Clinical Applications of Electrical Impedance Tomography

A thesis submitted to the University of Manchester for the degree of

Doctor of Philosophy (PhD)

in the Faculty of Biology, Medicine and Health

2017

Tanviha Quraishi

School of Medical Sciences

TABLE OF CONTENTS

Final word count of main text: **56,749**

LIST OF ABBREVIATIONS

ABP	Arterial blood pressure
ANS	Autonomic nervous system
ApEn	Approximate Entropy
AUC	Area under the curve
AWR	Awareness with recall
BBB	Blood-brain barrier
BEM	Boundary element model
BIS	Bispectral Index
BOLD	Blood-oxygenation-level-dependent
CBF	Cerebral blood flow
CBFV	Cerebral blood flow velocity
CBV	Cerebral blood volume
CEA	Carotid endarterectomy
CMFT	Central Manchester University Hospitals NHS Foundation Trust
CMR	Cerebral metabolic rate
CNS	Central nervous system
CPP	Cranial perfusion pressure
CSF	Cerebrospinal fluid
CT	Computed tomography
dc	Direct current
ECG	Electrocardiogram
EEG	Electroencephalogram
EGG	Electroglottograph
EIDORS	Electrical impedance and diffuse optical reconstruction software
EIT	Electrical impedance tomography
EITS	Electrical impedance tomography spectroscopy
EMG	Electromyography
EPSP	Excitatory post-synaptic potential
ESCoG	Sub-cortical EEG

ETAC	End-tidal anaesthetic concentration
FDG	Fluorodeoxyglucose
fEITER	Functional electrical impedance tomography with evoked response
FEM	Finite element model
fMRI	Functional magnetic resonance imaging
fps	Frames per second
FT	Fourier transformation
GA	General anaesthesia
GABA	Gamma amino butyric acid
HR	Heart rate
ICH	Intracranial hypertension
ICP	Intracranial pressure
i.v	Intravenous
LPV	Lung protective ventilation
MABP	Mean arterial blood pressure
MAP	Mean arterial pressure
MCA	Middle cerebral artery
MCAV	Middle cerebral artery blood flow velocity
MEG	Magnetoencephalography
MRI	Magnetic resonance imaging
NMDA	N-methyl-D-aspartate
NMR	Nuclear magnetic resonance
NIRS	Near-infrared spectroscopy
NVC	Neurovascular coupling
PET	Positron emission tomography
PONV	Post-operative nausea and vomiting
PNS	Peripheral nervous system
rABmtT	Regional arm-brain mean transit time
rCBF	Regional cerebral blood flow
REG	Rheoencephalography
ROC	Receiver operating characteristic
SE	Standard error

SPECT	Single-photon emission computed tomography
SQUID	Superconducting QUantum interference device
TBI	Traumatic brain injury
TCD	Transcranial Doppler
UCL	University college London
VALI	Ventilator associated lung injury
VEFR	Visually evoked cerebral blood flow velocity responses
VEP	Visual evoked potential
VILI	Ventilator induced lung injury
VM	Valsalva manoeuvre

LIST OF FIGURES

LIST OF TABLES

ABSTRACT

The University of Manchester
Tanviha Quraishi
Doctor of Philosophy (PhD)
Clinical Applications of Electrical Impedance Tomography
11th January 2017

INTRODUCTION Electrical Impedance Tomography (EIT) is an emerging clinical imaging technique. Functional EIT by Evoked Response (fEITER) was developed at the University of Manchester as a high-speed, functional brain imaging device for use at the bedside. This 32-electrode EIT system applies an injection frequency of 10kHz and captures data using a 10ms temporal resolution. This thesis reports on the first volunteer and patient trials undertaken using fEITER for the following conditions: **(a)** flashing visual sequence - 14 awake volunteers; **(b)** a voluntary Valsalva manoeuvre (VM) - 15 awake volunteers and **(c)** during the induction of anaesthesia - 16 elective surgical patients.
AIMS The research presented in this thesis was undertaken to differentiate between noise and physiological changes in raw fEITER data signals.
METHODS SNR was determined for fEITER. Raw fEITER signals were pre-processed to reduce noise and dominant trends before multiple comparisons between reference and stimulus data were undertaken. Histograms and ROC curves were produced to illustrate the difference between reference and stimulus fEITER data. AUC values for single-subject and pooled ROC curves were calculated to determine whether fEITER data can be reliably differentiated between reference and stimulus conditions. Approximate Entropy (ApEn) was applied to evaluate the regularity of high frequency components within fEITER data for each trial condition.
RESULTS Average SNR values for fEITER acquired using mesh and physical phantoms ranged from 62.94dB to 63.58dB, and 28.29dB to 31.45dB respectively. The following AUC values were acquired: Visual stimulus-frontal electrode pairs and electrode pairs overlying the visual cortex 0.520 and 0.505 respectively; VM: 0.658; and induction of anaesthesia: 0.547. The VM induced the greatest difference between pooled reference and stimulus data. Visual stimulation and induction of anaesthesia data showed poor distinction between pooled reference and stimulus data, although some single subject data did show a significant response. No significant differences were acquired for the comparison of ApEn-reference and ApEn-stimulus data for all trial conditions using a Wilcoxon's signed ranks test (visual stimulus-frontal electrode pairs: upper $p = 0.998$, visual stimulus-electrode overlying the visual cortex: upper $p = 0.980$; the VM: upper $p = 0.976$, and induction of anaesthesia: $p = 0.912$).
DISCUSSION Although single-subject and pooled fEITER data recorded during the VM produced the greatest differences between reference and stimulus measurements, stimuli such as visual flashes and induction of anaesthesia may not be large enough to induce quantifiable changes between reference and stimulus data recorded from single electrode pairs.Collectively, these results provide little evidence to show that pre-processing of raw fEITER data amplifies features in fEITER waveforms which may be representative of physiological changes induced by an applied stimulus.

DECLARATION

No portion of the work referred to in this thesis has been submitted in support of an application for another degree or qualification of this or any other university or other institute of learning.

COPYRIGHT STATEMENT

[i] The author of this thesis (including any appendices and/or schedules to this thesis) owns certain copyright or related rights in it (the "Copyright") and she has given The University of Manchester certain rights to use such Copyright, including for administrative purposes.

[ii] Copies of this thesis, either in full or in extracts and whether in hard or electronic copy, may be made **only** in accordance with the Copyright, Designs and Patents Act 1988 (as amended) and regulations issued under it or, where appropriate, in accordance with licensing agreements which the University has from time to time. This page must form part of any such copies made.

[iii] The ownership of certain Copyright, patents, designs, trade marks and other intellectual property (the "Intellectual Property") and any reproductions of copyright works in the thesis, for example graphs and tables ("Reproductions"), which may be described in this thesis, may not be owned by the author and may be owned by third parties. Such Intellectual Property and Reproductions cannot and must not be made available for use without the prior written permission of the owner(s) of the relevant Intellectual Property and/or Reproductions.

[iv] Further information on the conditions under which disclosure,publication and commercialisation of this thesis, the Copyrightand any Intellectual Property and/or Reproductions described init may take place is available in the University IP Policy see (http://documents.manchester.ac.uk/DocuInfo.aspx?DocID=24420), in any relevant Thesis restriction declarations deposited in theUniversity Library, The University Library's regulations (seehttp://www.library.manchester.ac.uk/about/regulations/) and inThe University's policy on Presentation of Theses

ACKNOWLEDGEMENTS

Firstly, I would like to express my sincere gratitude to my supervisors Professor Brian Pollard, Dr. Angella Bryan and Dr. Tom Marchant for the continuous support and encouragement they have provided me with throughout the completion of this thesis. The experience I have gained whilst being a part of Professor Pollard's research team has been invaluable and I am truly grateful for having the opportunity to undertake this PhD project.

I would like to thank Dr. Angella Bryan who has continually guided and motivated me through the various challenges we have faced. I'm extremely grateful to her for sharing her extensive knowledge and experience of undertaking clinical research. She has been a true inspiration and a continuous source of support.

I would also like to express my sincere gratitude and thanks to Dr. Tom Marchant for his continuous guidance and faith in me to complete this thesis. I am extremely grateful to him for joining the supervisory team and for imparting his knowledge and expertise of signal analysis techniques.

My sincere thanks also go to Dr. Chris Pomfrett. He co-invented fEITER and provided me with the invaluable opportunity to work with a brilliant invention.

I wish to acknowledge and thank my advisor Dr Rebecca Elliot for her help and guidance over the past 5 years.

I would also like to acknowledge and thank members of Professor Hugh McCann's research group from the School of Electrical and Electronic Engineering at the University of Manchester who were involved in producing fEITER.

I am grateful to Professor David Holder and his research group at University College London. Their expertise within EIT has been invaluable to this thesis.

I gratefully acknowledge my current and past colleagues within the Department of Anaesthesia at CMFT for their cheerful and willing support.

Words cannot express my gratitude towards my wonderful, loving parents Mr. & Mrs. N H Quraishi who have continually provided me with encouragement, love and strength in everything I've aimed to achieve.

I would also like to thank my siblings Yaqub and Hifza for consistently reminding me that there is light at the end of the tunnel. They have been a continuous source of motivation.

Finally, but by no means least, I would like to thank my loving husband Tabraiz for continually urging me to do better. He has provided me with endless support and encouragement throughout this journey for which I am truly grateful.

THE AUTHOR

The author gained a Bsc (Hons) in Neuroscience from the University of Manchester in 2007. As part of the undergraduate degree, the author undertook an industrial placement lasting 1 year until 2006, at Novartis AG Basel, Switzerland where she worked as a Laboratory Assistant within a cell screening group.
In 2009, she commenced employment within the Department of Anaesthesia as a Clinical Audit Facilitator at Central Manchester University Hospitals NHS Foundation Trust (CMFT) where she was involved in a multi-centre project concerning intra-operative fluid management. Following completion of the latter project, she joined a University of Manchester research group headed by Professor Brian Pollard and based within the same department as a Research Assistant to support EIT projects applied to anaesthesia. She is currently based within the Department of Anaesthesia at CMFT where she continues to work as a Research Assistant to support departmental research.

Chapter 1 Introduction

1.1 The Brain

The brain is the most sophisticated and complex organ within the body which functions to interpret the surrounding environment using sensory information transmitted via the nervous systems. The most crucial findings within neuroscience occurred during the nineteenth century where previous theories of physiological functions of the brain were challenged using scientific experimentation methods. Research undertaken during the nineteenth century provided fundamental evidence which enabled scientists to map anatomical regions of the brain to specific physiological functions. Animal experimentation and post-mortem observations firstly identified two distinct areas of the brain known as the cerebellum and cerebrum, more commonly named the brain stem and cerebral cortex respectively. Experimental ablation techniques performed on animals during the early nineteenth century showed that part of the cerebellum regulates respiration, cardiac function, coordination of movement and consciousness. During the latter part of the nineteenth century, individual case studies, post mortem examinations and electrical stimulation of the cerebrum identified functional areas of the cortex, conventionally described as lobes on the cortical surface. The human cortical surface is divided into four lobes namely: the frontal lobe, the parietal lobe, the occipital lobe, and the temporal lobe. Divisions of these lobes are formed by 2 distinct fissures on the cortical surface. The central sulcus forms a division between the frontal and parietal lobes, whereas the Sylvian fissure divides the frontal and temporal lobes (Figure 1.1). The frontal lobe encompasses important areas for voluntary movement including the primary motor cortex, the supplementary motor area and the premotor area. Auditory function is located within the temporal lobe. The occipital lobe functions as the primary visual centre of the brain and the parietal lobe contains somatic sensory areas (Bear et al., 2001). The human brain can be divided into 3 broad entities: the cerebrum, the cerebellum and brain stem; each of which contain further subdivisions relating to bodily functions.

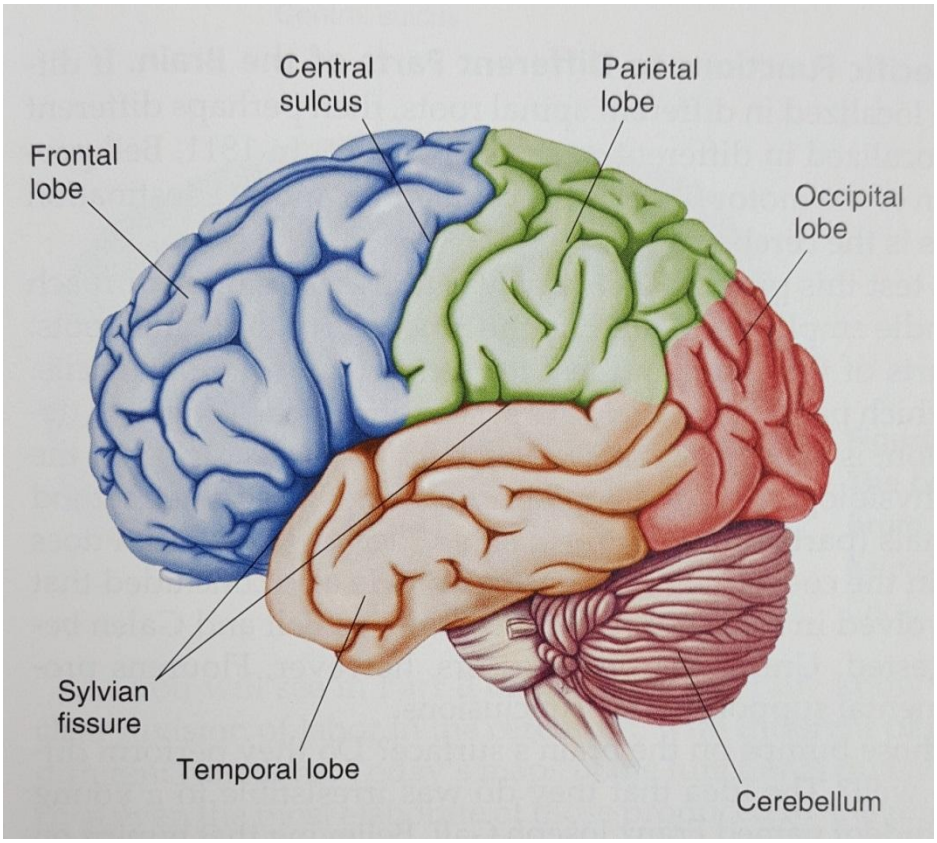

Figure 1.1 Lobes of the brain. The four lobes of the human brain can be traced on the cortical surface. The central sulcus separates the frontal lobe from the parietal lobe and the Sylvian fissure forms a division between the frontal and temporal lobes. The occipital lobe overlays the back of the brain above the cerebellum (Bear et al., 2001)

The cerebrum is considered the most highly evolved and superior structure within the brain. Anatomically, it covers the largest surface area in the brain and consists of two halves; the left and right cerebral hemispheres. The two hemispheres are separated centrally by the longitudinal fissure which extends from front to back (rostral to caudal). Connections between the two hemispheres are formed via a bridge-like structure known as the corpus callosum consisting of myelinated axonal fibres allowing the two halves to communicate. The outer layer of the cerebrum consists of grey cortical matter which forms the cerebral cortex. The cortex is associated with higher cognitive functions such as sensory and motor processing, perception of surroundings, planning and memory.

1.1.1 Communication in the Brain

The nervous system as a whole consists of a central and peripheral division more commonly known as the central nervous system (CNS) and peripheral nervous system (PNS). The CNS forms the brain and spinal cord whereas the PNS comprises nerves and nerve cells exterior to the brain and spinal cord which innervate the body. Cells of the brain broadly fall into one of two categories: neurons and glia. Neurons are the fundamental basis of communication within the nervous system. The description of a neuron comprises the soma (cell body), the dendrites (also known as neuritis) and the axons, all of which are highly specialised for their physiological function. The soma contains the nucleus of the neuron and other organelles such as mitochondria and endoplasmic reticulum which are common to other human cells. Branch-like extensions generating from the soma named dendrites serve to receive electrical impulses from neighbouring neurons. The dendritic membrane contains clusters of thousands of synapses which function to relay electrochemical signals to receptor proteins embedded in the membrane. The generated electrical signal, more commonly known as an action potential is then transmitted along the axon; a single fibre of nerve tissue projecting from the soma.

The action potential constitutes transmission of information along the neuron and enables communication within the nervous system via a rapid propagating electrical signal lasting approximately 2ms from beginning to end, with a peak amplitude of upto 100mV. Under resting conditions, the intracellular compartment of a neuron is negatively charged compared to the more positively charged extracellular environment. This naturally existing polarity of the neuron is recognised as its' resting potential. During an action potential, the resting membrane potential of a neuron changes from -65mV to +40mV caused by an influx of positively charged sodium (Na^+) ions into the nerve cell causing the membrane to depolarise (Bezanilla, 2006). Current knowledge on electrical properties of the axonal fibre during the generation and propagation of an action potential is built on pioneering research performed on the squid giant axon. Hodgkin and Huxley (Hodgkin and Huxley, 1939) measured action potentials propagating along the squid giant axon using micro-electrodes inserted into the live axon. Their investigations showed that the

action potential arises at the surface membrane of the nerve fibre and secondly, they quantified an absolute magnitude of the action potential as 90mV.

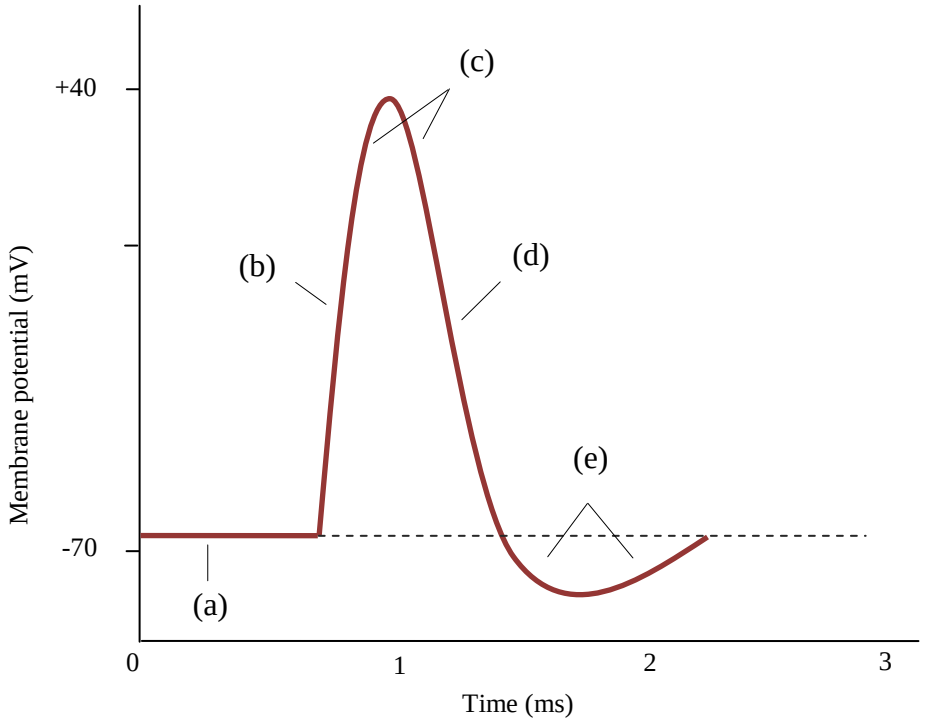

Figure 1.2 Illustration of the action potential. Phases of the action potential are displayed on the trace: (a) resting membrane potential; (b) rising phase; (c) overshoot; (d) falling phase; (e) undershoot.

A single action potential consists of distinct phases summarised in Figure 1.2. Firstly, the influx of positively charged Na^+ results in depolarisation of the membrane from the resting potential. Once depolarisation reaches a critical level (-65mV) termed the *threshold*, an action potential is generated. The 'rising' phase of the action potential describes the continuous influx of Na^+ across the membrane causing its' potential to increase further into the 'overshoot' phase. The membrane repolarises during the 'falling' phase of the action potential returning the membrane potential to a negative value. Repolarisation is caused by inactivation of Na^+ channels and also by the opening of potassium (K^+) ion channels across the membrane allowing the efflux of K^+ ions and causing the membrane potential to decrease. The decrease in membrane potential during this phase undershoots the original resting membrane potential due to further efflux of K^+ ions down their

concentration gradient. This part of the action potential is known as 'hyperpolarisation' and occurs prior to the membrane reverting to its resting potential. Inactive Na^+ channels and the delayed conductance of K^+ result in a refractory period during which it is impossible for an arriving stimulus to generate a further action potential (Bear et al., 2001, Kandel et al., 2000).

The axonal fibre functions as a conducting unit to transmit an action potential away from the soma to the axon terminal and can transmit signals along distances of less than 1mm to 3m (Kandel et al., 2000). The terminal end of an axon known as the pre-synaptic cell forms a connection onto the dendrite of a neuron which is termed the post-synaptic cell. The site of contact between the axon terminal and the post-synaptic cell is termed the synapse; the space between the two cells is known as the synaptic cleft. Action potentials propagating towards the axon terminal function to open voltage-gated calcium (Ca^+) channels located within close proximity of intrinsic synaptic vesicles containing neurotransmitter. The influx of extracellular Ca^+ ions induces these synaptic vesicles to fuse with the axon terminal membrane, resulting in the release of neurotransmitter via exocytosis (Borst and Sakmann, 1998). Following release of neurotransmitter molecules into the synaptic cleft, the molecules bind onto receptor proteins embedded in the membrane of the post-synaptic cell. Receptor proteins located in the post-synaptic membrane belong to one of the following two types of receptors: (a) transmitter-gated ion channels or (b) G-protein coupled receptors (GPCRs). The binding of neurotransmitter to either of these receptor types, stimulates structural changes in the receptor proteins, allowing the selective passage of ions through the post-synaptic membrane. Depending on the open channel selectivity induced by the neurotransmitter, the resulting membrane potential will propagate either an excitatory post-synaptic potential (EPSP) or an inhibitory post-synaptic potential (IPSP). Compared to transmitter-gated ion channels which allow the passage of ions through a central pore within them, GPCRs function to activate ion channels located within the post-synaptic membrane by activation of intrinsic mobile G-proteins which stimulate ion channels to open. In addition however, G-proteins can also function to stimulate the production of intrinsic second messengers within the cytosol which function to regulate ion channels and can also trigger alterations in cellular metabolism.

Glia support the physiological function of neurons within the brain. Although their role isn't central in the transmission of action potentials and electrochemical signals, optimal neuronal function is highly dependent upon the glia.

Glia are found in two forms within the brain: astrocytes and myelinating glia. Astrocytes are the most abundantly distributed glia in the brain and function to fill the extracellular spaces between neurons with a sponge-like formation. They modulate the extracellular fluid surrounding the neurons, firstly by confining released neurotransmitter to the post-synaptic cell and preventing neurotransmitter molecules from entering the extracellular space. Secondly, astrocytes have a protective role in the brain by removing excessive amounts of the neurotransmitter glutamate from the extracellular space. Excessive and prolonged release of the excitatory neurotransmitter glutamate has been shown to act as a neurotoxin leading to neuronal cell death.

Astrocytes also function to regulate the concentration of extracellular K^+ within the brain. Neuronal activity leads to the efflux of K^+ into the extracellular space. Resting levels of extracellular K^+ in the brain equate to 3mM. A single action potential causes an increase in extracellular K^+ concentrations of 1mM above resting levels; this increase in concentration correlates with the frequency of action potentials firing and also with the number of active neurons (Bilal, 2012). A build up of K^+ ions has been shown to disrupt the efficacy of synaptic transmission and can also alter the threshold of generating action potentials. Astrocytes regulate fluctuations in K^+ concentrations in the extracellular fluid firstly by uptake and accumulation of the excessive ions using ion channels and transporters, and secondly by dissipating the ions around the extracellular fluid known as spatial buffering (Gagnon et al., 2010).

Myelinating glia provide insulation to axonal fibres within the nervous system to increase the rate of nerve impulses propagating along the axon. Oligodendrogia are myelinated glia found in the CNS. A single oligodendrogia cell serves to insulate several axonal fibres. Action potentials are able to propagate the length of myelinated axons via gaps of exposed axonal membrane known as nodes of Ranvier.

Neurons are further categorised into the following 3 groups which reflect the number of processes extending from the soma: unipolar, bipolar and multipolar. The most abundantly found neuron type in vertebrates is the multipolar neuron which greatly varies in axon length and the number of dendritic branches extending from it.

1.1.2 Monitoring Brain Activity

The brain is central to regular functioning of the body by mediating nerve impulses, hormonal regulation and chemical messengers. Therefore, abnormalities in brain structure or function leading to potential disruption of the body's physiology must be appropriately diagnosed and accurately treated.

Conventional brain monitoring technologies within medicine provide useful tools to identify and diagnose abnormalities. Whilst the symptoms of neural damage or abnormalities are clinically identifiable, accurate diagnosis and treatment is dependent upon an imaging or monitoring intervention to anatomically locate the pathology within the brain. For example, epilepsy, stroke and tumours are all clinical conditions which exhibit distinct recognisable symptoms. However, precise localization of pathologies and treatment cannot progress without accurate imaging and monitoring techniques.

Technologies developed to monitor the brain target one of the following 3 physiological functions where pathological abnormalities may persist: (a) neural activity, (b) cerebral circulation and (c) anatomy.

Non-invasive monitoring of the brain clinically poses many challenges due to restricted access to the functional brain. Furthermore, there exist two separate temporal dimensions of functional brain activity. Measuring neural activity requires a sub-second temporal resolution commensurate with neuronal processing activity. Whereas measuring cerebral circulation requires a temporal resolution lasting several seconds commensurate with blood flow.

An ideal monitoring technique would successfully penetrate the protective layers surrounding the brain tissue including the hair, scalp, dura and encasing skull, whilst preserving the underlying brain tissue to be studied. For functional monitoring, a range of temporal resolutions would be desirable to differentiate between sub-second

neuronal activity and cerebral blood flow lasting several seconds. Finally, a high temporal resolution would enable accurate identification of anatomical abnormalities.

1.1.3 Imaging the Brain - Structural Imaging Techniques

Clinical techniques used to image the brain can be described as either structural imaging techniques or functional imaging techniques. The former refers to an image relating only to anatomy and provides no information on how the brain functions. The latter however, considers physiology of the brain by exploiting neural mechanisms, haemodynamic regulation or metabolism within the brain.
Considering structural imaging techniques first, conventional methods used within medicine to image anatomy of the brain are x-ray computed tomography (CT) and magnetic resonance imaging (MRI).

1.1.3.1 X-ray Computed Tomography (CT)

X-ray CT was first developed as a clinical imaging tool by Hounsfield in 1973 (Hounsfield, 1973) and it has since become an integral part of modern clinical medicine.
Conventional CT scanners operate by rotating X-ray breams around the head in the direction of the required cross-sectional plane. Each rotation corresponds to a single slice. As the patient moves through the scanner whilst X-ray beams are being projected, electronic sensors measure the projected X-ray beams. The radiopacity (resistance to X-rays) of different tissues within the head is computed to form a digitalised 2-D cross sectional sliced image which anatomically represents soft tissues of the brain. The time taken to perform a sequential CT scan of the brain is dependent upon equipment rotation speed. Spiral CT has gradually replaced sequential CT as X-ray beams are rotated continuously around the head therefore reducing the time required to perform a scan compared to sequential CT scanning. The spiralling nature of the X-rays allows multi-planar 3D images to be produced during a single scan. Movement artefact can also be eliminated from reconstructed images making it an ideal modality to image other areas of the body which are prone

to movement such as the lungs during respiration and bowels undergoing motility (Garvey and Hanlon, 2002).

Within clinical medicine, CT scans are most commonly used for diagnostic purposes and also to guide clinical treatment.

Patients presenting with a traumatic head injury routinely undergo a CT scan prior to treatment in order to determine the extent of damage to the skull and brain tissue. The acquired image can also be used to identify the incidence of a haemorrhage, haematoma, bruising to the brain and fractures on the skull. CT scanning is also widely used within neuro-oncology to identify the presence of a tumour or masses within the brain. Repeated CT scanning techniques also form an integral part of neuro-oncology treatment such as radiation therapy to monitor the progress and growth of tumours and masses within the brain.

For patients suffering a stroke, a CT scan is the primary investigative technique undertaken to diagnose the cerebral incident and in particular to rule out the incidence of a cerebral haemorrhage. To further explore an incident of stroke, CT is frequently coupled with angiography in a technique known as CT angiography which combines the CT anatomical image with a detailed angiography of the cerebral vasculature providing a high resolution image of vascular tissue within the brain. This combined method is particularly useful to identify vascular occlusions within the brain, although the impact of an occlusion on actual brain function cannot be determined using an anatomical image produced by CT (Miles, 2004).

CT is highly useful in a clinical setting due to the high resolution images it produces making it an ideal modality to anatomically locate specific areas of organs for accurate diagnosis, and also to guide precise surgical procedures such as needle biopsies. Despite the dramatic increase in CT use over the past several decades to improve patient healthcare, a major limitation of this modality is the radiation dose delivered to the patient making it unsuitable for repetitive imaging. The “organ specific dose” describes the calculated radiation dose delivered to the particular organ being imaged (Brenner and Hall, 2007, Davies et al., 2011) and is expressed in milligrays (mGy). Table 1.1 taken from a review conducted by Brenner (2007) (Brenner and Hall, 2007) lists the typical doses of organ specific dose of radiation which have been acquired from various studies (Table 1.1).

Table 1.1 List of organ specific radiation doses. This list has been adapted from a review undertaken in 2007 (Brenner and Hall, 2007).

Study type	Organ	Organ specific dose (mGy)
Dental radiography	Brain	0.005
Lateral chest radiography	Lung	0.15
Screening mammography	Breast	3
Adult abdominal CT	Stomach	10

The radiation doses emitted from CT scanning are considerably higher than x-ray radiation; x-ray examination of the adult abdomen will expose the patient's stomach to a radiation dose of approximately 0.25 mGy compared to a higher exposed dose of 10mGy using CT. Many of the potential risks associated with radiation exposure have been projected from studies undertaken on the atomic bomb survivors and survivors of nuclear disasters with particular focus on the incidence of cancer and genetic mutations caused by radiation exposure during pregnancy (Berrington de González et al., 2009, Brenner et al., 2001).

A recent retrospective cohort study examined the risks of developing leukemia and brain tumours in children and young adults who were exposed to CT radiation between 1985 and 2002. During follow-up, the authors reported an incidence of 0.04% and 0.07% for the diagnosis of leukemia and brain tumours respectively. Furthermore, a positive association was found between the amount of radiation exposure from CT scans with leukemia and brain tumours (Pearce et al., 2012). Although, the potential future risks of radiation are widely accepted, the benefits of CT technology currently outweigh the risks. The use of CT provides diagnostic accuracy using rapid scanning times. Furthermore, speedy scanning times also eliminate the need for sedation and anaesthesia in paediatric patients. Nevertheless, the associated potential risks of radiation have been acknowledged in the UK and protective legislations such as the Ionising Radiation (Medical Exposure) Regulations (Radiographers, 2011) ensure that CT scans are only undertaken when necessary and exposure remains within permitted radiation levels (Pearce et al., 2012). The most recent amendments to these regulations were made in 2011 (Society of Radiographers, 2011)

1.1.3.2 Magnetic Resonance Imaging (MRI)

The MRI technique was introduced into clinical practice in the 1980s and has since been utilised to study human brain anatomy and function, to aid neurodiagnosis. Cross-sectional images are generated from an MRI scan using nuclear magnetic resonance (NMR). The basic principles of clinical MR imaging are dependent upon hydrogen atoms; abundant in water and fat content within the body. The application of an external magnetic field within an MRI scanner causes the protons of some of the hydrogen atoms within the subject to align in parallel to the applied magnetic field, whereas other protons align in an opposite orientation to the applied magnetic field. A radio frequency pulse is then introduced which causes the unaligned protons to absorb energy from the externally applied force and resonate. Once the electromagnetic field is turned off, the protons release the absorbed energy and emit a radio signal which is captured as an electromagnetic signal (Wippold, 2007). The speed by which the protons return to their natural orientation is termed 'relaxation' and is defined by a time constant (T). Relaxation times are also dependent upon tissue type and the strength of the magnetic field applied. For example, within fat content, hydrogen has a slower relaxation time compared to hydrogen within water. These distinctions can be further subdivided into types of water content within a single organ system such as the brain, where the relaxation times of hydrogen can be seen to vary between the water content of CSF compared with the water content within grey and white matter of the brain. Due to differences in relaxation times within a single organ system, images produced using MRI can be optimised according to relaxation times to provide highly detailed and excellent contrast images between grey and white matter within the brain (Kandel et al., 2000, Shenton et al., 2012). Magnetic field gradients can be used to produce resonance frequencies of nuclei that are location dependent meaning a certain value of magnetic field can be associated with a specific location within the tissue of interest allowing tissue-specific details to be mapped into an image.

With a comparable spatial resolution to CT, MRI also possesses far better contrast resolution which makes it an ideal modality to image different tissue types. The technique is advantageous over CT, as it provides greater differentiation between

white and grey matters of the brain, allows multi-planar imaging to be undertaken (Duyn and Koretsky, 2011) and unlike CT, doesn't expose the patient to potentially harmful ionising radiation (Berlin, 2011, Dawson, 2004). However, despite obvious advantages, MRI is an expensive facility to set-up, requiring a shielded environment and highly expensive equipment. The imaging power of an MRI device is measured in Teslas which describes the magnetic field strength. Initial MRI systems operated using magnets that could attain field strengths of approximately one half of a Tesla which isn't sufficient to provide clinically useful images for diagnostic purposes. The use of superconducting magnets with field strengths ranging from 1.5 to 7 Tesla, provide the strength required for clinically useful images using MRI (Umutlu et al., 2014). The use of superconducting magnets provides a strong stationary magnetic field requiring appropriate and expensive screened facilities. Furthermore, ferromagnetic items in the surrounding area of the scanner can be particularly dangerous as they are literally projected towards the magnetic field.

Although the modality is non-invasive, MRI requires the patient to be placed into a restrictive scanning facility unsuitable for morbidly obese or claustrophobic patients. The tight space also limits the use of vital signs monitoring equipment for patients attached to several devices requiring close monitoring and access. Although, large diameter and upright scanners are now being produced to accommodate obese patients and also patients attached to additional clinical equipment (Sobol, 2012). MRI technology has, and continues to evolve since its original application within clinical practice in the 1980s. With increased capacities of magnetic fields and computing power, MRI is a powerful clinical imaging technique offering precise spatial detail for diagnostic purposes.

1.1.4 Imaging the Brain - Functional Imaging Techniques

Functional imaging techniques exploit haemodynamic, electrical and metabolic activity occurring in the brain to exhibit anatomical changes relating to physiological function.

Although CT and MRI are both highly useful to visualise high-resolution anatomical abnormalities in the brain caused by pathology or injury, images gained from these modalities provide no information on physiological function.

The following functional imaging modalities are most commonly used to image physiological changes in the brain: (a) positron emission tomography (PET), (b) functional MRI (fMRI) and (c) single-photon emission computed tomography (SPECT).

1.1.4.1 Positron Emission Tomography (PET)

PET is a nuclear imaging modality whereby gamma rays emitted by an administered positron-emitting radionuclide -more commonly referred to as tracers- are detected and reconstructed to form a tomographic image. A typical PET scan involves introducing a radioactive tracer isotope associated with a biologically active molecule, into the patients' circulation. Most PET scans utilise fluorodeoxyglucose (FDG); a tracer analogous to glucose which is used determine the metabolic activity of tissues as the radioisotope undergoes positron emission decay. Depending on the tracer used, it is possible to image a variety of functional processes occurring in a range of organs and tissues.

PET utilised for neuroimaging correlates areas of high radioactivity with increased brain activity. Standard FDG-PET has been used to localise epileptic foci as areas undergoing a seizure can be identified as having reduced metabolic activity (la Fougère et al., 2009). Similarly, FDG-PET has also been used to characterise neurodegenerative disorders such as Alzheimer's disease (McGeer et al., 1986) and in the differential diagnosis of Parkinsonian disorders relating to metabolic differences within areas of the brain (Eckert et al., 2005, Otsuka et al., 1996). The development of radiotracers which are structurally similar to neurotransmitters has enabled synaptic activity to be visualised within the brain using PET technology.

Radioligands specific for neuro-receptors such as dopamine, serotonin and acetylcholinesterase have been utilised in PET studies to determine the severity of neurological disorders such as Parkinson's disease (Antonini et al., 1995, Boileau et al., 2012, Brooks, 2003), major depressive disorders (Mayberg et al., 1988, Meyer et al., 1999, Shrestha et al., 2011) and anti-amyloid therapies for Alzheimer's (Nordberg, 2011).

PET is a widely used research and medical imaging tool with expanding clinical use within neuro-oncology for the detection of progressive tumour metastases and monitoring response to cancer therapy. In recent years the modality has been used in conjunction with a high resolution structural imaging technology such as CT or MRI to merge functional information with high-resolution anatomical images. The combination of PET/MRI has been of particular interest due to the higher soft tissue contrast provided by MRI whilst also eliminating additional doses of ionising radiation. However, the combination of PET with MRI has been a challenging concept to achieve requiring complete transformation of the PET detector design to make them compatible with the strong magnetic fields of MRI (Hu et al., 2014).

Despite advantages of being able to map a variety of physiological functions within the brain, PET has certain limitations which restrict its widespread use. The lack of expensive on-site cyclotrons used to produce radionuclides limits the use of some positron-emitting radioisotopes with short half-lives such as O-15 (oxygen-15) which has a half-life of 2 minutes. Radiation exposure to patients and staff as a result of PET scanning has also been the topic of various reviews debating the risks versus benefits of PET imaging. The overall exposure to ionising radiation inherent in imaging techniques such as PET is gradually increasing due to the diagnostic aid of these modalities for various pathologies in current clinical practice. In addition, imaging techniques are now more heavily relied upon for patient management.

PET and CT are considered to be sources of low-dose radiation (Huang et al., 2009, Guttikonda et al., 2014). Evidence from studies conducted on survivors from atomic disasters has established that high dose radiation exposure increases the risk of cancers and leukemias in a proportional manner with no safety threshold levels (Preston et al., 2007). Therefore, although low-dose radiation levels are deemed

acceptable, exposure at even these levels is considered to pose an increased health risk (Kumar et al., 2012, Leide-Svegborn, 2010, Nguyen and Wu, 2011).

1.1.4.2 Single-Photon Emission Computed Tomography (SPECT)

Similar to PET, SPECT is another radio nuclide based imaging method which has been applied to investigate cerebral haemodynamics, neurotransmitter and receptor abundance within the brain, and also receptor binding affinities using intravenously administered labelled compounds (Hill, 1980, Holman B and S., 1990). Many disease states are identified by functional changes prior to the manifestation of structural changes. For this reason, SPECT can be used as a complementary imaging technique to CT and MRI for increased imaging sensitivity to anatomically localise functional changes. Regional cerebral blood flow can be calculated from the time taken for an injected labelled compound to cross the blood-brain barrier (BBB). The time taken for the tracer compounds to enter neuronal cell bodies can also be determined and correlated with neuronal function (Devous Sr, 2005). Three-dimensional images representing the distribution of radionuclide within the brain are achieved using filtering techniques coupled with a rotating gamma camera (McArthur et al., 2011). Due to an increased rate of blood flow to grey matter containing cell bodies, SPECT is an ideal modality for differentiating between grey and white brain matter.

SPECT evaluations of cerebral perfusion have been useful in supporting the characterisation of dementia types and Alzheimer's disease. The technique has also been used to localise areas of a cerebral incident, foci of epilepsy and the progressive degeneration of dopaminergic neurones in Parkinson's disease (Brooks, 2005, Horky and Treves, 2011, McArthur et al., 2011).

The spatial resolution of this technique has been a concern for image interpretation when used as a single modality. Although combining the technology with high resolution CT imaging provides anatomically accurate information, this multi-modal technique is rarely considered essential. Once more however, the levels of exposure

to ionising radiation caused by SPECT and CT use, must be clinically justified (McArthur et al., 2011).

1.1.4.3 Functional MRI (fMRI)

fMRI shares the same basic principles as MRI however, fMRI exploits the different magnetic resonance between oxy- and deoxy-haemoglobin. fMRI measures the blood-oxygenation-level-dependent (BOLD) contrast and provides physiological information based on haemodynamic changes occurring within the brain. Areas of the brain which are highly perfused and receive greater amounts of oxygenated blood are associated with higher neural activity and metabolic demand. Deoxy-haemoglobin is paramagnetic and therefore reduces magnetic field homogeneity. The contrast between oxy- and deoxy-haemoglobin levels provides a BOLD signal contrast within the fMRI image as a result of local in-homogeneities in the main magnetic field. These in-homogeneities are related to physiological changes in haemodynamic demand. The BOLD signal has consequently been correlated with changes in neural activity in response to sensory stimuli and drug therapies crossing the BBB (Le Bihan et al., 1995, Silva et al., 2000, Yen et al., 2011). Similar to MRI, changes in magnetisation are used to reconstruct high-resolution images representing the contrast between regions of the brain which are highly perfused compared with areas containing increased levels of deoxy-haemoglobin. The role of fMRI within neurosurgery has also been reviewed as a comparative tool to predict neurological deficits pre-and post- neurological surgery (Ravn et al., 2014) as well as being used as a guide to precisely identify areas of cerebral function prior to neurosurgery (Matthews et al., 2006).

fMRI is considered a superior method of functional brain imaging compared to PET for two reasons. Firstly, fMRI has a greater spatial resolution (~3mm^3) compared to PET (5-10mm^3) (Bear et al., 2001) allowing physiological function in the brain to be located more precisely. Furthermore, repetitive imaging using fMRI carries no risk of exposing patients to harmful ionising radiation unlike PET, and is therefore considered to be completely non-invasive posing no health risks.

Despite the clinical uses of PET and fMRI a major limitation of using both techniques is that neither technology is portable therefore limiting their use in clinical situations such as the operating room. The patient has to be transferred to a specialised scanning facility for both fMRI and PET scanning which is unfeasible for a patient undergoing a surgical procedure and also carries significant risks for a ventilated critical care patient.

fMRI can localise haemodynamic activity with a spatial precision of millimeters using BOLD contrast, however the temporal resolution of this modality carries a haemodynamic delay of several seconds which is regarded as a limitation of the technique. Although the BOLD signal is correlated to neuronal activity, it is a not a direct measure of neural processing. To overcome this limitation and improve spatio-temporal resolution, the BOLD signal has been combined with neurophysiological measurements such as electroencephalography (EEG) in conjunction with fMRI to correlate haemodynamic physiology with cortical neural processing (Lemieux, 2004).

1.1.5 Physiological Monitoring of the Brain

Physiological monitoring techniques explore neural and haemodynamic processes occurring in the brain. These methods typically generate physiological waveforms which relate to functional activity. Physiological monitoring techniques currently used to monitor the brain can be broadly divided into techniques that monitor neural activity such as EEG and magnetoencephalography (MEG), and those which monitor cerebral haemodynamics such as transcranial Doppler (TCD) and near-infrared spectroscopy (NIRS).

1.1.5.1 Electroencephalography (EEG)

The first human EEG was captured by Hans Berger in the 1920's. He demonstrated its clinical utility to differentiate electrical activity between the awake and sleeping brain. The technique has since been extensively utilised in research to characterise the frequency and amplitude of electrical activity captured by EEG in various stages of sleep. It is also an important clinical tool to characterise immediate neuronal

responses to sensory stimuli (evoked responses) and is also heavily utilised for the diagnosis & management of epilepsy.

EEG captures the electrical activity of a population of cortical neurons firing action potentials using electrodes placed on the scalp. Potential differences at the cell membrane of neurones are produced by the influx and efflux of ions, generating excitatory or inhibitory currents. Although non-synaptic activity and synchronous action potentials can contribute to measured EEG activity, the primary source of EEG activity is generated by post-synaptic potentials of vertically aligned pyramidal cortical neurons, which are the major projection neurons in the cortex spanning cortical layers II, V and VI (Olejniczak, 2006).

Electrical activity is conducted through the various layers of tissues above the cortical surface before it can be measured using surface electrodes on the scalp. This conductivity is commonly known as volume conduction.

The summated electrical activity of cortical neurons is recorded as oscillations consisting of varying EEG band frequencies. The bandwidth of a typical clinical EEG recording ranges from 0.5 to 50Hz. The brain in a resting state produces a background electrical signal more commonly referred to as alpha rhythms occurring between 8-12Hz. Frequency signals deviating from the alpha (α) rhythms are generated from more complex cognitive activity (Olejniczak, 2006, Kennett, 2012). Beta (β) waves are identified at a frequency between 13-17Hz in response to intense concentration or alertness. Waveforms occurring in the β band frequency are accentuated by hypnotic drugs such as barbiturates and benzodiazepines. Theta (θ) and delta (δ) waveforms are typically slower and larger in amplitude and are captured at frequencies of 4-7Hz and < 3Hz respectively. EEG recorded during states of deep sleep typically generates δ waves. However when captured in awake states, these slow waves can also be symptomatic of sub-cortical lesions and pathological incidences of hydrocephalus (Fernández et al., 2000).

EEG captures electrical activity using an excellent millisecond temporal resolution allowing it to directly measure neuronal processing within the cortex. However, due to limitations in spatial resolution and sensitivity, EEG cannot identify single neuronal activity but instead captures synchronised electrical activity of neurons known as field potentials. Spikes manifested on a typical EEG trace represent field

potentials and summated electrical activity of neurons within the cerebral cortex. In addition, the amplitude of electrical activity measured at the surface is typically attenuated due to the layers of tissue between the EEG electrodes and the underlying cortical surface. It should also be noted that electrical activity originating from neurons lying within deeper structures of the brain such as the thalamus, brainstem and hypothalamus do not manifest on the surface EEG.

EEG can be combined with fMRI to overcome the poor spatial resolution. In turn the poor temporal resolution of fMRI is improved by the simultaneous use of EEG (Mullinger and Bowtell, 2011).

1.1.5.2 Monitoring Depth of Anaesthesia using EEG: the Bispectral Index

Monitoring depth of anaesthesia during surgery serves two clinical purposes. Firstly, it is imperative to ensure adequate unconsciousness, amnesia and analgesia is induced without excessive administration of the anaesthetic agent. Secondly, monitoring depth of anaesthesia is aimed to prevent the incidence of intra-operative awareness during surgery.

A detailed classification of anaesthetic stages produced by the inhalational anaesthetic agent diethyl ether was originally described by Arthur Ernest Guedel in 1937 (Guedel, 1937). Guedel's classification of anaesthesia comprised of 4 stages defined by various clinical observations such as analgesia, loss of the eyelash reflex, respiratory depression and muscle movement (Bhargava et al., 2004, Rani and Harsoor, 2012).

Frontal EEG has been shown to be a useful measure of depth of anaesthesia. In particular, general anaesthetic agents which act specifically on GABA receptors within the brain such as propofol and thiopentone, generate characteristic effects on frontal EEG relating to depth of anaesthesia. Whereas EEG activity during wakefulness is characterised by high frequency and low amplitude γ, β and α waves, EEG activity during GABA-ergic induced general anaesthesia (GA) predominantly features an increase in low frequency, high amplitude δ waves (Jagadeesan et al., 2013). During deeper levels of GA, EEG activity becomes suppressed with

characteristic ‘bursts’ of electrical activity known as burst suppression. A further increase in depth of anaesthesia results in almost constant suppression of EEG activity. This pattern of EEG activity is specific to states of coma and deep anaesthesia and therefore is not a visible feature of regular sleep EEG (Clark and Rosner, 1973, Jagadeesan et al., 2013). In its raw form, recognising specific features of frontal EEG relating to anaesthetic depth during surgery is difficult to identify and interpret without prior training. Consequently, a number of processing measures have been applied to EEG patterns relating to depths of anaesthesia in order to facilitate patient centred dosing of anaesthesia prospectively by the clinician. One processing technique commonly applied to the EEG signal is power spectral analysis. The distribution of EEG signal power over frequency is reflected by power spectral density. Spectral edge frequency and median edge frequency are two processing parameters formulated from the power spectrum. Spectral edge frequencies (SEF) derive single variables from raw EEG signals relating to depth of anaesthesia. SEF 95, SEF 90 and SEF 50 (median frequency) define frequency markers in Hz from the source gravity centre of the EEG band spectrum. Therefore, an SEF of 95% or 90% reflects the frequency boundary below which 95% or 90% of the total EEG power is situated (da Rosa and Rodrigues, 2011, Dressler et al., 2004, Schwender et al., 1996). In response to increasing levels of intravenously administered anaesthetic agents, SEF 95, SEF 90 and median frequency have been shown to decrease. As a result, it has been shown that SEF can be a useful measure for quantifying depth of anaesthesia during surgery and also during emergence from general anaesthesia (Schwilden et al., 1985). Whilst power spectral analysis provides an interpretation of the complex EEG signal relating to depth of anaesthesia, it also assumes that the EEG reflects a linear electrical process. This limitation prevents power spectral analysis to acknowledge characteristic features of signals generated from non-linear systems such as the brain. As power spectral frequency describes distribution of power as a function of frequency only, potential interactions in the EEG signal between oscillations occurring within different frequency bands are ignored (Tort et al., 2010). To overcome the limitation of solely using power spectral analysis when processing EEG signals for depth of anaesthesia monitoring, a more comprehensive signal processing technique can be applied to EEG data in order to acknowledge and

quantify non-linear features of the signal. Bispectral analysis is a processing technique which overcomes the limitations of power spectral analysis by detecting interfrequency interactions occurring within the sinusoidal components of the EEG signal (Sigl and Chamoun, 1994, Johansen and Sebel, 2000). A bispectrum generated from bispectral analysis contains characteristic features relating to altered physiological function within the brain such as anaesthetic induced unconsciousness. Extracting clinically relevant information from the bispectrum is difficult, requiring prior knowledge of interpretation. Within routine clinical practice, the application of bispectral analysis to monitor depth of anaesthesia has been exploited by commercially available devices such as the Bispectral Index® (BIS) (Covidien) monitor (Sigl and Chamoun, 1994, Jagadeesan et al., 2013). The Bispectral Index Scale (BIS, originally developed by Aspect Medical Systems, now Covidien) is a signal processing method which combines spectral and bispectral analysis with other features of the EEG such as burst suppression using a proprietary algorithm to derive a clinically useful index describing levels of consciousness. The BIS monitor generates a dimensionless number between 100 and 0 where 100 represents an awake state and 0 represents complete cortical suppression (Rampil, 1998). The BIS value is a statistically derived parameter which is based on the weighted sum of EEG factors such as time and frequency domains, combined with high-order spectral sub-parameters (Dou et al., 2014). The clinical use of BIS was aimed to supply anaesthetists with a single number reflecting the hypnotic effects of anaesthesia. The clinical benefits of using BIS were suggested to reduce the incidence of intra-operative awareness and improve post-operative outcomes by preventing excess anaesthetic administration. However, many research studies exploring the use of BIS have published conflicting results. Two large scale randomised, double blind trials undertaken in 2004 reported a reduction in intra-operative awareness with recall (AWR) following the use of BIS monitoring. Ekman, Lindholm et al., (2004) (Ekman et al., 2004) prospectively monitored a cohort of 4945 surgical patients using BIS. A recommendation of BIS values between 40 and 60 was applied during induction and maintenance of general anaesthesia. All patients were subsequently interviewed following surgery for an incidence of explicit recall during surgery. Results from the prospective patients were compared with a historical control group

consisting of over 7000 patients where no cerebral monitoring was applied during surgery. The authors reported a 0.04% incidence of explicit recall in the prospectively studied BIS group which was shown to be significantly lower than the incidence of recall reported in the control group: 0.18%. Awareness reported for patients in the BIS group was attributed to BIS values being higher than 60; although higher values were also recorded for other patients although no recall was reported for these patients. According to results from this large scale study, the use of BIS significantly reduces the incidence of explicit recall and awareness compared to patients receiving no cerebral monitoring during general anaesthesia.

Another study conducted in 2004 also explored the use of BIS monitoring to prevent the incidence of awareness in prospective surgical patients (Myles et al., 2004). Similar to the results reported by Ekman, Lindholm et al., (2004), a separate study also reported a reduction in the incidence of awareness during anaesthesia when BIS was used on 1225 surgical patients, compared to a prospective control group consisting of 1238 surgical patients, who received routine care without any cerebral monitoring technique (Myles et al., 2004).

Subsequent studies have reported conflicting data showing no significant decreases in the incidence of awareness during anaesthesia due to patients being monitored using BIS. In 2008, a study assessing the use of BIS to monitor depth of anaesthesia in order to prevent awareness, reported no significant differences in the incidence of awareness using BIS, compared to a patient group where standard end-tidal anaesthetic concentration (ETAC) was used to assess the levels of administered anaesthesia (Avidan et al., 2008). Similarly, in a later trial conducted on surgical patients considered to be at a high risk of awareness during surgery, the incidence of awareness reported for patients monitored with BIS compared to patients monitored using ETAC was not reported to be significantly different (Avidan et al., 2011).

The use of BIS in preventing excess administration of anaesthetic agents and improving post-operative recovery has also been a topic of considerable debate within literature. Whereas some trials have reported that the clinical use of BIS prevents excessive dosage of anaesthesia and therefore improves surgical outcomes (Chan et al., 2013, Punjasawadwong et al., 2007), data from other trials have provided conflicting results (Leslie et al., 2005, Mashour et al., 2012). Since it was

originally launched for clinical use, the BIS algorithm has undergone several alterations to reduce artefacts and improve performance. Recent modifications of the BIS algorithm consider the interference of frontal electromyography (EMG) activity to prevent false elevation of the BIS value as a result of low frequency frontal EMG activity (Baldesi et al., 2004). Significant hemispheric asymmetry has been reported using unilateral BIS monitoring from either side of the head (Pomfrett et al., 2009, Pomfrett and Pollard, 2009). Advancing from the traditional unilateral BIS monitoring system, a bilateral BIS monitor (BIS Vista™) has been launched to simultaneously monitor hemispheric differences during anaesthesia.

There is no doubt that there exists a clinical need to monitor depth of anaesthesia. As the functional target of anaesthesia is the brain, it is instinctive to monitor the delivery and effect of the agent on its target organ, relating to the drug dose provided. The BIS monitor aims to provide a solution to the clinical need of monitoring the effects of anaesthetic dose by monitoring the depth of hypnosis. Although generation of a BIS value considers altered electrical activity in the brain derived from frontal EEG activity, the actual BIS data provides no physiological information as to what neurological processes are occurring within the brain in response to administered anaesthesia. The precise mechanisms of how consciousness is lost and the absence of noxious perception during anaesthesia cannot be explained by a BIS value. In addition, BIS does not consider the effects of anaesthesia on deeper structures within the brain such as the thalamus which has been suggested to play an important role within consciousness (Alkire et al., 2000). Furthermore, BIS is not a universal depth of anaesthesia monitor for alternative anaesthetic agents which are not selectively active at the GABA receptor such as ketamine, nitrous oxide and xenon (Hirota, 2006). A further limitation of BIS is contamination of the BIS value caused by the electrical contribution of skeletal muscle activity measured using EMG. The EMG is a prominent source of interference within the BIS signal due to the administration of neuromuscular blocking agents during anaesthesia which vary the extent of paralysis (Russell, 2013). As the frequency of EMG activity overlaps with EEG activity within the range of 35-47Hz, the EMG has been shown to cause incorrect elevation of the BIS value due to the presence of high frequency and low amplitude EMG activity (Renna et al., 2002, Russell, 2013).

Despite the positive reports encouraging the use of BIS to determine the depth of anaesthesia, the limitations which have been discussed so far have highlighted that BIS cannot be reliably used in isolation to determine depth of anaesthesia. In order to develop a clinical device capable of monitoring anaesthetic depth on the brain it is first necessary to identify the precise mechanisms and targets of anaesthesia on functional activity within the brain. In addition, to study patient-centred anaesthetic depth within routine clinical practice, the precise effects of anaesthesia on the brain must also be isolated from other drug effects.

1.1.5.3 Magnetoencephalography (MEG)

Physiological processes occurring in organs such as the heart and brain generate electromagnetic potentials. Both the electrical and magnetic constituents of these potentials can be measured externally. The primary source of both EEG and MEG signals are the cortical pyramidal neurones. However, important differences in the orientation of the neurons and precise sources of measurements (intracellular and extracellular) which are used for EEG and MEG should be noted. Electromagnetic fields produced in the brain are generated from the depolarised/hyperpolarised post-synaptic potentials of cortical pyramidal neurons which are tangentially aligned to the scalp. In relation to the scalp, electrical potentials of cortical pyramidal neurons run in a parallel direction to the scalp whereas the emitted magnetic fields are released in a perpendicular direction.

Whereas the electrical constituent of neuronal activity in the brain is recorded on an EEG, the magnetic constituent of the electromagnetic field emitted by cortical pyramidal neurons is the source of MEG measurements (Babiloni et al., 2009, Sato and Smith, 1985).

As the amplitude of biological magnetic fields produced are extremely low, ranging from 10^{-13} to 10^{-10} tesla, highly sensitive monitoring devices are required to pick up the minute changes in the biomagnetic signals emitted from tissues which can be identified amidst a much larger, background magnetic field (Parra et al., 2004). Magnetic fields generated by the brain are measured using highly sensitive magnetic field detectors known as Superconducting QUantum Interference Devices (SQUID).

SQUID combat the challenge of measuring a weak magnetic field emitted by organs such as the heart or brain in the presence of the very large, naturally occurring magnetic field in the background. The first measurement of a magnetic field emitted by the human heart was measured at 5×10^{-7} gauss. Compared with the earth's steady magnetic field measured at approximately 0.5 gauss, the magnetic field produced from electrical currents of the heart was one million times smaller (Baule and McFee, 1963). Original measurements of magnetic fields emitted by the heart were undertaken using a single compacted detection coil in a shielded room to decrease the background magnetic field (Cohen, 1967). A similar method applied to the brain resulted in even weaker measurements of magnetic fields being captured from the scalp. The primary source of these measurements was produced by electrical alpha-rhythm currents which measured 1×10^{-9} gauss peak to peak. Signal averaging in respect to the electrical EEG signal was also applied to further remove background magnetic field from the acquired signal (Cohen, 1968). The subsequent application of SQUIDs enabled detection of the brain's magnetic field with increased sensitivity and also without the need for an electrical reference. This was achieved by the ability of SQUIDs to capture the magnetic field of direct current (dc) activity generated in the brain. The dc activity cannot be captured using EEG due to contact impedance occurring between the electrodes and the scalp. As there is no direct skin contact using MEG, magnetic field measurements generated by d-c activity can be reliably captured (Cohen, 1972). Major advances in technology have been undertaken over the years, which have enabled the original SQUID device containing single-channel sensors to evolve into instruments consisting of multiple SQUID sensors. Conventional MEG instrumentation consists of over 300 SQUID sensors contained within a helmet-like apparatus (Hari and Salmelin, 2012). MEG data is often superimposed on a high resolution image captured using MRI to create a magnetic source image (MSI).

MEG has several advantages over EEG. EEG measurements are generated by synchronous neuronal activity which therefore makes precise localisation of electrical signal generation a challenge. Although magnetic fields recorded in MEG are also generated from synchronous neuronal activity, MEG has a higher spatial resolution and therefore it is possible to localise origins of the magnetic field by

calculating the altered magnetic field as a function of its distance from the source (Kennett, 2012). MEG captures magnetic fields generated by intracellular ionic currents whereas EEG predominantly records extracellular electrical potentials. Furthermore, the layers of tissue surrounding the brain including the highly resistive skull attenuate the electrical signal measured by EEG, resulting in distortions when localising precise sources of activity (Shibasaki, 2008). In contrast, the skull is magnetically transparent therefore MEG eliminates any distortions caused by conductivity differences between the brain, scalp and skull. As a result, real time neuronal activity can be accurately determined using a spatiotemporal resolution of 0.1-1cm and 1ms, respectively (Wheless et al., 2004).

The temporal resolution of MEG exceeds that of EEG making it an ideal modality to record neuronal activity (Hari and Lounasmaa, 1989). MEG has been shown to be highly useful in investigating the pathology of CNS disorders such as epilepsy, Parkinson's and Alzheimer's disease (Stam, 2010). However, despite the technique being completely non-invasive, the small scale of the magnetic field emitted from the brain requires highly sensitive and specialised equipment. Unlike EEG technology which is highly portable and cost-effective, MEG recordings have to be carried out in expensive screened facilities to eliminate interfering sources of environmental magnetic fields. Despite MEG recording brain function with a more superior temporal and spatial resolution compared to EEG, the high cost involved in undertaking MEG recordings has limited its use as an established monitoring tool routinely used in clinical environments.

1.1.5.4 Monitoring Cerebral Perfusion using Near Infra-Red Spectroscopy (NIRS) and Transcranial Doppler (TCD)

Non-invasive monitoring techniques used for continuous cerebral perfusion monitoring include near-infrared spectroscopy (NIRS) and the transcranial Doppler (TCD).

The principle of NIRS was described in the 1970s by Jobsis (Jobsis, 1977) as a method to non-invasively monitor tissue oxygenation using NIR beams in the heart and brain. The optical properties of biological molecules change when they bind to oxygen, altering their absorption patterns and also their optical spectrums. The penetration of visible light by biological tissues is attenuated and varied due to blood, water and collagen content. Therefore visible light is unable to penetrate biological tissues at deeper distances. In contrast, the NIR spectrum which ranges from 700 to 1100nm, is capable of penetrating biological tissues at deeper distances of several centimetres (Jacques, 2013, Scheeren et al., 2012). In addition, NIR beams are also able to penetrate bone, making it an ideal modality to monitor transcranial cerebral oximetry. NIRS measures regional cerebral oxygen saturation to provide a continuous and real-time measure for adequate cerebral perfusion and oxygenation. Optical detectors placed on the head receive the emitted beam following penetration of photons through layers of cerebral tissue. The varying optical properties of oxy-haemoglobin and deoxy-haemoglobin allows the measurement of blood oxygenation within the brain which is correlated to neural activity (Murkin and Arango, 2009, Shibasaki, 2008).

As a clinical tool, NIRS is utilised as a continuous trend monitor during surgical procedures such as carotid endarterectomy (CEA) surgery where cerebral circulation can become compromised during clamping of the carotid artery. Various studies have shown NIRS to be a useful monitor for cerebral ischaemia during CEA (Hirofumi et al., 2003, Samra et al., 1996, Vets et al., 2004) and also as a predictor for reduced neurological function correlated with a reduction in cerebral oxygen saturation (Hirofumi et al., 2003).

TCD measurements are undertaken by a non-invasive Doppler probe emitting sound waves of a particular frequency range (1-2MHz) which are used to measure blood

flow velocity within cerebral blood vessels. Sound waves reflected by the movement of red blood cells are detected by a transducer and blood flow velocity can be determined from the resultant Doppler shift. TCD monitoring possesses a fast temporal resolution and therefore can be used to monitor rapid changes in cerebral haemodynamics (Markus, 2000). Limitations to TCD measurements are mostly associated with movement artefact which can distort the ultrasound signal. Reliable TCD application requires anatomical knowledge and technical skill to target the appropriate cerebral vessel through anatomical 'windows' in the skull. The TCD technique also assumes uniformity of vessel diameter and is therefore unsuitable for use in detecting changes in cerebral perfusion due to vasodilating and vasoconstricting drugs crossing the BBB (Panerai, 2009).

1.2 Electrical Impedance Tomography (EIT)

An ideal brain imaging modality would be portable, completely non-invasive and have the ability to monitor neural and haemodynamic physiology operating at two, variable temporal resolutions. Furthermore, a high spatial resolution would enable precise anatomical areas of the brain to be related to neural and haemodynamic functions. The latter is currently achieved using a combination of modalities such as EEG combined with fMRI to provide imaging of neural and haemodynamic brain function using a high spatio-temporal resolution. However, there still exist some limitations using combined methods such as the one described. As already mentioned, fMRI is not a portable technique therefore the subject or patient has to be taken to the scanning device. EEG monitors neural processing within the cerebral cortex which is useful for correlating fMRI activity with cortical functions such as movement, language and sensory processing. However EEG cannot monitor neural processing occurring in deeper areas of the brain. In addition, although highly perfused areas in deeper structures will be highlighted using fMRI, this will not provide a direct measure of neural activity in these areas when simultaneously measuring cortical EEG.

Due to many limitations in using a single or combined method of monitoring brain function, the neural basis underlying many physiological functions of the brain is still

poorly understood. Anatomical regions of the brain thought to be responsible for mediating states of consciousness have been identified using imaging modalities such as fMRI or PET. However, these results have been correlated with changes in blood flow and metabolic demand rather than actual neural processing within deeper structures of the brain. A portable device which would allow global neural activity to be visualised could revolutionise clinical brain imaging and further our current understanding of the brain. A portable technology would enable brain function to be monitored in a range of clinical environments such as critical care wards, the anaesthetic and operating rooms. Furthermore, a portable device may fulfill the possibility of being able to image the functional brain in an ambulance, GP practice or in the patient's home. For disease states such as stroke this could be a life-saving application where the decision to administer thrombolytics could be ascertained prior to the patient reaching hospital and therefore potentially minimising the devastating effects of a cerebral accident on the brain.

A suggested application for imaging global functional brain activity is electrical impedance tomography (EIT). EIT is an imaging technique which images the internal impedance of a given tissue or material. An EIT device essentially operates by injecting a current sequence of known amplitude and frequency into a tissue or material of interest using surface electrodes. Non-invasive EIT instruments utilise EEG type electrodes to measure boundary voltage data which is generated from the injected current. This information is then used to determine internal conductivity distributions and impedances to form a tomographical image. The technique benefits from numerous desirable features for a clinical imaging technique as it is portable, inexpensive, fast to perform and has been demonstrated to be completely non-invasive. Furthermore, compared with other medical imaging techniques such as PET and X-ray which expose patients to ionising radiation, EIT poses no risk or harm to its subjects making it suitable for repetitive use and continuous monitoring. As a brain imaging technique therefore, EIT holds great promise in providing a portable non-invasive imaging tool for rapidly visualising brain function in a range of clinical environments.

The technique of EIT was originally invented for geophysical investigations but has since been adapted for clinical imaging. The potential of EIT being used as a medical

imaging technique was first proposed by Henderson and Webster in 1978 (Wilson et al., 2001, Henderson and Webster, 1978) who suggested it's clinical utility for monitoring ventilation from the thoracic surface. Brown and Seagar (Brown and Seagar, 1987) subsequently developed the first commercially available EIT system to monitor ventilation and changes in the cardiac cycle. This prototype EIT system known as the Sheffield data collection system has since been utilised in numerous clinical trials and has also been the basis for the development of subsequent EIT systems used for monitoring ventilation and other physiological functions such as gastric motility, breast cancer screening, haemodynamic changes and more recently, functional brain activity.

1.2.1 EIT of Biological Tissues

The contents of biological tissues determine how injected current conducts through it. Bone and fat tissue are highly resistant and therefore poor conductors of electricity compared to muscle and nerve tissue which are less resistant to current flow. Tissue impedance as a measurement is defined as the opposition to the flow of an electric current and is largely, but not entirely, dependent upon two electrical properties of biological tissues: resistance and capacitance. Both the extracellular and intracellular fluid of a biological tissue contains sodium ions and is therefore highly conductive to injected current. These sodium-rich spaces encompass the 'resistant' component of a tissues' impedance measurement. The capacitance of biological tissues relates to the cellular lipid membrane which behaves as an insulator. The dielectric properties of biological tissues are highly dependent upon applied current frequency. EIT systems reported to date typically operate at frequencies between 100Hz to 100MHz, over which the resistance and reactance of biological tissues steadily decreases. This is due to higher current frequencies being able to pass more easily across the cell membranes. As current frequency increases, permittivity of the cell membrane decreases in a stepwise fashion termed as 'dispersions' described in the following three stages: (1) The alpha dispersion of the cell membrane occurs between applied frequencies of milli-Hz to 100Hz and is associated with ionic diffusion processes via gated channels at the cell membrane. At lower injected

frequencies the cell membrane is able to charge and discharge entirely. (2) The beta dispersion occurs at frequencies between 10kHz-100MHz due to cell membrane polarisation and the build-up of charges at the cell membrane. During beta dispersion, the cell membrane is only able to partially charge therefore permitting current to pass through the lipid cell membrane and enter the intracellular space. (3) The gamma dispersion occurring in the GHz range is related to polarisation of water, salt and protein molecules (Gabriel et al., 1996, Davalos and Rubinsky, 2004, Stuchly and Stuchly, 1980).

EIT systems utilising a low frequency current injection (typically below 100Hz) are constrained to the extracellular space and are typically applied to monitor haemodynamic changes occurring in tissues. EIT systems utilising higher frequency current injections (> 40 kHz) are able to penetrate the lipid cell membrane and can access sodium ions in both extracellular and intracellular spaces. Higher frequencies are therefore utilised by EIT systems to characterise and monitor intracellular properties (Oh et al., 2011, Prasad et al., 2008). Multi-frequency EIT systems, known as EIT spectroscopy, employ a range of current injecting frequencies for tissue characterisation, as biological tissues exhibit impedance differences which are variable as a function of the current injection frequency (Gagnon et al., 2010). Furthermore, the temporal resolutions can be coupled to appropriate injection frequencies to monitor specific physiological functions ranging from slow haemodynamic changes occurring over several seconds, to fast electrical and chemical changes occurring over milliseconds (Brown, 2003, Holder, 1992a, Schwan and Kay, 1957).

Impedance is therefore a dynamic form of measurement which, when measured over time, will be affected by various physiological mechanisms. Movement of extracellular water into the intracellular space, haemodynamic changes in velocity & volume and movement of ions across a cell membrane are all examples of physiological changes which would result in an impedance change. To date, the method of EIT has been applied to monitor various physiological functions such as ventilation, gastric emptying, breast cancer imaging, cerebral blood flow changes, and more recently, imaging neural activity of the brain.

1.2.2 Monitoring Ventilation using EIT

Maintaining respiration using a clinical device is known as ‘mechanical ventilation’ and is routinely utilised in medicine for patients unable to breathe by themselves. Ventilators are most commonly used in anaesthetised patients undergoing a surgical procedure and for more prolonged periods of time in critically ill patients within an intensive care setting. Clinicians are able to control the concentration of oxygen administered, respiration rate and tidal volume in accordance to the patients need. Although ventilation can be a life-saving intervention, its use can also lead to impaired lung function caused by physical mechanisms of ventilation. Ventilator-induced lung injury (VILI) or ventilator-associated lung injury (VALI) has been associated with the following two main triggers described in the literature:

1.) volutrauma caused by over-distension of the alveolar tissue
2.) atelectrauma caused by the transient inflation and collapse of the alveolar during the respiratory cycle (Albaiceta and Blanch, 2011, Gattinoni et al., 2010, Rocco et al., 2012).

Alveolar cell injury and rupture can cause interstitial oedema subsequently inducing an inflammatory response known as biotrauma. Systemic release of inflammatory mediators in mechanically ventilated patients has been associated with a risk of developing acute respiratory conditions such as pneumonia and pneumothorax. Prolonged inflammatory responses have also been shown to cause multi-organ failure (Slutsky and Tremblay, 1998, Ranieri et al., 1999, Kuiper et al., 2005). Extensive research over the past 40 years has highlighted the importance of lung protective ventilation (LPV) strategies for individual patients to avoid over-distension and mechanical trauma to the lung tissue whilst maintaining adequate gas exchange. Current methods employed to guide LPV involves high resolution imaging of the lungs (CT) which reveals regional lung air content and regional ventilation (Cinel et al., 2007). However, due to the patient being exposed to ionising radiation, CT is unsuitable for repetitive and continuous monitoring at the bedside. EIT has been proposed as an effective solution for non-invasive imaging of the lungs and for

the continuous monitoring of mechanically ventilated patients to guide LPV therapy at the bedside.

Due to the insulating properties of air, swelling of the air-filled alveoli during inspiration causes an increase in lung tissue resistance. The increase in resistance is measured as a conductivity change in boundary voltage measurements captured using EIT (Metherall et al., 1996). Portable EIT systems eliminate the need for patients to be transferred to a screening facility such as CT allowing bedside monitoring. Furthermore, EIT poses no risk of ionising radiation to the patient, making it an ideal technique for continuous and repetitive monitoring within the critical care environment.

Research conducted until now has described the following two areas of lung function which can be explored using EIT:

1.) Imaging intra-thoracic volume changes during respiration as a real-time monitoring tool to guide therapy

2.) Monitoring lung perfusion and gas exchange to detect abnormalities in lung function caused by pulmonary emboli and pulmonary oedema

Clinical studies adopting the use of EIT to monitor ventilation from the thorax have shown global impedance changes relating to both ventilation and the cardiac cycle. The rapid outflow of blood produced by the ventricles of the heart during ventricular systole, results in a sudden change in conductivity of the thorax as the ejected blood is supplied to the systemic and pulmonary circulation. Although the respiratory and cardiac cycles are isolated in frequency over a minute, both cycles often occur synchronously making it difficult to distinguish ventilation from perfusion when monitoring using EIT (Eyuboglu et al., 1989). The ability to distinguish between ventilation and perfusion is clinically relevant to assess an individual's potential gas exchange and therefore adapt individual ventilation therapy. As conventional imaging modalities are unable to assess both ventilation and perfusion at the bedside, EIT is a highly desirable monitoring tool for evaluating the distribution of ventilation and perfusion within the lungs.

A filtering technique must be applied to EIT data in order to separate the large changes in impedance elicited by ventilation from the much smaller electrical impedance changes resulting from perfusion (Eyuboglu and Brown, 1988). Fagerberg et al., (2009) demonstrated a method to distinguish between ventilation and perfusion in EIT data by implementing a large range of stroke volumes in a porcine model. To selectively monitor pulmonary perfusion using EIT, a brief apnoea was induced to eliminate the effects of ventilation on the EIT signal allowing prospective visualisation of pulse related impedance data. Pulse-synchronous impedance data was accurately captured using EIT across a range of stroke volume values. The study effectively demonstrated that EIT can be applied as a rapid and prospective method to distinguish between ventilation and pulmonary perfusion by comparing results with stroke volume data captured using the invasive pulmonary artery catheter. Fagerberg's study identified apnoea induction as an effective technique to eliminate the effects of ventilation from perfusion EIT data without the need for retrospective filtering, however this method is not deemed ideal to be used repetitively for continuous monitoring within a clinical setting (Grant et al., 2011). Various filtering techniques have also been applied to EIT data captured from the thorax to selectively identify changes in ventilation and perfusion. One method known as ECG-gated EIT has been applied in various studies to amplify cardiac perfusion signals captured using EIT. To implement this filtering technique, an ECG signal is simultaneously recorded from the individual. The QRS component of the ECG can then be utilised as a trigger for EIT data collection relating to a specific cardiac event such as the R-wave. Following a complete data cycle using ECG-gated EIT, temporal averaging of the data is undertaken to eliminate the effects of ventilation and noise from the perfusion data and therefore allowing pulsatile movement of blood within the lungs to be imaged (Eyuboglu and Brown, 1988, Eyuboglu et al., 1989, Pikkemaat and Leonhardt, 2010). Studies utilising ECG-gated EIT techniques to derive pulmonary perfusion data have demonstrated the importance of imaging blood flow in the lungs to identify abnormalities such as pulmonary emboli (Eyuboglu et al., 1989, Leathard et al., 1994). However, disadvantages of this filtering method have also been discussed relating to the long duration of time required to capture the recommended amount of cardiac cycle data

for reliable temporal averaging and also regarding the absence of a ventilation component during ECG-triggered data acquisition (Frerichs et al., 2009). Although, ECG-gated EIT is effective for evaluating pulmonary perfusion in isolation, the simultaneous assessment of ventilation and perfusion cannot be undertaken using this technique. Certainly, ECG-gated EIT could be applied retrospectively to EIT data to preserve the ventilation component of the EIT signal. However, this would limit the prospect of using EIT as real-time monitor for pulmonary perfusion.

Fourier transformation (FT) is another filtering technique applied to EIT data in order to isolate the components of ventilation and perfusion. FT examines changes in frequencies within a given signal over time. As ventilation and perfusion cycles operate at two different frequencies, these can be decomposed and expressed as different frequency components as demonstrated in a study undertaken by Kerrouche et al., (2001). In the aforementioned study, FT was successfully applied to EIT data captured from a single subject to differentiate between ventilation and perfusion data. In a later study undertaken by Frerichs, Pulletz et al., (2009), EIT data captured from ten intubated patients was evaluated to determine whether regional perfusion changes in the chest induced by unilateral and bilateral ventilation could be measured using EIT. Frequency filtering using FT was applied to the EIT data to separate ventilation and perfusion components. By reducing pulmonary perfusion to one lung during unilateral ventilation, the authors successfully demonstrated that EIT was capable of monitoring pulmonary perfusion in regions much smaller than previously reported. Similarly, Grant, Pham et al., (2011) reported the use of FT filtering on EIT data recorded from ten healthy subjects. Once the frequency characteristics of ventilation and perfusion were identified using FT, band pass filtering was applied to the separate EIT components relative to respiration and heart rates. Extracted impedance data was then reconstructed to reveal images representing impedance data for ventilation and perfusion (Suchomel and Sobota, 2013).

The use of EIT to image the cardiopulmonary system has been extensively researched and a number of physiological parameters have been shown to be reliably identified such as cardiac output monitoring (Frerichs, 2000, Smit et al., 2004) regional tidal volume (Dargaville et al., 2010, Pulletz et al., 2008, Karsten et al., 2011) and ventilation delay (Muders et al., 2009). Within the past 5 years,

commercial EIT devices have been launched to continuously monitor lung function. The PulmoVista® 500 was launched by Dräger as a bed-side monitor for continuous monitoring of ventilation within critical care. This device has recently been evaluated in a porcine model for the use of monitoring dependency of lung impedance on fluid balance (Schaefer et al., 2014) with the aim of a clinical use to diagnose the presence of pulmonary oedema or contusion. It operates using a belt of 16 electrodes placed around the chest. Current is injected in frequencies ranging from 80kHz to 130kHz, generating 10 to 30 images per second. A recent case study exploring the use of the PulmoVista® 500 to localise pulmonary embolisms in a porcine model showed the device was capable of detecting impedance changes due to large abnormalities in perfusion although smaller perfusion defects were not localised reliably (Sobota and Suchomel, 2013). The authors concluded that more studies are required to reliably use the PulmoVista® 500 for detection and localisation of pulmonary emboli.
Swisstom (Switzerland) have recently combined EIT technology with SALVIA Medical - an intensive care ventilation monitor - to produce a device which is able to continuously monitor pulmonary function within intensive care. The commercially available device is known as elisa 800^{VIT} and is advertised as being able to guide lung protective strategies for ventilated patients within intensive care (Swisstom, 2014).
Despite commercial devices being manufactured, EIT is still limited for widespread clinical applications to monitor and guide mechanical ventilation. It has been suggested that larger clinical trials relevant to clinical decision making may be required to support increased use within regular clinical practice (Frerichs et al., 2014).

1.2.3 Monitoring Gastric Motility using EIT

EIT has been used to generate sequential images of gastric contents relating to resistivity changes and therefore has provided a useful measure for the rate of gastric emptying. A consumed meal of known conductivity is used as a marker to monitor its progression through the gastric system using EIT. Difficulties in attaining high contrast measurements using EIT have been overcome by the use of markers in the

form of meals which are highly conductive in comparison to the gastric wall which is typically lower in conductivity. To avoid a further increase in gastric conductivity caused by acid release during digestion, drugs such as cimetidine have been used to suppress gastric acid release (Avill et al., 1987, Brown, 2003).
Baxter and Mangnall (1988) explored the effects of hydrochloric acid on gastric resistivity changes and found resistivity values related to changes in acid concentration and volume. The ability of using EIT as a method of recording peristaltic waves of the stomach wall during digestion has also been explored (Smallwood et al., 1994). Erol and Cherian (Erol et al., 1996b) used EIT to detect gastro-oesophageal reflux due to a change in pH. They attributed the large conductivity changes observed during reflux-free periods to gastric motility.

1.2.4 Breast Cancer Screening using EIT

EIT has undergone extensive research as a clinical imaging modality to screen for breast cancer due to its advantages compared to the currently used screening method: X-ray mammography.
Conventional breast cancer screening using X-ray mammography exposes the patient to harmful ionising radiation which itself increases the risk of cancer. In order to visualise maximum tissue area, compression of the breast is required which can be an uncomfortable, and sometimes a painful experience dependent on breast tissue density (Bayford, 2006). EIT is a completely non-invasive method of imaging and is therefore suitable for repetitive use if necessary as the patient isn't exposed to ionising radiation. EIT eliminates the requirement for an expensive screening facility and is therefore a more cost-effective solution. In terms of patient experience, the use of EIT would also eliminate the need for compression of the breast during a screening test and therefore improve patient experience.
Studies employing the use of EIT have successfully shown that breast cancer cells conduct injected current differently to healthy tissue as cancerous tissue has been shown to exhibit increased electrical conductivity compared to healthy tissue (Surowiec et al., 1988).

Jossinet utilised multiple frequency EIT measurements (impedance spectroscopy) to group excised breast tissue into anatomical and pathological categories using over 100 different impedivity spectra (Jossinet, 1998). Results from this trial suggested impedance spectroscopy can identify cancerous breast tissue and even distinguish its pathology from benign tumour tissue. In a later study, Gersing and Eberhard, (1999) monitored the effects of temperature on tissue properties and provided further evidence to support the use of EIT in differentiating between excised healthy and cancerous tissue. Significant contrasts were observed between the healthy and cancerous tissue in response to an increase in temperature, which was attributed to cancerous tissue lacking haemodynamic regulation in response to an increase in temperature (hyperthermia).

Despite evidence supporting the use of EIT for potential identification and characterisation of cancerous breast tissue, the difficulties in accurately capturing breast shape have somewhat limited the technique being adopted for clinical breast cancer screening. None of the existing EIT techniques used to date have accurately been able to capture breast shape. Most EIT systems operate by measuring the relative impedance change from a baseline measurement; allowing two physiological conditions to be compared. Images generated from these measurements are known as 'difference images.' Difference imaging reduces inaccuracies resulting from individual breast shape differences, and instrumentation errors can be easily identified and eliminated (Bayford, 2006). However, for the purpose of clinically diagnosing breast cancer, difference imaging is an unsuitable method of data capture as it is unfeasible to capture baseline data for the comparison of cancerous tissue. In these circumstances absolute imaging is required where an image of the absolute conductivity is used to construct an image without a reference voltage measurement. Although this method of imaging provides enhanced information regarding tissue conductivity, instrumentation effects such as electrode contact impedance cannot be accurately eliminated from measurements and therefore potential sources of error can be introduced. As a result, inconsistencies between available reconstruction models and measured data have been observed due to individual shape differences. However, inaccuracies using absolute imaging methods must be overcome for reliable results despite individual differences in breast shape and size.

The use of X-ray mammography is limited for younger women due to the technique showing greater sensitivity in older women and in breast tissue which is less dense (Carney et al., 2003). Within the UK, breast cancer is the most common cancer affecting women (Cancer Research UK, 2014), therefore early diagnosis is imperative for effective treatment. In theory, the use of EIT as a clinical imaging technique for breast cancer screening has various benefits outweighing current screening methods used. Compared to X-ray mammography, clinical EIT screening would be suitable for younger patients with no contraindications for pregnant or lactating women.

Despite the benefits however, there are concerns regarding accuracies in EIT reconstructions which have been highlighted. In addition, as benign tumours develop from constituents of healthy breast tissue, EIT cannot be used for the identification of benign tumours (Raneta et al., 2012).

EIT has recently been used in conjunction with traditional X-ray mammography to overcome the difficulties of image reconstruction due to individual shape errors (Choi et al., 2007). Combining EIT measurements with anatomically detailed images from MRI or CT scans have been used to minimise sources of error gained from absolute imaging techniques (Prasad et al., 2008). Although this seems like a practical solution to accurately capture individual breast dimensions for the use of absolute imaging, combining EIT with an expensive imaging modality would significantly increase costs and would still require transfer of the patient to a scanning facility. A more recent approach to minimise individual shape errors has been proposed (Forsyth et al., 2011) by the use of a hand held 3D scanning device to form an accurate 3D image of the breast. This application could eliminate the need to transport the patient to a scanning facility. Although image reconstructions of subjects are yet to be completed, the method proposes to minimise large sources of error caused by individual variability in breast shape and size.

A study conducted by Renata, Ondrus et al., (2012) compared the feasibility of using EIT in breast cancer diagnosis compared to the screening gold standard: X-ray mammography. In a study consisting of 808 patients, the sensitivity and specificity of X-ray mammography exceeded that of EIT. The incidence of false positives was also shown to be higher when using EIT compared to X-ray mammography. These

results have demonstrated that EIT in its current state of development cannot replace X-ray mammography for clinical screening of breast cancer until limitations providing accurate information on breast tissue structure have improved. However, the authors acknowledged the clinical potential of EIT to monitor physiological changes within breast tissue and suggested its use as an adjunct to current methods used for diagnosis, rather than a replacement.

1.3 Rheoencephalography (REG)

Electrical impedance measurements from peripheral areas of the body have demonstrated changes in conductivity relating to pulsatile blood flow, more commonly known as 'plethysmography.' The technique of plethysmography has specifically been used for monitoring changes in cerebral blood flow (CBF) and was first reported by Polzer and Schuhfried who measured pulsatile changes in impedance from a patient undergoing occlusion of a single carotid artery supplying the brain. The conductivity changes captured by surface electrodes applied to the head were related to CBF (Polzer and Schuhfried, 1950).

The term 'rheoencephalography' (REG) was coined by Jenkner in 1957 (Jenkner, 1957) to describe changes in CBF relating to the cardiac cycle and measured using surface electrodes to capture the impedance pulse waveform. The motivation for monitoring changes in CBF is clinically relevant following severe head trauma or relating to pathologies such as tumours and haematomas within the brain where CBF may be compromised due to brain swelling. In such cases, continuous bedside monitoring of CBF could provide important and rapid information to aid clinical intervention (Perez, 2014).

Despite various trials conducted since REG was originally described, the exact description of REG in terms of physiological function has yet to be clearly defined due to difficulties in solely measuring intracranial CBF without contamination from the external carotid circulation. As a result, the role of REG within diagnostic medicine as a reliable measure for cerebrovascular disease and CBF has undergone considerable debate.

Perez-Borja and Meyer (1964) measured REG from patients with known cases of cerebrovascular disease and compared these results to healthy subjects. An excitation frequency of 30kHz was injected across the head. The aim of their study was to evaluate the use of REG in clinically monitoring CBF changes to aid the diagnosis of cerebrovascular disease. During data acquisition, various manoeuvres known to influence CBF were performed such as compression of the carotid & jugular arteries and hyperventilation. A pressure cuff was also inflated around the head (below the level of surface electrodes attached to the head) in order to restrict carotid circulation. Results from this study showed considerable variations between recorded REG waveforms from each subject group, and also within the two subject groups. The authors reported difficulties in accurately identifying subjects who were diagnosed with cerebrovascular disease from healthy subjects using their REG waveforms. Use of the pressure cuff demonstrated that the REG waveform is considerably contaminated by external carotid circulation. Perez-Borja and Meyer concluded that the REG waveform doesn't exclusively reflect cerebral circulation and therefore REG could be a potentially misleading clinical measure to diagnose cerebrovascular disease. These findings were further supported by a similar study undertaken by Masucci et al., (1970).

Subsequent studies provided further evidence demonstrating how REG cannot be used as a reliable measure of intra-cranial CBF. In a study undertaken by Laitinen (1968), intra-cerebral impedance measured using invasive electrodes with an excitation frequency of 10kHz, showed significant variations when compared to REG traces recorded externally from the scalp; once more demonstrating the presence of extra-cranial carotid circulation on REG waveforms. These results were further supported by selective extra-cranial impedance traces which were shown to have temporal similarities to the REG (Laitinen, 1968).

The clinical value of REG capturing changes in CBF was reported in later studies undertaken in neonates where trends in REG were related to neuromotor outcomes. Gronlund, Kero et al., (1995) showed low pulsatile variability measured using electrical impedance from neonates and preterm babies correlated with abnormal neuromotor outcome at one year of age. A subsequent study carried out by the same group quantified tilt-induced changes in CBF measured by impedance from

premature infants (Gronlund et al., 1997). Results from the latter study correlated with previous findings from posture-dependent changes in middle cerebral artery blood flow velocity measured using Doppler ultrasonography (Anthony et al., 1993). It should be noted however, that these studies were undertaken in neonates; differences in skull, scalp and CSF resistivity between adults and neonates will affect impedance measurements recorded at the scalp (Gibson et al., 2000). Following years of conflicting evidence reported for REG, research into this technology continues due to the clinical benefits of a bed side monitor suitable for non-invasive and continuous evaluation of CBF.

For the majority of studies involving adult subjects, it has been established that the externally derived REG signal is contaminated by extra-cranial circulation. One particular study undertaken by Basano, Ottonello et al., (2001) aimed to evaluate the use of REG to monitor cerebral perfusion and therefore aid the diagnosis of brain death. The study measured REG data from mechanically ventilated and cerebrally dead patients. Surprisingly, when these data were compared to live subject data, the authors found the REG signals from both groups to be temporally comparable. The pulsatile waveform recorded from clinically brain dead subjects was attributed to residual extra-cranial blood flow through the scalp which was shown to be synchronous with the cardiac cycle prior to blood flow arrest (Basano et al., 2001). Subsequent research has explored the use of theoretical models to evaluate the various conductive layers of the head and the effect they have on impedance measurements relating to CBF and extra-cranial blood flow. The use of an optimal electrode arrangement to eliminate extra-cranial circulation from the REG has been suggested. Other factors such as scalp thickness, temperature and skull resistivity have also been explored for reliable monitoring of intra-cranial circulation (Perez et al., 2004).

A recent study has aimed to decompose the REG signal into intra- and extra-cranial components by applying an inflatable cuff around the head to avert extra-cranial circulation during REG measurements (Perez, 2014). This study utilised an injection frequency of 32kHz. Perez (2014) reported significant differences between waveforms representing intra- and extra-cranial blood flow. Plethysmographical measurements taken before and during cuff inflation to arrest extra-cranial blood

flow to scalp also demonstrated differences in waveforms derived from intra- and extra-cranial sources. Perez (2014) described the catenary waveform captured during cuff-inflation likely to be a representation of REG describing intra-cranial perfusion, whereas extra-cranial blood flow captured prior to cuff inflation was manifest as a saw-tooth waveform; a familiar sight in many REG reporting literature (Figure 1.3).

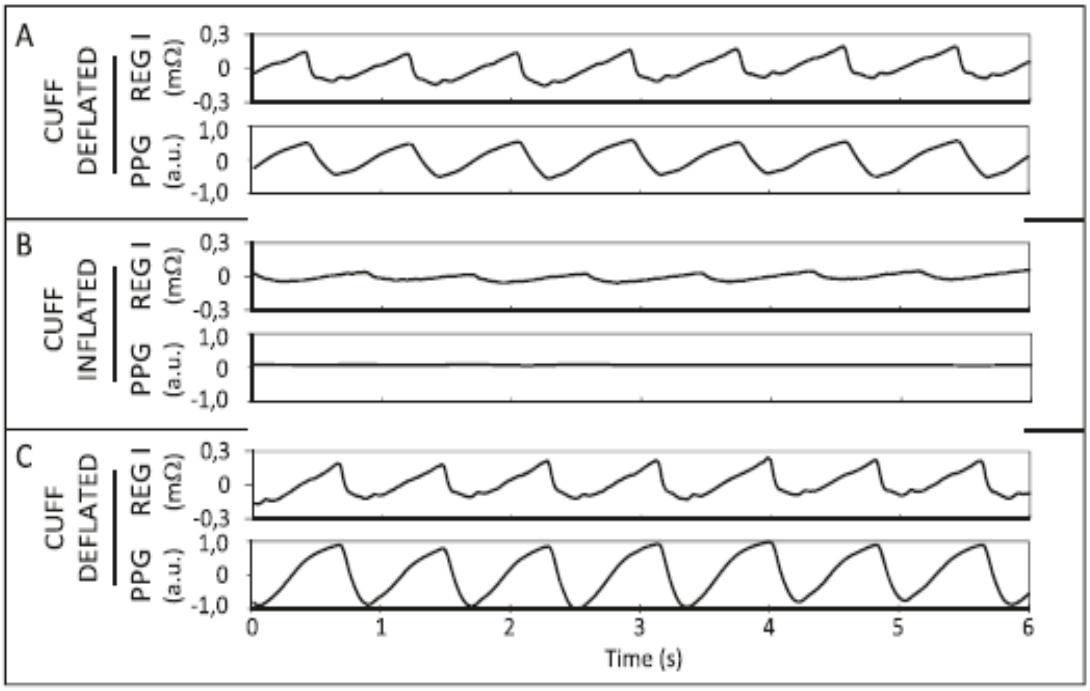

Figure 1.3 REG traces captured from the head. Plethysmographical signals captured from a single subject **(A)** before, **(B)** during and **(C)** following cuff inflation. REG signals are represented in the top trace in all three recording conditions. Figure taken from Perez (2014) (Perez, 2014).

The prospect of non-invasively measuring cerebral haemodynamics using a portable impedance device has motivated a vast amount of research undertaken to clearly define the REG signal. More recent research has aimed to decompose the REG signal to identify differences between intra- and extra-cranial haemodynamics. Although distinguishing results have been reported, intra-cranial CBF measured using REG has not undergone further isolation from other pulsatile dynamics occurring within the brain such as CSF movement.

Research conducted thus far has highlighted the importance of effective source separation of the REG signal for it to be used as a clinically useful physiological signal.

1.4 Exploring Functional Brain Activity using EIT

One of the most successful applications of EIT has been imaging ventilation of the lungs as discussed in section 1.2.2 of this thesis. Changes amounting to tens of percent have been recorded in boundary voltage measurements captured from the thorax during ventilation (Frerichs, 2000). Although image quality is compromised due to electrode positioning and limited prior information of lung position within individuals, low spatial resolution images generated using EIT can be used to identify anatomical areas and regional lung function with some confidence as the underlying physiology and anatomy of ventilation is well understood.

In contrast, EIT of the brain poses a unique technical challenge. Measurable changes in impedance and conductivity within the brain are caused by various physiological mechanisms. CBF and the osmotic movement of water into the extracellular space are categorised as slow changes occurring over several seconds. Whereas, the movement of ions across a cell membrane during neuronal depolarisation has a temporal resolution of several ms and is therefore categorised as a fast functional change occurring in the brain (Bayford, 2006, Holder, 2005). For an EIT system to capture functional activity of the brain, sufficient current must first be able to enter the brain by penetrating several protective layers. Firstly, the scalp is a moderately resistant tissue for injected current to penetrate through which can be aided by appropriate surface electrode contact. Secondly, the injected current will encounter the highly resistant pia matter and the skull; both tissues divert the injected current and prevent it from entering the brain (Holder and Tidswell, 2005). Finally, prior to reaching actual brain tissue, injected current must pass through the conductive CSF fluid.

Once boundary voltage measurements have been captured, the second challenge involves accurately identifying anatomy and physiological function within the brain

using high resolution imaging. Unlike ventilation, the anatomical location of functional neural processing within the brain is less clearly understood.

Research conducted over the past 2 decades has aimed to investigate and overcome the technical challenges of monitoring functional activity within the brain using EIT. A research group based at UCL has pioneered the use of EIT for functional brain imaging to investigate its clinical accuracy in identifying epileptic seizures, stroke and fast evoked responses.

According to the dielectric properties of biological tissues discussed in section 1.6.1, EIT can be used to explore physiological functions occurring in the brain. The path of a low frequency current (<100Hz) injected into the brain will be constrained to the extracellular space, blood volume and low-resistivity glial cells which are conductive to chloride and potassium ions (Gilad et al., 2007). During neuronal depolarisation, resistance of the neuronal membranes becomes less resistant to current flow therefore allowing it to enter the intracellular space. At higher injection frequencies (>40kHz), applied current is able to pass across the cell membrane capacitance and enter the intracellular space (Gilad et al., 2009).

Multi-frequency EIT systems are able to characterise tissue properties by utilising a range of current injection frequencies. By varying the frequency of current injections, a range of physiological mechanisms can be evaluated including metabolic and blood flow changes occurring in the extracellular space as well as intracellular activity caused by cell swelling and ionic movement across cell membranes. Low frequency measurements (current injections below 100Hz) are typically used to explore the extracellular properties of tissues such as shape and volume; as the cell membrane impedes low frequency current flow. High frequency current injections are able to penetrate the cell membrane and therefore these measurements are employed to investigate impedance changes occurring within the intracellular space.

Standard EIT involves capturing a change in voltage measured over time and therefore requires a baseline measurement to compare the recorded changes. Multi-frequency EIT offers an advantage over standard EIT as tissues are differentiated based on their conductivity properties to the frequency spectra applied, therefore eliminating the need for a baseline measurement. The use of multi-frequency EIT has

been of particular interest for diagnostic purposes specifically applied to distinguishing stroke type (Romsauerova et al., 2006b).

Compared to the changes captured from the thorax during ventilation, the amplitude of changes reported from EIT measurements of the brain have been much smaller. Cortical changes of approximately 5% were captured from the exposed cortices of anaesthetised rabbits during evoked responses using EIT at frequencies of 50 kHz. The changes were attributed to an increase in blood flow at the cortex following evoked activity. During an induced epileptic seizure, cortical changes of ~10% have been measured using EIT (Rao et al., 1997) which have been attributed to cell swelling. Induced stroke in anaesthetised rats caused impedance changes of over 100% measured using cortical electrodes (Holder, 1992b). These results captured from the exposed cortical surface have been translated following consideration of volume and conduction effects, to an estimated change between ~0.1% and 0.004% if recorded from the scalp surface using EIT injecting low frequency currents (below 100 Hz). This estimated change has been identified using anatomically realistic head models (Fabrizi et al., 2007, Holder and Tidswell, 2005, Gilad and Holder, 2009b). EIT systems utilised for human trials have been reported to be sensitive enough to capture the small impedance changes recorded using scalp electrodes to reflect functional activity in the human brain. During evoked visual activity in the brain, Gilad and Holder (2009b) reported changes of 0.001%; although slightly lower than the estimated changes predicted by modeling studies, the authors concluded these findings to be physiologically plausible as a reflection of visual evoked activity within the brain. The study was undertaken with the aim of imaging fast neuronal activity in the brain. However, results yielded changes which were too small to produce reliable images representing functional brain activity due to a poor signal-to-noise ratio caused by simultaneous EEG recordings.

Research conducted to date has explored the potential clinical use of EIT for imaging functional brain activity to diagnose cerebral incidents, map evoked responses and locate epileptic foci (Boone et al., 1994, Romsauerova et al., 2006b, Tidswell et al., 2001b). Studies conducted thus far have also highlighted important technical requirements to non-invasively capture functional brain activity using surface electrodes. Clinical studies undertaken on human subjects have reported changes

relating to physiological activity within the brain when evaluating raw EIT data. However, the production of tomographic images has been limited due to the small changes captured from the scalp in comparison to large levels of noise, resulting in a low signal-to-noise ratio.

1.4.1 Imaging the Brain using EIT

Forming a tomographic image using EIT is based on the principle of current flow through a volume conductor. The resulting volume distribution is a function of the conductivity distribution within the volume conductor. An EIT device operates by injecting a series of currents and measuring the voltage profiles from the periphery of the object to be imaged. A tomographic image representing internal conductivity distribution is produced using numerical reconstruction algorithms.

Reconstruction algorithms of EIT measurements consist of mathematical solutions to a forward and inverse problem. The forward problem can be defined as calculating boundary voltage and current values from known conductivity distributions within the area/tissue to be imaged. A mathematical model of the particular area to be imaged is often employed to solve the forward problem consisting of tetrahedral, volumetric elements which are coded for the conductivity of the various tissue types found in the subject. The model also accounts for spatial resolution dependent on the number and array of electrodes applied.

The main problem encountered in the EIT reconstruction processes is that the internal conductivity distribution is unknown and therefore the forward problem cannot be solved. In order to accurately image internal conductivity distributions of an object, boundary voltage data acquired by an EIT system must undergo simultaneous algorithms before the forward problem can be solved. This is known as the inverse problem which can be solved by *a priori* (theoretically deduced) information regarding the object or tissue to be imaged (Lionheart et al., 2005, Eyuboglu et al., 1989).

The inverse problem is solved by relating the externally recorded boundary voltage measurements to volumetric elements of the sensitivity matrix, and calculating internal conductivity distributions in order to solve the forward problem.

Reconstruction algorithms originally employed to image the brain utilised a head model resembling a sphere (Holder, 1992a, Towers et al., 2000, Boone et al., 1994) which is more commonly referred to as a finite element model (FEM) or boundary element model (BEM). Over the past two decades, head models have greatly improved in their geometric shape and conductivities of tissue properties to more closely resemble a generic human head. Models such as the University College London (UCL) head model which has been extensively used for reconstructions in research groups developing EIT for brain imaging, have been adapted to consider extracerebral layers of the head and increase precision in terms of geometrical shape (McCann et al., 2011). Reconstruction tools such as Electrical Impedance and Diffuse Optical Reconstruction Software (EIDORS), an online application developed at the University of Manchester, have supported the generation of accurate forward models for 2D and 3D image reconstructions (Adler and Lionheart, 2006, Lionheart, 2004).

Although the type and range of EIT reconstruction methods and algorithms adopted to date are beyond the scope of this introduction, the challenges of developing an accurate reconstruction method is a priority to establish EIT as a reliable imaging modality. Researchers have expressed the need for an optimised model calculation to eliminate errors and artefacts caused by individual geometrical differences in head shape (McCann et al., 2011). Prior knowledge of domain shape is an important requirement for accurate EIT reconstruction, particularly for absolute image reconstruction.

Until now, clinical images produced from boundary voltage measurements have assumed a linear solution to the inverse problem. Although simulated measurements of clinical tissues using tanks and phantoms produce accurate reconstructions using linear solutions to the inverse problem, clinical EIT measurements are highly dynamic and non-linear. Firstly, contact impedance between the electrode surface and tissue produces a base line drift which has to be removed and normalised prior to reconstructing meaningful changes measured by EIT. Secondly, the geometry of organs such as the lungs and gastric tissues undergo alterations in shape and size with physiological function such as respiration and gastric motility, which can introduce errors and motion artefacts in captured EIT data. Clinical EIT

measurements are highly non-linear as changes in tissue impedance do not result in linear changes in recorded voltage measurements at the surface (Bayford, 2006). Unlike an X-ray beam which proceeds linearly through the subject, an injected electrical current does not take a linear path due to differences in resistance within the body caused by medium such as blood or bone.

Nevertheless, clinically useful EIT reconstructions of the lungs have been presented by applying linear solutions similar to those employed in CT back-projection methods. Despite EIT measurements being non-linear, the relationship between changes in measured conductivity and lung volume during respiration has been established as linear since the 1980s, and has amplified the successful clinical application of EIT to monitor regional lung volume at the bedside (Harris et al., 1987). Some of the first clinical images of the lungs were presented using this reconstruction method (Brown and Barber, 1987).

Linear solutions have successfully been applied to localise evoked responses in the human brain using difference imaging between a baseline and stimulation condition (Tidswell et al., 2001b). The application of EIT to image the brain within an emergency or critical care environment has motivated a large amount of research with the aim of using EIT to rapidly diagnose the incidence of acute stroke and brain injury.

Within the realms of diagnosing stroke, the use of multi-frequency EIT has been explored as a tool to identify the type of stroke by differentiating between the incidence of haemorrhagic and ischaemic stroke. As multi-frequency EIT explores tissue properties using a conductivity spectrum, it has been suggested that an ischaemic area of the brain could be distinguished from the presence of blood in the incidence of a haemorrhagic stroke using a multi-frequency EIT system (McEwan et al., 2006). The application of EIT as a portable tool to rapidly identify stroke type would be clinically significant, as each type requires different avenues of treatment therefore, rapid diagnosis would ensure rapid treatment.

Difference imaging can avoid instrumentation errors due to measurements being taken in the same individual during two physiological states. However, for a clinical application of imaging stroke or brain injury using EIT, absolute imaging would be

essential to make a diagnosis, as a baseline measurement taken prior to the presented pathology would not be possible.

EIT data typically produces images which are poor in spatial resolution. This can be worsened by potential sources of error caused by instrumentation and inaccuracies in electrode placement. To reduce the effects of instrumentation errors on absolute EIT data, a frequency-difference method is often employed when using a multi-frequency EIT technique which is used to reconstruct images of conductivity differences between two applied frequencies (Ahn et al., 2010). However, the use of multi-frequency EIT is highly sensitive to modeling and instrumentation errors. In addition, bio-impedance of tissues also changes slowly with frequency (McEwan et al., 2007). Until now, linear solutions applied to frequency-difference EIT data with the aim of diagnosing brain injury or acute stroke in the human brain has been ineffective (Packham et al., 2012) further highlighting the requirement for non-linear solutions to reconstruct frequency-difference EIT data.

A recent publication has introduced a non-linear reconstruction method known as fraction reconstruction (Malone et al., 2014c) and phantom studies have assessed its use in reliably reconstructing images of the brain using frequency-difference EIT techniques. Potential sources of error when using fraction reconstruction have also recently been explored with the aim of using multi-frequency EIT to differentiate haemorrhagic stroke from ischaemic stroke. The study was conducted using a head shaped phantom and considered homogenous layers representing the brain, skull and scalp whilst also discussing the numerous sources of error (Malone et al., 2014a). Firstly, the presence of the skull limits a uniform distribution of current density throughout the brain resulting in a disparity of measurements, as areas with the highest current density (closest to the surface) will contribute most to measurements captured. The amplitude of current which can be injected by EIT systems is restricted to safety standards therefore an injected current of small amplitude will result in a recorded voltage measurement of even smaller amplitude. For accurate tomographic imaging, electrode positioning must be accurately represented for individual subjects. The use of a generic head model limits electrode representation. Skin to electrode contact impedance and stray capacitance also affect the signal-to-noise ratio. Malone, Jehl et al., (2014a) performed a simulation study using multi-frequency EIT to

investigate the effects of the modeling errors described to differentiate between simulated ischaemic and haemorrhagic stroke. The two pathologies were simulated using a perturbation placed in known positions within the head model. To simulate an ischaemic stroke, conductivity of the perturbation was set to the conductivity of the ischaemic brain.
Likewise, for simulation of the haemorrhagic stroke, conductivity of the perturbation was set to conductivity of blood. The following modeling errors were introduced:

(1) electrode positioning
(2) tissue conductivity
(3) contact impedance

Fraction reconstruction was performed to image the phantom under each error condition to determine whether or not simulated stroke type could be differentiated and whether or not these errors affected known positions of the perturbation. Results from this study demonstrated that electrode positioning severely affected image quality emphasising the importance of accurately recording electrode positions when reconstructing EIT data. Erroneous tissue spectra were also shown to affect the ability to distinguish between stroke types as the fraction reconstruction method assumes all known conductivities as being exact. For an error of 5% introduced into conductivity spectra, it was not possible to locate simulated haemorrhagic stroke and ischemic stroke could only be identified in a limited location. The overlapping conductivities for the tissue spectra at the applied frequencies caused difficulties in identifying healthy brain tissue from ischaemic tissue. The authors reported limited effects of erroneous contact impedances on image quality. Results from this study highlighted that a non-linear reconstruction method such as fraction-reconstruction, can potentially be applied to frequency-difference EIT data to differentiate stroke type. Results also emphasised the importance of accurate electrode placement on the head and how erroneous electrode positioning may lead to ambiguous results. Although the method has yet to be applied to human data, improvements in reconstruction methods applied to imaging the brain are bringing the technology of EIT one step closer to clinically useful applications within the field of neuroscience.

1.4.2 EIT Brain Imaging Systems: Sheffield

One of the first EIT systems to be developed was pioneered at Sheffield named the Mk1. Clinical EIT measurements of the lungs were recorded using this system and gave rise to the first images using EIT (Brown and Barber, 1987). Subsequent EIT machines produced since have been based on the Mk1 with various modifications to the number of electrodes applied, the current drive design and the frequency of current injected.

The main objective of EIT is to maximise current density within the chosen tissue (determined largely by the current drive design) in order to maximise sensitivity of the impedance measurements recorded in response to physiological changes in the tissue. The two main types of current drive designs to have been adopted in EIT systems to date are the adjacent and the current pattern drives. The former involves injecting current between two adjacent electrodes and resulting impedance measurements are recorded from other non-injecting electrodes around the tissue. Whereas, the latter (a current pattern drive) involves simultaneous current injections between different combinations of electrode pairs around the tissue. Similarly, resulting impedance measurements are recorded from all other non-injecting electrode pairs (Bayford, 2006, Brown, 2003).

The original Mk1 device operated using 16 surface electrodes with an adjacent current application design using an injection frequency of 50kHz. The system produced 2D difference images from a reference data set. Following development of the Mk1, the Mk2 system was also produced at Sheffield based on the former Mk1 design. However, unlike Mk1, the Mk2 system utilised a lower current injection frequency of 20kHz. The Mk2 was developed to monitor ventilatory and cardiac related changes in the lungs of 10 human subjects (Leathard et al., 1994). Despite poor spatial resolution, measurements with this system recorded large resistivity changes relating to pulmonary emboli.

The Mk3 system incorporated a revolutionary modification, in that it was the first system to be developed at Sheffield which employed a multi-frequency current injection pattern using eight different injection frequencies ranging between 9.6kHz and 1.2MHz. Injecting current at different frequencies allows the characterisation of

tissues related to an impedance spectrum. This system was utilised to monitor changes in impedance relating to ventilatory and fluid changes in the lung tissue of adults and neonates (Smallwood et al., 1999). The modified Mk3 system used 16 surface electrodes to inject an interleaved current design unlike previous systems which used adjacent drive patterns. This modification was made to avoid using multiplexers when alternating between current drive and measurement modes of electrodes. Compared to previous EIT systems, this modification also improved signal to noise ratio reported to be at 55dB. However, image reconstructions and measurements made at higher frequencies were problematic due to a poor signal to noise ratio which was reported to decrease as current injection frequency increased (Lu, 1995).

The latest system to be developed at Sheffield is the Mk3.5 system which is also a multi-frequency system similar to the Mk3. The Mk3.5 measures impedance using 8 surface electrodes at 30 different current injection frequencies (ranging from 2 kHz to 1.6 MHz) at a rate of 25 frames per second (fps). Similar to an earlier system developed at Sheffield, the Mk3.5 also injects current using an adjacent drive design. Although signal-to-noise ratio was reported to be lower than the previous system, the ratio was unaffected by a change in current injection frequency (Wilson et al., 2001). A summary of EIT systems developed at Sheffield is provided in Table 1.2.

Table 1.2 Sheffield EIT systems. A summary of Sheffield EIT systems produced and modifications to date.

System name	Number of electrodes	Injection pattern	Injection frequency
Mk1	16	adjacent	50 kHz
Mk2	16	adjacent	20 kHz
Mk3	16	interleaved	9.6 kHz - 1.2 MHz
Mk3.5	8	adjacent	2 kHz - 1.6 MHz

1.4.3 EIT Brain Imaging Systems: UCLH

A group based at University College London Hospitals (UCLH) developed one of the first EIT systems to image brain function in human subjects during epileptic seizures. The UCLH Mk1a is a multi-frequency system that operates using 16 electrodes to inject a single current injection frequency between 50Hz and 50kHz. Compared to adjacent current injection systems, the UCLH Mk1a utilises a diametrically opposed current injection design shown to reduce distortions and improve sensitivity of the reconstruction process (Bayford et al., 1996, Boone and Holder, 1996). Initial studies using the UCLH Mk1a were performed on saline filled cylindrical tanks containing perturbations of known impedance values. The portable Mk 1a system was designed to be used on ambulant human subjects at low frequencies to measure large impedance changes in the brain during epileptic seizures. Within the brain, an epileptic seizure results in the movement of water from the extracellular space into the intracellular space due to the influx of sodium and chloride ions causing an osmotic gradient (Boone et al., 1994). Initial tank studies conducted with this system utilised current injection frequencies as low as 1800Hz with the view that injected current will be completely constrained to the extracellular space in order for a greater change in impedance to be captured. If injected current is able to pass through the extracellular space and enter the intracellular space then the

movement of water from one medium to the other will ultimately result in no impedance change being captured. Results from the initial tank study showed acceptable images could be reconstructed using current frequencies as low as 1800Hz (Holder et al., 1999). Although the UCLH Mk1a demonstrated a low signal to noise ratio with acceptable images, the authors acknowledged that the low frequency measurements made on a saline tank could not simulate measurements from a human head due to the effects of high skin impedances using scalp electrodes. The UCLH Mk1a system was subsequently modified to be used with 64 electrodes and was named the UCLH Mk1b. This system also operated using diametric injections of low frequency current within a similar range to the previous Mk1a system (225Hz-77kHz). Although a multi-frequency system, the UCLH Mk1b was designed to operate at a single selectable frequency. Performance of the Mk1b system was evaluated in a trial using saline filled tanks containing a human skull. Images produced from this trial were deemed acceptable at lower frequencies and signal to noise ratio was also comparable to the most recent Sheffield EIT system (Mk3.5). However, similar to the first multi-frequency system developed at Sheffield (Mk 3), signal to noise ratio in the UCLH system altered with the frequency applied (Yerworth et al., 2002).

The UCLH Mk2 was developed as a hybrid system containing features from the Sheffield Mk3.5 and UCLH Mk1b systems. The UCLH Mk2 operates using a diametric current injection design between frequencies of 2kHz and 1.6MHz. Similar to the Sheffield Mk3.5 machine, Mk2 also measures impedance using multiple frequencies. Unlike the Sheffield system however, the UCLH Mk2 was designed to measure impedance at different current injection frequencies within a single time point, potentially allowing spectroscopic imaging of functional activity within the brain. Reasons for this modification were made with a view to use the system for diagnosing conditions such as stroke and traumatic brain injury where absolute imaging is required. However, due to instrumentation artefacts existing with this type of imaging, a difference imaging technique was proposed using the UCLH Mk2 where the differences between simultaneous measurements taken at various frequencies can be reconstructed, also known as EIT spectroscopy (EITS) (Yerworth et al., 2002). The UCLH Mk2 can measure impedance using up to 64 electrodes

allowing an increased spatial resolution. Yerworth, Bayford et al., (2002) compared performances of the UCHL Mk2, the Sheffield Mk3.5 and the UCLH Mk1b using impedance measurements taken from saline filled tanks containing test objects. The authors concluded that the increased number of electrodes adopted for the UCLH Mk2 system produced clearer resolution images although overall performance of the system was not as good as the Sheffield Mk 3.5 (Yerworth et al., 2003).

The multi-frequency UCLH Mk2 has since been utilised in human subjects to determine whether a suitable frequency range would distinguish between types of cerebral incidents. As a clinical tool, the authors suggested that multi-frequency EIT systems could provide rapid identification between an ischaemic and haemorrhagic stroke allowing urgent administration of thrombolytic drugs in patients suffering an ischaemic stroke (Romsauerova et al., 2006b). The trial was conducted in 3 patient groups exhibiting brain tumours, arteriovenous malformations and chronic stroke using a multi-frequency current injection range of 4kHz to 128kHz. The purpose of this work was to ascertain if the Mk2 was capable of identifying pathology in the stated patient groups using expected impedance values relating to the pathology. For example, brain tumours have a larger extracellular space, arteriovenous malformations cause an increase in blood volume and chronic stroke causes brain tissue to be replaced by highly conductive CSF. Raw data and images captured across the applied frequency range were evaluated for differences between pathological and normal brain regions for all three patient groups. Their results showed no reproducible differences between established pathologies and normal brain regions for the patient groups. The negative findings were attributed to instrumentation variability caused by the system operating across a range of applied frequencies resulting in greater changes due to instrumentation, compared to expected physiological changes.

Further modifications in EIT hardware have led to the development of the most recent system reported by UCLH: the UCLH Mk2.5. Modifications include an extended frequency spectrum to a lower limit of 20Hz (despite previous research suggesting injection frequencies above 10kHz should be used), and a more compact system designed to be worn on the head; shorter electrode wire length has been included to minimise stray capacitance (McEwan et al., 2006). Although human

studies have yet to be undertaken using this system, calibration studies carried out on tank tests have demonstrated its potential clinical use to non-invasively image and diagnose the incidence of acute stroke (Yerworth et al., 2003, McEwan et al., 2006). The potential application of EIT for neural imaging has been demonstrated at UCLH in a study undertaken by Gilad and Holder (2009b) where resistance changes caused by neuronal depolarisation in response to visual stimulation were recorded from human subjects. Resistance changes were recorded from the scalp overlying the occipital cortex using a low current injection frequency of 1Hz. From a total of 20 EIT recordings, significant changes were captured in 7 recordings according to the time course of a neural visual response. Although images could not be obtained due to a poor signal to noise ratio, the study demonstrated for the first time that EIT could successfully be used to capture sub-second neural responses from the scalp. A summary of EIT systems developed at UCLH is provided in Table 1.3.

Table 1.3 UCL EIT systems. A summary of UCL EIT systems produced and modifications in design.

System name	Number of electrodes	Injection pattern	Injection frequency
Mk 1a	16	diametric	50 Hz - 50 kHz
Mk 1b	64	diametric	225 Hz - 77 kHz
Mk 2	64	diametric	2 kHz - 1.6 MHz
Mk 2.5	64	diametric	20 Hz - 256 kHz

1.5 Functional EIT with Evoked Response (fEITER)

fEITER is a portable device developed at the University of Manchester with the aim of imaging functional activity within the brain (Figure 1.4). The system uses scalp electrodes to diametrically inject a randomised current pattern at 10kHz, coupled to a 10ms (100 fps) sampling rate.

An injection frequency of 10kHz falls within the boundaries of beta dispersion according to the bioimpedance properties of biological tissues discussed in section 1.6.1. Therefore, due to injected current at 10kHz being able to cross the lipid cell membrane, measurements at these frequencies will be sensitive to intracellular changes of neurons caused by synaptic activity and the influx/efflux of conductive ions. Therefore, regardless of a neurotransmitter mediating an inhibitory or excitatory response, intracellular conductivity will increase following opening of ion channels during neuronal depolarisation resulting in an impedance change.

The sub-second temporal resolution of fEITER is commensurate with neural processing activity. This feature supports the purpose of fEITER to investigate fast neural activity within the brain. Furthermore, the diametrically opposed current injection pattern avoids current being diverted across the skull and maximises current density within the brain improving sensitivity of conductivity changes occurring globally within the brain (Murphy et al., 1987, Yerworth et al., 2002, Bayford et al., 1996).

An earlier version of fEITER known as fEIT utilised 16 electrodes and a current injecting frequency of 9.6kHz (Towers et al., 2000). This system was used on human subjects to monitor areas of the brain activated in response to the presentation of sensory stimuli (Murrieta-Lee et al., 2004). Reconstructed images produced from this trial showed changes in conductivity relating to areas of the visual cortex (V1 to V4) in response to repetitive visual stimulation. The authors concluded that the rapid conductivity changes observed were due to functional changes occurring at the synaptic junction of visual neurons within the visual cortex, demonstrating the ability of fEIT to monitor sub-second functional activity within the brain relating to synaptic activity (McCann et al., 2006).

The present fEITER system is based on fEIT and comprises an additional feature of evoked response (ER). The ER component of the system was developed with the aim of capturing functional evoked responses from the brain. In addition, the ER could also be used to trigger an evoked potential by presenting sensory stimuli time-locked to specific features of a simultaneously recorded ECG such as the R-wave.

fEITER consists of two separate sub-system assemblies which form the base unit shown in Figure 1.4. The first assembly forms the EIT sub-system which drives current injection and measurement sequences to the headbox. The second sub-system forms the stimulus sequencing assembly which connects to a laptop for interface between the system and system operator during a fEITER trial. The latter sub-system generates stimulus sequences consisting of auditory tones and visual flashes delivered by headphones and goggles respectively, and controlled using *Signal* software (Version 3.09, Cambridge Electronic Design, Ltd.). Current of 1mA peak-peak is injected by fEITER using a montage of 32 scalp electrodes attached to the subject and in turn, connected to the headbox. During each measurement epoch, current is injected between 20 different combinations of diametrically opposed electrodes on the head. Measurements of resulting potential differences are captured from serial electrode pairs, excluding the injecting electrode pair. A complete epoch of fEITER lasts 60s and consists of 5998 frames of data. Measurements are acquired 100 times per second for 20 different current injection pairs, generating a total of 546 measurements for a single frame of data. Reconstructions from boundary voltage measurements recorded with fEITER have thus far been undertaken using the UCL 7-tissue head model (Table 1.4) (McCann et al., 2011).

The spatial resolution of fEITER is 7.74mm determined by the surface area of each electrode and each tetrahedral element within the 7-tissue UCL head model.

Figure 1.4 fEITER hardware. Photograph showing hardware components of the fEITER system composed of a base unit and headbox.

Table 1.4. The 7-tissue UCL head model The UCL head model is based on 7 tissues of the head listed in the table below. The conductivity values of each tissue are displayed in S/m (Siemens per meter), in addition to the number of tetrahedral elements and the average volume for each tissue.

Tissue type	Conductivity (S/m)	Number of tetrahedral elements	Average Elemental Volume ($x10^{-8}$ m^3)
Scalp	0.172	16427	9.88
Skull	0.050	11178	6.81
CSF	1.540	7585	3.38
Grey matter	0.345	12140	5.58
White matter	0.150	4740	7.44
Eyes	1.150	1235	0.80
Olfactory bulbs	0.110	31	10.97

fEITER has been built in accordance with British safety standards for a medical device (BS EN 60601-1) which defines the electrical limits for current applied to patients. The system has been classified as a 'Type BF' applied part, and preliminary studies have confirmed its compliance with this particular safety standard. Adherence to electrical safety standards are an obvious concern when undertaking a clinical trial using a new medical device on human subjects. These standards are also imperative for future CE marking of a novel medical device. The system has undergone an extensive MHRA approval process prior to clinical trials being commenced. Ethical considerations have also been explored and appropriate approvals were sought from South Manchester Local Research Ethics Committee (ISRCTN 93596854). In addition, external reviews of the fEITER software and safety aspects of the electronic design were completed independently to verify the instrument.

Preliminary results reported thus far from volunteer trials have explored the use of fEITER to capture neural evoked responses to manoeuvres such as the auditory startle reflex (McCann et al., 2011) and the Valsalva manoeuvre (VM) (Quraishi et al., 2011) (Appendix 5). Subsequent trials undertaken on patients have evaluated the use of fEITER to monitor functional activity within the brain during induction of anaesthesia (Bryan et al., 2011) (Appendix 5). A signal to noise ratio of over 90dB has been reported demonstrating its sensitivity to capture small changes of internal impedance using scalp electrodes (McCann et al., 2011).

fEITER can potentially provide a new approach to high speed imaging of functional brain activity at all depths within the brain. Unlike conventional brain imaging techniques which are often large installations requiring the patient to be transported to a scanning facility such as fMRI and PET, fEITER offers the potential of functional brain imaging at the bedside. Implementation of a sub-second temporal resolution coupled with a portable device suggests fEITER could potentially revolutionise aspects of medicine and healthcare where functional brain imaging techniques are employed. Within clinical areas concerning stroke and brain injury, functional imaging of the brain within a crucial timeframe could be vital for urgent diagnosis and treatment. For example, to limit ischaemic damage occurring in the brain, thrombolytic therapy following an acute stroke should be provided within a time period of 3 hours from initial stroke symptoms presented. However,

administration of the therapy is currently based upon results from a CT or MRI scan to differentiate between the incidence of ischemic and haemorrhagic stroke. Administration of thrombolytic drugs following haemorrhagic stroke could potentially be life-threatening by increasing bleeding within the brain. This is one area of medicine where EIT could provide rapid, bed-side monitoring of the brain to identify a cerebral incident without the need to transfer the patient to a scanning facility (Yerworth et al., 2003).

It has been suggested that functional EIT could potentially be applied to image the physiological process of consciousness. Consciousness has been proposed to be mediated by synchronous activity of neuronal networks forming neuronal assemblies within the brain (Greenfield and Collins, 2005), with varying levels of consciousness correlating with varying sizes of neuronal assemblies. The neural basis of consciousness is poorly understood as currently no functional imaging technique exists which can monitor sub-second changes within the brain correlating to neural activity. Anaesthesia has also been used as a tool to further investigate the neural mechanisms of consciousness using PET (Alkire, 2008), EEG (Boly et al., 2012) and fMRI (Schröter et al., 2012) techniques. However, neither PET nor fMRI possess a temporal resolution commensurate to neural processing within the brain therefore these modalities cannot directly measure and locate neural activity related to consciousness. Although EEG has a sub-second temporal resolution, neural activity in deeper areas of the brain cannot be explored using this technique. As a research tool, fEITER has the potential to investigate the neural basis of consciousness using a sub-second temporal resolution to capture neural activity at all depths of the brain. In addition, the precise targets of anaesethesia and drugs which are able to cross the BBB can potentially be explored.

Within clinical practice, fEITER could be a vital tool for bed side monitoring within departments such as the A&E, critical care wards and even within the operating room. Transferring patients from these environments to a scanning facility can be time consuming, hazardous for a critically ill patient and impossible during surgery. A portable technique such as fEITER could potentially eliminate the need to transfer patients to an imaging facility whilst providing a rapid diagnosis.

As mentioned previously in this thesis, imaging the brain using EIT poses a unique technical challenge. Unlike soft tissue systems such as the lungs, breast and prostate which have been successfully imaged using EIT, the brain is encased in the highly skull. For an EIT system such as fEITER to capture functional activity of the brain, sufficient current must first be able to enter the brain by penetrating several protective layers surrounding the brain (Bayford, 2006, Holder, 2005). Firstly, the scalp is a moderately resistant tissue for injected current to penetrate through which can be aided by appropriate surface electrode contact. Secondly, the injected current will encounter the highly resistant pia matter and the skull; both tissues divert the injected current and prevent it from entering the brain (Holder and Tidswell, 2005). Finally, prior to reaching actual brain tissue, injected current must pass through the conductive CSF fluid. The injected current amplitude by any EIT system is limited by medical safety regulations. In the case of fEITER, the injected current amplitude is measured at 1mA pk-pk, which is within the permitted limits according to BS EN 60601-1:2006 at the injected frequency. To ensure the injected current at particular amplitude is insensible to the subject, current injection frequency must also be limited to avoid inducing any sensations such as neuralgia. In addition, fEITER has been designed to acquire high precision measurements. According to published data, a reported SNR of 80dB is sufficient to obtain precise impedance changes of upto 1% induced by evoked responses. A SNR greater than 80dB has been reported for the fEITER system in tank conditions indicating the system has been built to sustain a high level of precision and performance (McCann et al., 2011, Towers et al., 2000). It must be acknowledged however, that fEITER is not yet fully developed. Although the system is medically safe for use within the anaesthetic and operating rooms, fEITER is not yet fully developed in terms of ergonomic design and most importantly reliable tomographical reconstructions.

The current process of electrode placement is based on the international 10-20 EEG electrode placement system. Accuracy of the reconstruction process is dependent upon precise electrode placement on the head. fEITER reconstructions which have been published thus far have used a realistic 7-tissue head model consisting of 53,336 tetrahedral elements (Bryan et al., 2011, McCann et al., 2011, Quraishi et al., 2013). Whilst the model is considered to be anatomically realistic, the model is

generalised to a human head and brain. Therefore, individual variance in head size and shape cannot be considered and is a source of inaccuracy when identifying precise anatomical locations within the brain. An ideal and more accurate scenario would be to reconstruct fEITER data using individual MRI scans of individual subjects to ensure anatomical accuracy and also to consider individual variance in head shape and size. Until now, only single subject reconstructions have been published for fEITER data despite there being a library of data acquired from multiple individuals who have volunteered as subjects in the fEITER trials. Although sub-second observations have been identified in published data so far, it is clear that further analysis of fEITER data is required in order to reliably ascertain the physiological processes that are being captured. In addition, until accurate tomographical reconstructions are undertaken for each subject tested using fEITER, physiological changes cannot be reliably localised within the brain.

1.6 Aims and Objectives of Thesis

There is evidence provided in literature where raw EIT waveforms have been evaluated to examine various physiological processes such as pulmonary ventilation, gastrointestinal emptying and cerebral blood flow (REG) (Bayford, 2006, Bodo et al., 2003, Erol et al., 1996a, Frerichs, 2000, Gilad and Holder, 2009b). There exists no guide however on pre-processing of raw EIT data prior to tomographical reconstructions being produced.

This thesis will report on the pre-processing of raw fEITER data acquired from trials due to be undertaken at the CMFT, for future tomographical reconstructions of pre-processed raw data. During the volunteer trial, fEITER will be used to monitor changes in boundary voltage measurements recorded from the head in response to volunteers being presented with visual stimulation and in response to a voluntary Valsalva manoeuvre (VM) being performed. The patient trial will consist of using fEITER to capture changes in boundary voltages during the induction of anaesthesia. From previous studies reported in literature, the use of neurophysiological and neuroimaging techniques have demonstrated that the trial conditions explored in the present study (visual stimulation, the VM and induction of anaesthesia) induce measurable changes in neuronal activity and cerebral blood flow (Bonmassar et al., 2001, Macey et al., 2012, Zhang et al., 2010). Therefore, the purpose of evaluating raw EIT waveforms recorded using fEITER is to investigate whether genuine physiological changes during evoked responses in volunteers and patients can be captured using fEITER. More specifically, it is anticipated that signal variability captured from individual fEITER measurement pairs may potentially reflect changes in physiology.

The primary aim of this thesis is to pre-process the raw fEITER waveforms captured during volunteer and patient trials to validate that the measurements recorded using fEITER are genuine signals reflecting changes in physiology and not noise. It is anticipated that pre-processed fEITER data will reflect changes in EIT induced by stimuli and sources of noise such as the inherent baseline drift within EIT will be eliminated by appropriate pre-processing techniques. In the future, pre-processing of EIT data may potentially form a crucial step prior to performing tomographical

reconstructions. In the present study, individual fEITER waveforms will be filtered for visible regular perturbations and for high frequency noise also. It is anticipated that underlying signals following filtering may be reflective of physiological changes induced by applied stimuli such as visual flashes, the VM and induction of anaesthesia.

The secondary aim of this thesis is to evaluate the high frequency components within fEITER waveforms. Whereas the primary aim of this thesis will regard high frequency components of the fEITER waveform as noise, the secondary aim of this thesis is to evaluate whether the high frequency components of the fEITER waveform reflect changes in physiology induced by applied stimuli.

Approximate entropy (ApEn) is a signal processing technique applied to physiological signals acquired from various body systems to identify deviations from regular physiological function which cannot be identified using descriptive statistical analysis techniques. ApEn has previously been applied to physiological signals measured from the brain such as EEG, intracranial pressure and cerebral blood flow to evaluate signal regularity and how pathophysiology can disrupt physiological signal regularity (Beaumont and Marmarou, 2002, Hornero et al., 2005, Pincus, 1995). By inducing evoked responses and changes in regular physiology within the brain, it is anticipated that a signal processing technique such as ApEn applied to high frequency components of fEITER signals may identify changes in measured boundary voltages from baseline induced by stimuli such as visual flashes, the VM and induction of anaesthesia. For the correct application of ApEn, the fEITER signal will be stationarised to remove the effects of a baseline drift. In addition, any dominant signals in the fEITER waveform occurring with visible regularity will also be removed prior to the application of ApEn.

1.7 An Introduction to the fEITER Trials at CMFT

The following section introduces the fEITER trials undertaken at CMFT. Firstly, the process of validating EIT systems using phantoms is introduced followed by an introduction of the stimuli presented to subjects as part of the volunteer and patient trials, namely: visual stimulation, the Valsalva manoeuvre and induction of anaesthesia. Finally the method of ApEn as a technique to evaluate raw fEITER data signals is also introduced here.

1.7.1 Validating EIT Systems using Phantoms

The performance of EIT systems is periodically validated using phantoms to produce reproducible results for calibration and comparison purposes. Validation is particularly crucial for EIT systems designed for use *in-vivo* since these are highly complex. Modifications to any part of the EIT system must be validated to ensure the system is acquiring data accurately and consistently whenever it is used (Gagnon et al., 2010, Holder and Tidswell, 2005).

The types of phantoms described in research can be divided into the following two categories: **mesh** and **physical** phantoms.

Mesh phantoms consist of impedance components such as active electronic elements, resistors alone, or in combination with capacitors. These phantoms are appropriate to acquire consistent and stable reproducible data to periodically assess the performance of an EIT system. In addition, mesh phantoms can be easily transported to test an EIT system in a variety of environments. A mesh phantom is essentially a physical version of a finite element model using resistors of known conductivity. Therefore, the overall electrical conductivity of a mesh phantom can also be altered by the addition of extra resistors (Gagnon et al., 2010).

The Cardiff phantom was one of the first mesh phantoms to be described in literature composed of 624 resistors with values of 51 and 100 Ohms (Ω) (Griffiths, 1988). Since then, the Cardiff phantom has been used to validate various EIT systems operating at a single-frequency and has also been used as the basis for the development of subsequent mesh phantoms described in literature (Holder and Tidswell, 2005, Riu and Anton, 2010).

The wheel phantom was subsequently developed to validate multi-frequency EIT systems and also to account for transfer impedances inherent of *in-vivo* measurements. The transfer impedance describes the change of injected current to the resultant measured voltage through biological tissues. Unlike the two-dimensional linear path of x-rays used in CT, the path of injected current through human tissue will be diverted three-dimensionally along the path of least resistance. Injected current through the head will therefore be diverted by the resistant skull resulting in a smaller proportion of the injected current entering the brain, hence the impedance will be transferred (Tidswell et al., 2001b). The wheel phantom consisted of 32 impedance elements divided equally between current injection and measurement elements (Griffiths, 1995).

Following the wheel phantom, two mesh phantom systems were produced with the aim of validating EIT systems developed to monitor functional changes in the thorax during ventilation named the Göttingen phantoms. The first Göttingen phantom consisted of 65 resistors and 16 impedance elements. Additional resistors were incorporated into the design to provide the option of two defined resistance values (Hahn et al., 2000). The second Göttingen phantom consists of 19 resistors compared to 65 in the first phantom. This phantom was also produced to be operated using a 16 electrode EIT system. Unlike the first phantom however, the second Göttingen phantom consisted of an inner ring of resistors allowing it to be used on EIT systems which operate using an adjacent injection drive design. As a result, in every position of current injected between two adjacent electrodes by the EIT system, the injected current was delivered through a central resistor in the inner ring (Hahn et al., 2008).

In 2010, Gagnon et al., (2010) (Gagnon et al., 2010) published their evaluations of a resistive mesh phantom compatible for use on a variety of EIT systems operating at a single or multiple frequencies. The resistive mesh phantom was built using 340 resistors whilst also integrating the effects of electrode impedances using models of silver/silver chloride electrodes (Ag/AgCl). Compared to the Cardiff phantom and second Göttingen phantom which produced signals of unrealistic frequency and amplitudes, the resistive phantom described by Gagnon et al., (2010) (Gagnon et al., 2010) was produced to generate realistic signals whilst also considering characteristic stray effects of *in vivo* EIT signals.

Whilst mesh phantoms provide a useful means for assessing the performance of an EIT system by assessing its' ability to generate stable and reproducible signals, they are limited to approximating signals within a two-dimensional homogenous medium. This is not reflective of *in-vivo* systems which are 3-dimensional and in-homogenous. In comparison, physical phantoms consist of a conductive medium such as gel or saline solution encased in a non-conductive tank with boundary impedance elements embedded within the surface. Impedance measurements are captured using surface electrodes which connect the EIT system to the tank. Known objects are placed into the conductive medium to create contrasting impedance measurements in an otherwise homogenous environment. Physical phantoms aim to provide a more realistic yet controlled environment to assess the ability of an EIT system to capture changes in impedance simulated by a known object in the three-dimensional homogenous environment (Yasin et al., 2011). Several EIT groups have used physical tanks to assess the ability of an EIT system to capture the presence of a conductivity target such as conductive metal, resistive Perspex objects and pieces of vegetables (Holder et al., 1999, Holder and Tidswell, 2005, Cherepenin et al., 2001). Compared to changes in *in-vivo* systems which produce lower contrasts using EIT, the aforementioned test objects within saline-filled tanks produce large impedance contrasts. To produce smaller contrasts within a physical phantom, EIT groups have employed the use of test objects such as gels or sponges inserted into the saline filled tank. As the saline solution slowly diffuses through the permeable pores of test objects, an impedance contrast is produced which is stable over time (Esler et al., 2010, Holder and Tidswell, 2005, Oh et al., 2008).

In relation to validating EIT systems suitable to capture changes in impedance from the head, the use of cylindrical physical phantoms have evolved to incorporate the geometry of a head. Developments to create a more realistic physical phantom were undertaken by producing a spherical tank compared to a cylindrical one. In order to resemble EIT measurements captured from a human head, a highly resistant layer simulating the skull was also fashioned using plaster of Paris (Liston et al., 2004, Holder and Tidswell, 2005). Studies have also adopted the use of a real human skull within a tank to create a more realistic phantom in addition to an external layer to simulate the impedance properties of the scalp and skin using the skin obtained from

a marrow (Liston et al., 2004, Tidswell et al., 2003, Tidswell et al., 2001a). The resulting effect has been a more realistic physical phantom modeled to incorporate the geometry and conductive layers of a biological system such as the human head. Despite advances, there are key limitations to using physical phantoms which affect the reproducibility of results over time. For example, the evaporation of conductivity medium, the osmotic change and ionic diffusion of organic test objects will cause variations in acquired results over time (Yasin et al., 2011). All physiological measurements are subject to noise in the form of movement, fluctuations in temperature and electronic interference. Compared to physical phantoms, although mesh phantom measurements are less likely to be affected by movement and temperature changes, they do not estimate the dynamics of signals acquired from three-dimensional objects such as biological tissue. Nevertheless, both types of phantoms described provide useful information regarding the performance of an EIT system and are recommended to be undertaken prior to embarking on EIT data collection from live subjects.

Voltage measurements acquired from phantoms are used to calculate reproducible values of signal-to-noise ratio (SNR) which describes the levels of a desired signal compared to background noise present in the measurement. SNR values determine the sensitivity of imaging systems using the average and standard deviation of a consecutive sequence of EIT measurements expressed in the unit of decibels (dB).

1.7.2 Visual Stimuli: Evoking a Visual Evoked Potential (VEP)

A visual evoked potential (VEP) describes the gross electrical change recorded from the occipital cortex of the brain, in response to a change in visual stimulation such as a flashing light. The electrical activity is captured using EEG at the occipital cortex. Multiple EEG signals are averaged to generate VEP waveforms which are frequently utilised as clinical tools to evaluate anterior visual pathway integrity encompassing the optic nerve, optic chiasm and neural radiation to the occipital cortex (Atilla et al., 2006, Vialatte et al., 2010).
There are two categories of visual stimulation clinically used to generate VEPs:

1.) flashing lights
2.) pattern stimuli such as checkerboards.

A flashing light stimulus is categorised as an unpatterned visual stimuli with variable light intensity and a variable presentation frequency. In comparison, patterned stimuli encompass the following 2 variations of checkerboards presented to the subject:

1.) pattern onset & offset, and
2.) pattern reversal

The pattern onset & offset stimuli is presented by displaying a checkerboard for a defined amount of time which represents the pattern onset. The checkerboard is then immediately replaced by an unpatterned display known as the offset. The offset is displayed for the same duration of time as the onset, and also consists of the same average luminance to avoid contamination of the VEP by varying the levels of luminance. The onset & offset sequence is repeatedly presented to the subject and resulting cortical VEPs are captured using EEG.

Unlike the pattern onset & offset sequence, pattern reversal has a continuous display of a checkerboard. Pattern reversal is achieved by alternating luminance levels

between half of the checkerboard (light or dark squares); luminance increases for one half whilst luminance decreases for the other half giving the illusion of the checks reversing in pattern by alternating between light and dark squares. The pattern reversal VEP captured is therefore the averaged response to the reversal.

'Transient' VEPs are generated when a stimulus is presented using a slow temporal rate up to, or below 4 flashes or pattern alternation per second, up to 4 per second. Transient VEPS are useful when analysing specific components of the waveform for clinical interest. For example the latency of the first positive peak following a flash or pattern reversal can be identified and measured. In comparison, 'steady state' VEPs are generated in response to visual stimuli presented using a high temporal rate above 10 flashes or 10 pattern reversal sequences per second. Steady state VEPs generate high frequency oscillations where specific component analysis is not possible. Instead, steady state VEPs are analysed by evaluating waveform amplitude and phase.

When used as a clinical tool, pattern visual stimuli are more widely used to generate reproducible and reliable VEPs with fewer inter and intra-individual variability compared to unpatterned stimuli. VEP investigations often lead to the diagnosis of demyelinating conditions of the visual system such as multiple sclerosis, familial ataxia and optic neuropathies. Patterned stimuli have also been shown to be a more sensitive probe when identifying minor visual pathway defects. This is due to the selection of variables such as stimulus size, orientation, luminance levels and field location, which allow specific sections of the visual pathway to be selectively tested. Field location in particular is a variable which can be used to reliably identify lesions affecting the retrochiasmal part of the visual pathway (Aminioff and Goodin, 1994, Korth and Nguyen, 1997).

The use of unpatterned stimuli to assess integrity of the visual pathway is limited due to the variability of responses observed amongst individuals and insensitivity when investigating clinical lesions (Groswasser et al., 1985). Nevertheless, flash VEP are still clinically useful for patients who are unable to focus or fixate on a pattern stimulus and also for patients who are too young or uncooperative. Unpatterned stimuli are also used to study steady state VEPs (Aminioff and Goodin, 1994, Aminoff, 1980).

1.7.2.1 Origin of the VEP

The VEP is largely a reflection of foveal activity and cone cell activation. Retinal synaptic projections from the central visual field are directed via the optic tracts to the lateral geniculate nucleus (LGN). Synaptic targets from the left and right LGN are relayed onto the primary visual cortex; an area of the occipital lobe which spans either side of the calcarine fissure, also termed V1 and the striate cortex. EEG electrodes placed onto the back of the head overlying the occipital cortex will therefore reflect central retinal activity. The time period analysed following visual stimulus presentation typically lasts between 200 and 500 milliseconds (Walsh et al., 2005).

As the primary function of the visual system is to identify shapes and edges, the alternating checkerboard pattern is the clinically preferred stimulus for generating a VEP. Furthermore, the visual response to a pattern stimulus is much larger and is deemed to bear a closer resemblance to the natural act of visual processing (Braddick and Atkinson, 2011, Kothari et al., 2014).

A typical transient VEP recorded using a reversing patterned stimulus (checkerboard) is shown in Figure 1.5. The waveform shows 3 identifiable features occurring at specific time points. An initial negative peak is seen at a latency of approximately 75ms following reversal of the checkerboard (N75). This is followed by a characteristic positive peak known as P100 at approximately 100ms. A second negative deflection is seen at a latency of approximately 145ms and is known as N145 (Aminoff, 1980, Harding et al., 1996, Odom et al., 2010). The P100 is generated in the striate cortex as a response to stimulation of the central visual field and therefore the latency of this response is accepted as a measure of retino-striate conduction time. A delayed P100 latency, a complete absence of the P100 or an abnormality in the amplitude of this response is a significant indicator of optic neuritis attributed to axonal damage within the visual pathway. Assessment of the P100 response is a clinically useful test for patients diagnosed with MS. MS is a neurological condition which affects the white matter of the brain and spinal cord. The condition causes optic neuritis as a result of demyelination of axonal fibres within the visual pathway (Halliday et al., 1973). Further specificity regarding the

location of damage within the visual pathway can also be gained from field selective VEP tests where the pattern reversal stimuli is presented individually to the left and right visual field (Walsh et al., 2005).

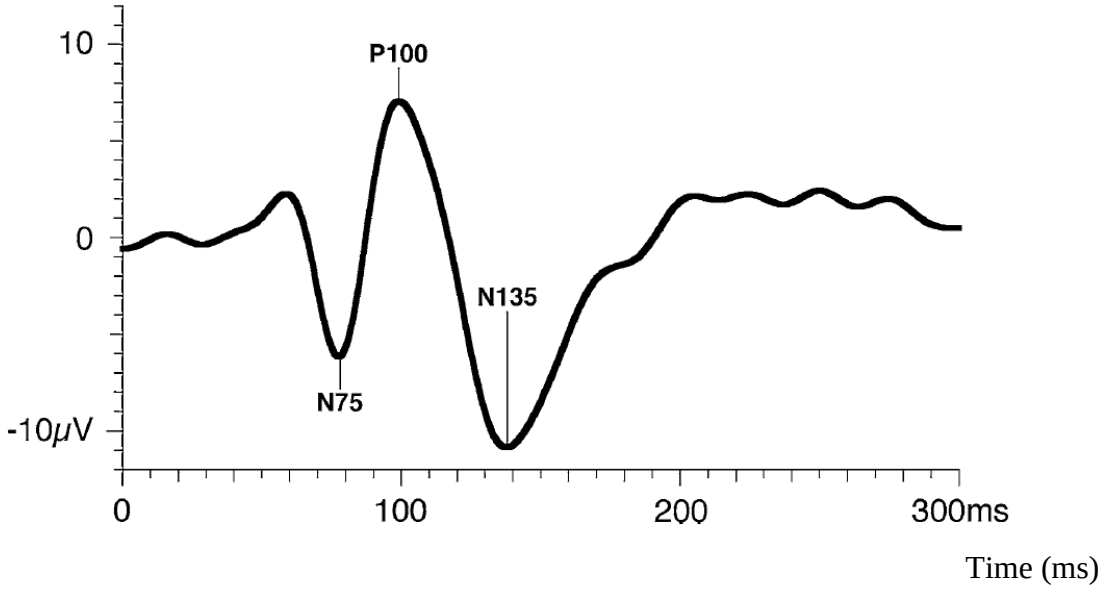

Figure 1.5 Characteristic VEP generated by a pattern reversal stimulus. Trace showing the characteristic features of a normal pattern-reversal VEP taken from Odom, et al (2010) (Odom et al., 2010).

The size of checks presented in pattern stimulus is traditionally expressed in terms of visual angle in minutes of arc. The retinal area can be divided into the following regions: the central foveal which spans 5º of visual angle, and the peripheral retina consisting of the para-foveal and peripheral region, spanning 8º of visual angle. In accordance to the retinal regions, it has been established that a VEP using a patterned stimulus is generated due to visual activity initiated centrally between 2 - 6º of visual field (Jones and Blume, 2000, Kothari et al., 2014). In a recent study undertaken by Kothari, Singh et al., (2014) (Kothari et al., 2014), the effect of altering the visual angle of a reversing checkerboard stimulus on the latency and amplitude of the major components of the VEP was evaluated. The authors aimed to identify an optimum visual angle among a range of check sizes which would generate a reliable pattern reversal VEP and allow accurate VEP interpretation. The authors reported that altering the size of the pattern stimulus (visual angle) affects components of the

recorded VEP. In addition, the authors also reported that optimum foveal stimulation was achieved using a visual angle of 120 minutes of arc as minimum P100 latency and substantial amplitude was observed using this visual angle (Kothari et al., 2014). The effect of viewing distance from the pattern reversal checkerboard stimulus on generated VEP components has also been investigated in a study undertaken by Shushtarian, Valiollahi et al., (2009) (Shushtarian et al., 2009). The authors concluded that a decrease in the distance between the subject and monitor leads to an increase of P100 latency and an overall reduction in P100 peak amplitude.

Other factors beyond the realms of a controlled clinical environment have also been shown to affect the recorded VEP such as subject gender and age. Reported latency variations between male and female subjects have been attributed to differences in average head sizes; a shorter P100 latency has been reported in female subjects due to a smaller average head size (Gregori et al., 2006). In addition, an increase in subject age has been shown to decrease P100 peak amplitude due to a reduction in visual acuity with increasing age (Halliday et al., 1973).

Figure 1.6 shows a characteristic VEP response to pattern onset & offset stimulus. Following pattern onset & offset, the first characteristic feature known as the C1 component occurs between a latency of 40 and 70ms followed by a secondary peak (C2 component) occurring at a latency of 100 to 130ms and finally the C3 component which occurs between 140 and 190ms (Di Russo et al., 2002, Harding et al., 1996).

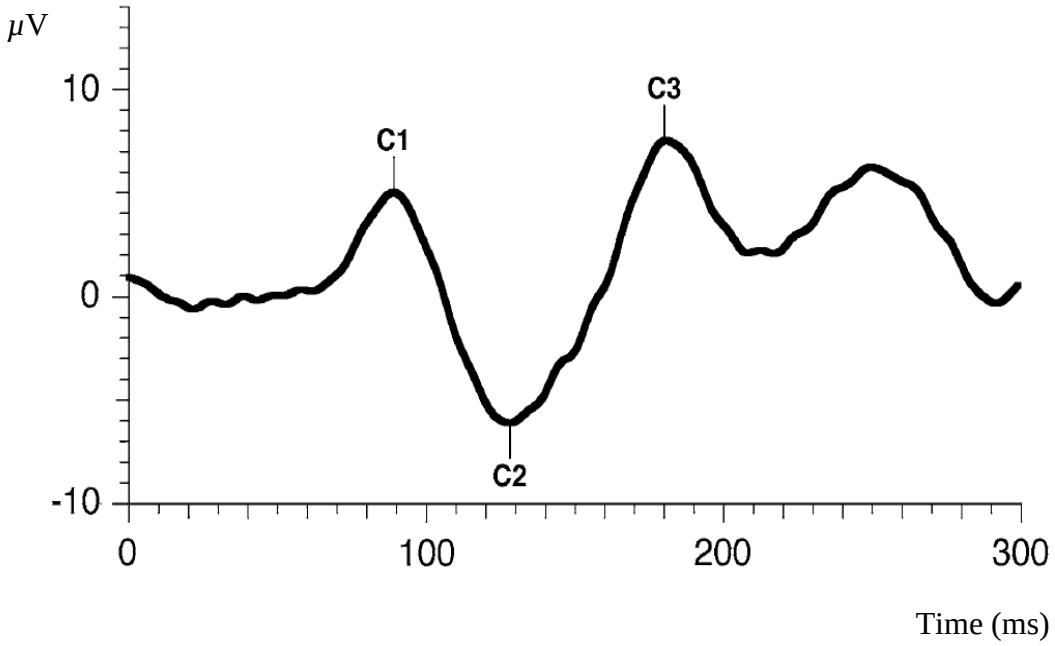

Figure 1.6 Characteristic VEP generated by a pattern onset/offset stimulus. Trace showing the characteristic features
of pattern onset/offset VEP taken from Odom, et al (2010) (Odom et al., 2010).

A VEP waveform generated from a flash stimulus is characteristically different from patterned stimulus. It typically consists of a series of peaks differing in polarity lasting for a latency of approximately 300ms with the first peak generated at approximately 30ms following the flash stimulus. A sequential nomenclature is used to evaluate these waveforms by numbering each negative (N) and positive peak (P) as shown in Figure 1.7. Although acknowledged as producing highly variable responses, literature suggests N2 and P2 components are the most robust and characteristic features generated using flash stimuli, occurring with a latency of approximately 90ms (N2) and 120ms (P2) (Aminioff and Goodin, 1994, Odom et al., 2010).

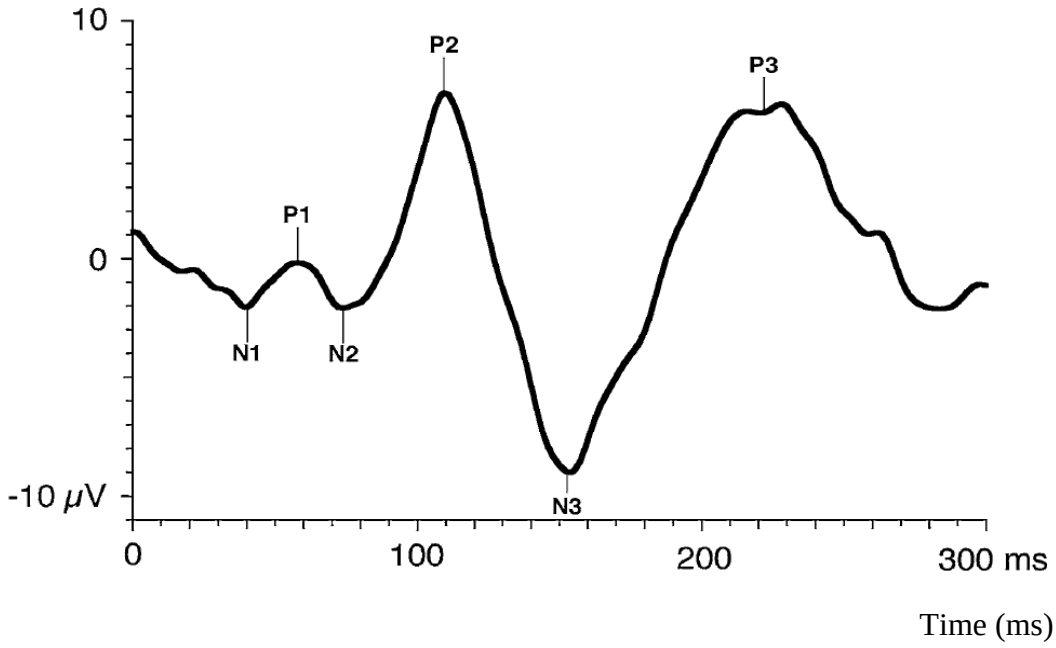

Figure 1.7 Characteristic VEP generated from a flash stimulus. Trace showing the characteristic features of a VEP generated from a flash stimulus taken from Odom et al, (2010) (Odom et al., 2010).

The neural source responsible for generating recognisable features of the VEP has been explored using high resolution imaging techniques such as MRI in conjunction with neurophysiology recordings made by EEG. Due to pattern stimuli generating more reproducible VEP waveforms compared to unpatterned stimuli, neural sources of these waveforms have been more consistently identified compared to flash VEPs. A number of visual-cortical locations have been identified as neural generators for components of pattern VEPs; the most common being the primary visual cortex which has shown to be most active in generating the major components of the pattern VEPs (N75 and C1). Earlier studies have combined the use of EEG with physical models of the head acknowledging conductivity of brain tissue, skin and skull to identify activation of the primary visual cortex during a VEP (Maier et al., 1987). The use of intracerebral and subdural electrodes has also confirmed early activation of this area during a VEP (Arroyo et al., 1997, Ducati et al., 1988). More recent studies have combined physiological recording techniques with high resolution imaging modalities to improve the overall spatio-temporal resolution compared with using either modality individually. High resolution imaging modalities such as MRI, fMRI and PET have been used in conjunction with EEG to compensate for the poor

temporal resolution of these modalities in order to identify a neural generator of early pattern stimulus VEP components (Bonmassar et al., 2001, DiRusso et al., 2001, DiRusso et al., 2005, Momose et al., 1997). MEG combined with EEG and fMRI has further explored the neural source of VEP components (Hashimoto et al., 1999, Shigeto et al., 1998, Hagler et al., 2009). Combining findings of past literature, the general consensus amongst investigators is that the origin of the C1and N75 components of the pattern VEP is located within the primary visual cortex. Generators of later VEP components has undergone some debate as investigations have located numerous areas responsible for eliciting the later components of pattern stimulated VEPs within the visual cortex including V1, V2, V3, V4 and extrastriate areas (Noachtar et al., 1993, Onofrj et al., 1995, Vanni et al., 2001).

Despite the advances in clinical brain imaging, electrophysiological techniques such as VEP recordings still provide great value in the diagnosis and management of neurological degenerative disorders, in particular managing multiple sclerosis (MS) patients. Although MRI is predominantly utilised to identify the presence of white matter lesions in patients recognised to be suffering from MS, recording VEPs is regarded as both complimentary to MRI and as a diagnostic tool on its own. A prospective follow-up study undertaken by Lee, Hashimoto et al., (1991) (Lee et al., 1991) over a period of 2 years compared the diagnosis of MS using MRI, with VEP results taken from patients who exhibited no symptoms of optic neuritis. Abnormal VEPs were detected in patients with no optic neuritis and normal MRI scans (Paty et al., 1988). Evaluation of the same patients following a 2 year period showed both MRI and VEP results were equivalent in the prognosis of developing MS.

VEPs are also clinically utilised to aid the prognosis of visual recovery following blindness due to head injury and/or trauma (Agarwal and Winny, 1999) and also to explore the loss of visual function as a result of chronic renal failure (Seymen et al., 2010). The reliable utility of clinical VEP recordings to explore visual function in cases of hereditary ataxias and hereditary motor and sensory neuropathies (HMSN) has been debatable. Earlier studies have reported VEP abnormalities associated with the neuropathies (Livingstone et al., 1981, Honan et al., 1993, Tackmann and Radu, 1980) whereas other investigations have shown no significant differences in VEP

latencies between control and study subjects, or in the normal responses of all inherited ataxia patients (Bird and Crill, 1981, Leblhuber et al., 1986).

1.7.2.2 Neurovascular Coupling (NVC) and VEP

Neurovascular coupling (NVC) is a term used to describe the synchronized relationship between neurological activity and the cerebrovascular response. The close integrated relationship between neurons, glia and astrocytes with vascular cells has been explored in various pathological conditions and a body of evidence now exists describing a functional neurovascular unit within the brain (Girouard and Iadecola, 2006). The precise mechanism of NVC has been attributed to a coordinated concert of activity involving ionic conduction, metabolic factors and neurotransmitters resulting in vasodilation or vasoconstriction of cerebral blood vessels.

fMRI is conventionally used to regionally map neuronal activity to vascular responses within the brain. Several studies have associated impaired NVC with pathological conditions such as Alzheimer's disease (Farkas and Luiten, 2001, Iadecola, 2004), stroke (Krainik et al., 2005, Blicher et al., 2012) and hypertension (Dunn and Nelson, 2014), collectively highlighting the importance of NVC regulation in the functional brain (Girouard and Iadecola, 2006).

NVC between cerebral blood flow in the posterior cerebral artery and VEPs has been investigated in a trial undertaken by Zaletel, Stucle et al., (2004). The relationship between visually evoked cerebral blood flow velocity (VEFR) and pattern reversal VEPs was monitored by simultaneously capturing cerebral blood flow velocity in the posterior cerebral artery using TCD whilst recording pattern reversal VEPs. Results from the study showed VEFR increased in response to increasing levels of visual contrast presented, providing evidence for a linear relationship between VEFR and VEP. An earlier study also employed the use of TCD to monitor the relationship between flash VEPs and cerebral blood flow in the posterior, basilar and middle cerebral arteries (Sturzenegger et al., 1996). Similar to the results mentioned above, blood flow velocity was shown to increase in the posterior artery in response to a flashing visual stimulus. The magnitude of increased CBF velocity in the posterior

artery was reported to be larger than that observed in the middle and basilar cerebral arteries. Brightness of the flashing stimulus was also reported to significantly influence the velocity response amplitude. These studies show that both flashing and pattern reversal visual stimulation causes measureable increases in cerebral blood flow velocity in the occipital lobe which have been attributed to NVC.
Using TCD however, is based on the assumption that vessel diameter remains constant (Newell et al., 1994) therefore although the study has provided evidence of a relationship between VEFR and VEP, the exact mechanisms of how NVC occurs cannot be further explained.

1.7.2.3 Using EIT to detect VEPs

The use of EIT to detect VEPs in human subjects has been explored by Professor David Holder's group based at UCL. The aim of their studies has been to capture a change in impedance during visual stimulation and relate these changes to an increase in blood flow and neuronal depolarisation. Regional CBF has been shown to increase in the visual cortex due to an increase in neural activity in this area. As blood is known to have a lower impedance than the brain, visual stimulation has been predicted to result in a decrease in impedance (Holder et al., 1996). In a study undertaken by Tidswell, Gibson et al., (2001b), non-invasive EIT measurements captured from human subjects during visual stimulation showed significant changes in impedance. Despite these encouraging results however, the study also highlighted some limitations with using EIT to isolate a single physiological function such as cerebral blood flow or neuronal depolarization. Absolute mean impedance change was calculated by averaging impedance values for electrodes which showed a significant impedance change. Contrary to the significant results observed for individual electrode data, no significant differences were observed for the absolute mean values between reference and visual stimulus conditions. Reconstructed images from this trial also failed to localise impedance changes to the visual cortex. This was attributed to the various physiological functions occurring in the brain at once during a VEP including regional increases and decreases in CBF and global neuronal depolarisation. Overall, the study highlighted the difficulty in relating the direction of

impedance changes with complex physiological activity occurring synchronously in the brain.

In a later study undertaken by Gilad and Holder et al., (2009b) visual stimulation was once more presented to human subjects to non-invasively capture impedance changes using EIT. The aim of this study was to assess the ability of EIT to capture fast neural activity during a VEP. Unlike in the study mentioned above, Gilad, Horesh et al., (2009) calculated changes in resistance from voltage measurements captured using EIT based on the hypothesis that synchronous neuronal activity and multiple action potentials at the visual cortex during a VEP would lead to an overall decrease in neuronal membrane resistance allowing low frequency currents (below 100Hz) to enter the intracellular space. During resting conditions therefore, low frequency currents would be confined to the extracellular space. Regardless of response direction (inhibitory or excitatory) a measureable change in resistance was expected to be recorded. Using EIT, current was injected between 2 pairs of electrodes placed on the scalp overlying the visual cortex. Results from the study showed significant differences in calculated resistance in 35% of individual recordings. The changes were shown to occur with a latency of 50ms to 250ms following stimulus presentation and peaked at a range of 100ms to 200ms. The results observed were credited as physiological and not artefact based on previous simulation studies (Gilad et al., 2007) which showed the injected amplitude of current used did not stimulate neuronal activity and therefore changes observed were not induced by the current injection itself. Although the significant results observed could not be translated into images due to a poor signal to noise ratio, the study did provide evidence that EIT as a technology could be used non-invasively to capture fast neuronal changes in the brain in response to visual stimulation.

Both aforementioned studies also show that analysis of EIT data as a physiological waveform can portray functional activity of the brain.

1.7.3 The Valsalva Manoeuvre (VM)

The Valsalva manoeuvre (VM) is named after anatomist Antonio Maria Valsalva who originally described use of the manoeuvre as a technique to inflate the Eustachian tubes. The VM is performed by sustaining a forced expiration against a closed airway (achieved by pinching the nose and keeping the mouth closed) and is characterised by a bursting sensation in the ear drums.

Since its original description, the manoeuvre has been recognised to cause characteristic changes in arterial blood pressure (ABP) and heart rate (HR). The changes in systemic pressure induced by the manoeuvre stimulate the sympathetic and parasympathetic branches of the autonomic nervous system (ANS) (Yale, 2005). Characteristic changes in systemic circulation occur in four well-defined stages illustrated on the top trace in Figure1.8: Stage I is recognised by a transient rise in MABP caused by the applied strain which increases intra-thoracic pressure. As the aorta is compressed, vagal tone increases (induced by the parasympathetic nervous system), causing a transient decrease in HR during this stage. MABP falls during stage IIa as a result of a decrease in atrial filling pressure. This is coupled by a reduction in cardiac output. A sympathetic response in stage IIb leads to a rise in peripheral vascular resistance, ABP and HR. Following release of the manoeuvre, stage III is characterised by a sudden fall in ABP caused by the abrupt fall of intra-thoracic pressure. HR increases following stage III. Finally, stage IV is recognised by a compensatory overshoot in ABP due to continued sympathetic autonomic tone. Stimulated arterial baroreceptors induce a reflex bradycardia before ABP and HR return to baseline values (Elisberg, 1963, Tiecks et al., 1996, Tiecks et al., 1995).

As a result of the VM inducing characteristic changes in ABP and HR, it is utilised as a clinical tool to evaluate autonomic function and cardiovascular integrity (Levin, 1966). The Valsalva ratio quantifies vagal function by considering HR ratio during stages II and IV. The ratio can be used to identify autonomic dysfunction which would be recognised by a loss of ABP overshoot and the characteristic bradycardia response (Hiner, 2005).

Due to the autonomic effects it exerts on blood pressure and heart rate, the VM is successfully used as a diagnostic test within cardiovascular medicine to detect left-

sided heart failure, systolic heart murmurs and left ventricular systolic dysfunction (Freeman, 2006). It is also used as a non-invasive aid to assess cardiac volume status and ventricular filling pressures in chronic heart failure patients (Felker et al., 2006). Cardiovascular circulation describes the vasculature between the body and heart whereas cerebral circulation encompasses the blood supply to the brain. Cerebral circulation is highly regulated by the autonomic nervous system to avoid any compromises of adequate blood supply to the brain which may lead to a cerebrovascular accident.

Although the VM is a natural reflex to regular processes such as defecation, lifting heavy weights and coughing, its effects on cerebral circulation mediated by the ANS can cause sensations of dizziness or fainting and in extreme circumstances, a cerebrovascular accident. Cerebral auto-regulatory mechanisms prevent extreme alterations to cerebral perfusion pressure and intracranial pressure during sudden positional changes (from supine to standing) and also during the VM when performed involuntarily or voluntarily (Chuang et al., 2005).

Although the autonomic effects exerted on systemic circulation during the VM have been widely studied, effects of the manoeuvre on cerebral circulation have been more challenging to evaluate due to limitations in measurement techniques and limited access to functional cerebral circulation in a living subject. Nevertheless, effects of the VM on cerebral circulation have been well characterised and further investigations have aimed to distinguish cerebral auto-regulatory mechanisms exerted by neural activity, from the mechanical influences. The primary motive behind understanding a neural component responsible for exerting autoregulatory processes following an autonomic strain has been to identify a particular area of the brain responsible for the rapid cerebral autoregulatory mechanisms exerted by the ANS. The voluntary VM has therefore been utilised in numerous studies as a tool to induce autoregulatory responses to maintain cerebral homeostasis. A range of studies have been undertaken to further understand the process of cerebral autoregulation induced by the VM including transcranial Doppler studies (TCD) to monitor blood flow velocity in cerebral arteries (Tiecks et al., 1995), functional MRI to image changes in blood flow (Henderson et al., 2002) and ganglionic blockades to specifically target autonomic outflow (Zhang et al., 2004).

Tiecks, Lam et al., (1995) utilised TCD to monitor characteristic effects of the VM on cerebral blood flow within the middle cerebral arteries illustrated on the bottom trace in Figure 1.8. Changes in middle cerebral artery blood flow measured using TCD during the VM were simultaneously compared to changes in systemic circulation.

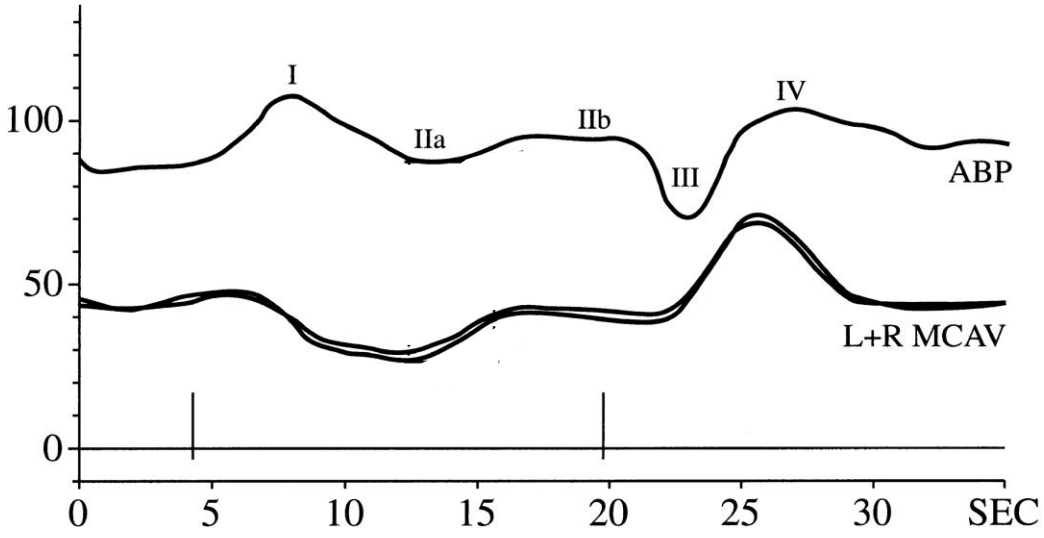

Figure 1.8 Changes in systemic and cerebral circulation induced by the VM in a single subject (adapted from Tiecks, Lam et al., 1995). Vertical lines on the x axis indicate timescale of the VM being performed. Percentage change is shown on the y axis. The top trace measures percentage change in ABP measured at the radial artery using a blood pressure monitor. The bottom trace shows percentage change of blood flow velocity in the left (L) and right (R) middle cerebral arteries (MCAV) measured simultaneously in the same subject using TCD. The four stages of the VM characterised by changes in ABP are illustrated along the top trace.

Tiecks, Lam et al., (1995) reported that percentage changes in cerebral blood flow velocity (CBFV) recorded from the middle cerebral arteries during the VM were comparable to the simultaneous changes captured in ABP characterised by the four defined stages of the manoeuvre. Although, the magnitude of changes recorded in cerebral blood flow were shown to be significantly greater than those observed in ABP, predominantly during stage II of the manoeuvre. The heightened increase in CBFV compared to ABP was attributed to an autoregulatory response involving

vasodilation of cerebral arterioles during stage II of the manoeuvre, stimulated by a fall in cranial perfusion pressure.

As expected, an increase in sympathetic tone following the release of the strain during stage III caused an overshoot in ABP which did not exceed the increase initially observed in stage I at the start of the manoeuvre. In contrast, the compensatory overshoot observed in CBFV following release of the strain in stage III was shown to exceed the level of CBFV increase measured during stage I. This stage was therefore considered to carry the highest risk for a cerebral accident.

The study demonstrated that the combined use of TCD and ABP pressure is a useful method for continuous monitoring of sympathetic outflow and cerebral autoregulatory responses. However it must be noted that the use of TCD assumes a constant vessel diameter during the manoeuvre therefore ruling out the possibility of dilation or constriction of the middle cerebral arteries. Furthermore, the results indicated that a neural mediator is responsible for exerting a greater overshoot in MCAV during stage IV compared to the overshoot observed in ABP. Although unresolved, the authors concluded that a neural component was responsible for mediating the cerebral autoregulatory response.

1.7.3.1 Identifying a Neural Component of the VM

In 2004, Zhang, Crandall et al., (2004) conducted a study to identify the neural components involved in mediating the cerebral haemodynamic autoregulatory response during the VM. Changes in CBFV during the VM were monitored in the presence of a ganglionic blockade. The blockade was used to inhibit autonomic ganglionic synapses and therefore inhibit any autonomic neural activity. The authors hypothesised that any differences observed in CBFV during the VM in the presence of a ganglionic blockade would differentiate cerebral autoregulatory responses mediated by mechanical factors from autoregulatory responses mediated by a neural component. CBFV was measured using TCD in nine healthy subjects who performed the VM before and following administration of an autonomic ganglionic blockade. Results showed that the characteristic changes in CBFV during the VM, without the ganglionic block, were significantly enhanced in the presence of a ganglionic

blockade. Under control conditions with no abnormalities in the autonomic regulatory system, a reduction in CBFV was observed during phases IIa and IIb of the VM, followed by a compensatory overshoot in CBFV during phase IV. As hypothesised by the authors, in the presence of a ganglionic blockade, CBF auto-regulatory mechanisms were inhibited leading to a greater reduction in ABP and CBF during stage II of the manoeuvre. Furthermore, in the presence of a ganglionic blockade during stage IV of the VM, there was no compensatory overshoot in ABP observed, whereas a heightened CBFV overshoot response was observed. The study demonstrated that autonomic neural activity is responsible for maintaining a relatively constant CBFV and is also receptive to a greater fall in ABP stimulating cerebral auto-regulatory responses. The characteristic changes observed in ABP during stages I and II of the VM were shown to be preserved in the presence of a ganglionic blockade demonstrating that these changes are mediated by mechanical effects rather than autonomic neural activity.

The precise location of a neural site responsible for exerting the autonomic effects of the VM on cerebral and systemic circulation has been the topic of numerous studies employing imaging techniques to identify a functional location within the brain. A network between various neuronal sites and the cardiovascular system, more commonly known as the brain-heart axis, has been identified in mediating autonomic outflow affecting systemic circulation during the VM (Nagai et al., 2010). The axis has been defined to consist of the insular cortices, anterior cingulate gyrus and the amygdala. In particular, the left and right insular cortices have been established as one of the initial neuronal sites activated in generating autonomic responses to the VM. Significant correlations in blood flow and neural activity at the insular cortex using fMRI have been made. More precisely, the left insular cortex has been shown to be activated during parasympathetic outflow resulting in bradycardia, whereas the right insular cortex has been shown to be associated with sympathetic autonomic tone leading to tachycardia (Henderson et al., 2002, Mendelowitz, 1999, Nagai et al., 2010). Although fMRI studies have shown consistent results in identifying the insular cortices, an isolated neuronal response cannot be identified using this modality due to a haemodynamic delay. fMRI measures blood-oxygenation-level-dependent (BOLD) signals and correlates highly perfused areas in the brain with an

increase in neuronal activity (section 1.4.3). As the BOLD signal is dependent upon haemodynamic activity within the brain, functional activity is captured using a temporal resolution of several seconds. A sub-second temporal resolution would be required to image a neural component associated with the VM. EIT technology proposes a potential solution to capture neuronal activity using a sub-second temporal resolution commensurate with neuronal processing activity. A technology such as fEITER which operates using a 10ms temporal resolution could potentially capture neuronal activity during the VM.

1.7.4 Induction of Anaesthesia

The term ‘anaesthesia’ was coined by Oliver Wendell Holmes in 1846 to describe a demonstration performed by William Morton where a patient undergoing surgery experienced a lack of sensation following inhalation of ether (Hudetz, 2012). The discovery of anaesthesia revolutionised clinical medicine by allowing a surgical procedure to be undertaken without any apparent suffering caused to the patient during surgery.

Induction of anaesthesia refers to the process of medically inducing a coma by the administration of one or more general anaesthetic agents resulting in an unconscious state. Although the molecular targets of general anaesthetic agents within the brain have been widely explored, the precise mechanisms of how anaesthetic agents produce a state of unconsciousness still remains unclear. This is partly due to a lesser understanding of how exactly consciousness arises within the brain and also due to the inability for researchers to anatomically identify a particular area within the brain which is responsible for a state of consciousness. Although it is extensively accepted that general anaesthesia (GA) results in amnesia, analgesia and suppression of one’s volition, the application of anaesthesia doesn’t result in complete suppression of neuronal activity within the brain (Garcia et al., 2010).

1.7.4.1 General Anaesthesia (GA): Molecular Targets within the Brain

GA is a pharmacological process whereby administered drugs bind to, and interact with receptors on the target organ of anaesthetic agents: the brain. Binding of these molecules causes an alteration of receptor function in a concentration dependent manner, leading to a global change in information processing within the CNS (Franks, 2008). Induction of anaesthesia using intravenous (i.v) agents is generally preferred over the use of inhalational agents due to a more rapid induction. The administration of an i.v anaesthetic agent leads to a cascade of physiological events. Firstly a rapid increase in plasma concentration of the anaesthetic agent occurs due to binding of the agent to plasma proteins within the blood. The remaining agent is essentially 'unbound' and is therefore able to cross the blood-brain barrier (BBB) to target the brain. The quantity of protein binding is dependent upon plasma concentrations, changes in blood pH levels and the presence of other pharmacological agents which may lead to displacement of the anaesthetic agent binding to plasma proteins. The rate at which the unbound form of the drug from the site of administration crosses the BBB leading to a loss of consciousness is often termed: "one arm-brain circulation time" and is largely dependent upon the cardiac output of the individual, the lipid solubility of the anaesthetic drug and the pK_a of the agent, coupled with the pH of the extracellular fluid (Fryer, 2004, Perouansky and Hemmings Jr, 2006).

Once the anaesthetic agents have crossed the BBB it is now widely accepted that functional mechanisms of general anaesthesia are exerted by these agents binding to specific proteins on neurons within the CNS and altering the function of ion channels. Under normal conditions, ion channels located within neurons functions to alter the electrical excitability of the neuron by mediating the influx or efflux of ions across the neuronal cell membrane. They type of ion crossing the neuronal cell membrane results in the propagation of excitatory or inhibitory signals (Garcia et al., 2010, Weir, 2006).

Within current clinical practice, there are 10 general anaesthetic agents that are used to induce and maintain GA in adults. These agents can be further sub-divided into

inhalation and i.v anaesthetic agents summarised in Table 1.5 (Garcia et al., 2010, Weir, 2006). Most i.v and inhalational anaesthetic agents are known to affect ligand-gated ion channels and two-pore domain K^+ channels.

Table 1.5 Commonly used inhalational and intravenous anaesthetic agents. Inhalational and intravenous anaesthetic agents which are most commonly used in adult clinical practice are listed below, corresponding to their receptor affinities.

Inhalational		Intravenous	
AGENT	RECEPTOR	AGENT	RECEPTOR
Nitrous Oxide	Glutamate - NMDA	Propofol	$GABA_A$
Isoflurane	$GABA_A$	Etomidate	$GABA_A$
Sevoflurane	$GABA_A$	Ketamine	Glutamate - NMDA
Desflurane	$GABA_A$	Methohexital	$GABA_A$
Xenon	Glutamate - NMDA	Thiopental	$GABA_A$

The two major cerebral targets of anaesthetics are N-methyl-D-aspartate (NMDA) and γ-amino butyric acid ($GABA_A$) receptors. Of the 10 agents categorised in Table 1.5, nitrous oxide, xenon and ketamine target glutamate receptors within the CNS by primarily blocking NMDA receptors. The NMDA receptor has a high affinity for naturally occurring neurotransmitters in the brain namely glutamate, glycine and D-serine. Binding of either of these excitatory ligands to the NMDA receptor located within the post-synaptic membrane, leads to an influx of positively charged Na^+ ions causing the post-synaptic neuron to depolarise. These receptors are therefore responsible for the propagation of fast excitatory neurotransmission within the brain. General anaesthetic agents that target the NMDA receptor work by inhibiting excitatory signals mediated by the NMDA receptor (Khan et al., 2014).
The majority of agents categorised in Table 1.5 mediate their sedative effects by modulation of the $GABA_A$ receptor which is a ligand-gated ion channel belonging to the Cys-loop family of ionotropic receptors. The $GABA_A$ receptor is formed from a combination of 5 of the following sub-units: α, β, γ, δ, ε, θ, π and ρ, which surround a central pore forming the ion channel. The $GABA_A$ receptor mediates chemical synaptic transmission and is located within the post synaptic membrane of excitable

neurons where it functions to propagate inhibitory neurotransmission within the CNS. The receptor is responsible for mediating approximately 40% of all fast inhibitory neurotransmission within higher centres of the CNS and is most abundantly found within the hippocampus, making it a central component of higher-order brain functions such as memory, learning, awareness and consciousness. The natural ligand for the $GABA_A$ receptor is synthesised from glutamate and is known as GABA. Following release of the neurotransmitter from the pre-synaptic neuron into the synaptic cleft, GABA binds to the $GABA_A$ receptor located on the post-synaptic neuron causing ion channels within the receptor to open and allow an inward movement of negatively charged chloride (Cl^-) ions against a concentration gradient. The inward movement of Cl^- ions results in the hyperpolarisation of the post-synaptic cell membrane. General anaesthetic agents that target the $GABA_A$ receptor allosterically enhance the effects of naturally occurring GABA therefore causing an overall increase in inhibitory neurotransmission (Weir, 2006, Khan et al., 2014, Garcia et al., 2010).

There exists a number of $GABA_A$ receptor isoforms consisting of different subunit compositions which determines the particular receptors' affinity to an agonist. Different isoforms of the $GABA_A$ receptor have demonstrated selectivity for different anaesthetic agents (Garcia et al., 2010, Weir, 2006). The most commonly identified isoform of the $GABA_A$ receptor found in the mammalian brain is composed of two α subunits, two β subunits and a single γ subunit. As well as being a primary target for intravenous anaesthetic agents such as propofol and etomidate, this particular $GABA_A$ receptor isoform also has a high affinity for benzodiazepines and barbiturates (Khan et al., 2014). There now exists a library of GA agents including both inhalational and i.v agents as listed in Table 1.5. However, due to the rapid induction properties of i.v agents coupled with a more rapid recovery time, i.v agents are the preferred choice for the induction of anaesthesia compared with inhalational agents. A number of studies have also shown that induction and maintenance of anaesthesia using i.v agents results in improved patient outcomes following surgery, demonstrated by an observed reduction in the incidence of post-operative nausea and vomiting (PONV) and early post-operative well-being (Dueck et al., 2005, Purdon et al., 2009).

1.7.4.2 Propofol

The most popular i.v anaesthetic agent used within clinical medicine to date is propofol due to its rapid recovery and anti-emetic properties. Propofol directly interacts with the $GABA_A$ receptor and potentiates inhibitory neurotransmission mediated by GABA (Uhrig et al., 2014). Following the administration of i.v propofol, the distribution half-life of the agent is 2-8 minutes before it is rapidly metabolised by the liver. The elimination half-life of propofol is between 4-7 hours. Due to extrahepatic metabolism of the agent by the lungs and kidneys, propofol clearance exceeds hepatic blood flow (Khan et al., 2014, Perouansky and Hemmings Jr, 2006).

1.7.4.3 Functional Targets of Propofol within the Brain

The mechanism of propofol binding to its molecular target within the brain is well understood. It has been established that different anaesthetic agents possess varying affinities for a range of molecular targets, i.e not all GA agents target a single receptor type (Garcia et al., 2010). Regardless of the molecular differences between general anaesthetic agents, ultimately their use produces a universal end point which is a state of unconsciousness, suggesting that the functional mechanisms underlying general anaesthesia and unconsciousness exceeds the simple binding of anaesthetic agents to molecular targets. The functional activity of how molecular targets instigate the cascade of activity leading to unconsciousness is still poorly understood. The use of functional monitoring techniques such as EEG and functional imaging modalities such as fMRI, PET and MEG are increasingly being used to further understand and localise a functional mechanism of how general anaesthetic agents lead to a state of unconsciousness (Alkire et al., 1995, Zhang et al., 2010). Exploring the precise neuronal targets of GA has often been coupled with research concerning consciousness as general anaesthetics provide an ideal tool to manipulate levels of consciousness (Långsjö et al., 2012).

1.7.4.4 Effects of Propofol on Cerebral Metabolic Rate (CMR) and Cerebral Blood Flow (CBF)

Baseline activity within the brain encompasses regional cerebral metabolic rate (CMR) and cerebral blood flow (CBF). Prior to exploring the effects of GA on functional connectivity within the brain, earlier studies have focussed on identifying the effects of general anaesthetic agents on baseline activity within regions of the brain. Regional changes in CMR and CBF in response to propofol administration have been related to functional changes in neuronal activity and therefore also linked to loss of consciousness. Intravenous general anaesthetic agents such as propofol cause a global reduction in CMR and CBF attributed to inhibitory neurotransmission caused by the stimulation of $GABA_A$ receptors. The link between loss of consciousness and a reduction in CMR was first reported by Alkire, Haier et al., (1995) using PET. CMR was measured using PET whilst propofol was titrated to subjects until loss of consciousness was achieved; defined by unresponsiveness to a verbal command. They found a global reduction of CMR throughout all areas of the brain by 30-70%. Non-uniform changes in certain areas were also identified; CMR within cortical regions were shown to decrease by 58% following propofol administration compared to a reduction of 48% recorded from sub-cortical regions (Miller and Ferrendelli, 1990, Shrestha et al., 2011). These differences showed that CMR depression within cortical regions was significantly higher than in sub-cortical regions suggesting that the anaesthetic effects of propofol on the brain are primarily due to cortical interferences. Regional CMR changes observed by Alkire, Haier et al., (1995) were later correlated with areas of the brain containing a high density of GABA receptors in a subsequent study conducted by Alkire and Haier (2001). Compared with isoflurane anaesthesia, relative glucose metabolic rates using propofol were reported to be lower in cortical regions such as the frontal, temporal, parietal and occipital lobes. In the following sub-cortical regions: basal ganglia, thalamus, hippocampus, midbrain and cerebellum, relative glucose metabolic rates were reported to be higher than those measured using isoflurane. Results from this study correlated areas in the brain containing high densities of $GABA_A$ receptors,

with a greater decrease in regional cerebral metabolism during propofol anaesthesia (Alkire and Haier, 2001).

Regional CBF (rCBF) during propofol anaesthesia has been explored in various studies to identify anatomical areas within the brain responsible for mediating behavioural effects of propofol such as sedation, amnesia and hypnosis. The aim of these studies was to identify a neural component of consciousness when considering a certain level of arousal exploited with the use of general anaesthetic agents. The use of PET in functional neuroimaging studies has enabled researchers to monitor changes in cerebral blood flow in response to titrated doses of anaesthesia. One such study investigated changes in rCBF in response to the titration of propofol (Fiset et al., 1999). The titration technique applied to awake volunteers allowed the researchers to induce varying levels of sedation and ultimately unconsciousness. The induction of unconsciousness was reported to result in a decrease of global CBF measured by PET. More importantly, large decreases in rCBF were observed in anterior regions of the brain encompassing the medial thalamus, the cuneus & precuneus, the posterior cingulated gyrus and a particular area of the prefrontal cortex known as the orbitofrontal cortex. Specifically, rCBF decreases in the medial thalamus were shown to supercede global decreases in CBF. The medial thalamus is an area which has previously been identified as a critical component of consciousness and arousal (Jasper, 1949). From their findings, Fiset, Paus et al., (1999) concluded that the regional decrease in CBF recorded within the medial thalamus in response to increasing concentrations of propofol, is a result of propofol acting on the reticulothalamic system as loss of consciousness is induced. Furthermore, the observed decrease in CBF within cortical regions was attributed to cortical deactivation by propofol. However, the authors were unable to establish whether the cortical decrease in CBF was a primary reaction to propofol induced anaesthesia, or a secondary outcome of disruption within the thalamocortical relay system resulting in reduced neuronal activity and hence a decrease in cortical CBF. As an additional measure of neuronal activity, the aforementioned study also employed the use of EEG recordings during loss of consciousness and results showed a prominent decrease in gamma (γ) activity. γ activity has been shown to be a property of the thalamocortical system linked to arousal and conscious processing

of the awake, and waking brain (Steriade, 1993). A reduction of γ activity during propofol anaesthesia reported by Fiset, Paus et al., (1999) therefore supports the idea that the thalamus and its' projections to cortical structures are central targets of the hypnotic effects exerted by propofol (Reed and Plourde, 2015).

A subsequent study also used PET to monitor changes in rCBF in response to thiopental and propofol (Veselis et al., 2004). The motive for undertaking this study was to explore whether these anaesthetic agents exercise different mechanisms of actions within the brain despite having a common affinity to the $GABA_A$ receptor. Although compared with thiopental, propofol was shown to exert a greater amnesic effect; both agents were shown to cause significant decreases in rCBF. However, more importantly, results from this study showed both agents exhibited distinct regional differences in their effect on CBF at similar pharmacologic effects when inducing sedation, hypnosis and amnesia. Despite both agents being active at the $GABA_A$ receptor, propofol was shown to decrease CBF in anterior regions of the brain including the ventrolateral prefrontal cortical regions, regions of the insula and the medial thalamus. In comparison, thiopental was shown to affect rCBF within posterior regions of the brain. These differences between anaesthetic agents were interpreted by suggesting that anterior regions of the brain are responsible for mediating changes in memory and hence these regions showed a decrease in CBF using smaller concentrations of propofol to induce amnesia. The observed sedative effects of thiopental were attributed to effects on cerebellar regions of the brain. The authors also reported that at larger concentrations, both agents affected similar cerebellar regions within the brain. Interestingly, results from this study showed that despite similar endpoints of anaesthesia exerted by both agents characterised by unresponsiveness, only propofol was shown to affect rCBF at the thalamus whereas, rCBF effects of thiopental were observed in cerebellar regions (Veselis et al., 2004). Although the disparity of effects observed between propofol and thiopental was attributed to small sample sizes, the study nonetheless demonstrated the diversity of anaesthetic agents and how agents with a selective affinity for the same receptor can mediate a universal endpoint of unresponsiveness via different regional mechanisms within the brain.

1.7.4.5 The Thalamus: A Neural Target of Anaesthesia

Having established that the $GABA_A$ receptors are the primary target for propofol within the brain, functional neuroimaging techniques have been employed to identify the precise neural location of propofol action and how these locations achieve a state of unconsciousness.

Zhang, Wang et al., (2010) used the BOLD-fMRI signal in the brain to identify the action sites of varying levels of administered propofol in the normal human brain of 10 subjects. A sedation scale was used to determine the level of consciousness following an infused dose of propofol. Levels of consciousness were identified as: awake, sedated, unconscious and conscious. In response to propofol administration, the authors reported an immediate decrease in the BOLD signal across all subjects in the hypothalamus, the frontal and the temporal lobes. Signal decreases in the thalamus were also observed in 50% of all subjects studied and the magnitude of signal decrease recorded in this area was significantly lower compared to decreases in the hypothalamus, frontal and temporal lobes. Prior to the aforementioned study, the thalamus had already been recognised as a common target of anaesthetic agents from a study conducted by Alkire, Haier et al., (2000). PET images of 11 anaesthetised subjects using halothane and isoflurane were statistically analysed to show regional metabolic suppression within the thalamus and midbrain reticular formation. The authors related their results to sleep-induced unconsciousness and suggested a similar mechanism is activated during anaesthesia whereby hyperpolarisation of thalamo-cortical neurons results in anaesthetic-induced unconsciousness. These findings have led to the theory of a ‘thalamic switch’ of consciousness (Alkire et al., 2000).

The thalamus behaves as a relay for cortical information processing using ascending and descending transmission pathways for various cortical regions. It has also been shown to be an important mediator for regulation of arousal (Schiff, 2008). Animal studies have shown that injections containing GABA agonists, similar to propofol, injected into an area contained within the thalamus known as the intralaminar nuclei resulted in rats falling asleep rapidly (Miller and Ferrendelli, 1990). In addition, excitatory stimulation of the same area with nicotine in rats has been shown to result

in the regaining of consciousness from anaesthesia (Alkire et al., 2007). The thalamus has been recognised as a common site of action for most anaesthetic agents and is also implicated as an important structure for regulating sleep and wakefulness. At a cellular level, general anaesthetics have been shown to hyperpolarise the resting membrane potentials of thalamo-cortical neurons (Nicoll and Madison, 1982) which has been supported further by evidence from more recent human neuro-imaging studies. One particular study conducted by Liu, Lauer et al., (2013) used fMRI to show functional connectivity in the thalamo-cortical system is reduced during deep sedation with propofol. Similar to previous studies undertaken, the authors suggested that the thalamo-cortical system is a principal component for the loss and return of consciousness. Despite the aforementioned evidence supporting the theory of a 'thalamo-cortical switch' of consciousness being a principle target of general anaesthetic agents, it has still not been possible to establish whether the effects of anaesthetic agents on this network are directly exerted, or a secondary result of modulation from other areas of the brain such as the cortex.

1.7.4.6 The Fronto-Parietal Cortex: A Neural Target of Anaesthesia

Conventional neuroimaging techniques allow a global image of the brain to be visualised. However, modalities such as PET and fMRI lack the temporal resolution to identify equivalent or sequential activation of neuronal networks within the brain. An indirect role of the thalamus in producing anaesthetic induced unconsciousness has been suggested by Velly, Rey et al., (2007) (Velly et al., 2007). This study employed the use of EEG combined with sub-cortical EEG (ESCoG) in twenty-five human subjects, to explore both cortical and sub-cortical changes within the brain during anaesthesia. EEG has the temporal advantage of a millisecond resolution allowing real time neuronal events to be captured. The limitation of monitoring only cortical activity using EEG was overcome by using deep brain electrodes to simultaneously capture electrophysiology from sub-cortical structures such as the thalamus. Results from this study showed changes in cortical activity occurred prior to the observed sub-cortical changes in response to induction with propofol.

Furthermore, the authors reported a significantly improved prediction of consciousness vs. unconsciousness from cortical EEG measurements compared to sub-cortical structures. From their observed results, Velly, Rey et al., (2007) concluded that thalamic effects of anaesthesia are in fact secondary to cortical activity and may be consequential to suppressed cortical activity caused by anaesthetic agents. It has therefore been suggested that the effects of anaesthesia on the thalamus may be secondary to cortical effects of general anaesthesia (Hudetz, 2012).

The fronto-parietal and frontal cortex have previously been identified as regions which are targeted and suppressed by general anaesthetic agents. As mentioned previously, propofol has already been shown to cause large reductions in CBF within these areas, demonstrated by Fiset, Paus et al., (1999) and Veselis, Feshchenko et al., (2004). A study undertaken by Boveroux, Vanhaudenhuyse et al., (2010) (2010) used fMRI to examine spontaneous fluctuations in the BOLD signal in healthy volunteers during various stages of propofol induced unconsciousness. Results from this study portrayed suppression of connectivity in the fronto-parietal cortex network during propofol-induced unconsciousness. A deterioration of connectivity between cortical and sub-cortical areas during propofol-induced unconsciousness was also demonstrated. Overall, it was concluded that propofol-induced unconsciousness was a result of deteriorated temporal connectivity within the brain, by specific targets of propofol within the fronto-parietal network. Although the study explored how thalamo-cortical connectivity is modulated with varying states of consciousness, the temporal neural correlates of consciousness targeted by anaesthetics remained unclear.

1.7.4.7 Evaluating Consciousness

Exploring the effects of anaesthesia forms the foundations of understanding the state of consciousness. In order to explain the phenomenon of consciousness, researchers have aimed to clarify the mechanisms of how anaesthetic agents manipulate consciousness in a reversible manner, eventually inducing a loss of consciousness. The mechanism of how general anaesthetic agents result in hypnosis and the loss of consciousness has been an intangible yet fascinating topic. How a range of anaesthetic agents with diverse binding properties ultimately lead to a common endpoint of unconsciousness has been of particular intrigue.

The next step in unravelling mechanisms of consciousness is to identify the precise neural components targeted by anaesthetic agents to induce unconsciousness. fMRI and PET have once more been employed in a number of studies aiming to resolve the precise neural correlates of consciousness. These studies have also used anaesthetic agents to vary consciousness levels whilst imaging regional activity within the brain. A PET study undertaken in 2012 (Långsjö et al., 2012) dissociated the epiphenomenal effects of anaesthesia such as changes in CBF, from the neural correlates of consciousness by using varying levels of anaesthetic agents. They also imaged a rapid return to consciousness using the unique anaesthetic agent: dexmedetomidine which allows the patient to regain consciousness whilst constant doses of the agents are still being administered (Maksimow et al., 2007). Dexmedetomidine was introduced into clinical practice in the 1990's as a short-term sedative. It is a pharmacological agonist at the α_2-adrenoceptor and results in sedative and analgesic effects whilst allowing subjects to be aroused. The key effects of dexmedetomidine binding at the α_2-adrenoceptor involve the efflux of potassium ions causing hyperpolarisation of the excitable neuronal membrane (Gertler et al., 2001). Therefore, regional activity in the brain captured during awakening whilst dexmedetomidine is still being infused could be identified as a neural correlate of consciousness, rather than a pharmacological target of the agent. Upon regaining consciousness, structures which were observed to effectively 'switch back on' were identified as the brainstem, thalamus, hypothalamus and anterior cingulate cortex. Limited activity was also observed within fronto-parietal cortical regions. The

authors concluded that the combined activity of the aforementioned structures forms a basic neural network to enable arousal upon regaining consciousness (Långsjö et al., 2012). A lack of cortical response upon regaining of consciousness was correlated to the gradual stages of emergence from anaesthetic-induced unconsciousness. The authors explained that emergence from anaesthesia encompasses autonomic arousal and brainstem reflexes which form the basis of consciousness. They suggested activity in higher processing areas such as the cortex would reflect a rich and wholesome conscious experience; absent during the initial stages of regaining consciousness from anaesthesia. The study successfully distinguished the minimal neural correlates of consciousness from pharmacological binding sites of the anaesthetic agents used. The authors also suggested that various networks within the brain are responsible for mediating altered states and levels of consciousness.

The state and level of consciousness has previously been attributed to neuronal assemblies existing within the brain by Baroness Susan Greenfield (Greenfield and Collins, 2005). Greenfield suggests consciousness as a whole arises as a result of multiple, transient neuronal assemblies -each potentially consisting of millions of brain cells- with the largest assembly dominating at one particular moment of consciousness. She also suggests that the net assembly size of neuronal networks can be used as a correlate to determine the level of consciousness. According to this theory of consciousness, it is presumed that neuronal assemblies within the brain during anaesthetic-induced unconsciousness would be substantially smaller and less dominant than neuronal assemblies during a conscious state. It is acknowledged that activity within the brain is not globally inhibited during anaesthesia. This notion is further supported by studies showing thalamo-cortical activity is not completely inhibited during propofol anaesthesia but instead information integration is impaired (Alkire, 2008, Dueck et al., 2005, Uhrig et al., 2014). One particular study implementing fMRI monitored changes in the primary and secondary auditory cortex in response to auditory stimulation during titrated doses of propofol anaesthesia (Dueck et al., 2005). Although a dose-dependent impairment of auditory function was reported, primary cortical responses to auditory stimuli were preserved even at

the highest doses of propofol indicating that anaesthetic-induced unconsciousness cannot be explained by complete cortical inhibition.

From the literature discussed, it is evident that anaesthesia-induced unconsciousness is not the result of a single anaesthetic target within the brain. As demonstrated by various neuroimaging studies undertaken in the past two decades, anaesthesia-induced unconsciousness is thought to be a cause of anaesthetic agents modulating functional connectivity of various structures within the brain. Research has also shown that unconsciousness during anaesthesia is not caused by complete de-afferentation of activity. The hypnotic mechanism of anaesthesia causing loss of consciousness is therefore assumed to be the result of functional connectivity being disrupted. Neuroimaging in its current form however is unable to confirm this possibility. One of the limitations which has so far prevented the precise neural correlates of anaesthesia-induced unconsciousness to be visualised in real time, has been the several second temporal resolution of functional imaging modalities used to date such as PET and fMRI (Greenfield and Collins, 2005). Although the spatial resolution of both modalities is excellent allowing precise areas of the brain to be identified, the time delay in capturing functional neuronal activity is in the region of 6-10 seconds (Greenfield and Collins, 2005). As a result, sub-second functional activity within the brain cannot be resolved using fMRI or PET. An obvious solution to overcome the poor temporal resolution of these modalities would be to combine the high resolution images obtained by fMRI and PET, with high temporal resolution monitoring techniques such as EEG. Although multimodal techniques have been employed in research (Purdon et al., 2009) these methods carry various technical and clinical challenges which prevent such measurements being applied to routine clinical practice to monitor patients during general anaesthesia. For example, when combined with fMRI, EEG electrodes and acquisition systems must be compatible with MRI technology (non-ferromagnetic) to prevent serious hazards and also to avoid interference with data acquisition and quality. Similarly, routine monitoring systems utilised in anaesthetic practice must also be compatible with MRI technology. Lastly, physiological observations such as blood pressure, heart rate, oxygen delivery must also be maintained; a difficult task to achieve whilst a subject or patient is inserted into a scanning facility. Furthermore, it is impossible for

surgical procedures to be performed within scanning facilities such as PET or fMRI meaning these methods cannot be used for continuous monitoring to observe the changes in the brain during surgical anaesthesia, and therefore limits the use of this technique.

1.7.5 Approximate Entropy (ApEn)

Approximate Entropy (ApEn) is a statistical measure for randomness and regularity pioneered by Pincus who successfully applied ApEn to time series data (Pincus, 1991). ApEn incrementally compares sections of time series data and calculates the logarithmic likelihood that a particular section retains similarities when compared to another incremental section of the same data set. Therefore, a complex and disordered time series data will be reflected by a large ApEn value. Complexity within the realms of physiology has been defined to reflect the presence of chaotic temporal features within healthy biological systems which represent regular physiological function. In comparison, a smaller ApEn value is seen to reflect a disruption of complexity within healthy biological systems (Lipsitz, 2002, Yentes et al., 2013). The historical development of quantifying regularity within a time series has generally been associated with entropy analysis such as Kolmogorov-Sinai (K-S) entropy which considers chaos and randomness within a system; the greater the entropy the greater the irregularity and complexity.

Unlike ApEn, entropy measures have been applied to infinite data sets containing limited or no noise; factors which are unavoidable in physiological measurements. The application of entropy to biological time series data will result in the analysis of system noise rather than the underlying physiological data. ApEn has been shown to be advantageous in evaluating short and noisy data sets with less than 50 data points. Whereas entropy is applied to linear data sets, ApEn is best applied to non-linear data sets such as biological signals. Physiological system data consist of multiple sequential signals which reflect biological processes. Measuring signal regularity and the persistence of certain signal sequences has provided a valuable tool to isolate pathological states or subclinical changes otherwise undetected using classical

techniques to quantify physiological signals, such as levels of mean and variability testing (Pincus and Goldberger, 1994b).

ApEn has been successfully applied to the respiratory, cardiac and central nervous systems as a diagnostic tool to correspond with pathology and also as a monitoring tool for clinically induced states such as anaesthesia. It has been a particularly useful statistical measure when evaluating heart rate within groups of individuals who show observed differences in waveform regularity despite having similar descriptive statistical values. In a study undertaken by Fleisher, Pincus et al., (1993) (Fleisher et al., 1993) ApEn was applied to ECG data recorded for pre-and post-operative conditions from non-cardiac surgical patients. The authors hypothesised that reduced ApEn values would distinguish patients demonstrating post-operative ventricular dysfunction. In accordance to the hypothesis, the authors reported significantly lower ApEn values in patients who demonstrated post-operative ventricular dysfunction compared to the cohort of patients who demonstrated no ventricular dysfunction post-operatively. The observed reduction in ApEn values associated with poor post-operative outcomes was attributed to a reduction in heart rate randomness coupled with an increase in recognisable features correlated with ventricular dysfunction. Consistent with earlier studies, the authors also observed distinctly lower ApEn values for older patients, supporting earlier theories that ageing results in reduced complexity of cardiovascular dynamics (Kaplan et al., 1991, Lipsitz and Goldberger, 1992).

Pincus and Goldberger (1994) (Pincus and Goldberger, 1994b) compared the heart rate traces of two pathologically distinct infant groups using ApEn. Their motive for comparison was to quantify the clearly observed differences in regularity between HR traces of the two groups, despite them having similar standard deviation and mean values. They found ApEn values were significantly lower for the pathologically abnormal group of infants compared to normal infant ApEn values. Pincus correlated a reduction in ApEn values with pathology using a hypothesis relating to perturbation and disease. In relation to HR, Pincus described a physiologically normal HR to be complex in nature as it is formed by the coherent interactions of physiological systems such as the autonomic nervous system (consisting of sympathetic and parasympathetic branches) with other internal and

external sources. It was hypothesised that disease and perturbation within a physiological system is the result of damaged coupling mechanisms and a discount of external influence leading to a physiological system which is effectively isolated from its expected functional input mechanisms. ApEn has been shown to correlate with this theory of physiological complexity where increasing values of ApEn are associated with greater system coupling and complexity, compared to decreasing values which have been shown to correlate with pathological conditions.

Similar to cardiovascular dysfunctions, ApEn has also been applied to EEG data captured during anaesthesia as an indicator of increasing anaesthetic depth. Increasing doses of anaesthetic concentrations results in intermittent bursts of high frequency EEG activity more commonly known as 'burst-suppression pattern.' In a study conducted by Bruhn, Ropcke et al., (2000) (Bruhn et al., 2000), ApEn values were shown to be inversely related to burst-suppression ratio. As burst-suppression ratio was shown to increase during isoflurane anaesthesia, ApEn values were shown to continuously decrease. The authors interpreted their results to signify that an increase in anaesthetic depth leads to a loss of system complexity and therefore lower ApEn values were obtained during increased depths of isoflurane anaesthesia. In comparison, during wakefulness, EEG is highly complex and disordered resulting in high ApEn (Jagadeesan et al., 2013). Results from a subsequent study also explored the use of ApEn applied to EEG for depth of anaesthesia monitoring during maintenance and recovery stages. The authors reported that ApEn could successfully differentiate between different stages of anaesthesia. Furthermore, comparison with BIS -a commercially available device which quantifies depth of anaesthesia (section 1.1.5.2) showed ApEn was more sensitive to changes in depth of anaesthesia, as the EEG response to recovery from anaesthesia was detected more rapidly using ApEn compared to BIS (Fan et al., 2010). Further applications to EEG data have shown ApEn to be a useful tool to detect pathologies such as epileptic seizures where ApEn values were once more shown to be lower for epileptic patients compared to non-epileptic EEG data (Srinivasan et al., 2007, Radhakrishnan and Gangadhar, 1998). Changes in ApEn values have also been shown to be reflective of changes in intracranial pressure (ICP) and intracranial hypertension (ICH). In a study undertaken by Hornero, Aboy et al., (2005), acute elevated levels of ICP in subjects

with severe traumatic brain injury (TBI) resulted in decreased values of ApEn, indicating reduced complexity in ICP beat morphology. Reduced ApEn values of ICP signals were also shown to coincide with episodes of ICH (Hornero et al., 2005). Results of this study also supported the potential use of ApEn as a tool applied to non-invasive monitoring such as EEG, ECG and ABP in the absence of continuous ICP monitoring to indicate elevations in ICH without the need to use invasive ICP monitoring interventions.

ApEn has also been applied to endocrine signals to determine the subtle effects of ageing, co-morbidities and gender on the secretory patterns of hormones such as insulin (Meneilly et al., 1997), cortisol and growth hormone (Charmandari et al., 2001, Gusenoff et al., 2001). Collectively, the aforementioned studies are a few of many examples demonstrating the application of ApEn to biological signal data. Results from various studies have demonstrated the advantages of using ApEn to interpret the regularity of biological signals. Given the noisy nature of real physiological signals, ApEn has been demonstrated to provide a solution for reliably analysing biological signal complexity and regularity.

1.7.5.1 Calculating ApEn

The calculation of ApEn (*m*, *r*, *N*) uses the following constant parameters: *m* and *r*. Where *m* is the window length or number of data points to be analysed within each section and *r* is an applied filter, calculated as a fraction of the standard deviation. *N* represents the number of data points.

The calculation is based on the analysis of ECG data using a series of R-R intervals where $u(i)$ denotes the i^{th} R-R interval. For the application of ApEn to other physiological time series data, the variable $u(i)$ represents measurement segments equally spaced in time. A sequence of vector time series representing *m* consecutive *u* values, starting with $u(i)$ are effectively formed. The following example illustrates the first 4 vectors formed from a time series data set: $x(1) = [u(1), u(2)]$, $x(2) = [u(2), u(3)]$, $x(3) = [u(3), u(4)]$, $x(4) = [u(4), u(5)]$.

Each vector is used as a template for comparison with all other vectors in the chosen time series to determine a conditional probability. The conditional probability

describes a calculated percentage of instances where the vectors close to the template vector matches the template vector within the tolerance limit set as *r*. ApEn then aggregates the conditional probabilities by measuring how many vectors are comparable when the window length is increased by 1: $m + 1$. Therefore, for N data points vector sequences from $x(1)$ through
$x(N - m+1)$, defined by $x(i) = [u(i),..., u(i + m - 1)]$ are formed. The distance $d[x(i), x(j)]$ between vectors $x(i)$ and $x(j)$ is then defined as the maximum difference in their numerical quantity. The sequence $x(1), x(2), x(3),..., x(N-m+1)$ is used to construct for each $i \leq N-m+1$, $C_i^m(r) =$ (number of $x(j)$ such that $d[x(i), x(j)] \leq r) / (N - m+1)$. The $C_i^m(r)$ calculates the regularity of patterns similar to a template pattern of window length m within a tolerance r. Next, $F^m(r)$ is defined as the average value of the natural log (ln) of $C_i^m(r)$. Therefore approximate entropy is defined as: ApEn (m, r, N) = $F^m(r) - F^{m+1}(r)$.
ApEn is independent of a scale or model and evaluates both obvious and obscure patterns in data where discriminatory features may not be clearly identified. Underlying episodic behaviour can be identified using ApEn which may not be clearly reflected in the peak occurrences or amplitude of a waveform (Hornero et al., 2005).

Chapter 2 General methods

In accordance with safety standards for undertaking a clinical trial using a non CE-marked medical device, fEITER met the requirements of the Medical device Directive, received a favourable ethical opinion from South Manchester Local Research Ethics Committee (LREC) and a 'no objection' response from the Medicines and Healthcare products Regulatory Agency (MHRA). The trial was registered as part of a portfolio study with ISRCTN under the following reference 93596854 and consisted of two parts: a volunteer trial and a patient trial.

2.1 Electrode Placement and Connection to fEITER

Anatomical landmarks on the head such as the nasion and inion, conventionally used in EEG electrode placement were used to locate precise areas for electrode placement on the scalp. 32 *ZipPrep*^{TM} (Covidien, UK), self-adhesive electrodes were attached to the scalp by parting the hair of each volunteer using a modified version of the routinely used 10-20 EEG electrode montage (Figure 2.1). An additional reference electrode was placed on the mastoid process of each volunteer. Once attached, all 33 electrodes were plugged into the fEITER head box. fEITER injected sinusoidal current of 1mA (peak to peak) in an opposite current injection pattern using an injection frequency of 10kHz. Current was injected in a randomised sequence between 20 diametrically placed electrode pairs illustrated in Figure 2.2 and listed in Table 2.1. The complete fEITER measurement index is presented in Appendix 1. The resulting serial voltage measurements were simultaneously recorded from pairs of non-injecting electrodes. The total current injection sequence for all electrode pair combinations was completed once every 10ms for a total of 60s. Each frame of data collected for 20 different injection sequences generates 546 voltage measurements. Following 60 seconds of data capturing time with fEITER, a total of 5997 data points are generated per injection sequence. Therefore, a complete fEITER data set considering all 546 voltage measurements captured over a single recording period lasting 60s generates a matrix of 3,270,540 data points.

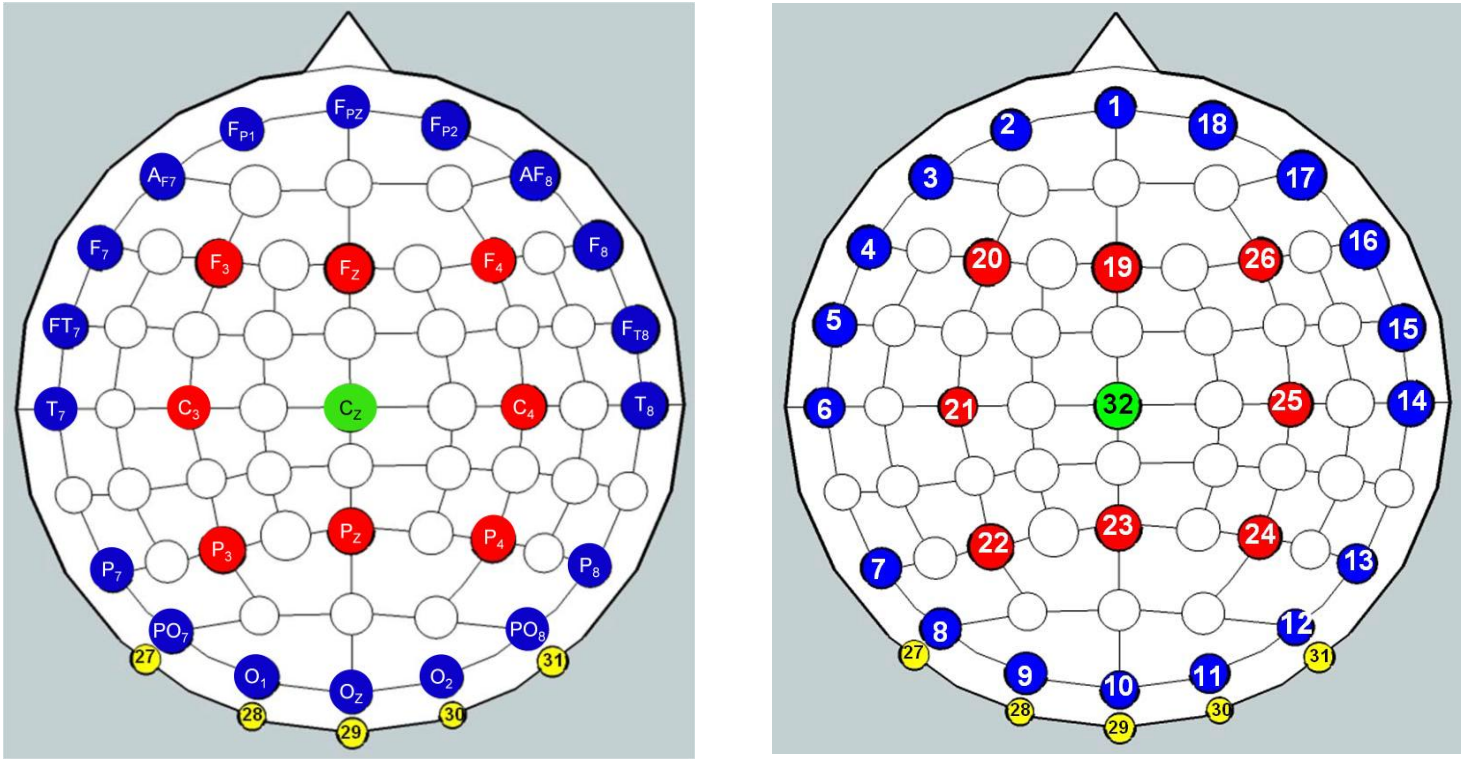

Figure 2.1 fEITER electrode montage. fEITER operates using 32 electrodes placed on the scalp in a montage based on the international 10-20 EEG system. An additional reference electrode is placed on the mastoid process (not shown in this figure). **(a)** Shows the fEITER montage using nomenclature from the 10-20 system; **(b)** shows the montage with numbers corresponding to each electrode position.

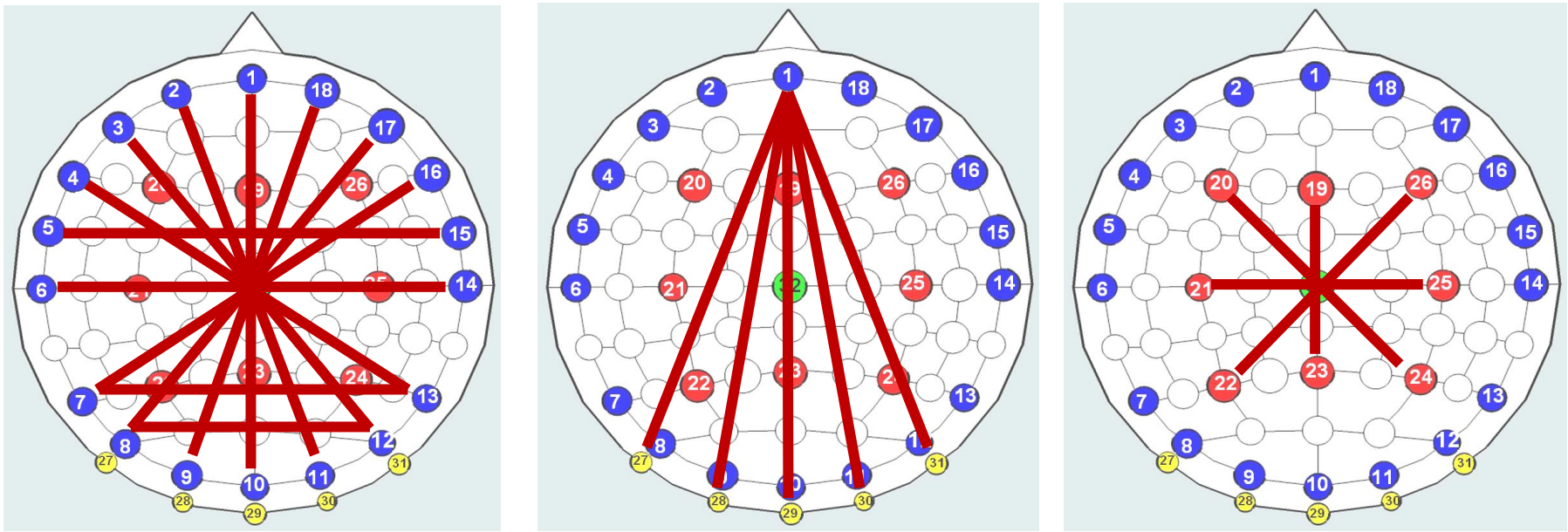

Figure 2.2 fEITER current injection patterns. The 20 different combinations of injection patterns utilised by fEITER are illustrated in this figure. The red lines represent the current injection sequences between 2 diametrically placed electrodes. In total, fEITER injects 20 current injection sequences per frame of data using a10ms frame rate.

Table 2.1 List of fEITER injection sequences. A list of the diametrically placed current injection pairs employed by fEITER which correspond to the illustrations in Figure 2.2.

1-10	2-11	3-12	4-13	5-15
6-14	7-16	8-17	9-18	7-13
8-12	1-27	1-28	1-29	1-30
1-31	19-23	20-24	21-25	22-26

2.2 Data Acquisition

Captured EIT data from the surface electrodes connected to the headbox were converted from a serial input to a parallel communication format by the fEITER base unit using a complex programmable logic device (CLPD) implanted within the base unit. Raw fEITER data was sampled at 500kS/s using a USB DAQCard-6221, the data acquisition and display was controlled by LabVIEW software (Version 7.1, National Instruments, UK) (McCann et al., 2011). Once the data acquisition period of 60s was complete, raw fEITER data was exported into *MATLAB* software (Version 7.10.0.499 – R2010a, The MathWorks, Inc.) where individually acquired voltage measurements were re-shaped to display each frame of data for all the voltage measurements within a single matrix (Appendix 2).

2.3 Bench Testing fEITER

Performance of the fEITER system was validated prior to undertaking volunteer and patient trials, using a mesh and physical phantom.

2.3.1 Measurements using a Mesh Phantom

The mesh resistor phantom used for validation purposes was produced by the Electrical Engineering group based at the University of Manchester consisting of 32 impedance elements. Each impedance element was electrically modeled to consider the Ag/AgCl electrode impedances used on human subjects. The connections were soldered onto a circuit board to directly fit within each of the 34 channels of the fEITER headbox illustrated in Figure 2.3.

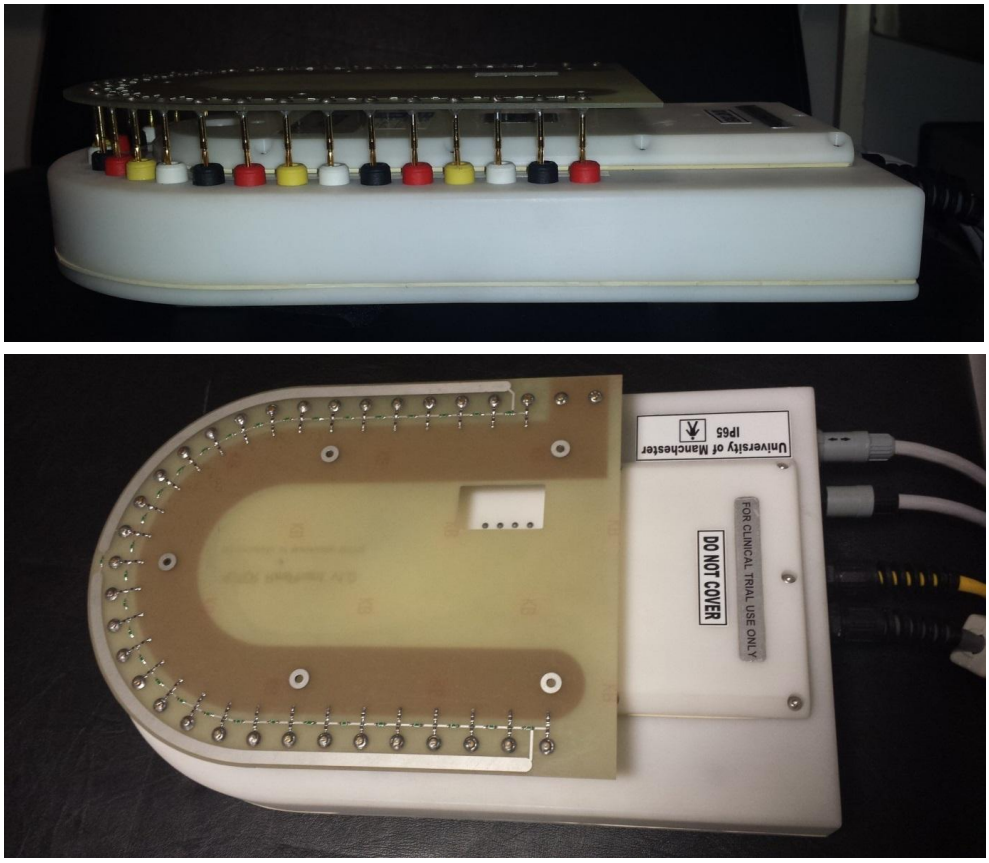

Figure 2.3 Mesh resistor phantom. The resistor phantom was engineered to plug directly into the fEITER headbox using 32 impedance elements.

Once the mesh resistor phantom was connected to the fEITER headbox as illustrated in figure 2.3, data capture using fEITER was commenced. Each data collection period lasted 60s (see section 2.1). Raw voltage measurements were acquired from the mesh phantom (see section 2.2), which were then used to calculate the SNR for the fEITER system. Raw fEITER data was exported into *MATLAB* software (Version 7.10.0.499 – R2010a, The MathWorks, Inc.) where individually acquired voltage measurements were re-shaped to display each frame of data for all the voltage measurements within a single matrix (Appendix 2).

A total of ten measurements were acquired using the mesh phantom in order to calculate an average SNR value. The standard deviation was calculated for each of the 546 voltage pair measurements across an epoch of 900ms (90 frames of data) to represent a sub-second functional response event (McCann et al., 2011). Therefore, a total of 49,140 data points were selected for SNR calculations.

2.3.2 Measurements using a Physical Phantom

Data from historical studies undertaken by the Electrical Engineering group at the University of Manchester was used to calculate SNR of the fEITER system using baseline and perturbation data. A physical phantom was adopted for the study in the form of a cylindrical tank containing 2 rings of 32 Ag/AgCl impedance elements. The elements were embedded into the boundary of the tank and were connected to the fEITER headbox via 32 touchproof leads. The experimental setup of the physical phantom is illustrated in Figure 2.4 The fEITER injection strategy was altered from a head strategy to a cylindrical tank injection strategy. Therefore, the sequence of electrode injection pairs was altered to induce diametric current injections around the boundary of a cylindrical tank. Serial voltage measurements were unchanged. Whereas the current injection strategy designed for the head consists of 546 different voltage measurements for each frame of data, the current injection strategy was designed for a cylindrical tank using two rings of sixteen electrodes consisting of 420 different voltage measurements for each frame of data.

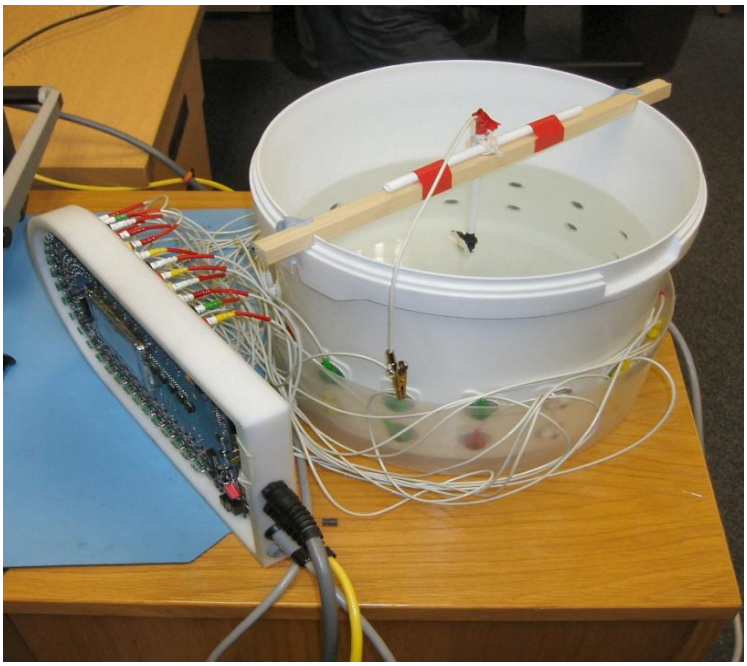

Figure 2.4 Physical phantom attached to the fEITER system. The cylindrical tank was filled with 0.2% saline and was attached to the fEITER head box during original functionality testing of the system at the University of Manchester. The tank contained 32 electrode contact points embedded into its boundary consisting of 16 electrode elements oriented in 2 rings.

The cylindrical tank was filled approximately 4 inches from the top with 0.2% saline solution. A solid object attached to a piece of string was suspended into the centre of the saline-filled tank using a wooden rod balanced on the edges of the tank to induce a contrast in voltage measurements within a homogenous environment (Figure 2.4). The solid object tied to the end of the string was suspended into the tank at the halfway point of fEITER monitoring at 30s. Therefore, 0s to 30s of fEITER recording time without the presence of a perturbation was considered as a baseline measurement whereas 30s to 60s of fEITER recording time following the introduction of the suspended object was considered a perturbation measurement.

Baseline Measurements

fEITER data was captured from the homogenous tank filled with the saline solution. Data was acquired as described in section 2.2 and raw fEITER data was subsequently exported into *MATLAB* software where individually acquired voltage measurements were re-shaped to display each frame of data for all voltage measurement within a single matrix (Appendix 2).

Baseline measurement analysis using fEITER were undertaken between 10s and 20s where no perturbation was introduced within the saline filled tank. The baseline data set used for further analysis consisted of 1000 data points for each injection and measurement electrode pair.
A total of 4 baseline measurements were collected.

Perturbation Measurements

A solid object was suspended centrally into the saline filled tank at 30s of fEITER recording time until 60s of fEITER recording was complete. Perturbation data was analysed from 50s to 60s to allow any movement within the saline-filled tank to settle following insertion of the perturbation. The perturbation data set for each injection and measurement pair consisted of 998 data points.
Once more, data was acquired as described in section 2.2 and was exported into *MATLAB* software. A total of 4 perturbation measurements were captured.

2.3.3 Calculating Signal-to-Noise Ratio (SNR)

Mesh Phantom Analysis

SNR in dB was calculated using the following formula:

$$SNR_i = 20 \log_{10} \frac{E[m_i]}{St.\ Dev[m_i]}$$

Where m_i represents the ith measurement and E represents the average for a particular injection measurement pair across 90 frames of data (Gagnon et al., 2010). The standard deviation (St. Dev) was calculated for each of the 546 measurement pairs across the 90 frames of data.
A single SNR value was calculated for each electrode measurement pair yielding a total of 546 SNR values calculated across 90 frames of data. For each of the 10 resistor phantom test undertaken, the range of SNR values (minimum and maximum) were exported in addition to an average SNR value calculated for each test.
Statistical analysis was undertaken on the exported SNR values using *StatsDirect* statistical software (Version 2.7.9, StatsDirect Ltd). Skewness was obtained between

-1 and 1 for the SNR values yielded from each resistor phantom test undertaken, indicating the data was normally distributed. A parametric test was therefore employed for statistical analysis. Statistical significance was accepted for $p < 0.05$ with a confidence limit of 95%. A box and Whisker plot was also constructed to display variability of the SNR values obtained using a resistor phantom.

Physical Phantom Analysis

Firstly, baseline and perturbation data were isolated from each of the four fEITER recordings. A SNR for each of the 420 injection measurements was calculated for all four fEITER recordings during baseline and perturbation. The 'signal' was defined as the difference between baseline and perturbation means. The 'noise' was calculated by averaging baseline and perturbation standard deviation values. Finally, 'signal' was divided by 'noise' for each of the 420 injection measurements pairs to determine SNR. Values were converted into dB by multiplying SNR values by $20 \log_{10}$.

A mean SNR using the physical phantom was determined by averaging the 420 SNR calculations for each of the four fEITER phantom measurements.

The averaged baseline and perturbation data were tested for normality. Skewness was obtained at 1.23 showing the data was not normally distributed. A box and whisker plot was constructed to display variability of the SNR values obtained.

2.4 Volunteer Trial

20 healthy volunteers were recruited for the trial following receipt of their written, informed consent (Table 2.2). Volunteers were provided with an information sheet and protocol for the trial at least 24 hours prior to recruitment (Appendix 3). Electrode placement and trials were undertaken in a darkened, quiet physiological measurement lab. All volunteers were asked to remain in a sitting position for the duration of the trial.

Each volunteer trial was commenced with a reference measurement where the volunteer was asked to sit still and quietly for the complete minute of fEITER recording time. Similar reference measurements were undertaken at various time-points within the complete trial for each volunteer. To capture evoked responses using fEITER, volunteers were presented with a sequence of visual flashes and were also asked to perform the Valsalva manoeuvre (VM) whilst monitoring using fEITER was undertaken.

Table 2.2 Volunteer demographics The table lists demographics of the volunteers recruited including age at the time of the trial and gender (M = Male; F = Female)

Volunteer number	Gender	Age at time of trial
1	M	47
2	M	37
3	M	38
4	M	47
5	M	29
6	M	41
7	M	55
8	F	56
9	F	25
10	M	56
11	M	48
12	F	29
13	M	34
14	M	46
15	F	31
16	F	35
17	M	56
18	M	46
19	F	41
20	M	36

2.4.1 Visual Stimulation

Visual responses were recorded using fEITER from 14 volunteers recruited for the study as described in section 2.4. fEITER was attached to each volunteer as described in section 2.1. Visual stimulation was presented to volunteers through goggles secured around the head and over the eyes using an elasticated strap. The goggles contained 2 rectangular blocks overlaying the eyes, each consisting of 20 LED light emitting diodes.

The goggles were connected to the fEITER base unit using digital output connectors to deliver a sequence of 20 flashes (1 flash per second) to subjects between 21.5s and 41.7s during a 60s data capturing period. Stimulus delivery was controlled by a digital analogue instruction using *Signal* software (Version 3.09, Cambridge Electronic Design, Ltd.) and the time point of each flash as a stimulus marker was simultaneously captured using *Signal* software.

Goggles were placed over the eyes in the desired position on the volunteer prior to the trial commencing and all volunteers were asked to keep their eyes closed for the total duration of recording time (lasting 60s) to avoid blinking artefact.

2.4.2 Valsalva Manoeuvre (VM)

Fifteen volunteers recruited for the study as described in section 2.4 were asked to perform the VM. fEITER was attached to each volunteer as described in section 2.1. During the fEITER trial, an ECG was simultaneously captured from each volunteer to identify the characteristic features of HR in response to the VM.

The VM was initiated by the volunteer at 10s by pinching the nose and keeping the mouth closed. The strain was held for 15s and released at 25s by commencing to breathe normally through an open airway. The volunteer was directed when to start and end the manoeuvre with a tap on the shoulder by a trial monitor at 10s and 25s. Following release of the manoeuvre, fEITER monitoring continued until 60s were complete. The volunteer remained as still as possible for the remaining 35s of monitoring time and kept their eyes closed throughout the minute. An ECG was captured for each volunteer simultaneous to the fEITER data using the data acquisition *Signal* software (Version 3.09, Cambridge Electronic Design, Ltd.) during the VM trial.

2.5 Patient Trial

20 patients due to undergo elective surgical procedures were recruited for the patient trial. All recruited patients were classified as fit and healthy and therefore graded I and II according to the American Society of Anesthesiologists (ASA) physical status classification system. The ASA classification system is a universal grading system consisting of 5 levels which is used to classify the risk of anaesthesia according to the pre-operative health of surgical patients (Brooks, 2003, Mayberg et al., 1988) (Table 2.3).

Patients were provided with an information sheet and protocol at least 24 hours prior to the trial (Appendix 3). Written, informed consent was gained from each patient. The demographics and surgical procedures for each recruited patient are detailed in Table 2.4. Electrode placement was undertaken on the ward prior to the patient being escorted to the anaesthetic room as described in section 2.1. Once in the anaesthetic room, fEITER was attached to the patient prior to being anaesthetised. Routine clinical practice was not interrupted by the fEITER trial.

Table 2.3 ASA classification scores. The American Society of Anaesthesiologists (ASA) 5 score grading system used to classify the preoperative physical health of patients undergoing a surgical procedure (Daabiss, 2011).

ASA classification	Description
I	Patient is fit and healthy
II	Patient has mild systemic disease
III	Patient has severe systemic disease which is not incapacitating
IV	Patient has severe systemic disease which is a constant threat to life
V	A moribund patient who is not expected to survive 24 hours with or without the surgical procedure

Table 2.4 Patient demographics. Demographics of recruited patients including: age at the time of the trial, gender of each patient (M=male; F=female) and the elective surgical procedure undertaken. Far right column details the amount of propofol administered to each patient.

Patient number (P)	Gender	Age at the time of the trial	Elective surgical procedure	i.v propofol administered (mg)
1	F	75	Cholecystectomy	200
2	F	78	Examination of upper gastrointestinal tract	130
3	M	74	Hernia repair	120
4	M	27	Hernia repair	200
5	M	76	Cholecystectomy	150
6	M	37	Hernia repair	200
7	M	72	Hemihepatectomy	110
8	M	27	Pyeloplasty	250
9	M	43	Hernia repair	200
10	M	50	Hernia repair	250
11	M	39	Hernia repair	250
12	M	65	Lymph node biopsy	150
13	M	70	Nephroureterectomy	200
14	M	68	Prostatectomy	200
15	M	60	Prostatectomy	190
16	M	51	Hemihepatectomy	200
17	M	21	Urethroplasty	150
18	M	53	Hemicolectomy	170
19	M	61	Prostatectomy	170
20	M	67	Liver resection	150

2.5.1 Induction of Anaesthesia

20 patients due to undergo elective surgical procedures were recruited for the trial as described in section 2.5. Electrode placement was undertaken as described in section 2.1 and fEITER was connected to the patient in the anaesthetic room. An intravenous bolus of propofol was administered by the anaesthetist to induce anaesthesia. Data capture using fEITER was commenced 10s prior to the administration of propofol; once fEITER recording commenced at 0s, an interval of 10s was noted by the anaesthetist before the intravenous bolus of propofol was injected at 10s to induce anaesthesia. Data acquisition by fEITER as described in section 2.2, continued until recording time was complete at 60s.

A 3-lead ECG trace was simultaneously recorded using the data acquisition *Signal* software throughout the patient trial. Continuous depth of anaesthesia monitoring was also undertaken using a Bispectral Index® (BIS) monitor (Vista, Covidien) which was updated every 5s (see section 1.5.1.2).

2.6 Data Analysis

Visual Stimulation – Frontal Measurements

fEITER data for 14 volunteers presented with a visual stimulus was imported into *MATLAB* software and pooled onto a single spreadsheet according to the 546 different electrode injection and measurement combinations (*MATLAB* script to import data is provided in Appendix 2). Therefore in the pooled data, a single data point for a particular electrode injection and measurement pair captured using fEITER, was the averaged response across 14 volunteers for that particular frame of data. Using the pooled data, an average baseline value for each electrode injection and measurement pair was calculated using data between 0s and 10s; an epoch consisting of 1000 data points. This period of data capture was considered a reference period where volunteers were sat still with their eyes closed prior to presentation of the visual stimulus. The average baseline value for each electrode injection and measurement pair was then used to calculate percentage differences for each data point within a particular electrode combination. This yielded a matrix containing percentage differences from baseline for each electrode injection and measurement pair across all 14 volunteers. Maximum percentage difference values for each electrode injection and measurement pair were selected from the data points

following delivery of the first visual flash at 21.5s until the end of the trial at 60s. These values were then sorted in order of size to yield a list of electrode injection and measurement pairs ranging from the pair which recorded the greatest percentage difference, to the smallest percentage difference value. The electrode measurement pair which yielded the greatest percentage difference following presentation of the first visual flash was identified as F_{PZ}_O_Z_AF_8_F_{P2}_ (inj_inj_meas_meas) which is referred to as 1_10_17_18 from here onwards. This electrode injection measurement pair was therefore isolated from each volunteer for further analysis. fEITER reference data for visual stimulation measurements was isolated from 0s to 20s prior to the first flash being presented to volunteers and consisted of 2000 data points,. The data signal captured at 1_10_17_18 for each volunteer was filtered for REG and high frequency noise (HFN).

Visual stimulation – measurements overlying the visual cortex

From published literature it is evident that the primary target for retinal stimulation using visual flashes is the primary visual cortex (Maier et al., 1987, Walsh et al., 2005). fEITER data captured from electrodes overlying the visual cortex was therefore selected for analysis to further explore EIT changes in a known area of activation during visual stimulation. For 13 volunteers presented with a visual stimulus the current injection pair F_{PZ}_I_Z (1_29) was selected for further analysis due to the injection pair being located centrally to the visual cortex. For all volunteers, measurement channels overlying the visual cortex in response to the current injection 1_29 were imported from *MATLAB* software into *Spike2* software in order to be visualised simultaneously in a single trace. The measurement pair e_{27}_e_{28} (27_28) was selected for further analysis as all measurements recorded from this particular measurement pair were deemed viable and contained no zero values.

Valsalva Manoeuvre (VM)

Raw fEITER data for 15 volunteers during the VM along with corresponding ECG data was firstly exported into *MATLAB* software and subsequently transferred into *Spike2* software (Version 7.03b, Cambridge Electronic Design, Ltd.) where the data was normalised for eyeballing (*Spike2* script is provided in Appendix 2).

Spike2 software was chosen to evaluate fEITER data captured during the VM for a number of reasons. Firstly, the software enables 500 waveforms to be visualised at once which was a desirable feature to eyeball and compare 546 channels of fEITER data captured during a single monitoring period. Secondly, the software also allows individual channel waveforms to be observed more closely. As the VM was a much larger stimulus compared to visual stimulation, fEITER channels which showed a more prominent response could be easily identified and compared visually. Finally, *Spike2* software enables the ECG to be imported and evaluated simultaneously with changes observed in fEITER waveforms during the VM.

From previous literature it is established that the VM affects blood flow velocity in the middle cerebral arteries. Imported waveforms visualized in *Spike2* software showed channels capturing fEITER data at the front of the head showed a greater response to the VM and also had a clear REG waveform. Therefore, a single measurement electrode pair attached to the area of the head overlying the middle cerebral artery territory was selected for further analysis for all volunteers performing the manoeuvre: 17_18. The injection electrode pair 1_10 was also chosen for further analysis due to its anatomical location of current injection along the middle cerebral arteries and also for comparative purposes to the frontal channels isolated from the same volunteers for further analysis in response to visual stimulation. fEITER reference data from VM measurements was isolated from 0s to 10s prior to volunteers initiating the VM, and consisted of 1000 data points. The data signal captured at 1_10_17_18 for each volunteer was filtered for REG and high frequency noise (HFN).

Induction of Anaesthesia

Raw fEITER data captured from each of the 20 patients during induction was firstly exported into *MATLAB* software and then transferred into *Spike2* software where the data was normalised for eyeballing as described in section 2.6 *Valsalva Manoeuvre (VM)*.

From neuroimaging research studies it has been noted that induction of anaesthesia using propofol leads to prominent functional changes in frontal regions of the brain (Långsjö et al., 2012, Zhang et al., 2010). Visual analysis of frontal fEITER measurements recorded during induction of anaesthesia in *Spike2* software

confirmed prominent changes occurring in frontal measurement channels following induction with propofol. Injection and measurement pair 1_10_17_18 were therefore selected for further analysis for all patients who underwent induction using propofol. Once more, the chosen injection measurement pair was also selected due to its anatomical location along the middle cerebral artery.

fEITER reference data from induction measurements was isolated from 0s to 10s prior to the intravenous bolus of propofol being administered, and consisted of 1000 data points. The data signal captured at 1_10_17_18 for each patient was filtered for REG and HFN.

2.6.1 Filtering the REG Frequency

Power spectral density (PSD) estimation was used to identify the REG frequency in the reference data of all volunteers and patients. PSD is a useful signal processing application which displays the variations in power of a signal, as a function of frequency (Stearns, 1990, Kuc, 1988). As the fEITER signal is a representation of varying electrical quantities of voltage against time, Fourier analysis was applied to the waveform to examine its spectral content. Fourier analysis and Fourier transforms explore the relationship between a time domain of a signal and the corresponding frequency domain by assuming that signals are composed of a number of sinusoidal signals. Therefore, a given signal can be represented as a linear arrangement of multiple sinusoidal signals and one can determine the frequency components of the overall signal by examining the frequencies, amplitudes and phases of the individual sinusoidal signals which the given signal is made up of (Sinha, 2010, Brigham, 1988).

PSD is best estimated by computing the autocorrelation of the data sequence and windowing this to reduce variance before calculating the Fourier transform of the result. In-depth guides to estimating PSD are available from various sources of literature (Champeney, 1974, Texas-Instruments, 1980, Papoulis, 1962). To identify the REG frequency from fEITER waveforms, the latter PSD estimation method was used where firstly autocorrelation of the sample data was determined to effectively remove phase and trends from the data signal to ultimately produce a clean PSD estimate. The autocorrelated data was then multiplied by an appropriate window function before the Fourier transform of the product was computed.

Each step of the PSD estimation and filtering undertaken in *MATLAB* software is illustrated in Figures 2.5-2.7 (script provided in Appendix 2). Data sequences for each volunteer and patient were imported into *MATLAB* software. Firstly, the reference measurements were isolated from the total signal (Figure 2.5a). The sample autocorrelation of the reference data was determined (Figure 2.5b) before a Hanning window function was applied (Figure 2.5c). Finally, the Fourier transform of the product was computed (Figure 2.5d).

As suggested by clinical data, the REG waveform was observed at a frequency almost simultaneous to heart rate at approximately 1Hz (Bodo, 2010). Once the REG frequency was identified, first order differencing was applied to the whole data signal prior to filtering the REG (Figure 2.5e-f). An inherent feature of EIT signals is a baseline drift which is primarily attributed to contact impedance between the electrode and skin surface. As a result, clinical EIT measurements are known to be highly non-linear as changes in tissue impedance do not result in linear changes of recorded voltage measurements captured at the skin surface (Bayford, 2006). For the effective application of signal processing techniques to a time series data such as EIT measurements captured using fEITER over time, it is necessary to stationarise the signal. A stationary time-series reflects a data series which is constant over time, therefore descriptive statistical properties over time such as mean and variance remain constant throughout the time series. Conversely, a time-series which is not stationary will have a varying mean over time therefore rendering the application of further signal processing techniques to analyse the time-series less effective. To remove the effects of drifting within the raw EIT signals and to stationarise the signal, first-order differencing was applied to fEITER data. First order differencing effectively removes trends and cycles such as a drift within a time-series data whilst preserving the fundamental signal. First order differencing is undertaken by computing the difference between consecutive data points i.e. subtracting one point from another (Chatfield, 1989, Nason, 2006, Biglan et al., 2000).

A Hanning window was applied to the first 100 points of the differenced data signal to remove any offset within the data and ensure the first data point is a zero value. Finally, a band pass filter using *MATLAB* software was applied to the windowed data to filter out the REG frequency occurring at approximately 1Hz. The REG signal typically manifests as a sawtooth waveform thought to reflect physiological changes in intra-cerebral and extra-cerebral blood flow at a frequency similar to heart-rate

(Bodo, 2010) (see section on REG). Although the exact cut off points specified for the band pass filter varied for all volunteers, the most dominant frequency of 1Hz was incorporated into the band pass filter. Therefore, all band pass filtering frequencies which were applied to fEITER data, varied between the ranges of 0.71Hz and 1.73Hz using a filter order of 5.

An example data signal filtered for REG is illustrated in Figure 2.5f (MatLab script used for filtering is provided in Appendix 2). Figure 2.6 shows the PSD estimation of differenced fEITER data prior to (Figure 2.6a) and following the band pass filter for REG (Figure 2.6b). The most dominant frequency at approximately 1Hz has been filtered out from the data and is absent in Figure 2.6b. An attempt to filter out the remaining REG frequency spectrum greater than 1Hz using a second band pass filter or using a band pass filter encompassing a greater range of low frequencies resulted in a loss of low frequency components in the fEITER signal as illustrated in Figure 2.6c. Therefore, only the most dominant REG frequency as identified in Figure 2.5d was filtered from the fEITER data.

a.)

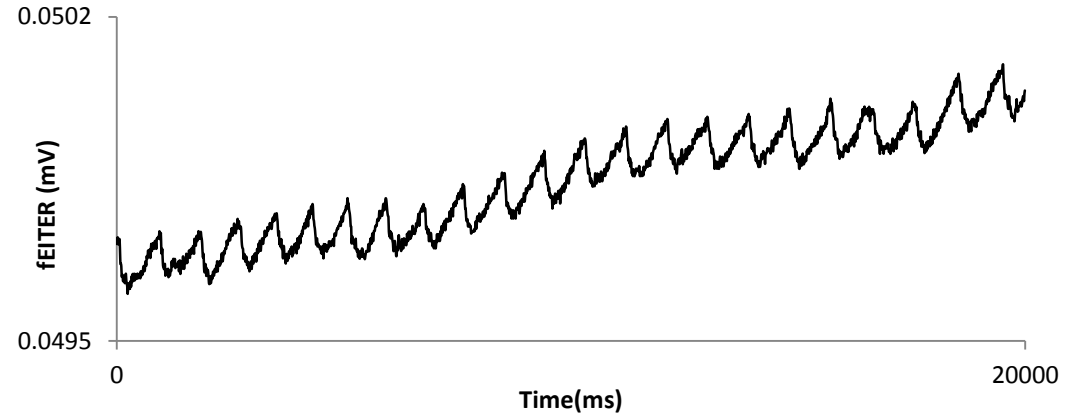
0.0502
fEITER (mV)
0.0495
0
20000
Time(ms)

b.)

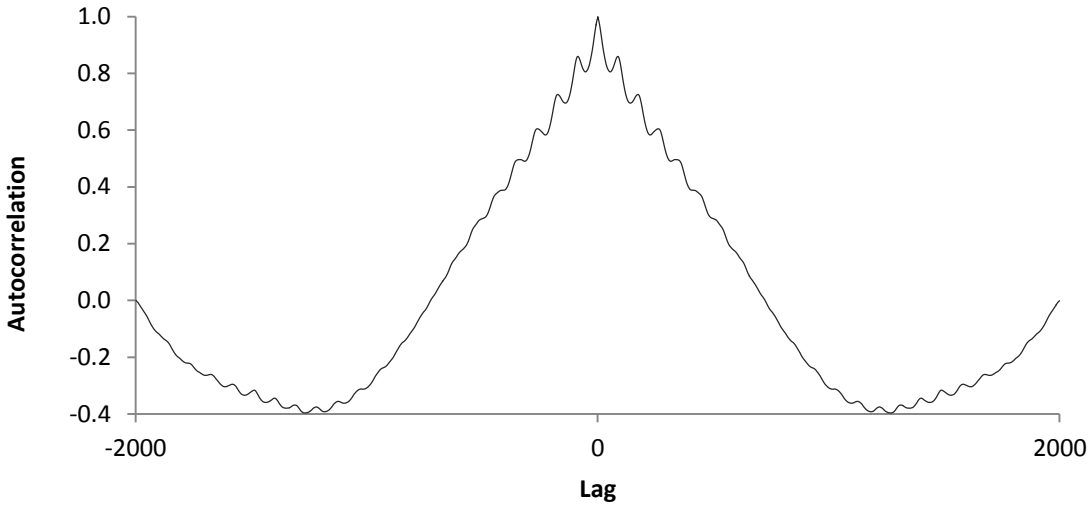
1.0
0.8
0.6
0.4
0.2
0.0
-0.2
-0.4
Autocorrelation
-2000
0
2000
Lag

c.)

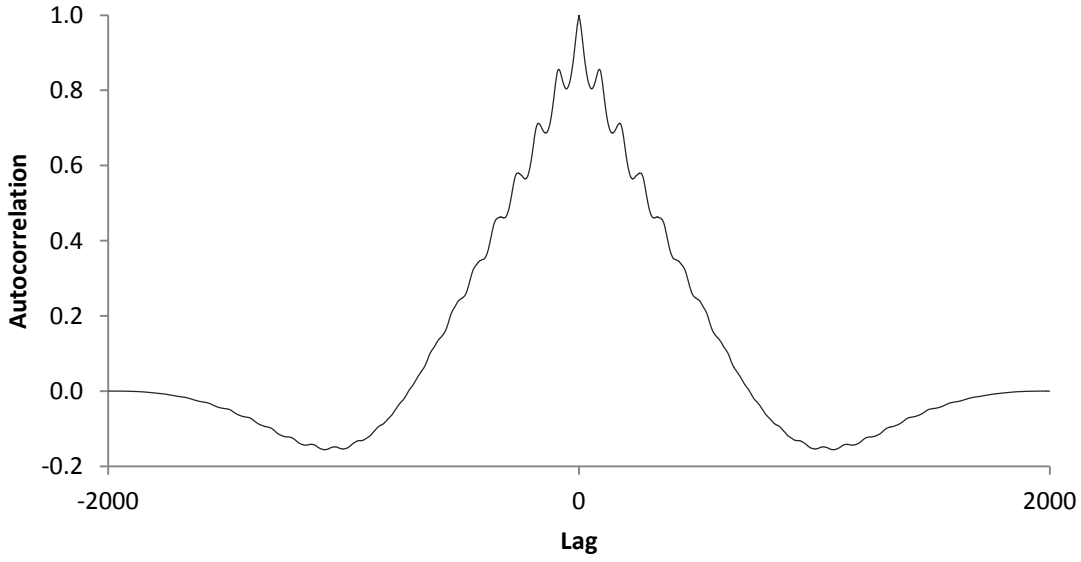
1.0
0.8
0.6
0.4
0.2
0.0
-0.2
Autocorrelation
-2000
0
2000
Lag

d.)

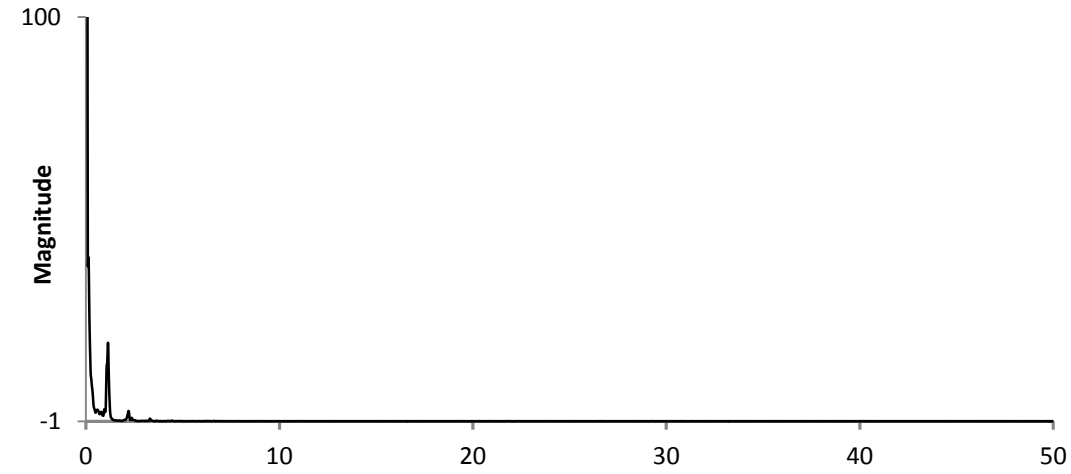
100
Magnitude
-1
0
10
20
30
40
50
Frequency (Hz)

e.)

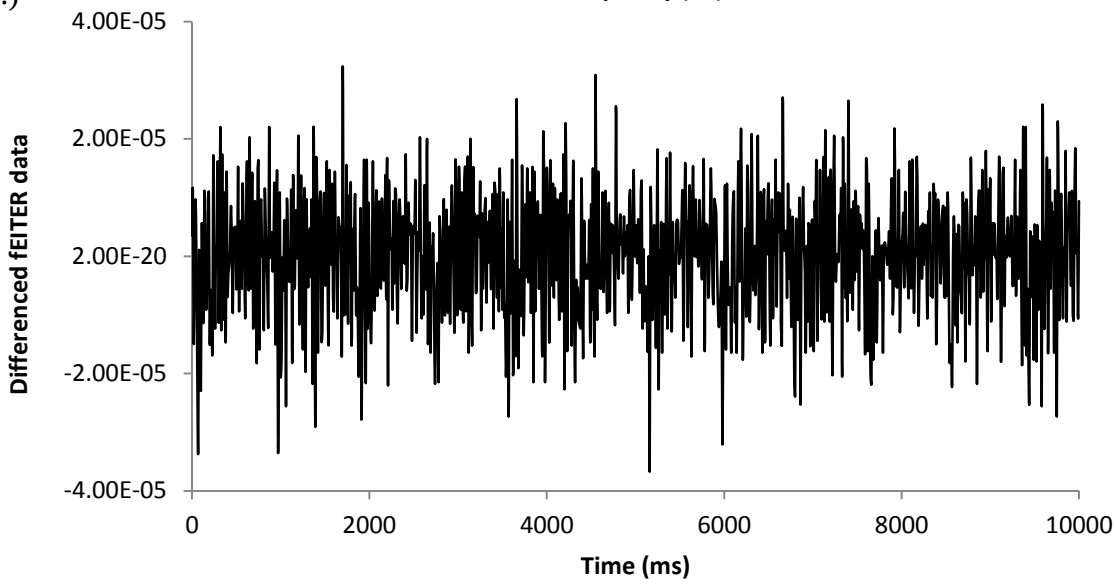
4.00E-05
2.00E-05
2.00E-20
-2.00E-05
-4.00E-05
Differenced fEITER data
0
2000
4000
6000
8000
10000
Time (ms)

f (i)

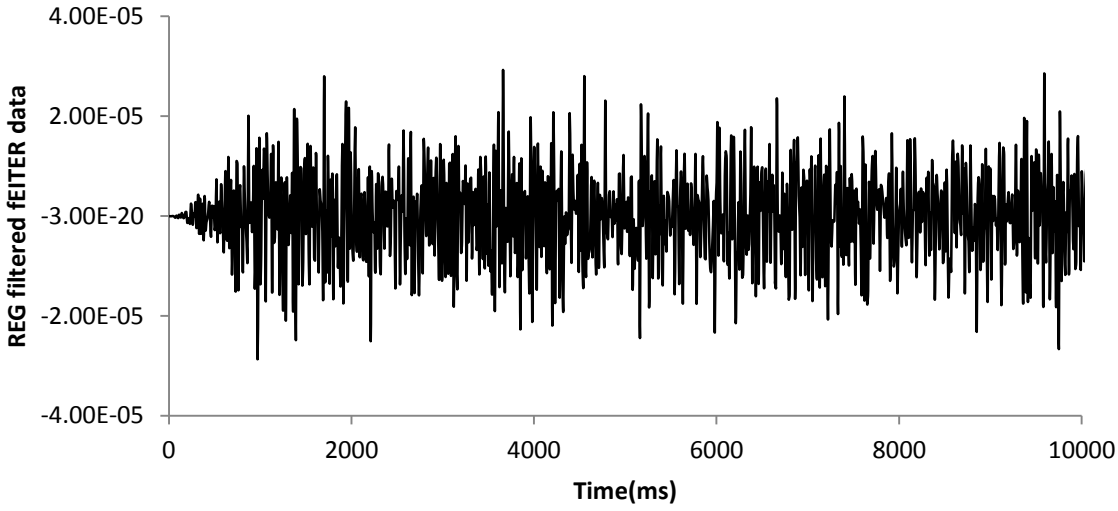
4.00E-05
2.00E-05
-3.00E-20
-2.00E-05
-4.00E-05
REG filtered fEITER data
0
2000
4000
6000
8000
10000
Time(ms)

f (ii)

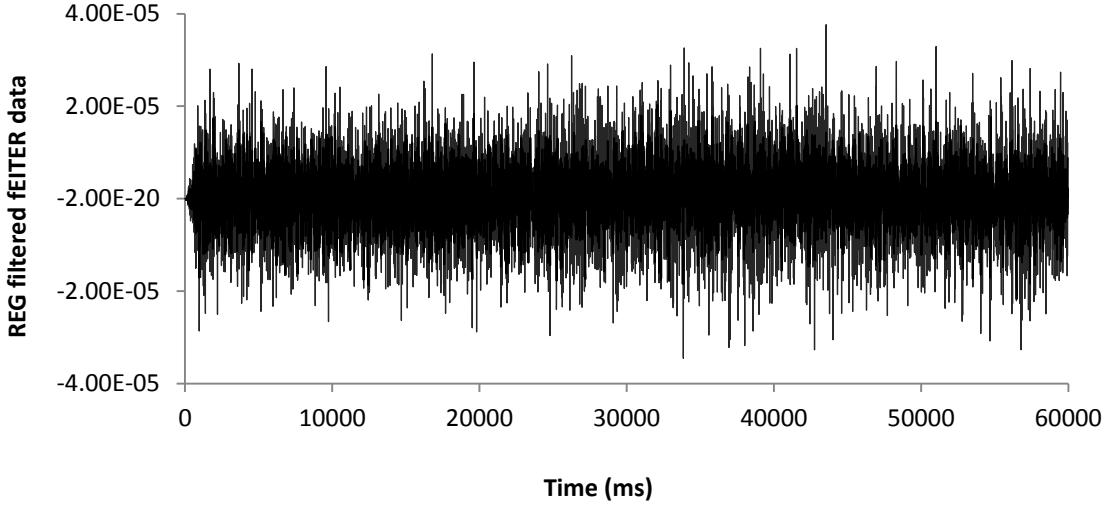

Figure 2.5 PSD estimation: a.) Raw fEITER data for the reference period consisting of 2000 data points. **b.)** Autocorrelation of the reference data signal. **c.)** Autocorrelated data has been windowed using the Hanning window function. **d.)** Fourier transform of the windowed product showing the PSD estimation. **e.)** First order differencing was applied to the whole fEITER data signal consisting of 5997 data points **f(i).** fEITER data signal which has been filtered for REG using a band pass filter, 0s to 10s of the data is displayed. **f(ii)** Complete 60s of fEITER data signal which has been filtered for REG.

a.)

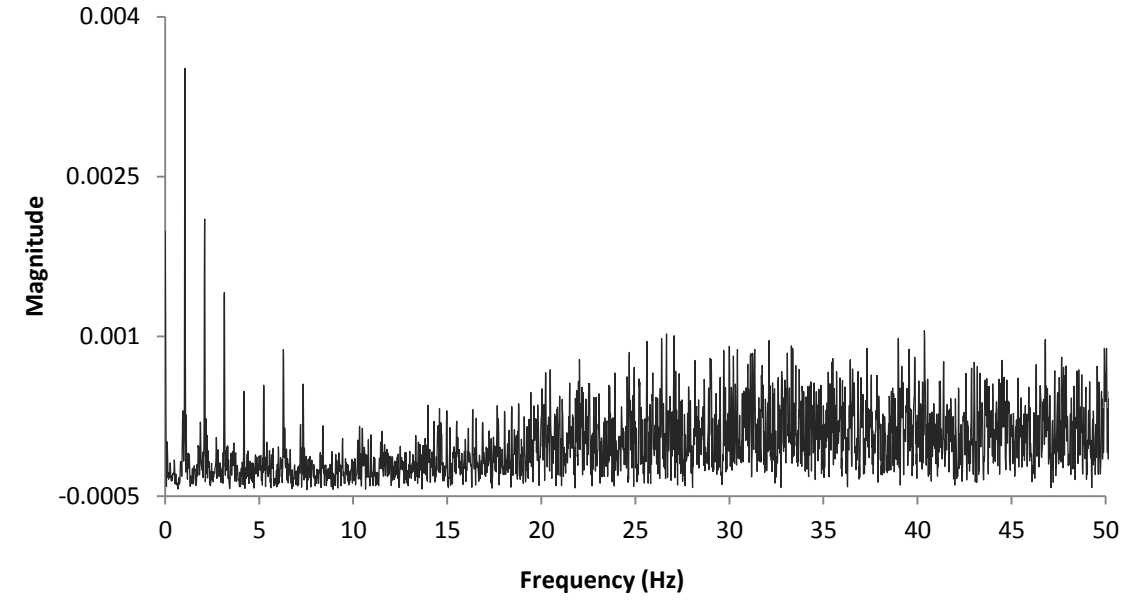
0.004
0.0025
0.001
-0.0005
Magnitude
0
5
10
15
20
25
30
35
40
45
50
Frequency (Hz)

b.)

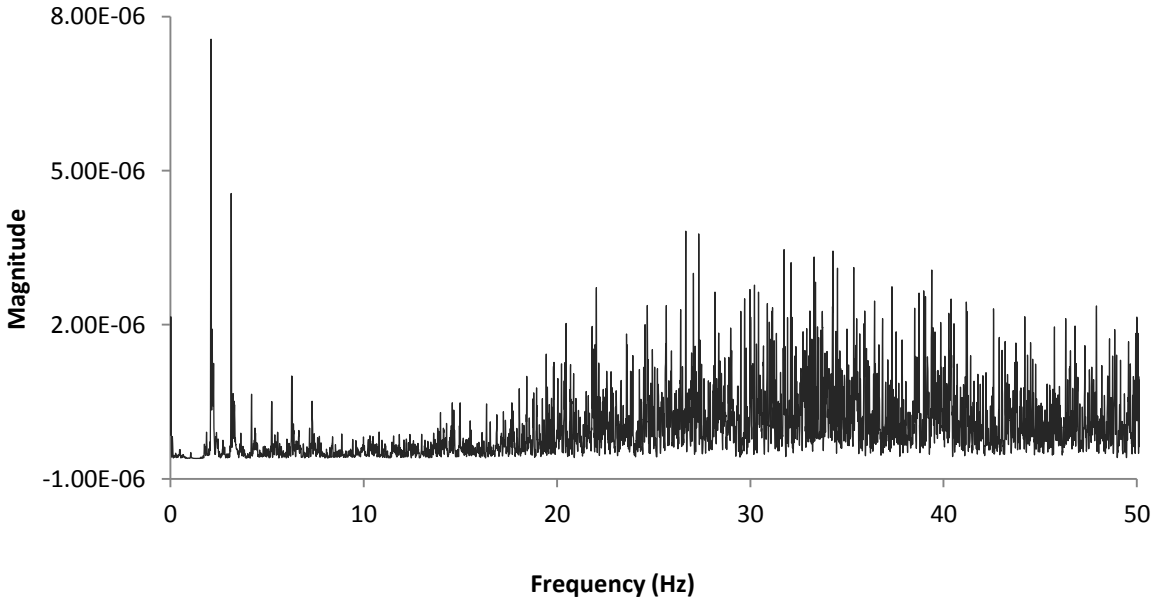
8.00E-06
5.00E-06
2.00E-06
-1.00E-06
Magnitude
0
10
20
30
40
50
Frequency (Hz)

c.)

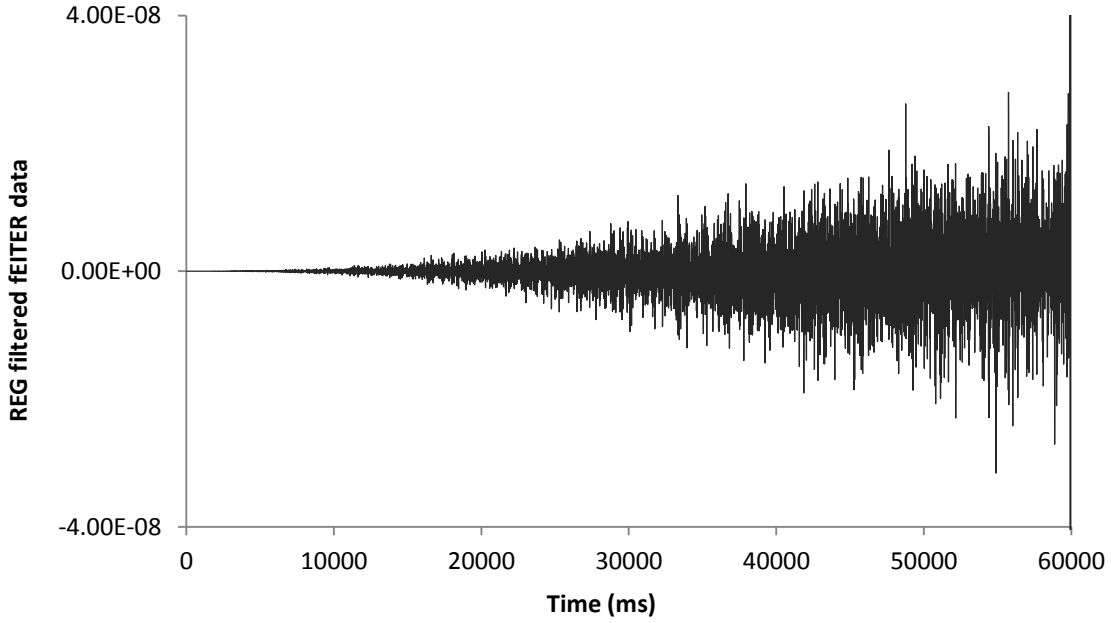

Figure 2.6 PSD estimation of differenced fEITER data: a.) PSD estimation of first order differenced fEITER shown in Figure 2.5. This figure of PSD estimation displays the low frequency spectrum of the REG. The most dominant frequency of REG can be identified at approximately 1Hz. **b.)** PSD estimation of first order differenced data which has been filtered for REG using a band-pass filter as described in Figure 2.5f. The most of dominant frequency of REG occurring at 1Hz is absent following the application of a band pass filter. **c.)** Resulting fEITER data filtered for REG using a large band pass filter frequency range to encompass the REG frequencies identified in Figure 2.6b. A loss of low frequency components are displayed.

2.6.2 Filtering High Frequency Noise (HFN)

Once REG was filtered from the data signal, a second PSD estimate was applied to the filtered signal to identify HFN components (Figure 2.6b). Similar to the PSD method described in section 2.6.1, the sample autocorrelation of the whole filtered signal was determined before applying a Hanning window to the whole signal. Finally HFN components were identified by computing the Fourier transform of the filtered signal. To remove HFN components, a low pass filter was applied using a signal frequency value and a filter order of 2 in *MATLAB* software. A frequency of 3.69Hz was used in the low-pass filter and was applied to all REG filtered data signals (script for HFN filtering provided in Appendix 2). Figure 2.7a and 2.7b illustrates an example fEITER data signal in its raw form and once it has been filtered for REG and HFN.

a.)

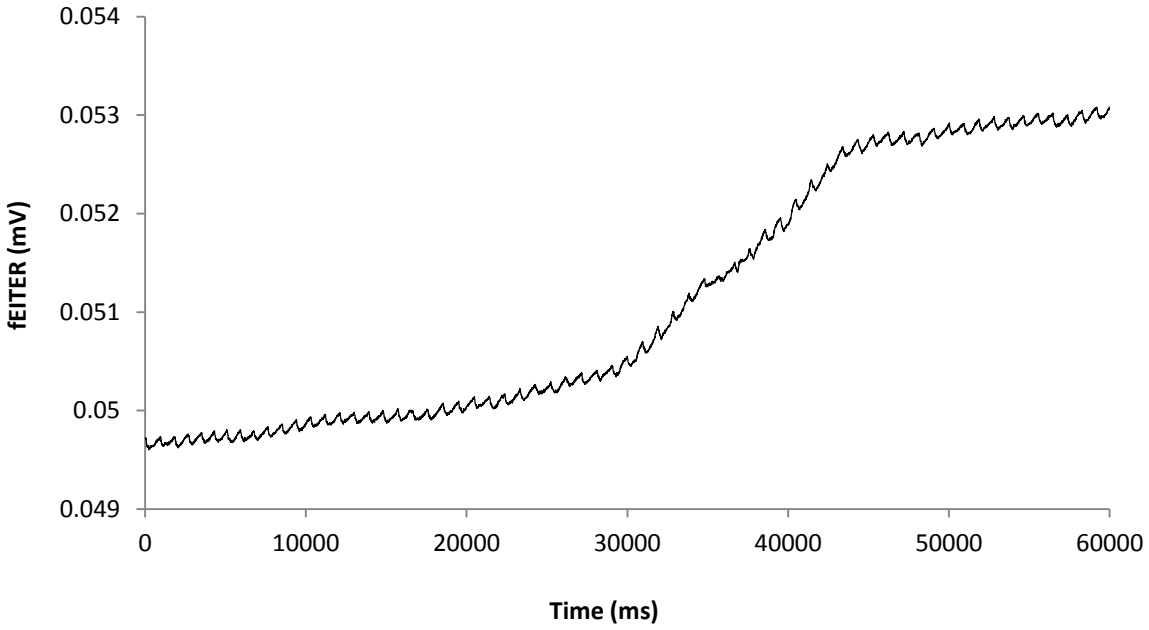

b.)

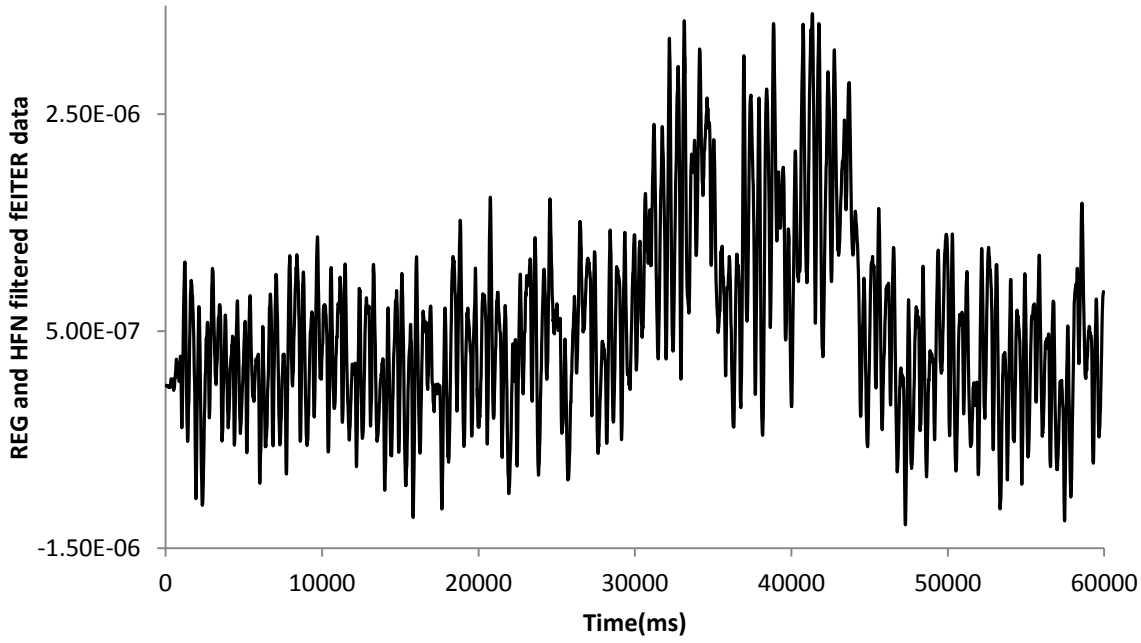

Figure 2.7 fEITER data filtered for REG and HFN: a.) Raw fEITER data captured from an individual volunteer during the presentation of a visual flashing sequence which commenced at 21s. **b.)** Graph displaying fEITER data illustrated in Figure 2.7(a) which has been differenced and filtered for REG and HFN.

2.6.3 Histograms of Multiple Comparisons

Previous analysis of fEITER data comprised of comparing single epochs of reference and stimulus data. Whilst statistical comparisons between reference and stimulus data yielded significantly different results, comparisons between two epochs within a reference measurement were also shown to be significantly different. To compensate for the highly varied characteristic of the fEITER waveform consisting of continuous perturbations, it was deemed more appropriate to undertake multiple comparisons between randomly selected epochs of data from the filtered waveforms. Multiple comparisons were used to reveal the statistical compatibility when exploring reference-reference comparisons versus reference-stimulus comparisons.

REG and HFN filtered data signals for each volunteer were imported into *MATLAB* software and multiple comparisons of randomly selected samples from reference and stimulus sections of the data were undertaken. Reference and stimulus sections of the filtered data were specified within the *MATLAB* code. The number of random samples to be selected was defined as 5000 using a sample length of 50 data points for each comparison. As a total, 5000 comparisons were deemed sufficient to encompass the complete reference and stimulus periods of data therefore providing a comprehensive comparison of the whole reference and stimulus periods of data.

Two random samples selected from the specified reference section were used to calculate a t-statistic reference value using mean and standard deviation values yielded from the 2 samples. This process was repeated 5000 times using randomly selected data segments from reference data. Secondly, mean and standard deviation values from one randomly selected reference sample and one randomly selected stimulus section were used to produce a t-statistic stimulus value. Once more, this comparison was repeated 5000 times using randomly selected data segments from reference and stimulus data. Therefore, two columns consisting of 5000 t-statistic values were produced for each volunteer. One column represented t-statistic values from reference-reference comparisons, whereas the second column contained t-statistic values generated from reference-stimulus comparisons. It was anticipated that t-statistic stimulus values produced from the latter comparison between reference and stimulus samples would generate a higher t-statistic value indicating a larger variation between the mean of randomly selected reference and stimulus samples. A lower t-statistic value was expected from the comparison of randomly

selected samples from the reference segment of data indicating a greater probability of means from reference samples being similar to each other. To demonstrate the difference in t-statistic values yielded from the multiple comparisons of randomly selected samples, two histograms were produced for each volunteer representing the distribution of t-statistic values derived from the comparison of randomly selected reference samples *vs*. reference samples and reference samples *vs.* stimulus samples. For each volunteer, two columns of data were yielded: t-statistic reference and t-statistic stimulus. Finally, the two columns of data generated for each volunteer/patient (t-statistic reference and t-statistic stimulus) were pooled for the total number of volunteer/patients. The pooled data was then used to produce a single histogram representing the pooled distribution of t-statistic values from multiple random comparisons undertaken across all the volunteers/patients (script for multiple comparison and histograms is provided in Appendix 2).

2.6.4 Producing ROC Curves

Using the t-statistic values calculated from the comparison of randomly selected segments from reference and stimulus measurements as described in the previous section (2.6.3), ROC curves were produced for each volunteer as an alternative method to visually represent the statistical compatibility of the comparisons undertaken. ROC curves are traditionally used as a tool to evaluate the ability of a diagnostic test to predict a dichotomous result (positive/negative), usually reflecting the presence or absence of a clinical condition (Florkowski, 2008, Hajian-Tilaki, 2013). The true positive rate, also described as sensitivity, is plotted against the false positive rate which is also described as 1-specificity. In relevance to clinical diagnosis, the sensitivity describes the probability of a positive test when a disease or condition is present. This is plotted against the probability of a positive test when the disease or condition is absent (1-specificity). Data can therefore be divided into two columns, one representing results where a condition tested for is known to be present and the other representing test results in known negative cases.

The two columns of t-statistic values for individual subjects were imported from *MATLAB* software into *StatsDirect* statistical software (Version 2.7.9, StatsDirect Ltd). To produce the ROC curves, t-statistic stimulus values were assigned as the true positive rate (sensitivity) and t-statistic reference values were assigned as the

false positive rate (1-specificity). A single ROC curve was produced per volunteer/patient. Area under the ROC curve (AUC) was calculated in *StatsDirect* software using the extended trapezoidal rule (Hanley and McNeil, 1982, Fawcett, 2006b, Bradley, 1997, Hajian-Tilaki, 2013). A single ROC curve was produced using pooled t-statistic values across all volunteers/patients and once more AUC for the pooled ROC curves was calculated as described above. A maximum AUC value of 1 indicates the comparison is highly effective in differentiating between the two groups and there exists no overlap between the two groups being tested. An AUC value of 0.5 indicates that there is no discrimination between the two groups. Therefore, a greater difference in t-statistic ref and t-statistic stim values would be reflected by a AUC value closer to 1. Comparisons where t-statistic ref values were indistinguishable from t-statistic stim values would be reflected in the generated ROC curves with an AUC close to 0.5.

2.7 ApEn Analysis

ApEn was applied to fEITER measurements in order to analyse the subtle changes which may be present in high frequency components within the fEITER signal in response to stimulation. REG was filtered from fEITER data as it is a highly regular component of acquired signals which could dominate ApEn results. Once REG was filtered, ApEn was applied to reference and stimulus fEITER data to explore any changes in high frequency components in response to visual stimulation, the VM and induction of anaesthesia.

2.7.1 ApEn applied to Visual Stimulation Data

Frontal Measurements

Frontal measurements (1_10_17_18) from 14 volunteers during visual stimulation were isolated as described in section 2.6 *Visual stimulation – frontal measurements*. As described in section 2.6.1, REG was filtered from the data signal of each volunteer using a band pass filter.

To calculate ApEn, REG filtered data signals for each volunteer were sectioned for reference and stimulus measurements. Reference measurements captured prior to any visual stimulation were isolated between 0s and 20s and consisted of 2000 data

points. Stimulus measurements were isolated during the stimulus period where visual flashes were presented between 21.5s and 41.5s, and also consisted of 2000 data points. ApEn was calculated for reference and stimulus conditions for each volunteer data set using *MATLAB* software (Script provided in Appendix 2).

Measurements overlying the Visual Cortex

ApEn was also applied to data acquired from anatomical locations overlying the visual cortex of 13 volunteers. It is evident from literature that the primary target of visual stimulation using flashes is the visual cortex. This has been confirmed by imaging studies using fMRI and electrophysiological studies using EEG to capture VEPs from the visual cortex (Di Russo et al., 2002, Lee et al., 1991). Therefore ApEn was applied to fEITER data captured from areas overlying the visual cortex to explore any changes in measured voltages in response to visual stimulation. The current injection pair F_{PZ}_I_Z (1_29) was selected for further analysis using ApEn due to the injection being located centrally to the visual cortex. For all volunteers, measurement channels overlying the visual cortex in response to the current injection 1_29 were imported from *MATLAB* software into *Spike2* software in order to be visualised simultaneously in a single trace. The measurement pair e_{27}_e_{28} (27_28) was selected for further analysis as all measurements were deemed viable captured from this particular measurement pair and no zero values were recorded.
REG was filtered from the selected injection measurement pair 1_29_27_28 as described in section 2.6.1 using a band pass filter. From 13 volunteers, a REG frequency could not be identified in 3 volunteers. For these volunteer responses where REG could not be identified, first order differencing was applied to remove any effects of drifting from the data signal prior to further analysis using ApEn. Reference measurements captured prior to any visual stimulation were isolated between 0s and 20s and consisted of 2000 data points. Stimulus measurements were isolated during the stimulus period where visual flashes were presented between 21.5s and 41.5s, and also consisted of 2000 data points. ApEn was calculated for reference and stimulus conditions for each volunteer using *MATLAB* software (Script provided in Appendix 2).

2.7.2 ApEn applied to VM Data

Frontal measurements (1_10_17_18) from 15 volunteers who undertook the VM were selected as described in section 2.6 *Valsalva Maneouvre (VM)*. As described in section 2.6.1, REG was filtered from the data signal of each volunteer using a band pass filter.

To calculate ApEn, REG filtered data signals for each volunteer were sectioned for reference and stimulus measurements. Reference measurements captured prior to the VM being initiated were selected between 0s and 10s and consisted of 1000 data points. Stimulus measurements were selected between 10s and 25s, during the VM being performed, and consisted of 1500 data points. ApEn was calculated for reference and stimulus conditions for each volunteer using *MATLAB* software (Script provided in Appendix 2).

2.7.3 ApEn applied to Induction of Anaesthesia Data

Frontal measurements (1_10_17_18) from 20 patients who underwent anaesthetic induction were selected as described in section 2.6 *Induction of Anaesthesia*. As described in section 2.6.1, REG was filtered from the data signal of each patient using a band pass filter. The induction of anaesthesia period was regarded from the administration of propofol at 10s until complete induction of anaesthesia which continued until 60s. Therefore, for valid ApEn calculations comparing a similar number of data points between reference and stimulus conditions, individual reference measurements lasting 60s which were recorded at 1_10_17_18 from each patient were also selected. REG was filtered from reference measurements of each patient as described in section 2.6.1 using a band pass filter. ApEn was calculated for reference measurements consisting of 5997 data points for each patient. For stimulus conditions, ApEn was calculated from induction of anaesthesia measurements using data captured from the administration of propofol at 10s until induction of anaesthesia was complete at 60s. This data set consisted of 4998 data points (Script provided in Appendix 2).

2.7.4 Choice of Constant ApEn Parameters

Based on previous statistical validation studies undertaken, the fixed values of *m* and *r* were set at *m*=2 and *r*=0.25 x standard deviation respectively (Pincus, 1991, Pincus et al., 1993, Pincus and Goldberger, 1994a). Setting *m* as 2 for data sets consisting of 1000 or more data points has been shown to provide statistically valid ApEn values. While a large data set may look regular, setting *m* to higher values will typically result in small, or even zero matches for segments of data. Setting *m* as 2 allows a greater number of matching segments to be identified whilst also being superior to *m*=1. As the specified selections of data consisted of 1000 or more data points, *m*=2 was deemed acceptable to reliably calculate ApEn.

The constant parameter *r* is selected as a tolerance filter between the values of 0.1 x standard deviation and 0.25 x standard deviation. Pincus and Goldberger (1994b) described smaller values of *r* resulting in inaccurate probability estimates whereas larger values of *r* greater than 0.25 x standard deviation can cause a loss of relevant information due to tolerance levels being larger than the signal structure. For the present study, a tolerance level of 0.25 x standard deviation was chosen based on statistical validity achieved using this filter level described in literature (Pincus, 1995, Pincus and Goldberger, 1994b). In addition, the SNR for fEITER has been reported as being larger than 3dB (McCann et al., 2011) which satisfies the constant parameters of *m* and *r* to gain reliable statistical validity (Pincus and Goldberger, 1994a).

2.7.5 Statistical Analysis of ApEn Data

In total, four sets of ApEn values were generated consisting of reference and stimulus values for the following trials: **1)** Visual (frontal), **2)** Visual (visual cortex), **3)** Valsalva manoeuvre and **4)** Induction of anaesthesia.

ApEn values calculated for reference and stimulus data for each trial condition were exported from *MATLAB* into *StatsDirect* statistical software for statistical analysis. For each trial condition, reference ApEn values were statistically compared to stimulus ApEn values using a Wilcoxon's signed ranks test. Statistical significance was accepted for an upper sided $p < 0.05$ corresponding to a confidence limit of 95%.

Chapter 3 Results

3.1 Validating the fEITER System using Phantoms

3.1.1 Mesh Resistor Phantom

The average, minimum and maximum values for SNR calculated from each of the 10 mesh resistor phantom trials undertaken are presented in Table 3.1.

Table 3.1. fEITER SNR values from a mesh resistor phantom. Average SNR values calculated from ten consecutive resistor phantom tests. Each SNR value was calculated using 90 frames of data then averaged across the 546 measurement pairs.

Resistor phantom test	Average SNR value (dB)	Minimum SNR value (dB)	Maximum SNR value (dB)
1	63.38	36.51	96.01
2	63.52	36.32	97.27
3	63.31	36.56	98.04
4	63.33	36.47	98.12
5	62.94	36.37	95.21
6	63.34	36.29	95.64
7	63.58	36.37	96.51
8	63.14	36.39	97.61
9	63.00	36.74	97.79
10	63.32	36.43	96.86

The average SNR calculated for 10 consecutive resistor phantom trials ranged between 62.94 and 63.58dB (Table 3.1). For all ten phantom tests reported, 98% of all SNR values acquired were greater than, or equal to 40dB and 54% of all SNR values acquired were greater than, or equal to 60dB.

To test for repeatability and consistency over time, average SNR values for the ten tests were statistically compared with one another. No significant differences were shown to exist between the average SNR values obtained (Figure 3.1).

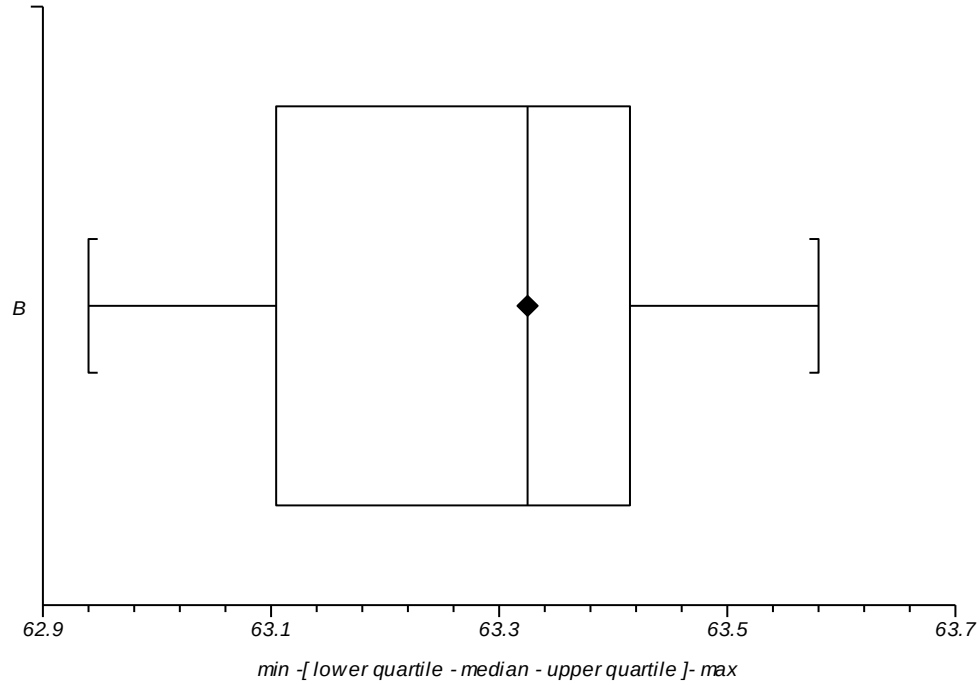

Figure 3.1 Box & whisker plot: fEITER SNR values using a resistor phantom. Average SNR values listed in Table 3.1are illustrated as a box & whisker plot. Median SNR: 63.33; min SNR: 62.94; max SNR: 63.58.

3.1.2 Physical Phantom Measurements

SNR values

A single injection measurement pair recorded from a physical phantom tank test using fEITER is represented in Figure 3.2. A distinct change in captured fEITER voltage can be observed in Figure 3.2 occurring at 30s, as a result of the perturbation being inserted into the homogenous saline-filled tank.

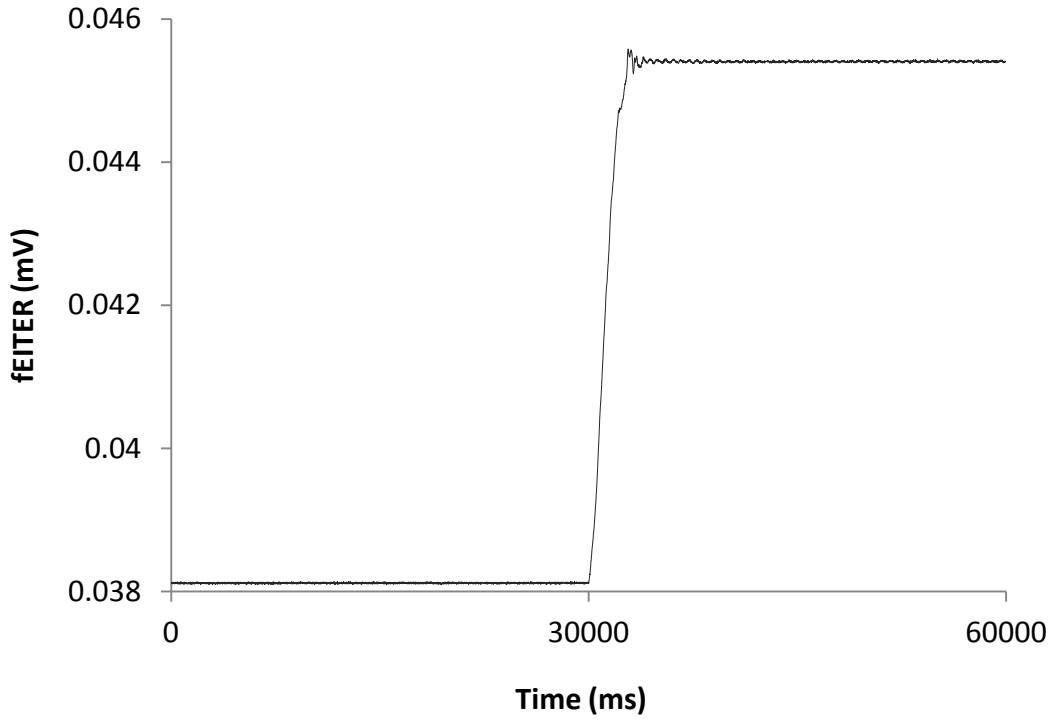

Figure 3.2 Example fEITER data recorded from a physical phantom. fEITER data recorded from the physical phantom at electrode injection and measurement pair 1_9_26_27. A perturbation was introduced into the saline filled tank at 30s where a clear change in recorded fEITER voltage can be observed.

The average SNR calculated for the four physical phantom trials ranged between 28.29 dB and 31.45 dB. Average SNR values calculated for the physical phantom trials are presented in Table 3.2. To test for repeatability and consistency over time, average SNR values for the four tests were statistically compared with one another in a box and whisker plot illustrated in Figure 3.3. No significant differences were shown to exist between the average SNR values obtained (Figure 3.3).

Table 3.2. fEITER absolute SNR values from a physical phantom. Average SNR values calculated from four physical tank measurements. Average SNR values were calculated from baseline and perturbation measurements.

Physical phantom test	Average SNR value (dB)	Minimum SNR value (dB)	Maximum SNR value (dB)
1	29.57	28.66	63.04
2	31.45	20.46	61.83
3	28.52	17.48	54.11
4	28.29	19.41	47.47

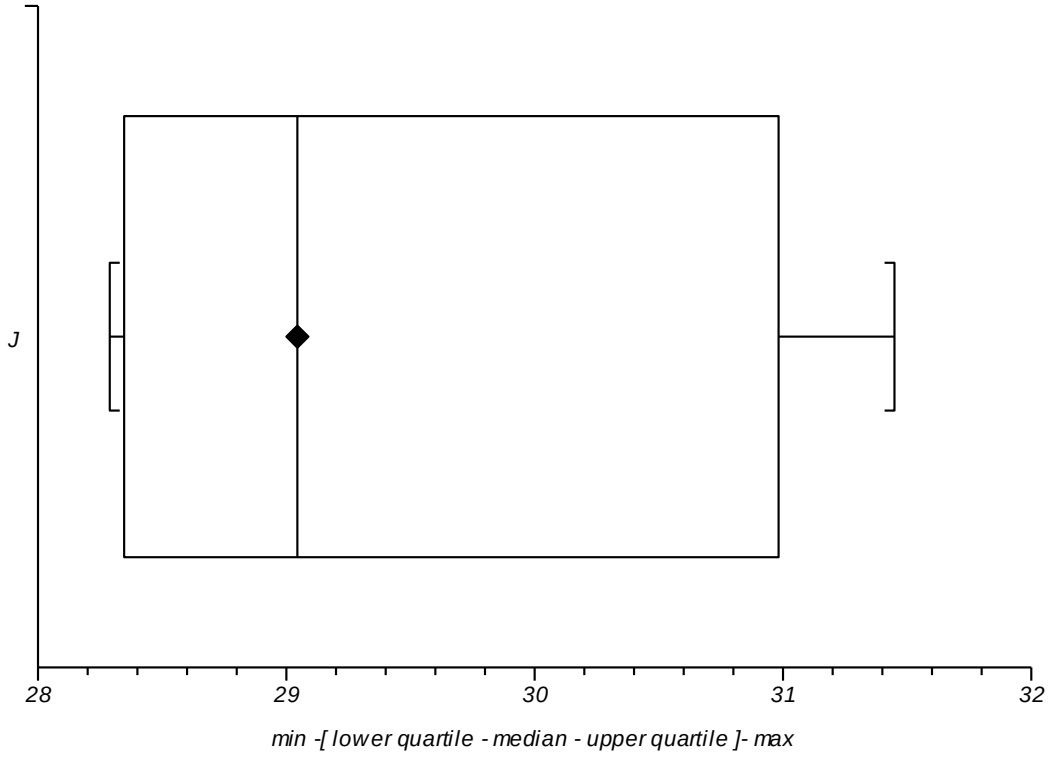

Figure 3.3 Box & whisker plot: fEITER SNR values using a physical phantom. Average SNR values listed in Table 3.2 are illustrated as a box & whisker plot. Median SNR: 29.04; min SNR: 28.29; max SNR: 31.45.

3.2 Histogram and ROC curve analysis

Visual Frontal Measurements

Raw fEITER data for each volunteer presented with visual stimuli was filtered for the REG and HFN. Figure 3.4a-c demonstrates examples of fEITER data captured from 3 different volunteers during the presentation of visual flashes. Raw fEITER data captured from 3 individual volunteers during visual stimulation is shown in Figures 3.4a (i), 3.4b (i) and 3.4c (i). Filtered fEITER data for the 3 volunteers following the removal of REG and HFN is demonstrated in Figures 3.4a (ii), 3.4b (ii) and 3.4c (ii)

Three examples of histograms generated for each volunteer from t-statistic values presenting comparisons of reference data with reference data and stimulus data are illustrated in Figures 3.4a (iii), 3.4b (iii) and 3.4c (iii). The two sets of t-statistic values generated for each volunteer were pooled across the total number of volunteers generating pooled t-statistic reference and pooled t-statistic stimulus values. Pooled t-statistic values are represented on a single histogram shown in Figure 3.4d. Figure 3.4d demonstrates little observable difference between pooled t-statistic stimulus values compared to pooled t-statistic reference values.

Individual t-statistic values for each volunteer were used to create ROC curves. Three examples of ROC curves representing 3 volunteers are illustrated in Figures 3.4a (iv), 3.4b (iv) and 3.4c (iv).

The pooled t-statistic values across all volunteers were used to create a single ROC curve illustrated in Figure 3.4e with an AUC value of 0.520. AUC values generated from individual ROC curves are presented in Table 3.3 ranging from 0.502 to 0.787. From 14 AUC values presented in Table 3.3, 13 values fall within 95% confidence limits between 0.404 and 0.741.

Visual Measurements overlying the Visual Cortex

Figures 3.5a (i), 3.5b (i) and 3.5c (i) are examples of raw fEITER data captured from the back of the head from three different volunteers during visual stimulation. Raw fEITER measurements recorded from the back of the head during the presentation of visual flashes were filtered for REG and HFN. From a total of 13 volunteers studied, REG could not be identified in 3 volunteers. For these 3 volunteers, only HFN noise was filtered from their fEITER data. Examples of REG and HFN filtered data

captured from the same three volunteers during visual stimulation are shown in Figures 3.5a (ii), 3.5b (ii) and 3.5c (ii).

Three examples of histograms generated for each volunteer from t-statistic values representing the comparison of reference data with reference and stimulus data are illustrated in Figures 3.5a (iii), 3.5b (iii) and 3.5c (iii). t-statistic values for each volunteer were pooled to yield t-statistic reference and t-statistic stimulus values. Pooled t-statistic values were used to create a single histogram illustrated in Figure 3.5d to demonstrate observable differences between reference and stimulus data.

ROC curves were produced for each volunteer using single-subject t-statistic values. Three examples of individual ROC curves are illustrated in Figures 3.5a (iv), 3.5b (iv) and 3.5c (iv). AUC values were calculated for each ROC curve and are represented in Table 3.4. A single ROC curve was also produced using the pooled t-statistic values shown in Figure 3.5e with an AUC value of 0.505. Excluding one AUC value presented in Table 3.4, fall within 95% confidence limits between the AUC range of 0.484 and 0.574.

The Valsalva Manoeuvre (VM)

Raw fEITER data for each volunteer performing the VM was filtered for the REG and HFN. Figure 3.6a-c demonstrates fEITER data captured from 3 different volunteers during the VM. Figures 3.6a (i), 3.6b (i), and 3.6c (i) show raw fEITER data. Figures 3.6a (ii), 3.6b (ii) and 3.6c (ii) illustrate REG and HFN filtered fEITER data.

Three examples of histograms generated for each volunteer from t-statistic reference and t-statistic stimulus values are shown in Figures 3.6a (iii), 3.6b (iii) and 3.6c (iii). Pooled t-statistic values across all volunteers are represented on a single histogram shown in Figure 3.6d. The pooled histogram displays some separation between reference and stimulus data. In particular, greater t-statistic stimulus values in small frequencies can be observed which represent greater variation in mean values of randomly selected epochs of stimulus data.

Three examples of ROC curves which were subsequently produced using the t-statistic values for individual volunteers are illustrated in Figures 3.6a (iv), 3.6b (iv) and 3.6c (iv). Once more, pooled t-statistic values across all volunteers were used to produce a single ROC curve illustrated in Figure 3.6e with an AUC of 0.658. AUC

values generated from individual ROC curves for all volunteers are presented in Table 3.5 and range from 0.508 to 0.873. Individual AUC values for all volunteers fall within 95% confidence limits between 0.472 and 0.874.

Induction of Anaesthesia

Raw fEITER data recorded from 19 patients undergoing induction of anaesthesia was filtered for REG and HFN. Simultaneously recorded bilateral BIS data (left and right) captured for each patient was pooled and averaged for 60s of monitoring time during induction. Following induction with propofol at 10s, bilateral BIS values for each patient can be seen to consistently decrease indicating increased depth of anaesthesia as induction progresses. (Figures 3.7a(ii), 3.7b(ii) and 3.7c(ii). Prior to induction during the reference period where each patient was awake and fully conscious, the average bilateral BIS values was calculated as 91.7 (left sided BIS) and 93.2 (right sided BIS). At the end of fEITER recording time at 60s following induction with propofol, the average bilateral BIS values was recorded at 41.4 (left) and 44.1 (right).

Raw fEITER data captured from three different patients during induction is illustrated in Figures 3.7a (i), 3.7b (i) and 3.7c (i). Filtered fEITER data for the same three patients following the exclusion of REG and HFN is shown in Figures 3.7a (ii), 3.7b (ii) and 3.7c (ii). Histograms were generated from the filtered data of each patient using t-statistic values. Figures 3.7a (iii), 3.7b (iii) and 3.7c (iii) illustrate histograms representing t-statistic reference and t-statistic stimulus values. The two sets of t-statistic values generated for each patient were subsequently pooled across all patients. The pooled t-statistic values across all patients during induction of anaesthesia are represented on a single histogram shown in Figure 3.7d. t-statistic values calculated for each patient were also used to produce individual ROC curves. Three examples of patient ROC curves are illustrated in Figures 3.7a (iv), 3.7b (iv) and 3.7c (iv). Once more, pooled t-statistic values were used to create a single ROC curve illustrated in Figure 3.7e. AUC value for the pooled ROC curve was calculated as 0.547. Individual AUC values generated from single patient ROC curves produced are represented in Table 3.6. From 19 patient AUC values shown in table 3.4, 18 AUC values were shown to fall within the 95% confidence limits between 0.470 and 0.645.

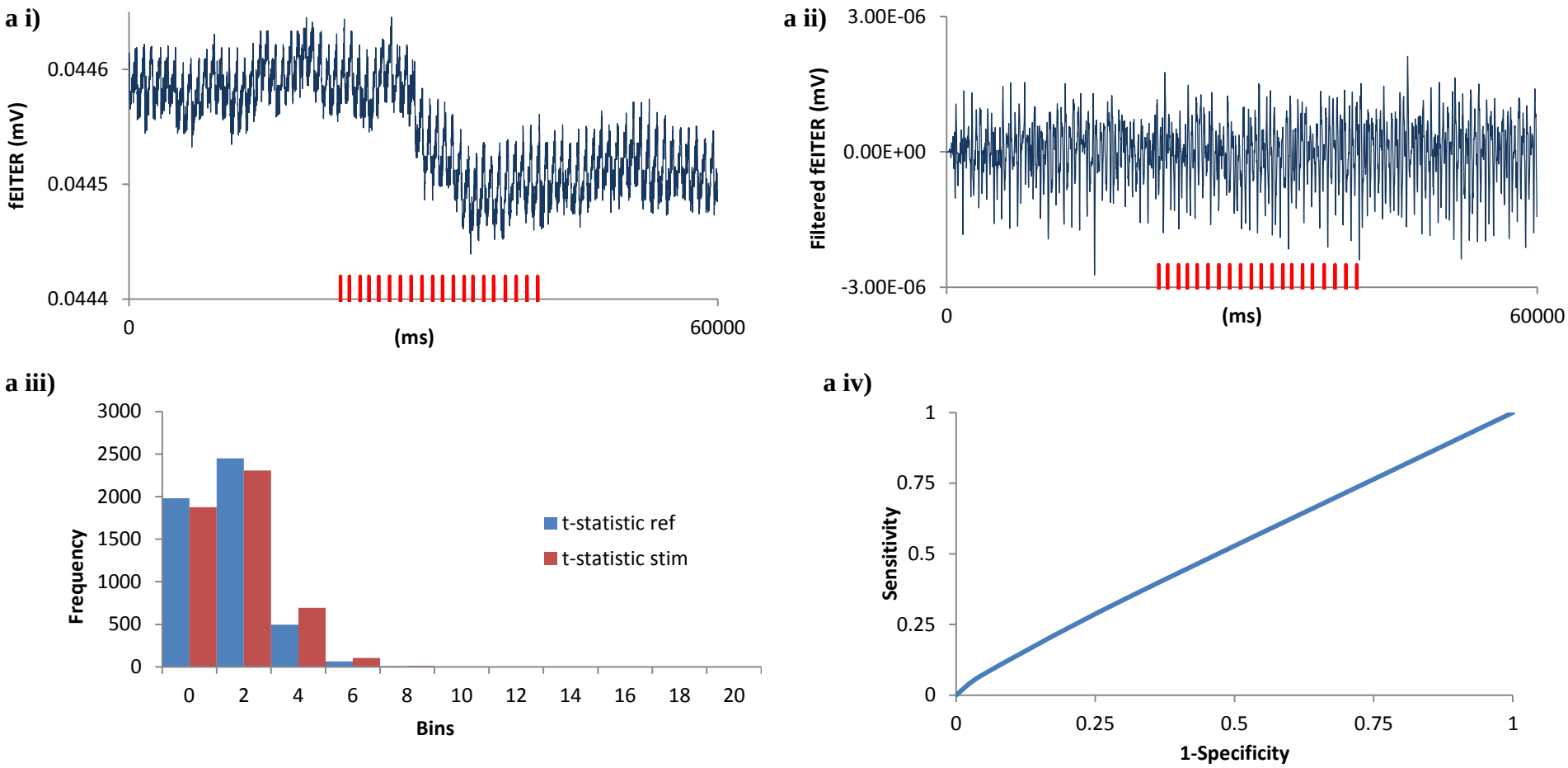

Figure 3.4a) Single volunteer (V8) fEITER data analysis during visual stimulation (frontal measurements). **a i)** Raw fEITER data for V8 during visual stimulation. Twenty visual flashes were presented to volunteers between 21.5s and 41.7s represented by vertical red lines along the x axis. **a ii)** Filtered fEITER data for REG and HFN. **a iii)** Histogram generated from t-statistic comparisons of randomly selected reference values with randomly selected reference and stimulus values. **a iv)** ROC curve produced from t-statistic values, AUC = 0.525.

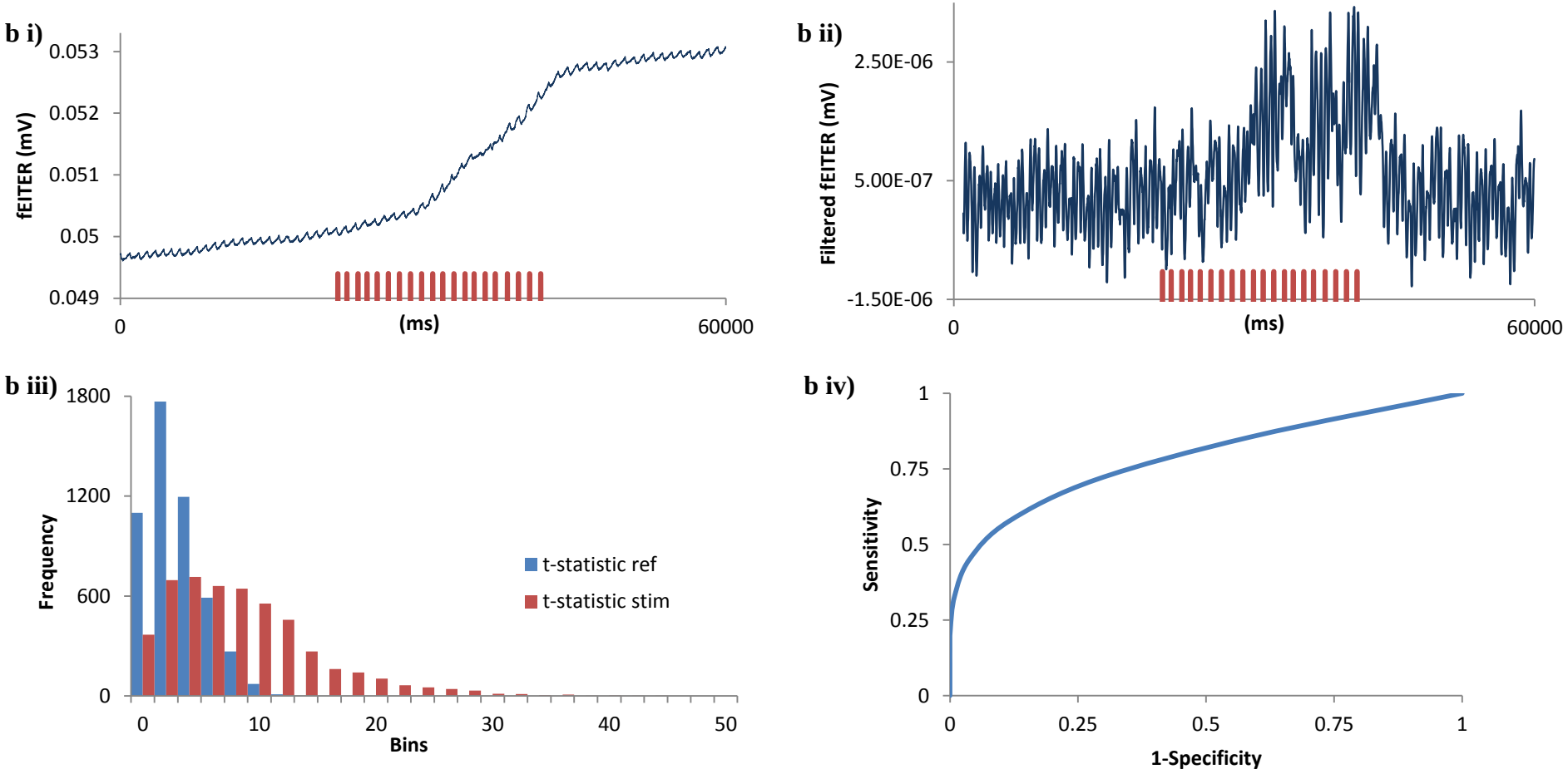

Figure 3.4b) Single volunteer (V12) fEITER data analysis during visual stimulation (frontal measurements). **b i)** Raw fEITER data for V12 during visual stimulation. Twenty visual flashes were presented to volunteers between 21.5s and 41.7s represented by vertical red lines along the x axis. **b ii)** Filtered fEITER data for REG and HFN. **b iii)** Histogram generated from t-statistic comparisons of randomly selected reference values with randomly selected reference and stimulus values. **b iv)** ROC curve produced from t-statistic values, AUC = 0.787.

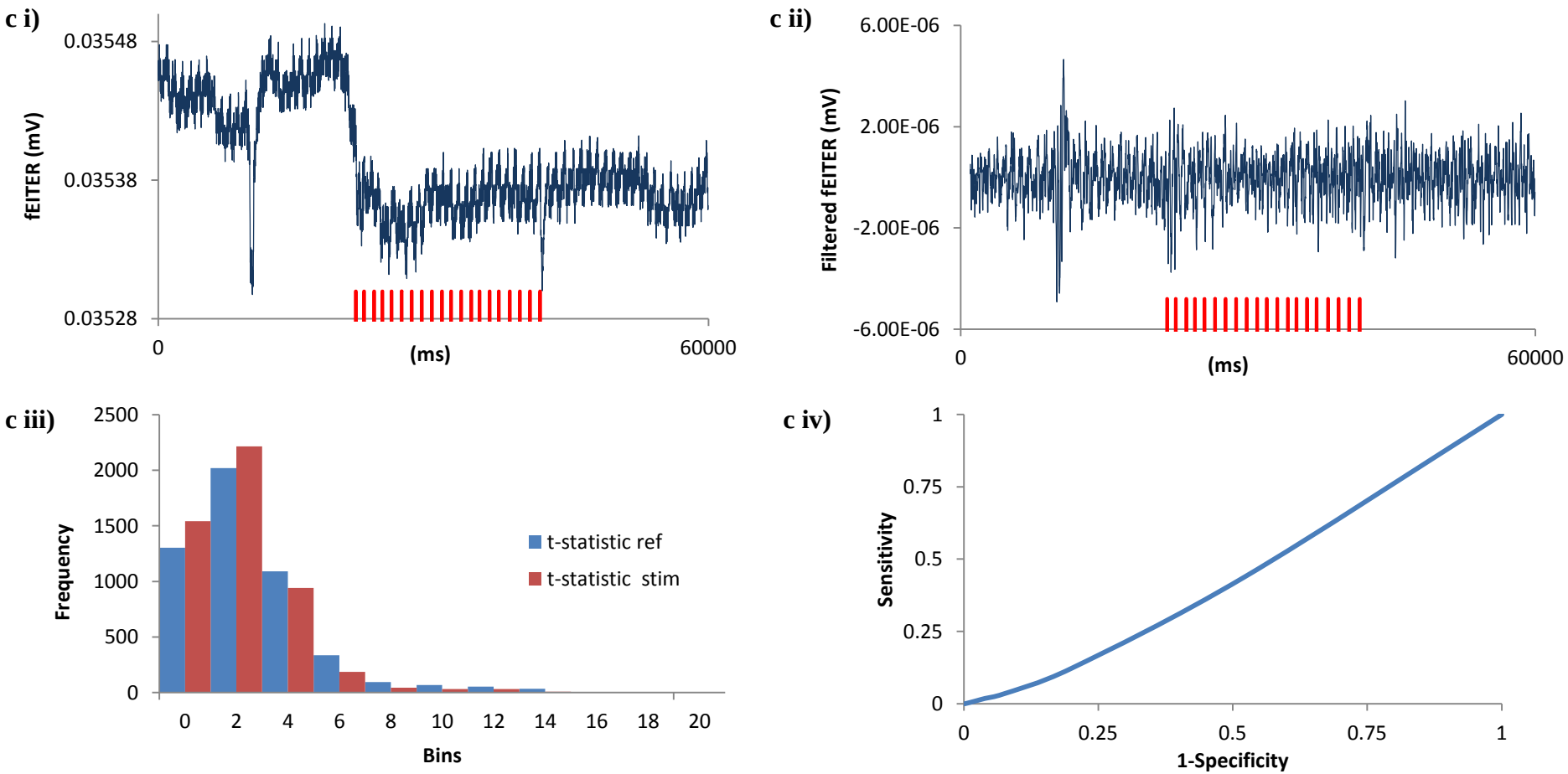

Figure 3.4c) Single volunteer (V13) fEITER data analysis during visual stimulation (frontal measurements). **c i)** Raw fEITER data for V13 during visual stimulation. Twenty visual flashes were presented to volunteers between 21.5s and 41.7s represented by vertical red lines along the x axis. **c ii)** Filtered fEITER data for REG and HFN. **c iii)** Histogram generated from t-statistic comparisons of randomly selected reference values with randomly selected reference and stimulus values. **c iv)** ROC curve produced from t-statistic values, AUC = 0.557.

d.

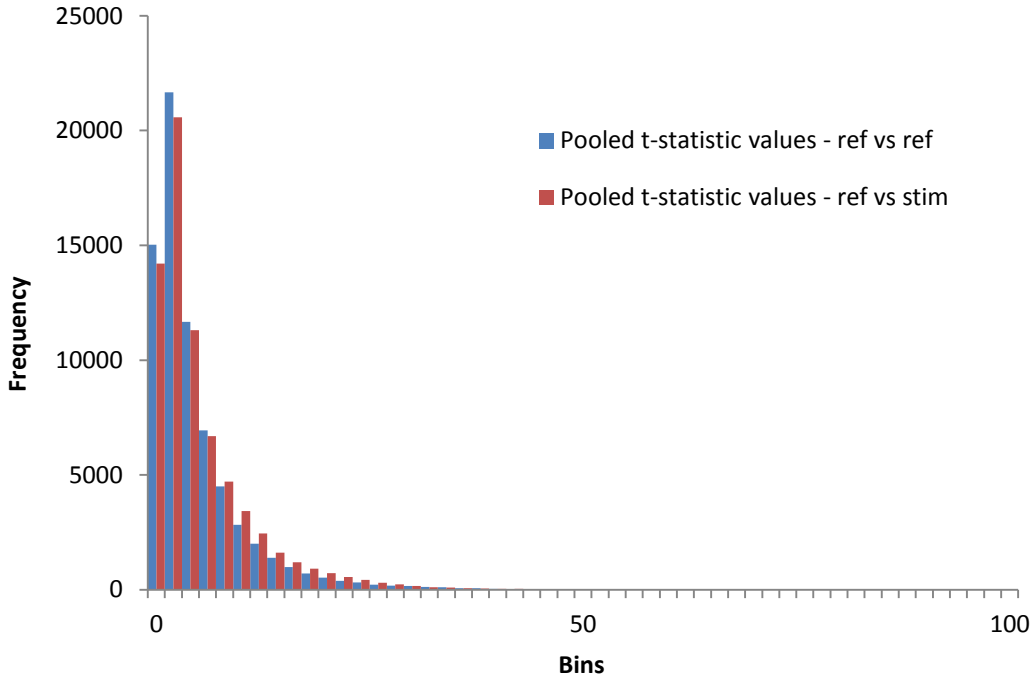

Figure 3.4d) Visual stimulus (frontal measurements) histogram of pooled t-statistic values. t-statistic values generated for each volunteer were pooled to produce a single histogram representing pooled t-statistic values for ref *vs*. ref (70,000 data points) and ref *vs*. stim (70,000 data points) comparisons during the presentation of visual flashes.

e.

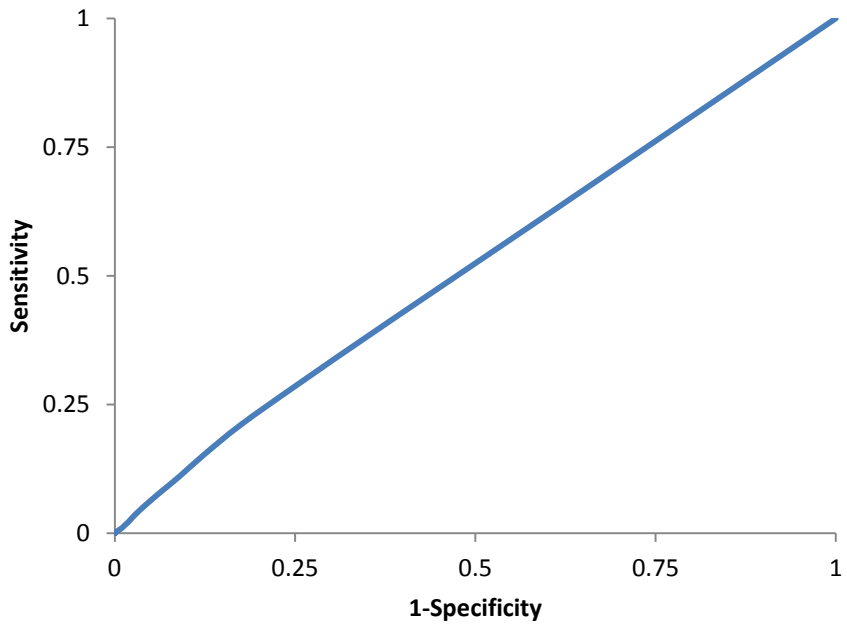

Figure 3.4e) ROC curve of pooled t-statistic values for the visual stimulus (frontal measurements). Pooled t-statistic values across all volunteers during the presentation of visual flashes were used to produce a single ROC curve with AUC value of 0.520.

Table 3.3 Visual stimulus (frontal measurements): AUC curve values for individual volunteer ROC curves. A list of AUC values calculated from individual ROC produced for each volunteer using t-statistic values calculated during the presentation of visual flashes.

Volunteer number in thesis	ROC AUC value
1	0.512
2	0.595
3	0.502
5	0.690
6	0.504
7	0.532
8	0.525
9	0.502
10	0.568
11	0.529
12	0.787
13	0.557
14	0.554
15	0.658

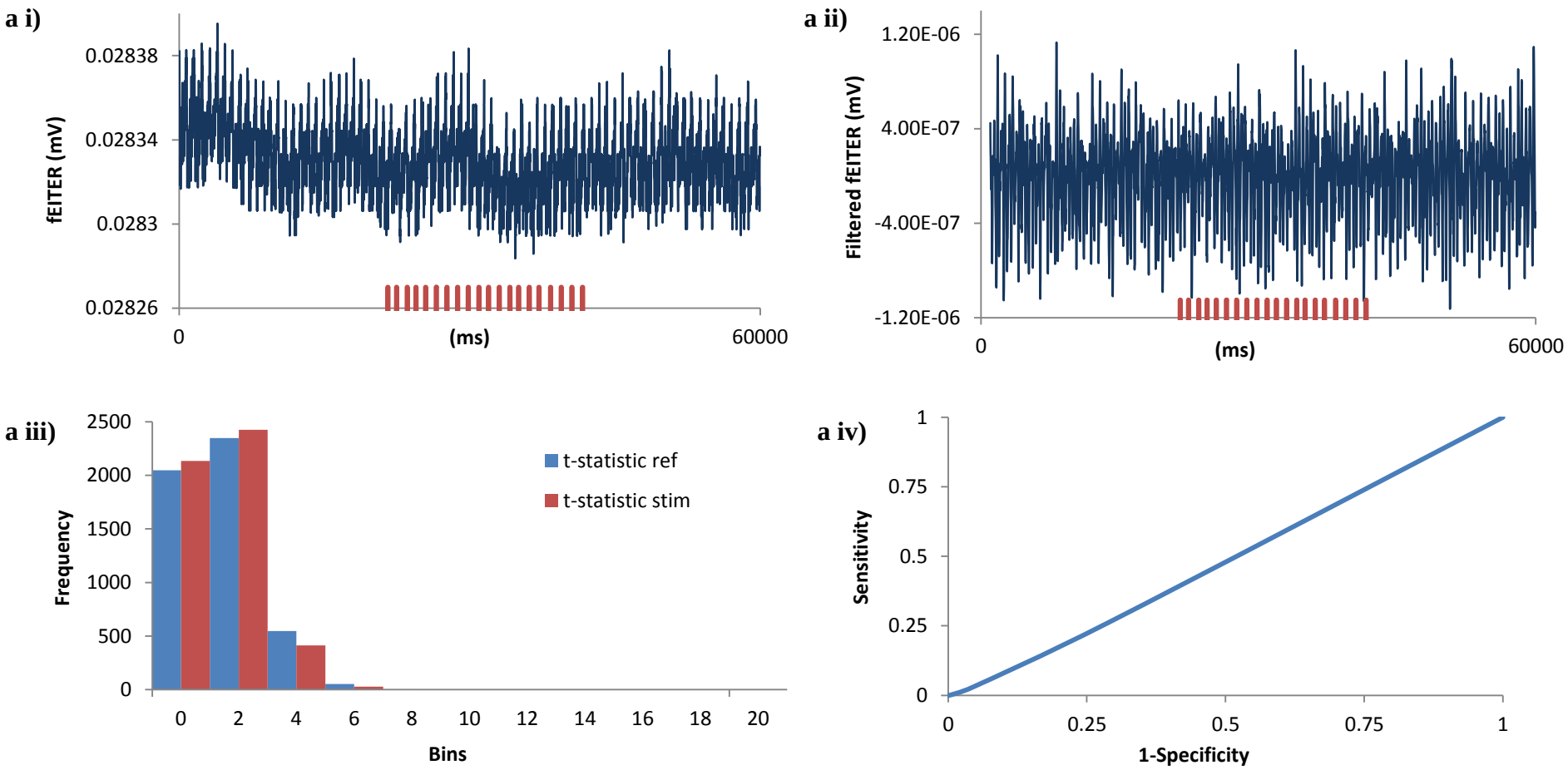

Figure 3.5a) Single volunteer (V8) fEITER data analysis during visual stimulation (measurements overlying the visual cortex). **a i)** Raw fEITER data for V8 during visual stimulation. Twenty visual flashes were presented to volunteers between 21.5s and 41.7s represented by vertical red lines along the x axis. **a ii)** Filtered fEITER data for REG and HFN. **a iii)** Histogram generated from t-statistic comparisons of randomly selected reference values with randomly selected reference and stimulus values. **a iv)** ROC curve produced from t-statistic values, AUC = 0.515.

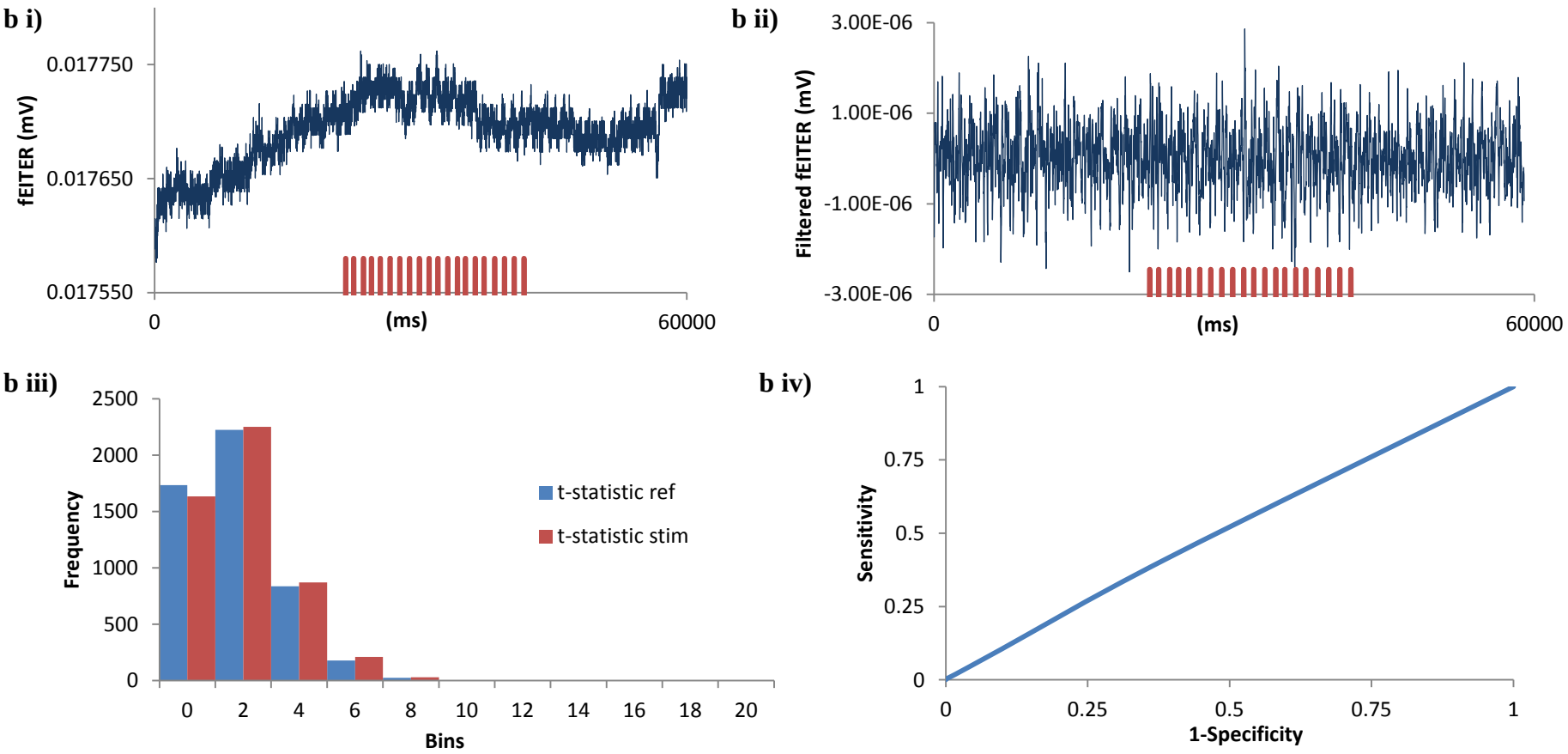

Figure 3.5b) Single volunteer (V12) fEITER data analysis during visual stimulation (measurements overlying the visual cortex). **b i)** Raw fEITER data for V12 during visual stimulation. Twenty visual flashes were presented to volunteers between 21.5s and 41.7s represented by vertical red lines along the x axis. **b ii)** Filtered fEITER data for REG and HFN. **b iii)** Histogram generated from t-statistic comparisons of randomly selected reference values with randomly selected reference and stimulus values. **b iv)** ROC curve produced from t-statistic values, AUC = 0.515.

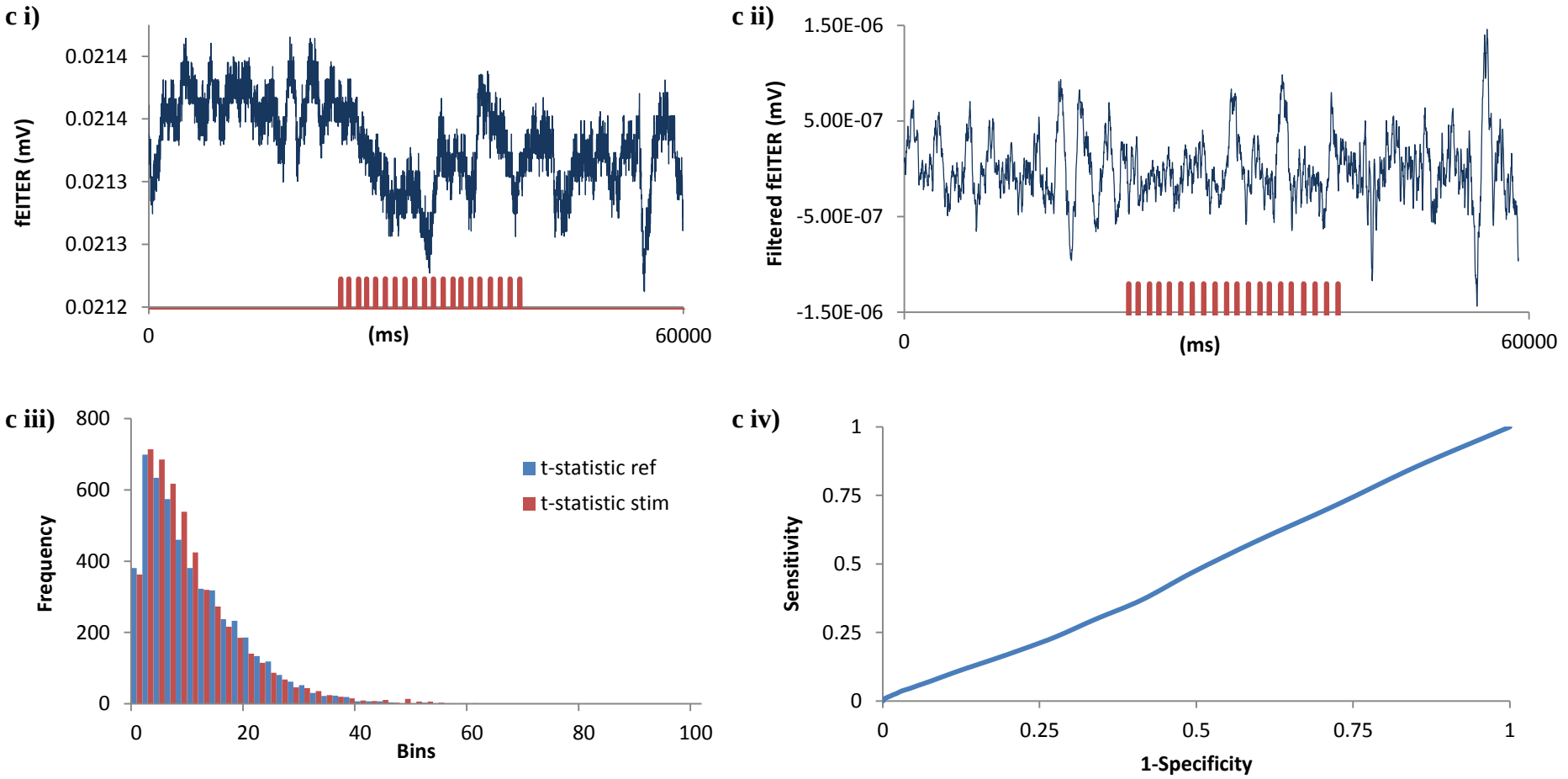

Figure 3.5c) Single volunteer (V13) fEITER data analysis during visual stimulation (measurements overlying the visual cortex). **c i)** Raw fEITER data for V13 during visual stimulation. Twenty visual flashes were presented to volunteers between 21.5s and 41.7s represented by vertical red lines along the x axis. **c ii)** Filtered fEITER data for REG and HFN. **c iii)** Histogram generated from t-statistic comparisons of randomly selected reference values with randomly selected reference and stimulus values. **c iv)** ROC curve produced from t-statistic values, AUC = 0.516.

d.

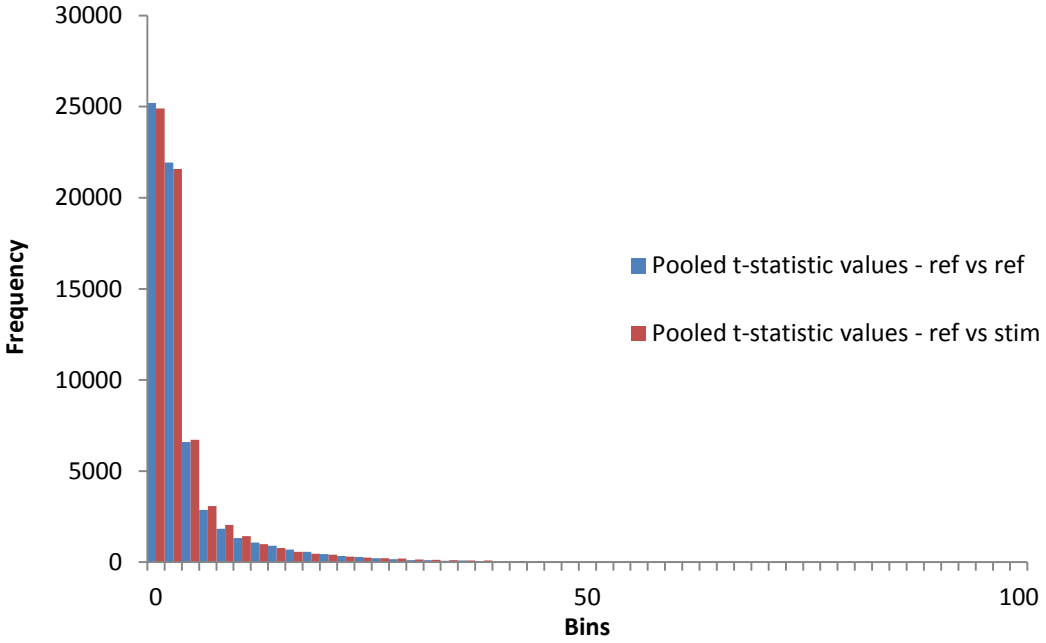

Figure 3.5d) Visual stimulus (measurements overlying the visual cortex) histogram of pooled t-statistic values. t-statistic values generated for each volunteer were pooled to produce a single histogram representing pooled t-statistic values for ref *vs*. ref (65,000 data points) and ref *vs*. stim (65,000 data points) comparisons during the presentation of visual flashes.

e.

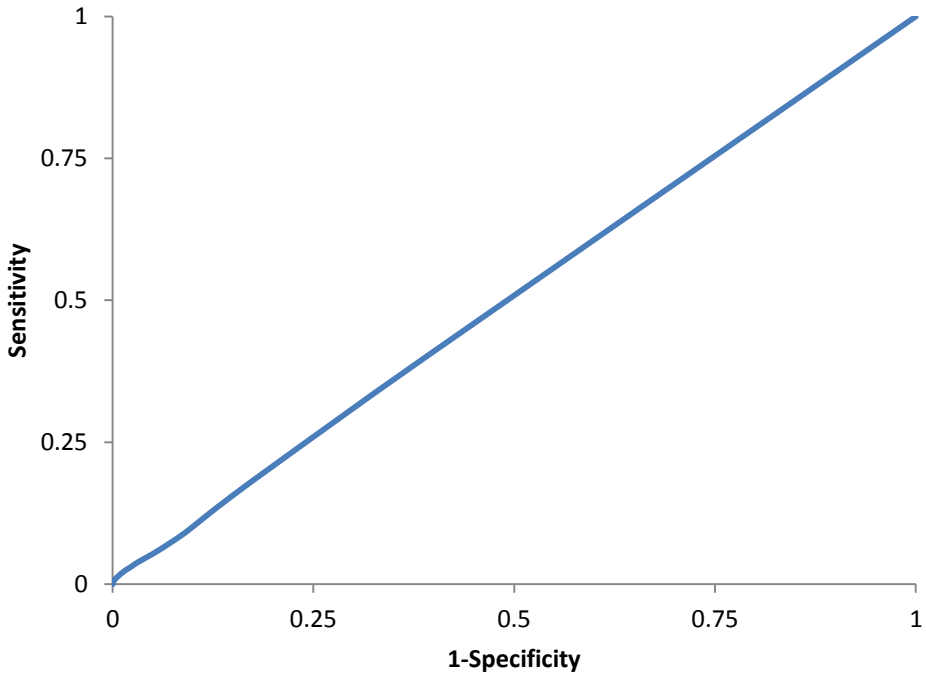

Figure 3.5e) ROC curve of pooled t-statistic values for the visual stimulus (measurements overlying the visual cortex). Pooled t-statistic values across all 13 volunteers during the presentation of visual flashes were used to produce a single ROC curve with AUC value of 0.505.

Table 3.4 Visual stimulus (measurements overlying the visual cortex): AUC values for individual volunteer ROC curves. A list of AUC values calculated from individual ROC curves produced for each volunteer using t-statistic values calculated during the presentation of visual flashes.

Volunteer number	ROC AUC value
1	0.576
2	0.514
3	0.514
5	0.535
6	0.502
7	0.516
8	0.515
9	0.544
10	0.521
11	0.534
12	0.515
13	0.516
15	0.569

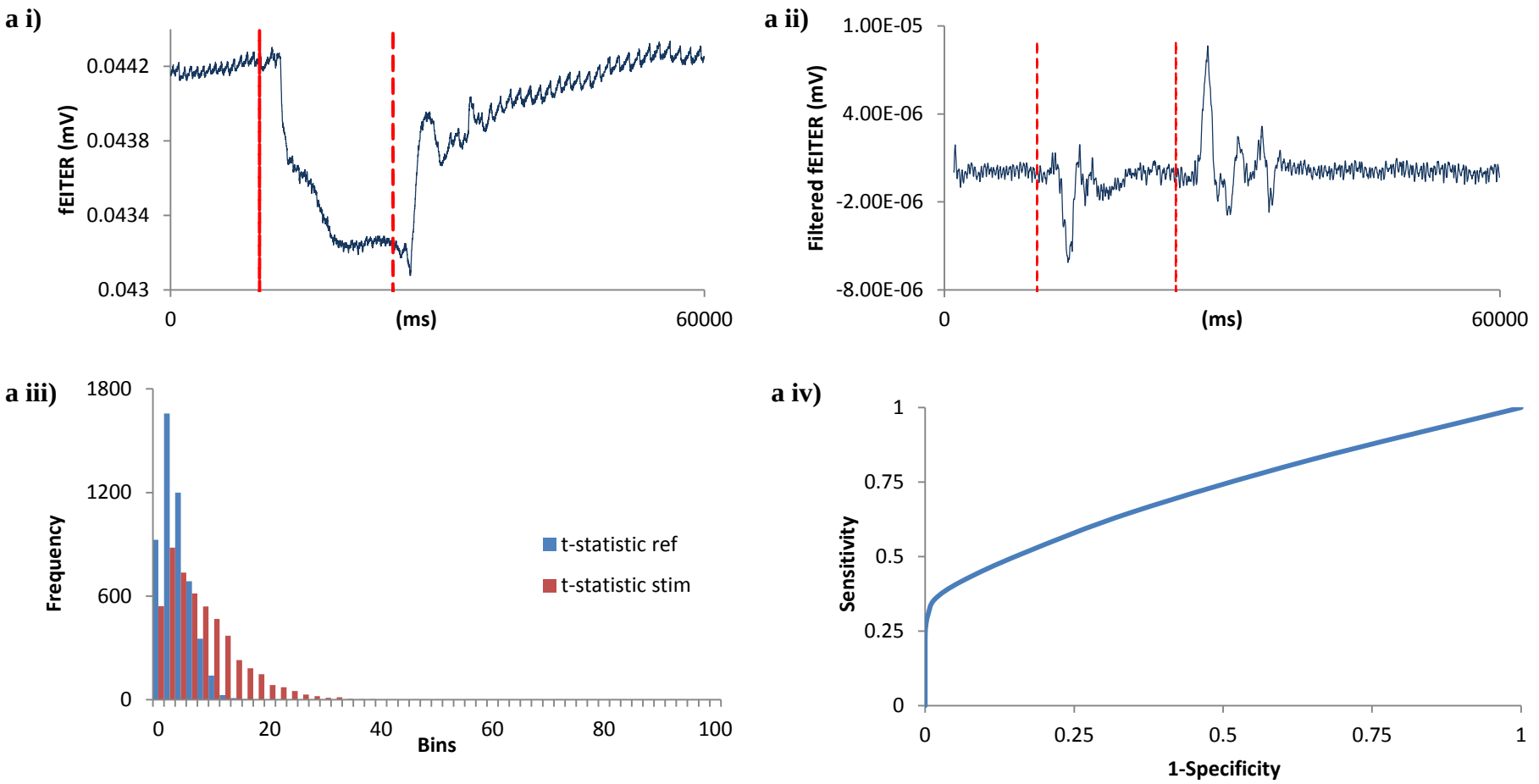

Figure 3.6a) Single volunteer (V8) fEITER data analysis during the VM. **a i)** Raw fEITER data for V8 during the VM. The VM was initiated at 10s and released at 25s as indicated by the vertical red lines. **a ii)** Filtered fEITER data for REG and HFN. **a iii)** Histogram generated from t-statistic comparisons of randomly selected reference values with randomly selected reference and stimulus values. **a iv)** ROC curve produced from t-statistic values, AUC = 0.722

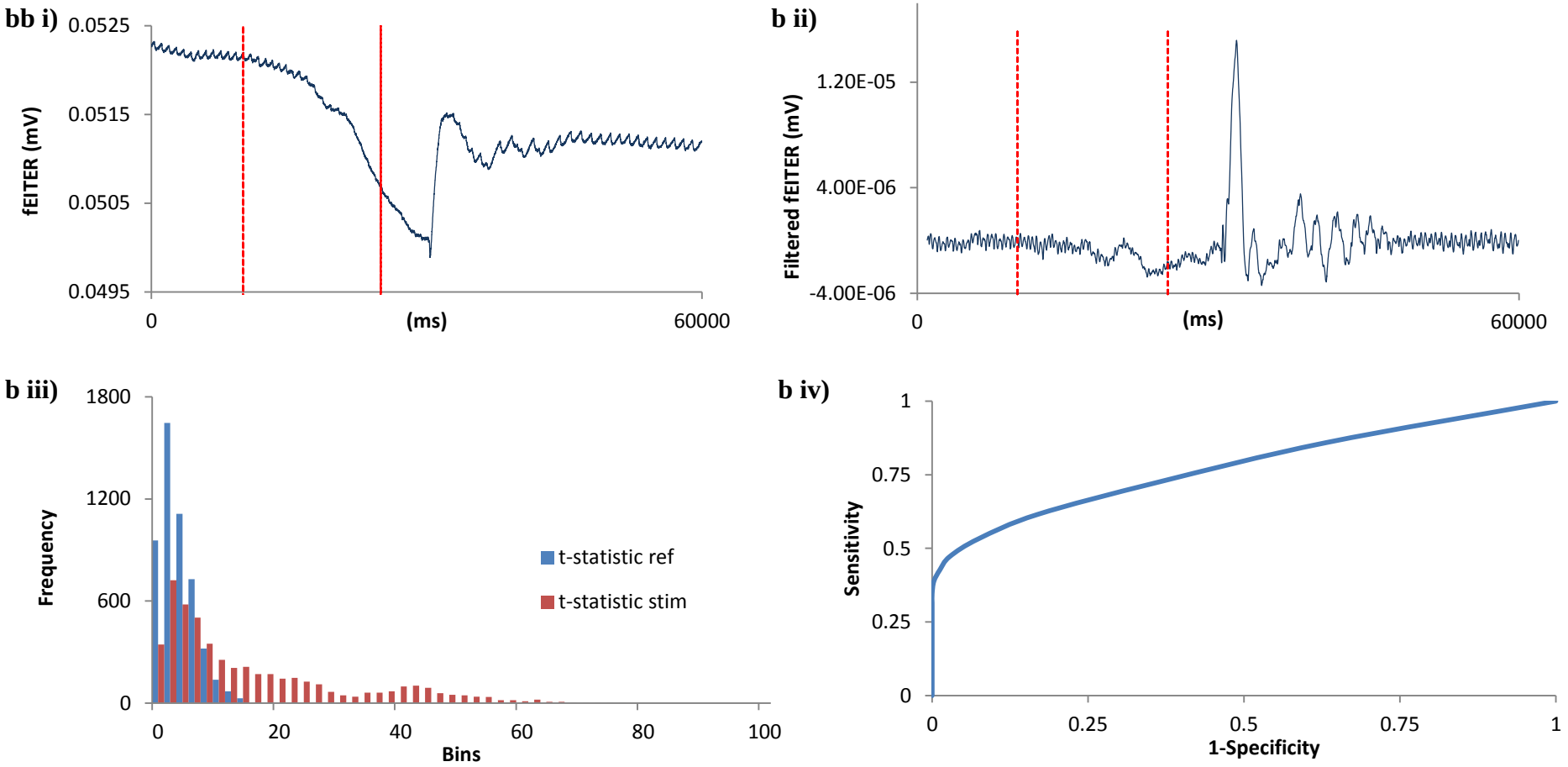

Figure 3.6b) Single volunteer (V12) fEITER data analysis during the VM. b i) Raw fEITER data for V12 during the VM. The VM was initiated at 10s and released at 25s as indicated by the vertical red lines. **b ii)** Filtered fEITER data for REG and HFN. **b iii)** Histogram generated from t-statistic comparisons of randomly selected reference values with randomly selected reference and stimulus values. **b iv)** ROC curve of t-statistic values, AUC = 0.778

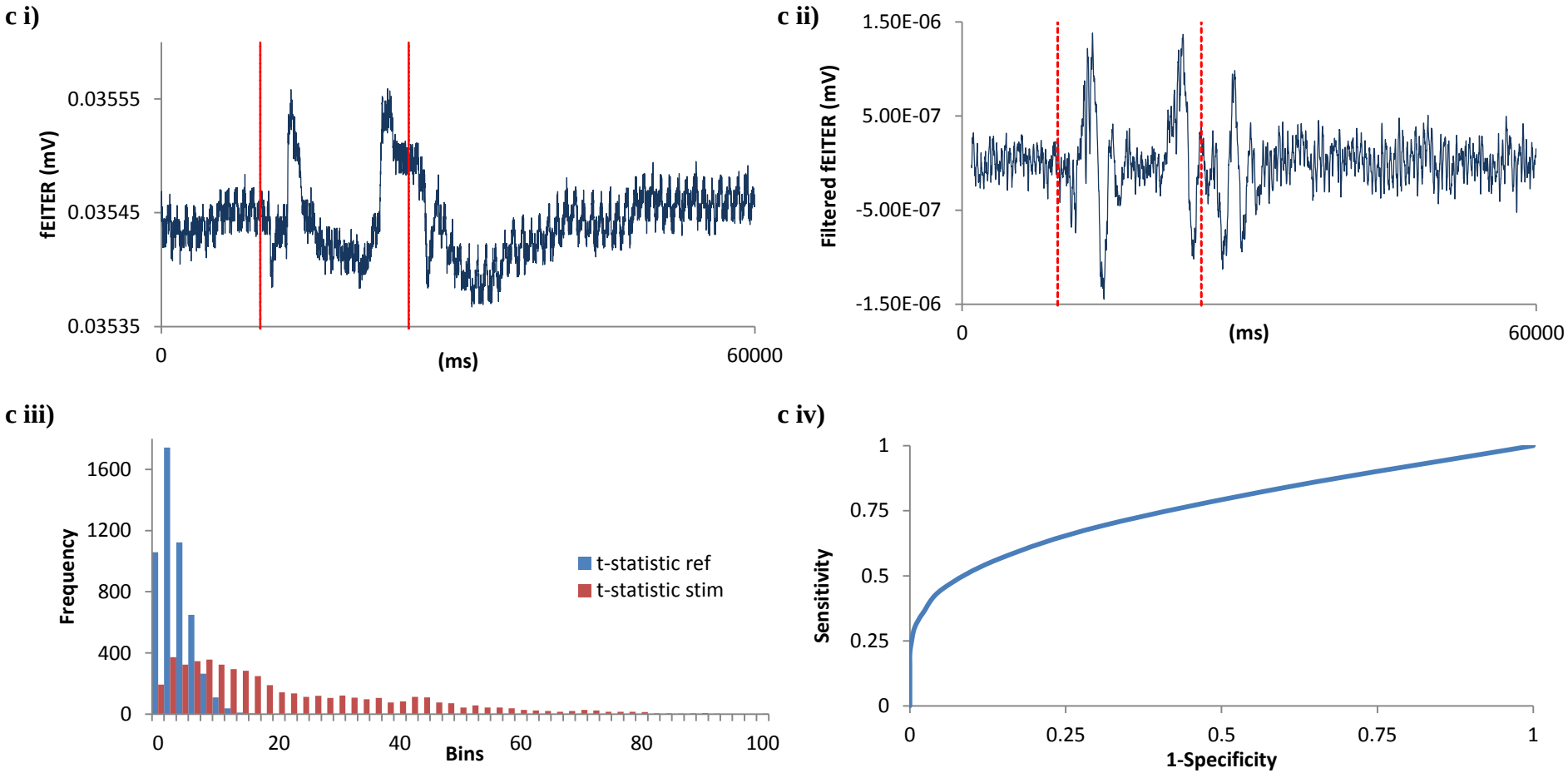

Figure 3.6c) Single volunteer (V13) fEITER data analysis during the VM. c i) Raw fEITER data for V13 during the VM recorded. The VM was initiated at 10s and released at 25s as indicated by the vertical red lines. **c ii)** Filtered fEITER data for REG and HFN. **c iii)** Histogram generated from t-statistic comparisons of randomly selected reference values with randomly selected reference and stimulus values. **c iv)** ROC curve produced from t-statistic values, AUC = 0.765

d.

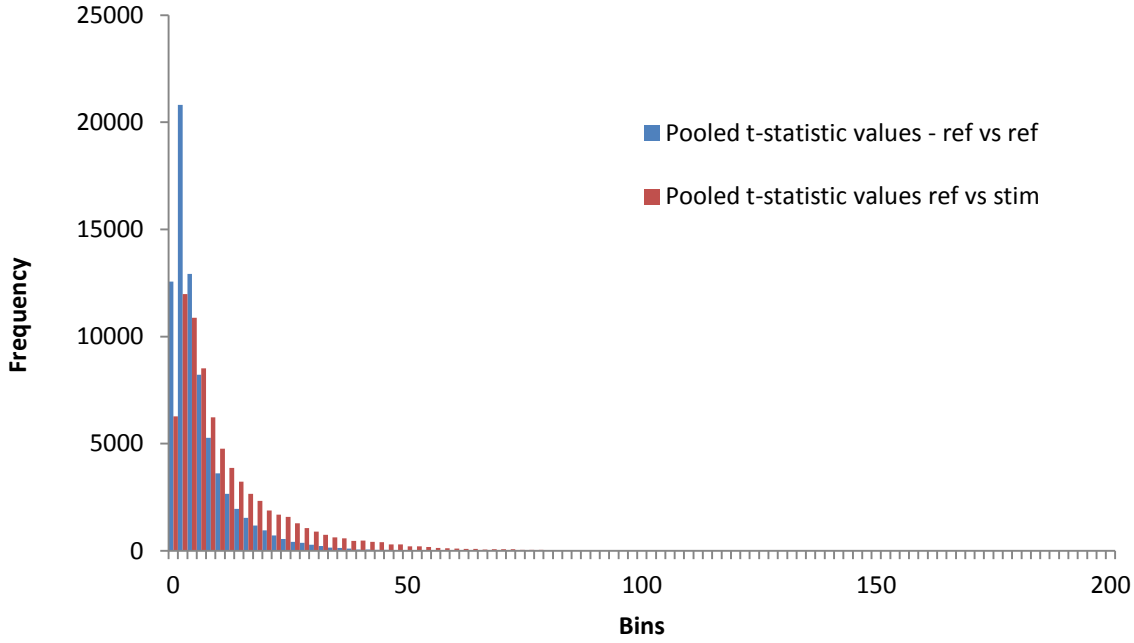

Figure 3.6d) VM histogram of pooled t-statistic values. t-statistic values generated for each volunteer were pooled to produce a single histogram representing pooled t-statistic values for ref *vs*. ref (75,000 data points) and ref *vs*. stim (75,000 data points) comparisons.

e.

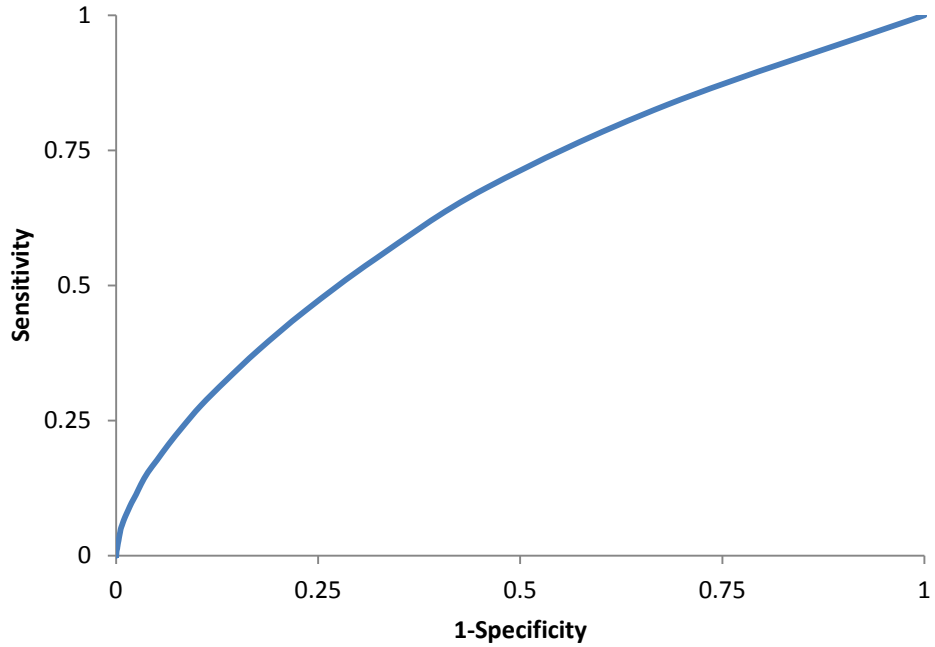

Figure 3.6e) ROC curve of pooled t-statistic values for the VM. Pooled t-statistic values for all 15 volunteers during the VM were used to produce a single ROC curve with AUC value of 0.658

Table 3.5 VM: AUC values for individual volunteer ROC curves. A list of AUC values calculated from individual ROC produced for each volunteer using t-statistic values calculated during the VM

Volunteer number	ROC AUC value
1	0.572
2	0.692
3	0.707
4	0.873
5	0.65
6	0.584
7	0.508
8	0.722
9	0.564
10	0.711
11	0.735
12	0.778
13	0.765
14	0.684
15	0.549

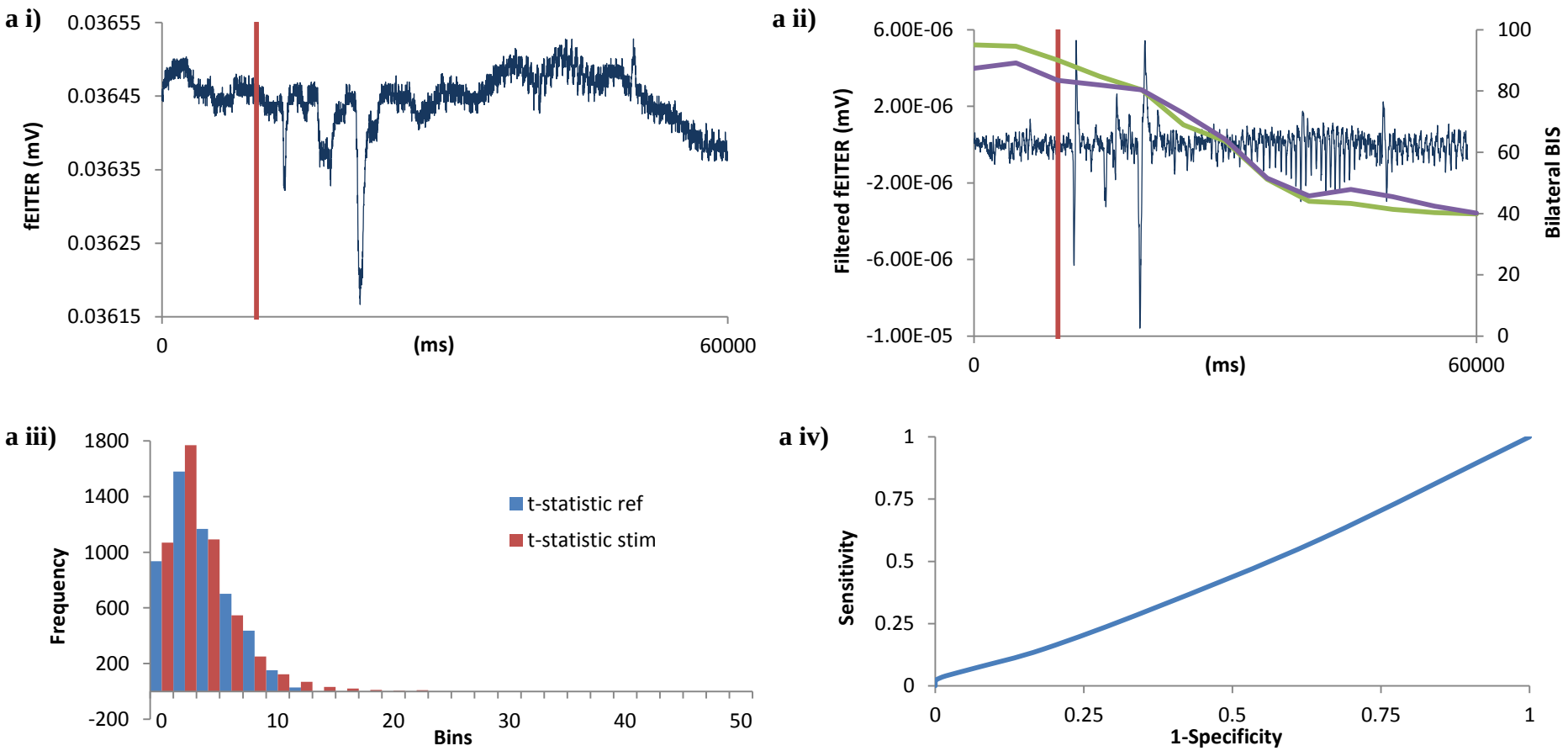

Figure 3.7a) Single patient (P04) fEITER data analysis during induction of anaesthesia with propofol. **a i)** Raw fEITER data for P04 during induction. Propofol was administered intravenously at 10s indicated by the vertical red line along the x axis. **a ii)** Filtered fEITER data for REG and HFN. Simultaneously bilateral recordings of BIS are plotted on the secondary y axis. Left BIS is represented by the green line whereas right BIS is represented by the purple line. **a iii)** Histogram generated from t-statistic comparisons of randomly selected reference values with randomly selected reference and stimulus values. **a iv)** ROC curve produced from t-statistic values, AUC = 0.537

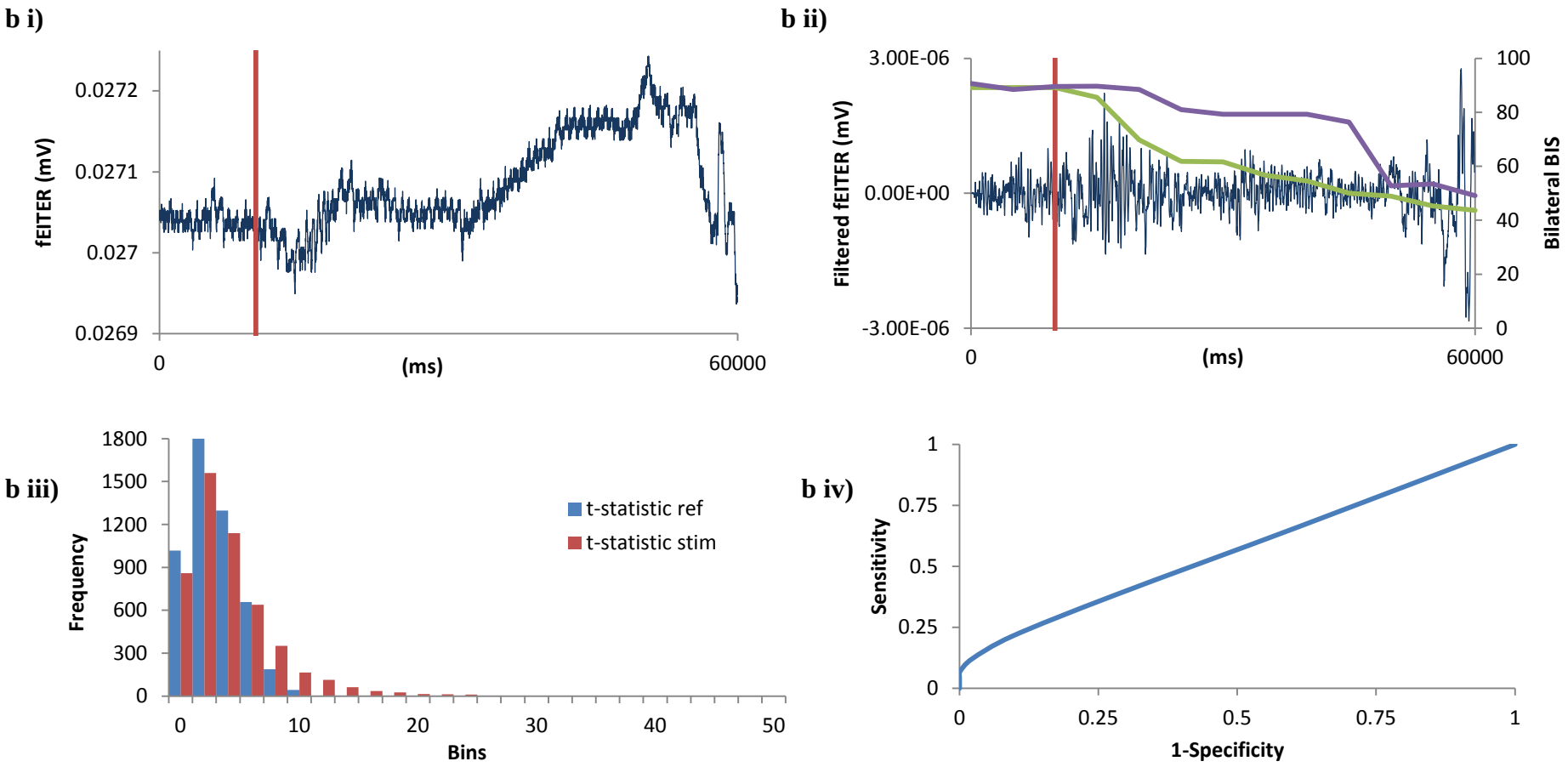

Figure 3.7b) Single patient (P15) fEITER data analysis during induction of anaesthesia with propofol. **b i)** Raw fEITER data for P15 during induction. Propofol was administered intravenously at 10s indicated by the vertical red line along the x axis. **b ii)** Filtered fEITER data for REG and HFN. Simultaneously bilateral recordings of BIS are plotted on the secondary y axis. Left BIS is represented by the green line whereas right BIS is represented by the purple line. **b iii)** Histogram generated from t-statistic comparisons of randomly selected reference values with randomly selected reference and stimulus values. **b iv)** ROC curve produced from t-statistic values, AUC = 0.568

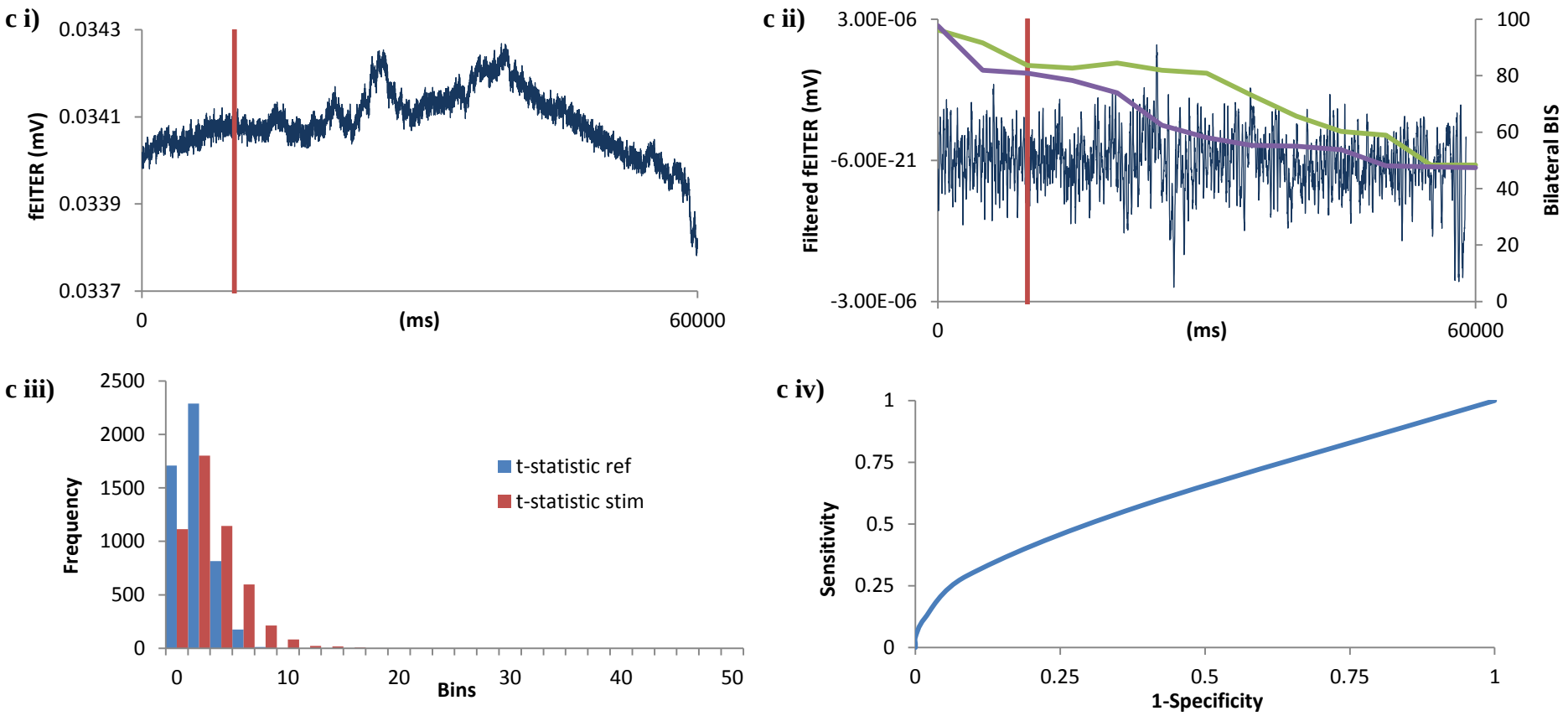

Figure 3.7c) Single patient (P22) fEITER data analysis during induction of anaesthesia with propofol. **c i)** Raw fEITER data for P22 during induction. Propofol was administered intravenously at 10s indicated by the vertical red line along the x axis. **c ii)** Filtered fEITER data for REG and HFN. Simultaneously bilateral recordings of BIS are plotted on the secondary y axis. Left BIS is represented by the green line whereas right BIS is represented by the purple line. **c iii)** Histogram generated from t-statistic comparisons of randomly selected reference values with randomly selected reference and stimulus values. **c iv)** ROC curve produced from t-statistic values, AUC = 0.637

d.

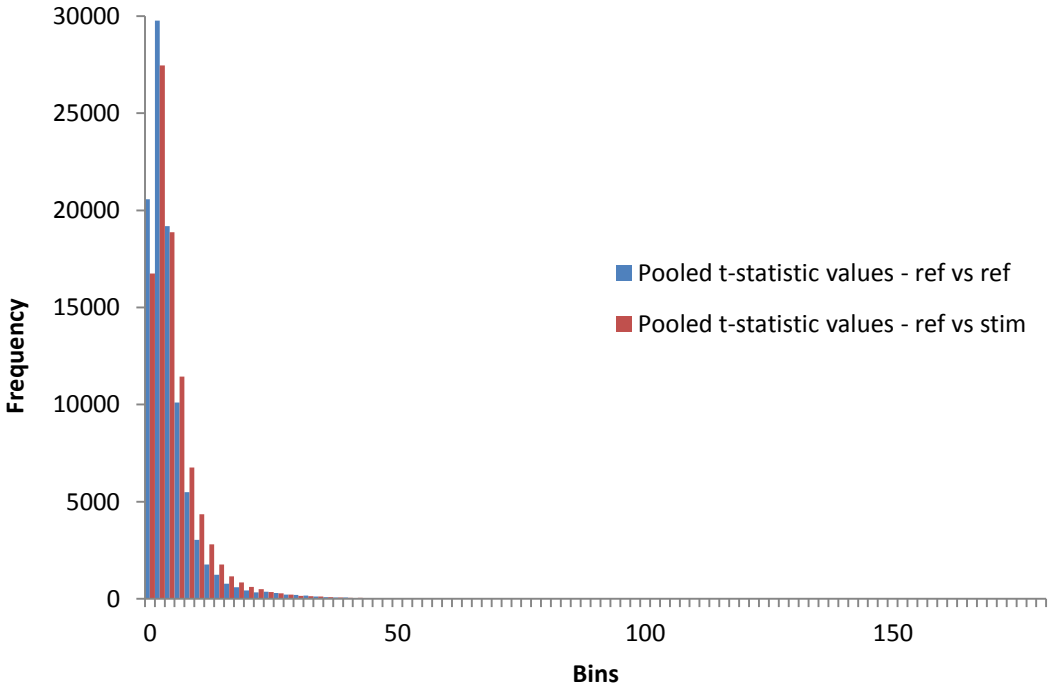

Figure 3.7d) Induction of anaesthesia histogram of pooled t-statistic values. t-statistic values generated for each patient were pooled to produce a single histogram representing pooled t-statistic values for ref *vs*. ref (95,000 data points) and ref *vs*. stim (95,000 data points) comparisons during induction to anaesthesia.

e.

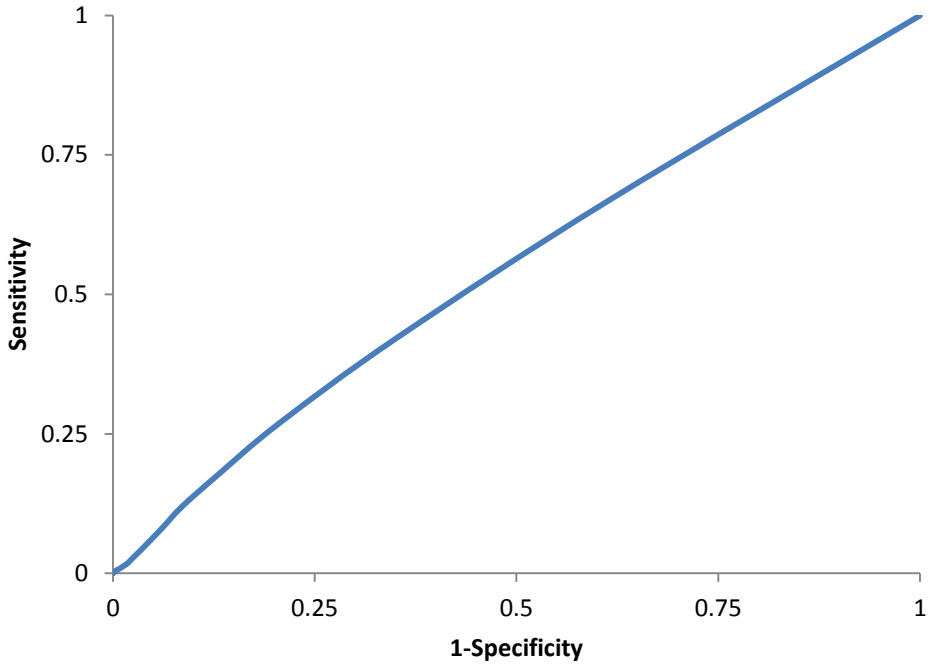

Figure 3.7e) ROC curve of pooled t-statistic values for induction of anaesthesia. Pooled t-statistic values across all patients during induction of anaesthesia were used to produce a single ROC curve with AUC value of 0.547.

Table 3.6 Induction to anaesthesia: AUC values for individual patient ROC curves. A list of AUC values calculated from individual ROC curves produced for each patient using t-statistic values calculated during the induction of anaesthesia.

Induction	
Patient number	ROC AUC value
P01	0.616
P02	0.542
P03	0.550
P04	0.537
P05	0.518
P06	0.531
P07	0.51
P09	0.649
P11	0.502
P12	0.584
P14	0.599
P15	0.568
P17	0.524
P18	0.537
P19	0.523
P20	0.575
P22	0.637
P23	0.533
P26	0.528

3.3 ApEn Results

Approximate Entropy (ApEn) was applied to high frequency components of fEITER data retained in the signal for reference and stimulus conditions for each volunteer and patient. The data was filtered for REG only. Four sets of ApEn values calculated for four trial conditions are presented in Tables 3.7a to 3.7d representing visual frontal measurements (Table 3.7a), visual cortical measurements (Table 3.7b), Valsalva manoeuvre (VM) (Table 3.7c) and induction of anaesthesia (Table 3.7d). Statistical analysis was undertaken to compare volunteer and patient reference ApEn values with stimulus ApEn values calculated for each trial condition. ApEn values were expected to be greater for reference values in comparison to ApEn stimulus values. To test this hypothesis, ApEn reference values were statistically compared to ApEn stimulus values using a Wilcoxon's signed ranks test. An upper sided *p* value is presented for statistical analysis of the present results to test the alternative hypothesis of x values (ApEn reference) being larger than y values (ApEn stimulus). Differences between the two values in each trial condition (ApEn stimulus subtracted from ApEn reference) are presented as bar charts in Figures 3.8a to 3.8d to illustrate the direction of change in ApEn values during the presented/performed stimuli.

For frontal fEITER measurements during visual stimulation, ApEn values calculated for each volunteer during reference and stimulus conditions were shown to be non-significantly different (Table 3.7a) (Wilcoxon's signed ranks test, upper $p = 0.998$). From a total of fourteen volunteers presented with visual flashes, ApEn values calculated for stimulus conditions were greater than ApEn values calculated during reference conditions for eleven volunteers (Figure 3.8a).

For fEITER measurements captured from the back of the head overlying the visual cortex during visual stimulation, ApEn values calculated for reference and stimulus conditions were shown to be non-significantly different (Table 3.7b) (Wilcoxon's signed ranks test, upper $p = 0.980$). From a total of thirteen volunteers who were presented with visual flashes, ApEn values calculated for stimulus conditions were shown to be greater than ApEn values calculated for reference conditions for nine volunteers (Figure 3.8b).

For the VM, ApEn values calculated for each volunteer during reference and stimulus conditions were shown to be non-significantly different (Table 3.7c)

(Wilcoxon's signed ranks test, upper $p = 0.976$). From a total of fifteen volunteers who performed the VM, ApEn values calculated for stimulus conditions were greater than ApEn values calculated during reference conditions for twelve volunteers (Figure 3.8c).

Complete 60s monitoring of fEITER measurements under reference conditions was undertaken in sixteen patients prior to induction of anaesthesia. Therefore, ApEn was calculated using fEITER data for sixteen induction patients. For fEITER measurements captured from patients prior to and during induction of anaesthesia, ApEn values calculated for reference and stimulus conditions were shown to be non-significantly different (Table 3.7d) (Wilcoxon's signed ranks test, $p = 0.912$). From a total of sixteen patients who were monitored using fEITER during induction of anaesthesia, ApEn values calculated during induction were shown to be greater than ApEn values calculated during reference conditions for ten patients (Figure 3.8d).

Table 3.7a) Volunteer ApEn values during visual stimulation (frontal measurements). ApEn values calculated for fEITER data captured during visual stimulation (frontal measurements) which was filtered for REG only. 0s to 20s of fEITER data was selected as reference data and ApEn was calculated for this data set (ApEn – Ref). Stimulus data was isolated between 21.5s and 41.5s during the presentation of visual flashes, and ApEn was also applied to this data set (ApEn – Stim).

Volunteer	ApEn - Ref	ApEn - Stim
1	1.665	1.663
2	1.532	1.600
3	1.574	1.660
5	1.507	1.595
6	1.382	1.368
7	1.667	1.649
8	1.590	1.649
9	1.626	1.655
10	1.523	1.635
11	1.623	1.684
12	1.745	1.746
13	1.422	1.483
14	1.619	1.641
15	1.419	1.616

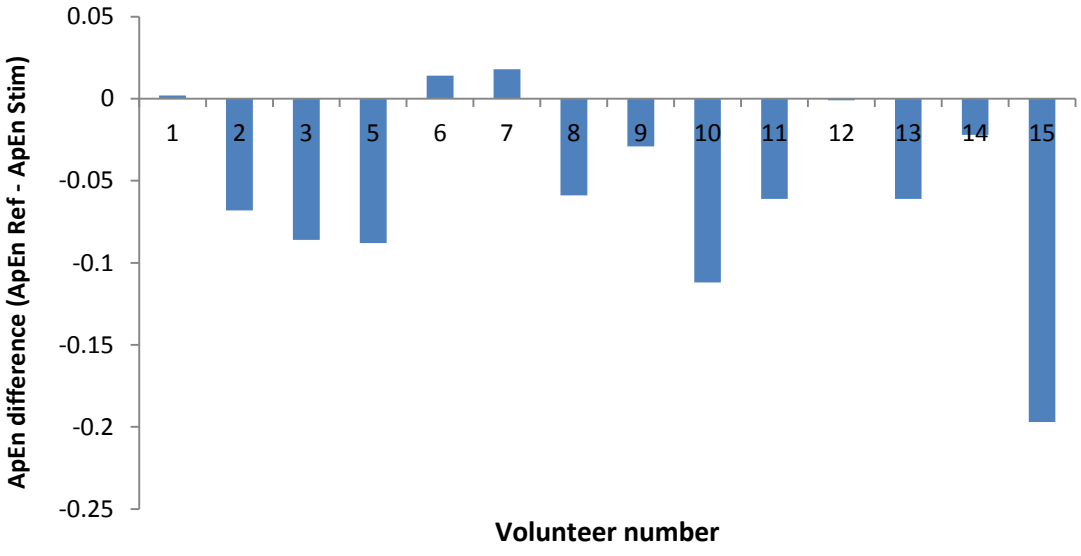

Figure 3.8a) ApEn differences for visual stimulation – frontal measurements. Bar chart displaying the difference in ApEn entropy calculated for reference and stimulus conditions for visual stimulus fEITER data captured at the front of the head in 14 volunteers (Table 3.7(a)). ApEn stimulus values were subtracted from ApEn reference values to display the direction of differences between the two values. From a total of 14 volunteers, ApEn stimulus values were greater than ApEn reference values for 11 volunteers.

Table 3.7b) Volunteer ApEn values during visual stimulation (measurements overlying the visual cortex). ApEn values calculated for fEITER data captured during visual stimulation (measurements overlying the visual cortex) which was filtered for REG only. 0s to 20s of fEITER data was selected as reference data and ApEn was calculated for this data set (ApEn – Ref). Stimulus data was isolated between 21.5s and 41.5s during the presentation of visual flashes, and ApEn was also applied to this data set (ApEn – Stim).

Volunteer	ApEn - Ref	ApEn - Stim
1	1.492	1.571
2	1.527	1.646
3	1.627	1.640
5	1.185	1.249
6	0.505	0.627
7	1.517	1.542
8	1.668	1.671
9	1.535	1.534
10	1.527	1.485
11	1.422	1.586
12	0.926	0.894
13	1.532	1.532
15	0.810	1.070

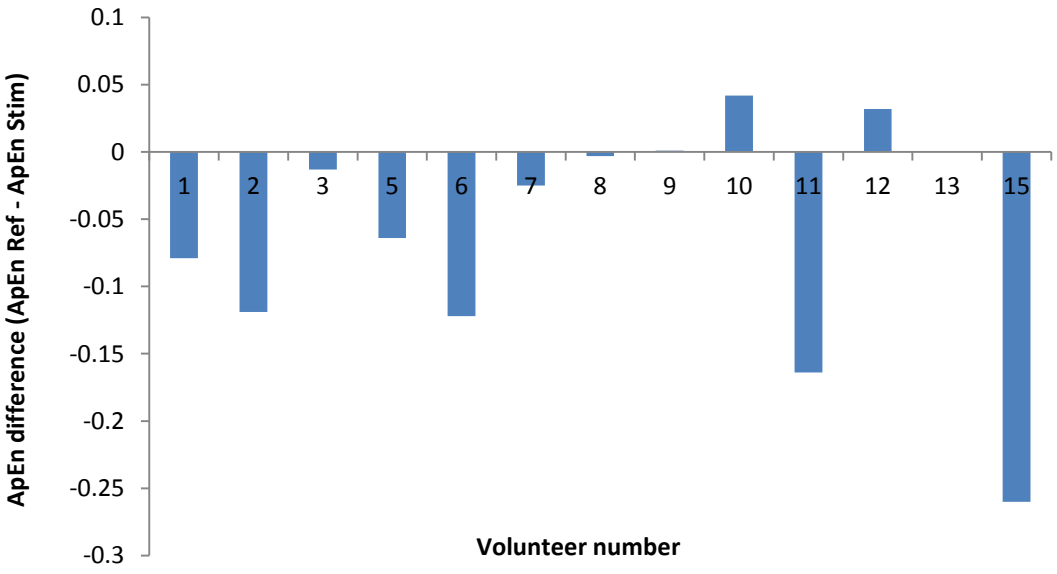

Figure 3.8b) ApEn differences for visual stimulation –measurements overlying the visual cortex. Bar chart displaying the difference in ApEn entropy calculated for reference and stimulus conditions for visual stimulus fEITER data captured from the back of the head in 13 volunteers (Table 3.7(b)). ApEn stimulus values were subtracted from ApEn reference values to display the direction of differences between the two values. From a total of 13 volunteers, ApEn stimulus values were greater than ApEn reference values in 9 volunteers.

Table 3.7c) Volunteer ApEn values during the VM. ApEn values calculated for fEITER data captured during the VM which was filtered for REG only. 0s to 10s of fEITER data was selected as reference data and ApEn was calculated for this data set (ApEn – Ref). Stimulus data was selected between 10s and 25s during periods of the VM being performed, and ApEn was also applied to this data set (ApEn – Stim).

Volunteer	ApEn - Ref	ApEn - Stim
1	1.496	1.615
2	1.535	1.563
3	1.424	1.504
4	1.552	1.627
5	1.549	1.623
6	1.403	1.462
7	1.461	1.598
8	1.508	1.661
9	1.482	1.603
10	1.531	1.612
11	1.636	1.517
12	1.607	1.691
13	1.531	1.498
14	1.465	1.491
15	1.615	1.503

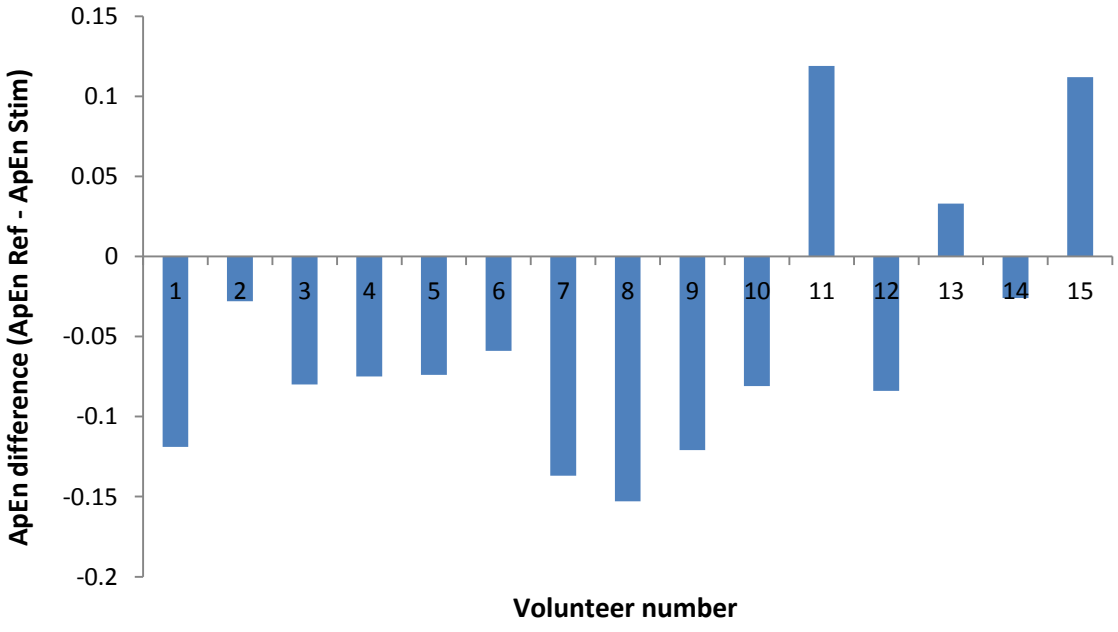

Figure 3.8c) ApEn differences for the VM. Bar chart displaying the difference in ApEn entropy calculated for reference and stimulus conditions for fEITER data captured during the VM in 15 volunteers (Table 3.7(c)). ApEn stimulus values were subtracted from ApEn reference values to display the direction of differences between the two values. From a total of 15 volunteers, ApEn stimulus values were greater than ApEn reference values in 12 volunteers.

Table 3.7d) Patient ApEn values during induction of anaesthesia. ApEn values calculated for fEITER data captured at rest (reference) and during induction of anaesthesia which was filtered for REG only. Reference fEITER data for each patient lasting 60s was selected and ApEn was calculated for this data set (ApEn – Ref) following REG filtering. Stimulus data was selected from induction fEITER measurements recorded from each patient following the administration of propofol at 10s.ApEn was calculated for stimulus data between 10s and 60s (ApEn – Stim).

PATIENT	ApEn - Ref	ApEn - Stim
P01	1.673	1.674
P02	1.741	1.600
P03	1.616	1.682
P04	1.685	1.583
P05	1.427	1.605
P06	0.996	1.476
P07	1.434	1.539
P09	1.661	1.748
P11	1.598	1.612
P12	1.593	1.504
P14	1.516	1.509
P17	1.498	1.799
P18	1.576	1.566
P19	1.491	1.381
P20	1.711	1.973
P26	1.540	1.693

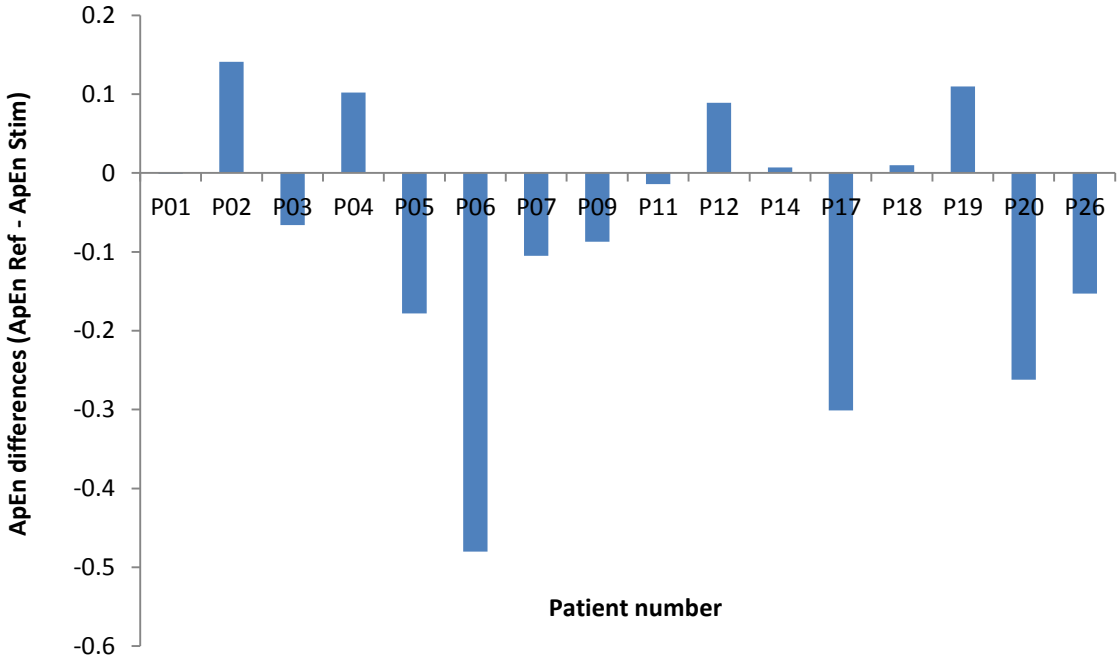

Figure 3.8d) ApEn differences for induction of anaesthesia. Bar chart displaying the difference in ApEn entropy calculated for reference and stimulus conditions for fEITER data captured during induction of anaesthesia in 16 patients (Table 3.7(d)). ApEn stimulus values were subtracted from ApEn reference values to display the direction of differences between the two values. From a total of 16 patients, ApEn stimulus values were greater than ApEn reference values in 10 patients.

Chapter 4 Discussion

4.1 Validating the fEITER System: Phantom Measurements

The observed SNR values which were achieved using the resistor phantom applied to fEITER are comparable, and in some instances superior to SNR values reported in literature for other EIT systems developed for clinical applications such as: the ITS P1000 (Murrieta-Lee et al., 2004, Tang et al., 2010), the Sussex MK4 system (Bilal, 2012), the Sheffield Mk3.5 (Wilson et al., 2001) the Sheffield Mk3a (Wilson et al., 2001) and the UCLH Mk1b (Yerworth et al., 2002). SNR values reported in literature for the latter EIT systems are summarized in Table 4.1 and were acquired using saline filled tank phantoms.

Table 4.1 SNR values of clinical EIT systems. A summary of reported SNR values for EIT systems developed for clinical applications.

EIT system	Reported SNR (dB)
ITSP1000	50-60dB
Sussex Mk4	40dB
Sheffield Mk3a	30dB
Sheffield Mk3.5	40dB
UCLH Mk1b	50dB

The maximum range of SNR reported in the present study for resistor phantom measurements is also comparable to previous SNR values reported for fEITER using mesh phantoms (Davidson et al., 2010, McCann et al., 2011). These results demonstrate that fEITER can be considered to be a stable EIT system with low-noise and accurate performance. Maximum SNR values gained from the present resistor

phantom measurements have not decayed since previous publications dating back to 2010 prior to the volunteer and patient trials being undertaken.

Results reported from physical phantom measurements demonstrate that the introduction of a perturbation in the form of a solid object within a homogenous saline-filled tank results in an observable difference in measured voltages using fEITER. Also, results from physical phantom measurements show that fEITER is capable of capturing a contrast in a homogenous medium such as a saline filled tank. Ideally, data recorded from a three-dimensional physical tank in the present study would be reconstructed to demonstrate the ability of an EIT system to accurately locate a contrast in measured voltage induced by a perturbation using tomography. These reconstructions would form the basis for clinical applications of an EIT system with the incentive of accurately reconstructing changes in biological tissues. Although historical tank data presented in the current study was not reconstructed, original functionality testing of fEITER undertaken using the same cylindrical tank with an alternative perturbation did result in the successful reconstruction of physical phantom tests to show a contrast in voltage measurements over time.

A sponge soaked in a highly concentrated saline solution compared to the saline solution in the cylindrical tank was used as a perturbation for tomographical reconstructions of fEITER data. The soaked sponge was inserted into the saline filled tank and fEITER recording was commenced. One minute recordings of fEITER measurements were reconstructed over time to show a change in conductivity from baseline following the insertion of the soaked sponge. Three reconstructed frames from a single recording epoch lasting 60s are presented in Figure 4.1.

The reconstructed reference frame (Figure 4.1(a)) shows the homogenous medium within the tank with no perturbation and therefore no contrast can be visualised. Following the insertion of the perturbation represented in red against the turquoise homogenous background, the impedance contrast can be seen to change over time (Figure 4.1(b) and (c)) as the homogenous bathing fluid permeates the sponge soaked in a more concentrated saline solution. In addition, diffusion of the contrasting saline solution from the sponge can also be seen to extend across the homogenous medium within the tank over time. Although the experiment did not result in precise boundaries of the sponge being visualised, the reconstructions validate the ability of fEITER to capture a change in impedance over time in relation to a baseline.

(a)

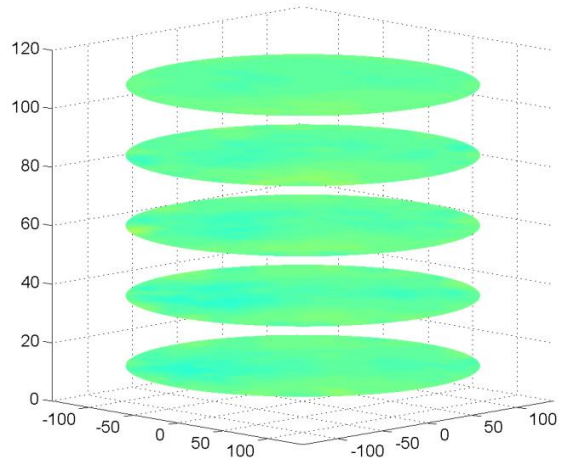

(b)

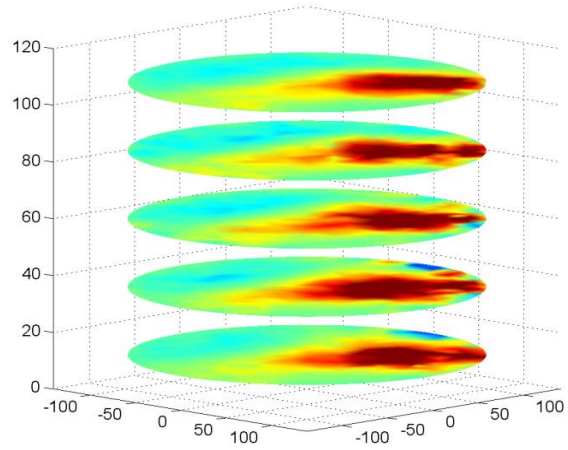

(c)

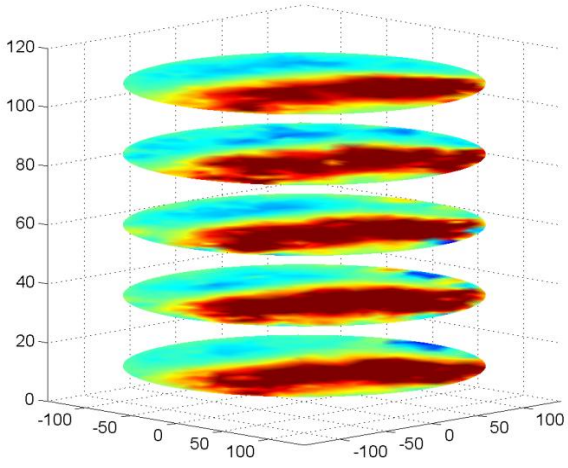

Figure 4.1 Tank reconstruction using fEITER. Reconstructed frames of data captured at 5s during a baseline recording **(a)** at 37s containing the perturbation **(b)** and at 55s containing the perturbation **(c)**. Turquoise represents a homogenous medium captured at baseline where as red represents the perturbation.

There are various limitations of using both mesh and physical phantoms to validate clinical EIT systems which have been acknowledged in literature (Gagnon et al., 2010, Holder and Tidswell, 2005, Yasin et al., 2011). Firstly, mesh phantoms cannot simulate the signal dynamics captured from three-dimensional objects such as biological tissue. Their use however is invaluable and crucial prior to undertaking EIT measurements *in-vivo* in order to assess the stability of an EIT system and also to ensure that the EIT system is capable of capturing a dominant signal compared to background and system noise (Gagnon et al., 2010, Holder and Tidswell, 2005, Yasin et al., 2011).

Physical phantoms are inherently subject to more measurement errors compared to mesh phantoms (Oh et al., 2008) attributed to evaporation of saline within the exposed tank and subtle movements and vibrations within the homogenous medium. Previous literature reporting the SNR of the fEITER system has adopted the use of both mesh and physical phantoms where SNR has been determined using the following calculation:

$$\mathrm{SNR}_i = 20 \log_{10} \frac{\mathrm{E}[m_i]}{\mathrm{St.\ Dev}[m_i]}$$

Where m_i represents the ith measurement and E represents the average for a particular injection measurement pair across 90 frames of data (Gagnon et al., 2010). The present study reports a more accurate SNR by quantifying a real change in voltage signal induced by a perturbation within a physical phantom. Whilst maximum results of SNR using the mesh resistor phantom in the current study are comparable to previously published results (Davidson et al., 2010, McCann et al., 2011), physical phantom data analysis undertaken has resulted in a much lower SNR (average SNR between 28.29dB and 31.45dB). These results should be acknowledged as an assessment of the fEITER system performance by considering a real change in signal and calculation of noise in order to determine a SNR. Although, the present analysis resulted in a lower average SNR value, maximum SNR values reported for the physical measurements (between 47.7dB and 63.04dB) are still comparable to SNR values reported for other EIT systems developed for clinical

applications (Table 4.1). Similar to previous literature reporting fEITER SNR values, it is unclear from reports of other EIT systems whether quoted SNR values are an average value or the maximum SNR determined. The current analysis aims to provide a comprehensive validity of the fEITER system using two different phantom types.

As with other physical phantoms developed for EIT validation, a considerable limitation of the physical phantom reported in the present study is that a cylindrical tank cannot simulate real signal dynamics captured from a biological tissue such as the head. There exist many layers external to the brain which injected current must penetrate before reaching the brain. To overcome this limitation, many studies including those involving fEITER have adopted the use of head shaped physical phantoms which consider the geometric shape of a head and incorporate biological layers of tissue external to the brain such as the skull and skin (Liston et al., 2004, Tidswell et al., 2003, Tidswell et al., 2001a) . A SNR of 80dB was reported for fEITER using a head shaped physical tank (Robinson, 2011). However as mentioned previously, although the geometric shape of a head was considered in the mentioned study, no change in the signal was induced to calculate the SNR. In addition, the various layers of tissue surround the brain were also not considered. Although the presented analysis in this thesis has provided a more comprehensive evaluation of SNR for the fEITER system, a head shaped tank considering the layers of tissue types surrounding the brain would provide a more accurate understanding of fEITER SNR.

4.2 Histogram and ROC curve analysis

4.2.1 Visual Stimulation: Frontal Measurements

fEITER data during visual stimulation was recorded from frontal electrodes of 14 volunteers and was filtered for REG and HFN. Individual histograms were produced for each volunteer using filtered fEITER data captured during visual stimulation. Single-subject histograms that were produced using t-statistic ref and t-statistic stim values were varied in displaying differences between reference and stimulus measurements. Whereas individual histograms for single subjects illustrated in Figures 3.4a(iii) and 3.4c(iii) demonstrate a large overlap between the t-statistic ref and t-statistic stim values, the histogram presented in Figure 3.4b(iii) for V12 shows

a greater difference between t-statistic ref and t-statistic stim values. Specifically, higher t-statistic stim values represent a larger variation between the mean of randomly selected reference and stimulus samples in contrast to a smaller variation between the means of randomly selected samples within the reference period. The examples of single-subject histograms illustrated in Figures 3.4a-c(iii) are reflective of filtered fEITER data for each volunteer presented in Figures 3.4a-c(ii). Following the presentation of the first visual flash to V12, filtered fEITER data can be seen to change before returning to baseline following the end of visual stimulus (Figure 3.4bii). Pooled t-statistic ref and t-statistic stim values across 14 volunteers were used to generate a single histogram (Figure 3.4d) which shows almost complete overlap between t-statistic ref and t-statistic stim values. The pooled ROC (Figure 3.4e) further represents the overlap in t-statistic ref and t-statistic stim values. An AUC value of 0.520 was achieved for the pooled ROC curve which demonstrates poor separation between pooled reference and stimulus fEITER comparisons.

4.2.2 Visual Measurements overlying the Visual Cortex

fEITER data was captured from the back of the head overlying the visual cortex during visual stimulation from 13 volunteers. From this data set, REG could only be identified in 10 individuals. For volunteer data where REG could not be identified, only HFN was filtered. fEITER measurements pairs located at the back of the head were noisy in nature therefore providing a plausible explanation as to why an REG frequency could not be identified in 3 volunteers. In its current state of development, fEITER does not provide a signal quality index unlike commercial monitoring devices used on the head such as the BIS Vista™; a depth of anaesthesia monitor. BIS provides a continuous signal quality index by measuring impedance from electrodes in contact with skin at regular time intervals. As a result, BIS data which does not surpass a certain level of signal quality can be excluded from analysis (Luebbehusen, 2005). A similar feature developed for the fEITER system in the future would enable users to identify the quality of data captured and eliminate poor quality data.

Single-subject histogram and ROC curves were produced for each of the 13 volunteers using t-statistic ref and t-statistic stim values. From example histograms illustrated in Figures 3.5a-c(iii) for 3 volunteers, it is evident that t-statistic ref and

stim values overlap therefore demonstrating that fEITER data captured from areas of the head overlying the visual cortex during reference periods cannot be distinguished from data captured during visual stimulation. The poor distinction between reference and stimulus data recorded from the back of the head during visual stimulation was further reiterated by individual ROC curves produced using t-statistic ref and stim values calculated for individual volunteers. Single-subject AUC values presented in Table 3.4 range between 0.502 and 0.576 which further demonstrates that visual simulation does not induce detectable changes in fEITER data recorded from electrodes overlying the visual cortex. Pooled t-statistic ref and t-statistic stim values across all 13 volunteers were used to produce a single pooled histogram and pooled ROC curve. Once more pooled data presented in Figures 3.5d and 3.5e reiterates the poor distinction between t-statistic ref and t-statistic stim values, supported by an AUC value of 0.505.

4.2.3 The Valsalva Manoeuvre (VM)

Filtered fEITER data for individual volunteers (Figures 3.6a-c(ii)) show observable changes in response to the VM being performed.

From individual histograms produced for the VM using t-statistic values (Figures 3.6a-c(iii)), a clear distinction can be observed between t-statistic ref and t-statistic stim values. As anticipated, the histograms produced for individual volunteers demonstrated that the comparison between randomly selected reference and stimulus samples generated higher t-statistic values indicating a larger variation between the mean of randomly selected reference and stimulus samples. Conversely, lower t-statistic values were generated from the comparison of randomly selected samples from the reference segment of data indicating a greater probability of means from reference samples being similar to each other. There is some overlap visible in single-subject VM histograms and also within the pooled histogram illustrated in Figure 3.6d. This demonstrates that although the majority of t-statistic ref and t-statistic stim values were distinctly different, a small proportion of comparisons generated similar t-statistic values.

Pooled t-statistic ref and stim values generated for individual volunteers who performed the VM are represented in a single ROC curve presented in Figure 3.6e. From the ROC curve it is evident that pooled t-statistic ref and t-statistic stim values

can be distinguished from each other which is reflected by an AUC value greater than 0.6 (0.658). From the pooled results presented in this thesis, it can be concluded that voluntary performance of the VM causes changes in measured fEITER data which can be differentiated from reference measurements. These results can be attributed to changes in low frequency fEITER signals captured during the VM. Individual AUC values calculated from single-volunteer ROC curves also show that the majority of volunteer fEITER data could be differentiated between reference and stimulus periods as, out of 15 volunteers, only 5 volunteers had an AUC value between 0.5 and 0.6. ROC curves for 10 volunteers generated an AUC value of greater than 0.6; the largest AUC value reported as 0.873 was acquired for Volunteer #4 (Table 3.5).

Overall, this data set shows that following filtration of the fEITER signal for REG and HFN, low frequency components still show a visible difference between reference and stimulus data in response to the VM being performed.

4.2.4 Induction of Anaesthesia

fEITER was used to capture data from 19 patients undergoing induction of anaesthesia using propofol. BIS data was simultaneously recorded to monitor the increase in depth of anaesthesia in response to propofol administration. Pooled bilateral BIS values decreased from 91.7 and 93.2, to 41.4 and 44.1 for left and right BIS respectively indicating that patients were fully anaesthetised during fEITER monitoring time following induction with propofol (Ekman et al., 2004, Myles et al., 2004).

Raw fEITER data recorded for each patient during induction was filtered for REG and HFN before t-statistic ref and t-statistic stim were calculated. Individual histograms which were produced using single-subject t-statistic values demonstrated an overlap between t-statistic ref and t-statistic stim values with few patients exhibiting greater t-statistic stim values. Individual ROC curves were produced for each patient using t-statistic ref and t-statistic stim values. From the list of AUC values calculated for individual ROC curves it is evident that there is subtle distinction between t-statistic ref and stim values of each patient as individual AUC values range from 0.502 to 0.649 with only 3 patients' data exhibiting an AUC value of over 0.6 (Table 3.6). A single histogram and ROC curve were produced using

pooled t-statistic values across all patients. From the pooled histogram illustrated in Figure 3.7d, t-statistic ref and stim values can be seen to overlap largely and there is only a small frequency of larger t-statistic values representing stimulus data. Greater t-statistic stim values would indicate a greater variation between the means of reference and stimulus data. However, from the results presented it can be concluded that there is little difference between pooled fEITER data which was captured during a reference period and pooled fEITER data which was captured following the administration of propofol during the induction period.

This is further demonstrated by an AUC value of 0.547 generated from the ROC curve of pooled t-statistic values indicating poor separation between fEITER data captured during reference and induction (Baumann et al., 2015, Fawcett, 2006a).

4.3 ApEn Analysis

ApEn was applied to fEITER data which was filtered for REG only. For these analyses, HFN was preserved in the data to explore the high frequency components within the fEITER signal and to evaluate whether changes which were not visually obvious could be detected using a physiological signal analysis tool such as ApEn. There is no published data to date which reports the application of ApEn to EIT measurements of the head. Therefore the application of ApEn to EIT data recorded using fEITER is a novel analysis technique whereby changes in fEITER data have been evaluated as changes within a physiological signal.

ApEn is a statistical method used to explore and quantify regularity within time series data such as physiological signals (Yentes et al., 2013). fEITER waveforms are highly irregular in nature, consisting of small perturbations underlying a saw tooth signal representing the REG. Furthermore, EIT data similar to physiological signals are highly non-linear and non-stationary in character. Therefore, conventional analysis techniques such as the comparison of means are not sufficient to fully quantify changes in complex waveforms such as fEITER data. In literature, ApEn analysis has been shown to correlate with subclinical changes which have remained undetected using classical analysis techniques such as levels of mean and variability testing which are typically used to evaluate time series and physiological data (Pincus and Goldberger, 1994b). Regularity within a data set is determined by data being followed by similar data and is represented by smaller ApEn values

indicating greater regularity. In contrast, irregularity within a time series means there is less chance of data points being similar to each other or being repeated. Irregularity within a data set implies greater randomness and complexity and is represented by larger ApEn values (Balasis et al., 2011). Healthy biological systems are regarded as highly complex and irregular involving coherent interactions with other physiological systems signified by larger ApEn values. Disease and perturbation within a physiological system is hypothesised to result from the decoupling of interactions with other physiological mechanisms therefore reducing complexity and increasing regularity within a physiological system indicated by smaller ApEn values.

4.3.1 ApEn applied to Visual Stimulus Data – Frontal Measurements

ApEn values calculated for single-subject fEITER responses measured from the front of the head during visual stimulation were shown to be non-significantly different from reference ApEn values. ApEn values calculated for the visual stimulation period were shown to be larger in 11 volunteers from a total of 14 volunteers.
In literature, entropy analysis of event related potentials undertaken on EEG data have revealed a decrease in entropy values during event related potentials such as visual responses. Entropy values are accepted to be lower for predictable signals indicating regularity, and are shown to increase with signal randomness (Heisz and McIntosh, 2013). Therefore, in the present study, ApEn values were expected to decrease during visual stimulation by assuming that the presentation of a repetitive visual flashing sequence would stimulate event related potentials. Contrary to expectations however, ApEn values calculated for REG filtered fEITER data were shown to increase during periods of visual stimulation in 11 out of 14 volunteers. As expected, ApEn values were shown to decrease during visual stimulation in only 3 out of a total of 14 volunteers. From these results it can be concluded that ApEn cannot be applied successfully to fEITER data acquired from frontal measurements during visual stimulation as ApEn values were not shown to decrease uniformly across all volunteers during the presentation of visual flashes. From these data there was no evidence found to support the possibility of high frequency components

within fEITER data consisting of physiological oscillations which may reflect changes in neural dynamics during visual stimulation.

4.3.2 ApEn applied to Visual Stimulus Data - Measurements overlying the Visual Cortex

ApEn values were calculated for single-subject filtered fEITER data recorded from electrodes overlying the visual cortex during the presentation of visual flashes. The visual cortex is the primary target of central retinal activity and has been shown to be a highly active area during a VEP (Maier et al., 1987, Walsh et al., 2005). Therefore, fEITER data acquired from electrodes overlying the visual cortex were evaluated using ApEn. In particular, high frequency components of the fEITER signal were evaluated following fEITER data being filtered for REG to explore whether high frequency components within the fEITER signal undergo any detectable changes quantified by ApEn in response to visual stimulation. For fEITER data captured from the back of the head of 13 volunteers who were presented with a visual flashing sequence, ApEn values were shown to be non-significantly different between reference and stimulus conditions. Compared to reference data, ApEn values were expected to decrease during the presentation of visual flashes indicating greater regularity during the stimulus presentation period (Heisz and McIntosh, 2013). Contrary to expectations however, ApEn values during visual stimulation were shown to decrease in only 4 out of 13 volunteers. For 9 volunteers, ApEn values calculated during visual stimulation were greater than reference ApEn values. Once again from the results presented it can be concluded that high frequency components of fEITER data recorded from electrodes overlying the visual cortex and quantified by ApEn, do not display the expected changes in regularity induced by a visual stimulus. No evidence was found to conclude that high frequency components preserved in the fEITER data which was filtered for REG only, contain signal features reflecting neural dynamic changes in the visual cortex during visual stimulation.

4.3.3 ApEn applied to VM Data

The VM has been shown to disrupt cerebral autoregulatory mechanisms within the brain causing characteristic changes in ICP and CBF (Tiecks et al., 1995, Zhang et al., 2004). Autoregulation of ICP and CBF is a complex physiological system maintained by a combination of autonomic, chemical and metabolic mechanisms. Under resting conditions, it can be assumed that autonomic, chemical and metabolic influences form a highly complex system mediating optimum cerebral autoregulation. During reference periods therefore, ApEn values for fEITER responses were expected to be larger indicating an irregular and complex data series. The VM is established to cause a disruption of complex cerebral autoregulatory mechanisms and therefore this disruption was expected to result in smaller ApEn values being recorded during periods of the VM. ApEn values calculated for single-subject fEITER responses during the VM were shown to be non-significantly different between reference and stimulus (VM) conditions. Contrary to expectations, in the majority of volunteers (12 out of 15 subjects) ApEn was shown to be greater during periods of the VM in comparison to reference conditions. The non-significant differences observed between reference and VM data suggests that the application of ApEn to fEITER data recorded during the VM does not result in expected differences described in literature.

4.3.4 ApEn applied to Induction of Anaesthesia Data

ApEn has been extensively applied to depth of anaesthesia data to quantify changes in EEG during the induction and maintenance period. Specifically during induction, it has been acknowledged that changes in EEG data are highly non-linear therefore, the application of analysis methods appropriate to non-linear signal dynamics are required. As a results, ApEn has been successfully used as an index of consciousness and depth of anaesthesia applied to EEG data (Li and Li, 2014). In particular, ApEn has been shown to decrease with increasing depths of anaesthesia indicating a decoupling of complex neural dynamics during the transition from a conscious state to being anaesthetised (Fan et al., 2011, Balcı et al., 2010). In the present study, ApEn values calculated for reference data were shown to be non-significantly different to ApEn values calculated during induction of anaesthesia. In accordance with literature, ApEn was shown to decrease during induction in only 6 patients from

a total of 16, although this difference was not significant. For the remaining 10 patients, ApEn was observed to increase during induction of anaesthesia contrary to published data. Due to the differences between reference and induction ApEn values being non-significantly different, it can be concluded from the present results that ApEn cannot be reliably applied to fEITER data to quantify changes in regularity induced by anaesthesia.

Chapter 5 Conclusions

fEITER data captured from the volunteer and patient trials was filtered and analysed in two parts. Firstly, t-statistic comparisons were undertaken between pairs of randomly selected epochs of data which had been filtered for REG and HFN. The REG was a visibly regular component of the fEITER signal data which has shown to be reflective of extra- and intra-cerebral blood flow changes (Bodo, 2010, Perez, 2014). The aim of the present analysis was to evaluate fundamental changes within the fEITER data therefore it was intuitive to remove dominating trends such as the REG using filtering techniques.

In addition, first order differencing was also applied to raw data to minimise trends within the signal induced by the baseline drift common to EIT measurements.

For individual subject data, 5000 comparisons were undertaken for reference and stimulus data which generated 5000 t-statistic values for each data set (reference and stimulus) per individual. Each epoch of data which was randomly selected, consisted of 50 data points. A larger epoch of data consisting of 100 data points was considered as well as a smaller epoch of data consisting of 25 data points. Neither variation in epoch length provided a significant change in the distribution of t-statistic values acquired, therefore it was deemed appropriate to use an epoch of data consisting of 50 data points.

The second stage of analysis involved the application of ApEn to data which had been filtered for REG only to allow the analysis of more subtle differences in high frequency components between reference and stimulus data.

5.1 Visual Stimulus – Frontal and Visual Cortex Data

During visual stimulation, frontal fEITER measurements and fEITER measurements captured from the back of the head overlying the visual cortex were considered for further analysis.

Classical evaluation of visual responses captured from areas of the head overlying the visual cortex involves averaging multiple EEG responses to a visual stimulus in order to extract meaningful information regarding latency and amplitude of a VEP. Averaging multiple responses effectively amplifies meaningful data within a signal

and assumes signal variability surrounding the key signal component (the VEP) is noise. In the present study, fEITER data acquired from the front of the head was evaluated due to electrodes on the forehead having excellent contact with the scalp aided by the absence of hair on this area. Therefore signal quality was expected to be greater in this area. In addition, percentage change of the fEITER signal in response to a visual flash was also evaluated; the electrode pair exhibiting the greatest percentage change across all volunteers was situated at the front of the head and was therefore evaluated further. Electrodes overlying the visual cortex were selected for further analysis as the visual cortex is the primary target of retinal stimulation using a visual stimulus such as a flashing sequence. Therefore, it was anticipated that activity within this area of the brain would be reflected in EIT data captured using fEITER.

EIT has previously been applied to human subjects to evaluate VEPs generated within the visual cortex. Professor David Holder's group based at UCL have undertaken numerous studies to display a change in measured impedance during visual stimulation and relate these changes to an increase in CBF and neuronal depolarisation within the visual cortex. As a result of neural activity increasing in the visual cortex during visual stimulation, regional CBF is also expected to increase within the visual cortex. Overall visual stimulation has been predicted to result in a decrease in impedance due to blood having a lower impedance than the brain (Holder et al., 1996). In a study undertaken by Tidswell et al., (2001b), non-invasive EIT measurements captured from human subjects during visual stimulation demonstrated significant changes in impedance although the authors were unable to determine whether the changes observed were due to cerebral blood flow or neuronal depolarisation. Absolute mean impedance change was calculated by averaging impedance values for electrodes which showed a significant impedance change. Contrary to the significant results observed for individual electrode data, no significant differences were observed for the absolute mean values between reference and visual stimulus conditions. Reconstructed images from this trial also failed to localise impedance changes to the visual cortex. This was attributed to various physiological functions occurring in the brain at once during a VEP such as regional increases and decreases in CBF and global neuronal depolarisation. Overall, the study highlighted the difficulty in relating the direction of impedance changes with simultaneous physiological activity within the brain. Later studies aimed to

distinguish regional CBF changes from neuronal responses to visual stimulation by the application of varying current injection frequencies.

A comparable study undertaken in human subjects (Gilad and Holder, 2009b) monitored impedance changes of fast neuronal activity using scalp electrodes overlying the occipital cortex during visual evoked responses induced by a pattern reversal stimuli. Results from this study showed a percentage decrease in resistance of 0.001 ± 0.0005% captured using EIT. These results were accepted to be genuine physiological responses to visual stimulation in accordance to previous modeling studies undertaken by the same group (Holder et al., 1996).

From the comparisons undertaken in the present study using pooled t-statistic values, no evidence was found to show reliable differences exist between fEITER reference and visual stimulation data for frontal fEITER measurements and also for fEITER measurements overlying the visual cortex. ApEn analysis applied to reference and visual stimulus fEITER data also demonstrated no significant differences. Potential causes of the negative outcomes observed will be discussed below.

There are key differences between previous EIT studies conducted using visual stimuli and the present study. Firstly, it must be acknowledged that traditional VEPs captured using EEG in response to visual stimulation are the result of averaged multiple responses to a visual stimulus (Li and Li, 2014). Similarly, EIT studies which have reported significant differences in impedance in response to VEPs have evaluated averaged EIT responses in response to a visual stimulus. Professor David Holder's group averaged EIT responses over 6 subjects presented with a pattern visual stimulus whilst simultaneously capturing EEG to confirm a genuine VEP. Although a poor SNR prevented EIT data to be reconstructed into an image, the study reported significant decreases in measured resistance (Gilad and Holder, 2009b).

Likewise, a study employing the use of an earlier version of fEITER known as fEIT (Towers et al., 2000) was used on human subjects to monitor areas of the brain activated in response to the presentation of sensory stimuli (Murrieta-Lee et al., 2004). Although the presented results were gained from only 2 subjects, EIT data acquired from voltage pairs were averaged to show significant differences in impedance between reference and VEP data. The authors concluded that the rapid conductivity changes observed were due to functional changes occurring at the synaptic junction of visual neurons within the visual cortex (McCann et al., 2006).

EIT data from this trial was reconstructed and demonstrated changes in conductivity relating to areas of the visual cortex (V1 to V4) in response to repetitive visual stimulation.

Analysis undertaken in the present study evaluated single responses to visual stimulation which could be regarded as a limitation of this study and a possible reason for why differences between t-statistic values calculated for reference and stimulus conditions were not observed. VEPs are regarded as a mean response of the brain to repeated visual stimulation. Individual signal fluctuations occurring over time are disregarded as noise within a signal which amplifies repetitive components such as the VEP.

A further limitation of the present study was that no measure of signal quality was assessed for fEITER data therefore levels of noise within a signal could not be determined. The effect of excess noise on the fEITER signal can be recognised from voltage measurements captured from the back of the head overlying the visual cortex, specifically for 3 of the volunteers where the REG frequency could not be identified. Large levels of noise within these data may be a plausible explanation for REG not being clearly identified in these volunteers. Furthermore, increased noise levels would also dominate the application of ApEn preventing more subtle components such as high frequency oscillations to be explored.

From the results presented it is evident that presentation of a visual stimulus does not result in measureable changes in fEITER data compared to reference data measured at rest. Although larger AUC values were acquired for some individual subjects demonstrating little difference between frontal reference and stimulus data recorded during a visual stimulus, pooled data consisting of over 65000 data points could not be used to reliably distinguish between fEITER reference and stimulus data. In addition, the application of ApEn did not demonstrate changes in high frequency components of the fEITER signal in response to a visual stimulation.

5.2 The Valsalva Manoeuvre (VM)

The VM is an established clinical diagnostic tool which is used to evaluate autonomic function due to the characteristic effects the manoeuvre elicits on cerebral and systemic circulation (Carrasco-Sosa and Guillén-Mandujano, 2012, Felker et al., 2006). Within the brain, the VM has been shown to induce an autoregulatory

response mediated by the ANS to directly influence CBFV and ICP (Hiner, 2005, Prabhakar et al., 2007). fMRI studies have identified the insular cortex as the primary anatomical region responsible for mediating autonomic outflow in response to an autonomic strain such as the VM (Nagai et al., 2010). The aim was of the present study was to evaluate fEITER signals captured in response to a large voluntary strain established to cause characteristic physiological changes in CBF and ICP in healthy individuals.

From the t-statistic comparisons undertaken, pooled data consisting of 75,000 data points was used to create a single ROC curve to display differences between reference and stimulus fEITER data. The AUC value of 0.658 generated from the pooled ROC curve demonstrates that there is relative distinction between fEITER data recorded during reference periods compared with fEITER data captured during the VM. However, ApEn analysis showed no significant differences between ApEn calculated for reference and ApEn calculated during the VM.

Collectively, these results demonstrate that following filtering of the REG and HFN, fEITER data captured during the VM can be distinguished from reference data. This is more clearly demonstrated by individual volunteer AUC values presented in Table 3.5. These data indicate that a more clear distinction between fEITER reference and stimulus data can be made from single subject data compared to pooled results. However, the results presented also demonstrate that high frequency components within the fEITER data do not demonstrate meaningful data within the fEITER signal as ApEn calculations for reference versus stimulus data were shown to be non-significantly different suggesting high frequency components within the fEITER signal may be representative of noise.

5.3 Induction of Anaesthesia

Pooled t-statistic values for induction patients generated 95,000 data points from which a single ROC curve was produced. AUC value of the pooled ROC curve was stated as 0.547 indicating poor separation between reference and stimulus fEITER data. Furthermore, ApEn comparisons of fEITER data filtered for REG only, demonstrated no significant differences between reference and stimulus data captured during the induction period. ApEn has previously been applied to BIS data captured during induction of anaesthesia to demonstrate a reduction in ApEn values

following the administration of an anaesthetic agent. As anaesthesia is induced and consciousness is gradually lost, reduced ApEn values reflect a decoupling of complex neural networks within the brain (Balcı et al., 2010, Fan et al., 2011). In the present study, although simultaneously recorded BIS data was shown to consistently decrease in each patient following the administration of propofol, ApEn analysis of high frequency components within fEITER signals did not decrease during the induction period as expected.

Results from t-statistic comparisons of the filtered fEITER signal suggest no differences in reference fEITER signals are caused as a result of anaesthetic induction. In addition, results from the ApEn analysis demonstrate that high frequency components within the fEITER signal are not representative of meaningful signal variability as the differences between reference and stimulus ApEn values were non-significant.

5.4 Thesis Conclusions

The aim of the present study was to evaluate the changes in single subject fEITER data in the presence of a performed or presented stimulus. Firstly, filtering techniques were applied to raw fEITER data using PSD estimation to reduce dominant components such as the REG, and sources of high frequency noise before multiple random comparisons were statistically performed between epochs of reference and stimulus fEITER data. Secondly, high frequency components were preserved in the fEITER signal which was filtered for REG only in order to evaluate whether subtle changes in high frequency components are reflective of changes between reference and stimulus fEITER data. ApEn was applied to fEITER data filtered for REG only in order to evaluate the high frequency components within the fEITER signals.

ApEn is a statistical method used to explore and quantify regularity within time series data and was deemed an appropriate tool to evaluate raw fEITER signals captured during an applied stimulus such as the VM, visual flashes and induction of anaesthesia. In order for accurate application of ApEn applied to fEITER data it was important to remove visible regular components such as the REG which would dominate the ApEn. A band pass filter was applied to fEITER data to remove the REG component. The most dominant frequency identified from PSD estimation was

at 1Hz; the band pass filter was applied to remove this frequency. Despite removing the most dominant frequency of the REG from the fEITER signal, components of the REG were still present within the signal as the REG waveform manifests as a sawtooth perturbation consisting of many small spikes. From PSD estimation, smaller frequencies were also identified which would contribute to the overall sawtooth perturbation of the REG. However, application of a larger band pass filter resulted in losing the majority of the fEITER signal. Therefore, only the most dominant component of the REG was effectively removed from the fEITER signal which resulted in the remaining signal still containing some REG components. This is one potential cause of inaccuracy for the application of ApEn and therefore a potential contributing factor to the poor difference observed between reference and stimulus data. Accurate application of ApEn requires a signal to be stationary which results in the mean, variance and autocorrelation of a time series being consistent over time (Pincus and Goldberger, 1994a). fEITER data in its raw form can be regarded as non-stationary due to the baseline drift common to EIT measurements. In order to stationarise fEITER data and remove the inherent baseline drift, first-order differencing was applied to the fEITER signal (Hyndman and Athanasopoulos, 2013, Leuthold et al., 2005). Whilst first-order differencing is highly effective in removing trends within a time-series, it should be acknowledged that the process of subtracting one data point from the next can also reduce sensitivity of the captured signal and therefore subtle signal components may have potentially been lost during the first-order differencing process. Furthermore, the process of first-order differencing may also have contributed to the analysis being less sensitive to changes in the mean fEITER signal level.

In addition to removing the most dominant frequency of the REG at approximately 1Hz, removal of HFN components resulted in the assumption that only relevant fEITER data was preserved for further analysis and all sources of potential contamination such as REG and HFN were removed. In fact, one of the major limitations of analysing fEITER data using a thorough analysis technique as described in this thesis is that there is no prior knowledge of the exact physiological changes, if any, being captured from the scalp using fEITER. Filtering techniques are highly useful when known physiological process can be effectively isolated. In the current study, there was prior knowledge of a single physiological change being captured using fEITER. The acquired signal could be representative of multiple

physiological changes occurring simultaneously within the head at a single time-point. Furthermore, noise in a human volunteer cannot be accurately quantified using physical phantoms typically used within the field of EIT to determine SNR of an EIT system. Therefore, although HFN components were removed in the present study using PSD estimation techniques, it is unknown whether sources of noise were still retained within the fEITER data.

Although the application of filtering techniques to EIT data is not novel, there exists no literature describing the application of filtering and de-trending methods to fEITER data (Bryan et al., 2011, Davidson et al., 2010, McCann et al., 2011, Quraishi et al., 2011, Robinson, 2011). Instead raw fEITER data has been used in the past to form reconstructions of the brain relating changes in conductivity to functional changes in physiology (Bryan et al., 2011, McCann et al., 2011, Quraishi et al., 2011).

The reconstruction process of EIT data integrates multiple simultaneous EIT voltage measurements to produce a tomographic image representing changes in conductivity within the tissue of interest (Lionheart, 2004, Liston et al., 2004). There are examples in literature where EIT data has been filtered prior to the reconstruction process. Most of these examples exist for EIT data captured from the thorax to visualise changes in ventilation and perfusion. ECG-gated EIT is a filtering technique used to amplify cardiac perfusion signals recorded using EIT. To implement this filtering technique, an ECG signal is simultaneously recorded from the individual. The QRS component of the ECG can then be utilised as a trigger for EIT data collection relating to a specific cardiac event such as the R-wave. Following a complete data cycle using ECG-gated EIT, temporal averaging of the data is undertaken to eliminate the effects of ventilation and noise from the perfusion data and therefore allowing pulsatile movement of blood within the lungs to be imaged (Eyuboglu and Brown, 1988, Eyuboglu et al., 1989, Pikkemaat and Leonhardt, 2010). Imaging studies utilising ECG-gated EIT as described above have been successfully implemented to identify abnormalities such as pulmonary emboli (Eyuboglu et al., 1989, Leathard et al., 1994). EIT data captured from the thorax has also been transformed using FFT to isolate the components of ventilation and perfusion (Kerrouche et al., 2001, Frerichs et al., 2009). As ventilation and perfusion cycles consist of different functional frequencies, EIT data differentiating the two

have been successfully reconstructed (Grant et al., 2011, Suchomel and Sobota, 2013).

The examples of literature discussed above have been applied to EIT data where there is extensive prior knowledge of physiological information; both heart and ventilation rate can be easily evaluated using alternative monitoring techniques allowing simple separation of the two functions monitored using EIT data. This is not the case for EIT data recorded from the head which is a further limitation of the present study. EIT measurements of the brain pose a highly technical challenge in that there are multiple processes occurring simultaneously within the brain such as changes in CBF, the osmotic movement of water into the extracellular space, changes in ICP and CSF and the movement of ions across cell membranes during neuronal depolarisation. Multiple physiological changes occurring at a single time point would contribute to measureable changes in impedance. However, unlike the separation of ventilation and perfusion, simultaneously occurring physiological processes in the brain captured using EIT cannot be isolated without *a prioi* information. This raises an important question to the validity and accuracy of the reconstructions which have previously been performed for fEITER data without the knowledge of specific physiological processes being reconstructed.

From the analysis and results presented in this thesis the following overarching conclusions can be made:

Once the REG and HFN have been filtered, differences in reference and stimulus data can be determined for fEITER data captured during the VM. Individual volunteer differences have been shown to be more prominent than pooled differences. Pooled data for induction of anaesthesia resulted in an AUC value greater than 0.5 indicating some separation between reference and stimulus fEITER data. However, these differences are not large enough to reliably distinguish between reference and stimulus data during induction of anaesthesia. Both the VM and induction are large stimuli, the effects of which can be observed on raw fEITER data. Furthermore, both stimuli are established to cause large global changes in physiological functions within the brain. It can be concluded that when evaluating single-subject variability of fEITER data, it may be necessary to induce large changes in order to establish a reliable difference between reference and stimulus measurements recorded using fEITER.

The evaluation of fEITER data during the presentation of a visual stimulation failed to demonstrate differences in reference and stimulus data. It can be concluded that the visual response induced by a flashing sequence was too small to show single-subject variability of fEITER data therefore no statistically significant differences could be demonstrated. Similar to EIT studies reported in literature, it would be instinctive to perform future studies where multiple responses to flashing visual sequences presented to a single subject are captured using fEITER which can be subsequently averaged to reveal a visual response. The advantage of performing such studies in the future would be that inducing a visual response could be isolated to the visual cortex and would not induce global changes within the brain unlike the VM and the induction of anaesthesia.

High frequency components evaluated using ApEn applied to single-subject fEITER data failed to demonstrate differences between reference and stimulus data for all trials evaluated. Although data was effectively stationarised using first-order differencing, subtle changes in high frequency components of the fEITER signal may still have been dominated by low frequency perturbations from the regular REG component within the signal.

At its current stage of development and from the analysis undertaken in the present study, it can be concluded that pre-processed fEITER data cannot be tomographically reconstructed for the trial conditions presented in this thesis. Without a clear understanding of how measured fEITER data relates to physiological processes occurring within the brain during a presented stimulus, reconstructions of raw fEITER data cannot provide reliable or robust information on physiological activity within the brain. The work presented in this thesis however will form the foundation for further anlaysis of fEITER data as a physiological signal in order to establish the exact sources of activity being measured.

In theory, a portable EIT technology has the potential to allow brain imaging at the bedside within a range of clinical environments. For example, this would be highly useful within the discipline of anaesthesia to monitor depth of anaesthesia currently undertaken using spectral analysis monitors such as BIS. Although they are portable, monitors such as BIS are ineffective in providing information relating to functional physiology within the brain. There are no spatial indications of anaesthetic drugs within the brain and depth of anaesthesia is correlated to an indexless scale. If the technique of EIT could be further developed as a functional bedside brain imaging

device EIT could potentially be used to localise functional changes occurring in the brain during induction and during increasing depths of anaesthesia. The application could also be extended to image the regional effects of other drugs crossing the BBB, broadening the application of EIT within clinical medicine.

Extending from the realms of the anaesthetic and operating rooms, altered levels of consciousness are frequently encountered within critically ill patients requiring a reliable assessment of varying states of consciousness. Arousal and awareness at the patient's bedside within critical care is often evaluated by 'consciousness scales' and the patient's responsiveness to commands, rather than obtaining objective assessments using functional neuroimaging techniques (Laureys et al., 2002). Once again a portable EIT device could satisfy the clinical needs mentioned above to provide an objective assessment of conscious states at the bedside within critical care. Not only would the need to transport critically ill patients to functional neuroimaging facilities be eliminated, but a portable EIT device would also provide the opportunity for continuous monitoring at the bedside. There is no doubt that a clinical requirement for a bedside brain imaging device capable of imaging fast neuronal processing exists. However it must be acknowledged that the technique of EIT in its current stage of development cannot fulfil this clinical need due to numerous technical issues which may never be overcome. When considering the tomographical end-point of EIT, almost all EIT techniques result in low-resolution conductivity images due to the inverse problem and a lack of precise anatomical information. It would seem logical to increase the number of surface electrodes to enhance spatial resolution, however this enhances the problem. Decreasing the proximity between surface electrodes results in smaller voltages being recorded and an overall reduction in the SNR (Holder, 2004, Holder, 2005, Woo, 2011). An EIT monitor capable of capturing fast neuronal processing would require boundary voltage measurements sensitive enough to record an internal change in conductivity induced by neuronal processing (Brown, 2003). A range of studies have indicated that changes relating to neuronal activity are not large enough to cause a measurable change on the surface of the head (Gilad and Holder, 2009b, Tidswell et al., 2001b). Furthermore, as in the present thesis, large changes in conductivity measured from the surface of the head cannot be attributed to a single physiological process within the head such as neuronal activity despite attempts to minimise influences within the signal from other physiological processes such as blood flow. The EIT group based

at UCL have achieved imaging of impedance changes with a temporal resolution of 2ms in the rat somatosensory cerebral cortex using epicortical electrodes (Aristovich et al., 2016). Although the technique of EIT has been used in this publication, measurable changes relating to neuronal depolarisation have only been acquired using invasive electrodes as the conductivity changes stated are too small to be captured from non-invasive surface electrodes. It has been acknowledged within the EIT community that a considerable technical advancement is required to improve the sensitivity of EIT measurements of small conductivity changes within the head relating to neuronal activity. Without such developments, it is currently an unrealistic ambition for existing EIT technologies such as fEITER to be able to reliably and non-invasively capture neuronal activity from the surface of the head. The application of EIT within the clinical field of stroke has also been explored by various research groups. The differentiation between ischaemic and haemorrhagic stroke has been of particular interest as, following ischaemic stroke, tissue impedance measured from a low-frequency current injection (below 20kHz) has been shown to increase as result of cell swelling due to the movement of extracellular fluid, into cells (Holder and Tidswell, 2005, Romsauerova et al., 2006b, Schaefer et al., 2002). In comparison, following haemorrhagic stroke, overall tissue impedance decreases due to the conductivity of blood being greater than the conductivity of brain tissue (Bonmassar et al., 2010, Holder and Tidswell, 2005). Consequently, the application of a multi-frequency EIT technology (MFEIT) also known as EIS, is highly desirable as a diagnostic tool to characterise the frequency responses between the incidence of ischaemic and haemorrhagic stroke. As a baseline measurement is not required when using EIS, it is considered advantageous for diagnostic purposes compared to EIT. Within current clinical practice, the diagnosis of stroke is undertaken using CT or MRI requiring the patient to be transferred to an imaging modality which may compromise the short time-window allowed for the successful administration of thromolytics in the incident of an ischaemic stroke. It has been proposed that a portable EIS monitor available within an accident & emergency or critical care environment may provide rapid diagnosis of acute stroke at the bedside, eliminating the need to transfer patients to an imaging facility and also eliminating the use of ionising radiation (Holder, 2004, Holder and Tidswell, 2005, Romsauerova et al., 2006b).

The application of EIS has shown to be promising for the characterisation of various tissue systems including the lung(Gao et al., 2014), breast (Zheng et al., 2008) and prostate (Mishra et al., 2012).

As acknowledged previously within this thesis, imaging the brain using EIT or EIS presents a unique challenge compared to imaging soft tissue systems such as the lungs, breast and prostate due to the brain being encased in the highly resistant skull. The injected current amplitude cannot be increased beyond medical safety regulations, limiting the maximum current density at all depths of the brain when using a spectrum of injection frequencies, resulting in a low SNR (Malone et al., 2014b). Current research investigating the use of EIS applied to the brain for stroke-type differentiation concerns minimising reconstruction artefacts and instrumentation errors caused by electrode positioning, contact impedance and tissue conductivity spectra in realistic simulations of the head (Malone et al., 2014b, Dowrick et al., 2016). Results from simulation studies have provided the foundation for further validation tests to be undertaken in physical phantoms prior to any human studies being performed (Malone et al., 2014b, Jehl and Holder, 2016). Once more, it must be acknowledged that despite the theoretical potential of an EIS sysetm capable of differentiating between haemorrhagic and ischaemic strokes, existing multi-frequency systems are only being applied to phantom and anilmal simulations of stroke. The most recent in-vivo experiments to image stroke at UCL were undertaken in anaesthetised rats using invasive intra-cerebral and skull electrodes (Dowrick et al., 2016) and further publications from this group are exploring methods to improve the ill-posed inverse problem applied to multi-frequency EIT imaging (Jehl and Holder, 2016). The current publications within the field of EIS for stroke imaging once more demonstrates that pioneering EIT groups such as UCL are still at a premature stage of developing a clinical EIS modality which would be suitable for applications on the human head using non-invaisve electrodes.

The suggestion of using EIT and EIS in conjunction with an established high-resolution imaging modality such as MRI has been continuously recommended as a research ambition in literature (Holder, 1987, Woo, 2011). A multi-modal technology combining a high resolution anatomical image of the brain with conductivity changes acquired by EIT would certainly improve the inherent problems of poor image resolution acquired with EIT. Furthermore, this may also provide the technical validation required to analyse EIT data and images. The

development of such a multi-modal technology would however require significant investment and extensive research. More importantly, such developments may compromise the most desirable features of EIT technology, these being low production costs, non-invasiveness and portability for use at the bedside.

Although the potential of EIT and EIS within clinical medicine is compelling, the development of a medical device encompassing the technology is still highly speculative.

At this present time, the technology of EIT still requires extensive practical research to amplify the low signals acquired from the scalp compared to background noise. The necessary technical breakthrough which is needed will only be accomplished with considerable mathematical expertise, collaboration from the wider EIT community and substantial monetary investments.

Specific steps would then need to be undertaken to produce a medical device suitable for clinical use, including patenting the technology, CE marking and multi-centre clinical trials. The latter would take several further years of research and potentially millions of pounds worth of investment. Similar to the BIS monitor developed over numerous years of research costing millions of pounds; EIT as a bedside brain imaging technology has no gold standard to validate EIT signals acquired from the scalp. Clinical studies undertaken using the BIS technology used predictive probability outcome measures to compare with various BIS values. Similarly, it will be imperative to firstly validate EIT acquired signals and tomographical images from the head prior to developing an EIT medical device for clinical use.

The general findings of the present thesis suggest that producing a commercial EIT or EIS device may be a task too great for the immediate future when considering the lack of significance acquired from pooled data. However, there is some optimism associated with single subject measurements presented in this thesis which may fuel further research into the technology. The future of EIT and EIS may be restricted to being used as a clinical research tool only, not a commercial medical device.

Chapter 6 Future Work

There now exists a library of fEITER data which has been recorded as part of the volunteer and patient trials undertaken at CMFT. The work presented in this thesis will form the foundations for future analysis of existing data and will also provide motives for further research.

fEITER has been used to explore the response of only a single well-defined autonomic challenge until now: the Valsalva manoeuvre (VM). From the results presented in this thesis, the VM produced the greatest distinction between reference and stimulus data when comparisons of t-statistic values were undertaken. In addition, prior to filtering the data, changes in the REG and fEITER waveform could be visualised as a result of the manoeuvre being undertaken which was attributed to the VM being a strong stimulus affecting various physiological systems within the brain and body. The changes observed in the present study have provided a motive to explore other autonomic strains and their effects on fEITER data captured from the head in a volunteer study proposed to be undertaken at CMFT. The responses to autonomic challenges such as the Mueller's manoeuvre (MM) and the hand grip test will be explored using fEITER in future studies. Similar to the characteristic effects of a large stimulus such as the VM on cerebral blood flow and pressure, the MM and the hand grip test have also been shown to induce characteristic changes in neuronal activity and cerebral haemodynamics (Carrasco-Sosa and Guillén-Mandujano, 2012, Macey et al., 2012). It is anticipated that results from this study will provide further understanding of fEITER responses recorded during autonomic challenges. From the data presented in this thesis, the amplitude of REG changed in responses to the VM being performed, reflecting the characteristic changes induced by the VM on cerebral and systemic circulation. Therefore, changes in REG during autonomic strains will also be evaluated in the future trial to gain further insight into the physiological responses captured in the form of REG and how this is affected during a voluntary autonomic strain. This follow-on study has received a favourable ethical opinion from South Manchester Local Research Ethics Committee (LREC) (Appendix 3).

Unlike fEITER responses recorded during the VM, single pair voltage measurements during a visual stimulus provided no evidence for significant differences in fEITER

data between reference and stimulus conditions. This was attributed to a visual response being too small to show a significant change in voltage measurements recorded from a single electrode pair. It would be instinctive to average multiple fEITER responses to a flashing visual sequence recorded multiple times from the same electrode pair to attenuate any signal variability and in turn to amplify the visual response recorded from the visual cortex.

Averaging multiple visual responses is common practice within EEG recordings to amplify the VEP (Aminioff and Goodin, 1994, Halliday et al., 1973) and this method has also been applied to evaluate visual responses captured using EIT in previous studies (Gilad and Holder, 2009b, Murrieta-Lee et al., 2004). Whereas in the current study a flashing visual sequence was only presented to a single volunteer twice, in future studies it would be proposed to present a visual flashing sequence upto 5 times to a single volunteer in order to average the responses recorded from a single electrode pair.

In order to fulfil the tomographical end-point of fEITER, EIT and reconstruction expertise is vital. We aim to continue collaboration with the EIT group based at UCL headed by Professor David Holder. Although pooled data has provided little evidence to show that quantifiable physiological changes can be captured using fEITER, the reconstruction process could be deemed as a more sensitive approach to visualise global changes occurring at all depths of the brain. Unlike the analysis undertaken in the present study which has only considered changes recorded from single electrode measurement pairs, the process of tomographic reconstruction of fEITER data will explore simultaneous changes recorded from a total of 546 electrode pairs.

The next stage of developing the fEITER system further will inevitably involve the application of multiple injection frequencies; ideally a spectrum which would encompass the present current injection frequency of fEITER of 10kHz. Capturing responses induced by the same stimulus using different injection frequencies may potentially eliminate contamination of the fEITER signal by the dominant REG. UCL have already explored the use of multi-frequency EIT systems applied to the head (McEwan et al., 2007, McEwan et al., 2006, Romsauerova et al., 2006b) therefore future collaboration with this group will provide important avenues for the development and future applications of fEITER.

With further development, a fast, functional brain monitoring EIT device may be a useful tool to continuously monitor patients undergoing particular surgical procedures that are associated with adverse neurological outcomes. Patients requiring coronary-artery bypass surgery are typically characterised as older and often suffering from vascular disease. A major concern for this patient group undergoing coronary-artery bypass surgery has been the incidence of post-operative neurological disorders including stroke and cognitive decline. Although the precise mechanisms of post-operative neurological disorders have not been identified, the use of cardiopulmonary bypass during surgery has been attributed as a possible cause of adverse post-operative neurological outcomes (Bartels et al., 2013, Norkiene et al., 2010, Selnes et al., 2012). It has been proposed that continuous intra-operative monitoring of the brain using EIT during cardiopulmonary bypass may provide further information on physiological function within the brain by exploring sub-second and slower changes occurring at all depths of the brain. In addition, a portable EIT device would enable post-operative monitoring to be continuously undertaken on the critical care unit or post-operative ward, to further understand the incidence of post-operative neurological dysfunction.

Collectively, the work presented in this thesis has highlighted the potential clinical applications of EIT to monitor functional brain activity. More importantly, results have also highlighted areas of fEITER research requiring further research prior to undertaking tomographical reconstructions.

REFERENCES

1. ADLER, A. & LIONHEART, W. R. B. 2006. Uses and abuses of EIDORS: an extensible software base for EIT. *Physiological Measurement,* 27**,** S25.
2. AGARWAL, A. K. & WINNY, G. C. 1999. Role Of ECT Phenothiazine Combination In Schizophrenia. *Indian Journal of Ophthalmology,* 47**,** 233-236.
3. AHN, S., JUN, S. C., SEO, J. K., LEE, J., WOO, E. J. & HOLDER, D. 2010. Frequency-difference electrical impedance tomography: Phantom imaging experiments. *Journal of Physics: Conference Series,* 224**,** 012152.
4. ALBAICETA, G. & BLANCH, L. 2011. Beyond volutrauma in ARDS: the critical role of lung tissue deformation. *Critical Care,* 15**,** 304.
5. ALKIRE, M. D. MICHAEL T., HAIER, P. RICHARD J., BARKER, P. M. D. STEVEN J., SHAH, NITIN K., WU, M. D. JOSEPH C. & KAO, P. M. D. JAMES Y. 1995. Cerebral Metabolism during Propofol Anesthesia in Humans Studied with Positron Emission Tomography *Anesthesiology,* 82**,** 393-403.
6. ALKIRE, M. D. MICHAEL T., MCREYNOLDS, B. S. JAYME R., HAHN, B. A. EMILY L. & TRIVEDI, AKASH N. 2007. Thalamic Microinjection of Nicotine Reverses Sevoflurane-induced Loss of Righting Reflex in the Rat. *Anesthesiology,* 107**,** 264-272.
7. ALKIRE, M. T. 2008. Loss of effective connectivity during general anesthesia. *Int Anesthesiol Clin.,* 46**,** 55-73. doi: 10.1097/AIA.0b013e3181755dc6.
8. ALKIRE, M. T. & HAIER, R. J. 2001. Correlating in vivo anaesthetic effects with ex vivo receptor density data supports a GABAergic mechanism of action for propofol, but not for isoflurane† ‡. *British Journal of Anaesthesia,* 86**,** 618-626.
9. ALKIRE, M. T., HAIER, R. J. & FALLON, J. H. 2000. Toward a Unified Theory of Narcosis: Brain Imaging Evidence for a Thalamocortical Switch as the Neurophysiologic Basis of Anesthetic-Induced Unconsciousness. *Consciousness and Cognition,* 9**,** 370-386.
10. AMINIOFF, M. J. & GOODIN, D. S. 1994. Visual evoked potentials. *Journal of Clinical Neurophysiology,* 11**,** 493-9.
11. AMINOFF, M. 1980. *Electrodiagnosis in Clinical Neurology,* New York, Churchill Livingstone Inc.
12. ANTHONY, M. Y., EVANS, D. H. & LEVENE, M. I. 1993. Neonatal cerebral blood flow velocity responses to changes in posture. *Archives of disease in childhood,* 69**,** 304-8.
13. ANTONINI, A., VONTOBEL, P., PSYLLA, M., GUNTHER, I., MAGUIRE, P. R., MISSIMER, J. & LEENDERS, K. L. 1995. Complementary Positron Emission Tomographic Studies of the Striatal Dopaminergic System in Parkinson's Disease. *Arch Neurol,* 52**,** 1183-1190.
14. ARISTOVICH, K. Y., PACKHAM, B. C., KOO, H., SANTOS, G. S. D., MCEVOY, A. & HOLDER, D. S. 2016. Imaging fast electrical activity in the brain with electrical impedance tomography. *NeuroImage,* 124, Part A**,** 204-213.
15. ARROYO, S., LESSER, R. P., POON, W., WEBBER, W. R. S. & GORDON, B. 1997. Neuronal generators of visual evoked potentials in humans: visual processing in the human cortex. *Epilepsia,* 38**,** 600-10.

16. ATILLA, H., TEKELI, O., ÖRNEK, K., BATIOGLU, F., ELHAN, A. H. & ERYILMAZ, T. 2006. Pattern electroretinography and visual evoked potentials in optic nerve diseases. *Journal of Clinical Neuroscience,* 13**,** 55-59.
17. AVIDAN, M. S., JACOBSOHN, E., GLICK, D., BURNSIDE, B. A., ZHANG, L., VILLAFRANCA, A., KARL, L., KAMAL, S., TORRES, B., O'CONNOR, M., EVERS, A. S., GRADWOHL, S., LIN, N., PALANCA, B. J. & MASHOUR, G. A. 2011. Prevention of Intraoperative Awareness in a High-Risk Surgical Population. *New England Journal of Medicine,* 365**,** 591-600.
18. AVIDAN, M. S., ZHANG, L., BURNSIDE, B. A., FINKEL, K. J., SEARLEMAN, A. C., SELVIDGE, J. A., SAAGER, L., TURNER, M. S., RAO, S., BOTTROS, M., HANTLER, C., JACOBSOHN, E. & EVERS, A. S. 2008. Anesthesia Awareness and the Bispectral Index. *New England Journal of Medicine,* 358**,** 1097-1108.
19. AVILL, R., MANGNALL, Y. F., BIRD, N. C., BROWN, B. H., BARBER, D. C., SEAGAR, A. D., JOHNSON, A. G. & READ, N. W. 1987. Applied potential tomography. A new noninvasive technique for measuring gastric emptying. *Gastroenterology,* 92**,** 1019-26.
20. BABILONI, C., PIZZELLA, V., GRATTA, C. D., FERRETTI, A. & ROMANI, G. L. 2009. Chapter 5 Fundamentals of Electroencefalography, Magnetoencefalography, and Functional Magnetic Resonance Imaging. *In:* LUCA, R., DARIO, I. & LEOPOLD, S. (eds.) *International Review of Neurobiology.* Academic Press.
21. BALASIS, G., DAGLIS, I. A., ANASTASIADIS, A. & EFTAXIAS, K. 2011. Detection of dynamic complexity changes in Dst time series using entropy concepts and rescaled range analysis. *In:* LIU, W. & FUJIMOTO, M. (eds.) *The dynamic magnetosphere.* New York: Springer.
22. BALCı, C., KARABEKIR, H. & SIVACI, R. 2010. Determining entropy values equivalent to the bispectral index values during sevoflurane anaesthesia. *Archives of Medical Science : AMS,* 6**,** 370-374.
23. BALDESI, O., BRUDER, N., VELLY, L. & GOUIN, F. 2004. Spurious bispectral index values due to electromyographic activity. *European journal of anaesthesiology,* 21**,** 324-325.
24. BARTELS, K., MCDONAGH, D. L., NEWMAN, M. F. & MATHEW, J. P. 2013. Neurocognitive outcomes after cardiac surgery. *Current Opinion in Anesthesiology,* 26**,** 91-97.
25. BASANO, L., OTTONELLO, P., NOBILI, F., VITALI, P., PALLAVICINI, F. B., RICCA, B., PRASTARO, T., ROBERT, A. & RODRIGUEZ, G. 2001. Pulsatile electrical impedance response from cerebrally dead adult patients is not a reliable tool for detecting cerebral perfusion changes. *Physiological Measurement,* 22**,** 341.
26. BAULE, G. & MCFEE, R. 1963. Detection of the magnetic field of the heart. *American Heart Journal,* 66**,** 95-96.
27. BAUMANN, P., FOUZAS, S., PRAMANA, I., GRASS, B., NIESSE, O., BÜHRER, C., SPANAUS, K. & WELLMANN, S. 2015. Plasma Proendothelin-1 as an Early Marker of Bronchopulmonary Dysplasia. *Neonatology,* 108**,** 293-296.
28. BAXTER, A. J., MANGNALL, Y. F., LOJ, E. H., BROWN, B., BARBER, D. C., JOHNSON, A. G. & READ, N. W. 1988. Evaluation of applied

potential tomography as a new non-invasive gastric secretion test. *Gut,* 29**,** 1730-5.
29. BAYFORD, R. H. 2006. BIOIMPEDANCE TOMOGRAPHY (ELECTRICAL IMPEDANCE TOMOGRAPHY). *Annual Review of Biomedical Engineering,* 8**,** 63-91.
30. BAYFORD, R. H., BOONE, K. G., HANQUAN, Y. & HOLDER, D. S. 1996. Improvement of the positional accuracy of EIT images of the head using a Lagrange multiplier reconstruction algorithm with diametric excitation. *Physiological Measurement,* 17**,** A49.
31. BEAR, M. F., CONNORS, B. W. & PARADISO, M. A. 2001. *Neuroscience. Exploring the brain. Second edition,* Maryland, Lippincott Williams & Wilkins.
32. BEAUMONT, A. & MARMAROU, A. 2002. Approximate Entropy: A Regularity Statistic for Assessment of Intracranial Pressure. *In:* CZOSNYKA, M., PICKARD, J., KIRKPATRICK, P., SMIELEWSKI, P. & HUTCHINSON, P. (eds.) *Intracranial Pressure and Brain Biochemical Monitoring.* Springer Vienna.
33. BERLIN, L. 2011. Communicating the Harmful Effects of Radiation Exposure from Medical Imaging: Malpractice Considerations. *Health Physics,* 101**,** 583-588.
34. BERRINGTON DE GONZÁLEZ, A., MAHESH, M., KIM, K. & ET AL. 2009. PRojected cancer risks from computed tomographic scans performed in the united states in 2007. *Archives of Internal Medicine,* 169**,** 2071-2077.
35. BEZANILLA, F. 2006. The action potential: From voltage-gated conductances to molecular structures. *Biological Research,* 39**,** 425-435.
36. BHARGAVA, A. K. M., SETLUR, R. M. & SREEVASTAVA, D. M. M. 2004. Correlation of Bispectral Index and Guedel's Stages of Ether Anesthesia. *Anesthesia & Analgesia,* 98**,** 132-134.
37. BIGLAN, A., ARY, D. & WAGENAAR, A. C. 2000. The Value of Interrupted Time-Series Experiments for Community Intervention Research. *Prevention Science,* 1**,** 31-49.
38. BILAL, R. 2012. *Investigation of undesired errors relating to the planar array system of electrical impedance mammography for breast cancer detection.* Master of Philosophy, University of Sussex.
39. BIRD, T. D. & CRILL, W. E. 1981. Pattern-reversal visual evoked potentials in the hereditary ataxias and spinal degenerations. *Annals of Neurology,* 9**,** 243-250.
40. BLICHER, J. U., STAGG, C. J., O'SHEA, J., OSTERGAARD, L., MACINTOSH, B. J., JOHANSEN-BERG, H., JEZZARD, P. & DONAHUE, M. J. 2012. Visualization of altered neurovascular coupling in chronic stroke patients using multimodal functional MRI. *J Cereb Blood Flow Metab,* 32**,** 2044-2054.
41. BODO, M. 2010. Studies in Rheoencephalography (REG). *Journal of Electrical Bioimpedance,* 1**,** 22.
42. BODO, M., PEARCE, F. J., MONTGOMERY, L. D., ROSENTHAL, M., KUBINYI, G., THUROCZY, G., BRAISTED, J., FORCINO, D., MORRISSETTE, C. & NAGY, I. 2003. Measurement of brain electrical impedance: animal studies in rheoencephalography. *Aviation, space, and environmental medicine,* 74**,** 506-11.

43. BOILEAU, I., PAYER, D., HOULE, S., BEHZADI, A., RUSJAN, P. M., TONG, J., WILKINS, D., SELBY, P., GEORGE, T. P., ZACK, M., FURUKAWA, Y., MCCLUSKEY, T., WILSON, A. A. & KISH, S. J. 2012. Higher Binding of the Dopamine D3 Receptor-Preferring Ligand [11C]-(+)-Propyl-Hexahydro-Naphtho-Oxazin in Methamphetamine Polydrug Users: A Positron Emission Tomography Study. *The Journal of Neuroscience,* 32**,** 1353-1359.
44. BOLY, M., MORAN, R., MURPHY, M., BOVEROUX, P., BRUNO, M. A., NOIRHOMME, Q., LEDOUX, D., BONHOMME, V., BRICHANT, J., TONONI, G., LAUREYS, S. & FRISTON, K. 2012. Connectivity changes underlying spectral EEG changes during propofol-induced loss of consciousness. *J Neurosci.,* 32**,** 7082-90. doi: 10.1523/JNEUROSCI.3769-11.2012.
45. BONMASSAR, G., IWAKI, S., GOLDMAKHER, G., ANGELONE, L. M., BELLIVEAU, J. W. & LEV, M. H. 2010. On the Measurement of Electrical Impedance Spectroscopy (EIS) of the Human Head. *International journal of bioelectromagnetism,* 12**,** 32-46.
46. BONMASSAR, G., SCHWARTZ, D. P., LIU, A. K., KWONG, K. K., DALE, A. M. & BELLIVEAU, J. W. 2001. Spatiotemporal Brain Imaging of Visual-Evoked Activity Using Interleaved EEG and fMRI Recordings. *NeuroImage,* 13**,** 1035-1043.
47. BOONE, K., LEWIS, A. M. & HOLDER, D. S. 1994. Imaging of cortical spreading depression by EIT: implications for localization of epileptic foci. *Physiological Measurement,* 15**,** A189.
48. BOONE, K. G. & HOLDER, D. S. 1996. Current approaches to analogue instrumentation design in electrical impedance tomography. *Physiological Measurement,* 17**,** 229.
49. BORST, J. G. G. & SAKMANN, B. 1998. Calcium current during a single action potential in a large presynaptic terminal of the rat brainstem. *The Journal of Physiology,* 506**,** 143-157.
50. BOVEROUX, P., VANHAUDENHUYSE, A., BRUNO, M.-A., NOIRHOMME, Q., LAUWICK, S., LUXEN, A., DEGUELDRE, C., PLENEVAUX, A., SCHNAKERS, C., PHILLIPS, C., BRICHANT, J.-F., BONHOMME, V., MAQUET, P., GREICIUS, M. D., LAUREYS, S. & BOLY, M. 2010. Breakdown of within- and between-network Resting State Functional Magnetic Resonance Imaging Connectivity during Propofol-induced Loss of Consciousness. *Anesthesiology,* 113**,** 1038-1053.
51. BRADDICK, O. & ATKINSON, J. 2011. Development of human visual function. *Vision Research,* 51**,** 1588-1609.
52. BRADLEY, A. P. 1997. The use of the area under the ROC curve in the evaluation of machine learning algorithms. *Pattern Recognition,* 30**,** 1145-1159.
53. BRENNER, D. J., ELLISTON, C. D., HALL, E. J. & BERDON, W. E. 2001. Estimated Risks of Radiation-Induced Fatal Cancer from Pediatric CT. *American Journal of Roentgenology,* 176**,** 289-296.
54. BRENNER, D. J. & HALL, E. J. 2007. Computed Tomography — An Increasing Source of Radiation Exposure. *New England Journal of Medicine,* 357**,** 2277-2284.
55. BRIGHAM, E. O. 1988. *The Fast Fourier Transform and Its Applications,* Prentice-Hall Signal Processing Series.

56. BROOKS, D. J. 2003. PET Studies on the Function of Dopamine in Health and Parkinson's Disease. *Annals of the New York Academy of Sciences,* 991**,** 22-35.
57. BROOKS, D. J. 2005. Positron Emission Tomography and Single-Photon Emission Computed Tomography in Central Nervous System Drug Development. *NeuroRX,* 2**,** 226-236.
58. BROWN, B. H. 2003. Electrical impedance tomography (EIT): a review. *Journal of Medical Engineering & Technology,* 27**,** 97-108.
59. BROWN, B. H. & BARBER, D. C. 1987. Electrical impedance tomography; the construction and application to physiological measurement of electrical impedance images. *Medical progress through technology,* 13**,** 69-75.
60. BROWN, B. H. & SEAGAR, A. D. 1987. The Sheffield data collection system. *Clinical Physics and Physiological Measurement,* 8**,** 91.
61. BRUHN, J. M. D., ROPCKE, H. M. D., REHBERG, B. M. D., BOUILLON, T. M. D. & HOEFT, A. M. D. P. D. 2000. Electroencephalogram Approximate Entropy Correctly Classifies the Occurrence of Burst Suppression Pattern as Increasing Anesthetic Drug Effect. *Anesthesiology,* 93**,** 981-985.
62. BRYAN, A., POMFRETT, C. J. D., DAVIDSON, J. L., POLLARD, B. J. P., QURAISHI, T., WRIGHT, P., ROBINSON, R., AHSAN, S. T. & MCCANN, H. 2011. Functional Electrical Impedance Tomography by Evoked Response (fEITER): a new device for the study of human brain function during anaesthesia. *British Journal of Anaesthesia,* 106**,** 428-429.
63. CANCER RESEARCH UK 2014. Cancer Research UK (2014). Cancer Statistics Report: Cancer Incidence and Mortality in the UK, September 2014.
64. CARNEY, P. A., MIGLIORETTI, D. L., YANKASKAS, B. C., KERLIKOWSKE, K., ROSENBERG, R., RUTTER, C. M., GELLER, B. M., ABRAHAM, L. A., TAPLIN, S. H., DIGNAN, M., CUTTER, G. & BALLARD-BARBASH, R. 2003. Individual and Combined Effects of Age, Breast Density, and Hormone Replacement Therapy Use on the Accuracy of Screening Mammography. *Annals of Internal Medicine,* 138**,** 168-175.
65. CARRASCO-SOSA, S. & GUILLEN-MANDUJANO, A. Dynamics of autonomic activity during Mueller and Valsalva maneuvers assessed by time-frequency analysis of cardiovascular variability. Computing in Cardiology, 2011, 18-21 Sept. 2011 2011. 201-204.
66. CARRASCO-SOSA, S. & GUILLÉN-MANDUJANO, A. 2012. Response patterns of arterial pressure and heart period to Mueller manoeuvre and their comparison to those of Valsalva manoeuvre. *Clinical Physiology and Functional Imaging,* 32**,** 253-261.
67. CHAMPENEY, D. 1974. Fourier transforms and their physical applications by D. C. Champeney. *Acta Crystallographica Section A,* 30**,** 126.
68. CHAN, M. T. V. M. F., CHENG, B. C. P. M. F., LEE, T. M. C. P., GIN, T. M. D. F. F. & THE, C. T. G. 2013. BIS-guided Anesthesia Decreases Postoperative Delirium and Cognitive Decline. *Journal of Neurosurgical Anesthesiology,* 25**,** 33-42.
69. CHARMANDARI, E., PINCUS, S. M., MATTHEWS, D. R., DENNISON, E., FALL, C. H. D. & HINDMARSH, P. C. 2001. Joint Growth Hormone and Cortisol Spontaneous Secretion Is More Asynchronous in Older Females

Than in Their Male Counterparts. *The Journal of Clinical Endocrinology & Metabolism,* 86**,** 3393-3399.
70. CHATFIELD, C. 1989. Non-linear and non-stationary time series analysis. *International Journal of Forecasting,* 5**,** 428-429.
71. CHEREPENIN, V., KARPOV, A., KORJENEVSKY, A., KORNIENKO, V., MAZALETSKAYA, A., MAZOUROV, D. & MEISTER, D. 2001. A 3D electrical impedance tomography (EIT) system for breast cancer detection. *Physiological Measurement,* 22**,** 9.
72. CHOI, M. H., KAO, T.-J., ISAACSON, D., SAULNIER, G. J. & NEWELL, J. C. 2007. A Reconstruction Algorithm for Breast Cancer Imaging With Electrical Impedance Tomography in Mammography Geometry. *Biomedical Engineering, IEEE Transactions on,* 54**,** 700-710.
73. CHUANG, Y. M., HU, H. H. & PAN, P. J. 2005. Cerebral Syncope: Insights from Valsalva Maneuver. *European Neurology,* 54**,** 98-102.
74. CINEL, I., JEAN, S. & DELLINGER, R. P. 2007. Dynamic Lung Imaging Techniques in Mechanically Ventilated Patients. *Intensive Care Medicine.* Springer Berlin Heidelberg.
75. CLARK, M. D. DONALD L. & ROSNER, P. D. BURTON S. 1973. Neurophysiologic Effects of General AnestheticsI. The Electroencephalogram and Sensory Evoked Responses in Man. *Anesthesiology,* 38**,** 564-582.
76. COHEN, D. 1967. Magnetic fields around the torso: production by electrical activity of the human heart. *Science,* 156**,** 652-4.
77. COHEN, D. 1968. Magnetoencephalography: evidence of magnetic fields produced by alpha-rhythm currents. *Science,* 161**,** 784-6.
78. COHEN, D. 1972. Magnetoencephalography: detection of the brain's electrical activity with a superconducting magnetometer. *Science,* 175**,** 664-6.
79. DA ROSA, A. C. & RODRIGUES, J. P. M. 2011. Dream therapy: correlation of dream contents with encephalographic and cardiovascular activations. *In:* CVETKOVIC, D. & COSIC, I. (eds.) *States of consciousness. Experimental insights into meditation, waking, sleep and derams.* Springer-Verlag Berlin Heidelberg.
80. DAABISS, M. 2011. American Society of Anaesthesiologists physical status classification. *Indian Journal of Anaesthesia,* 55**,** 111-115.
81. DARGAVILLE, P., RIMENSBERGER, P. & FRERICHS, I. 2010. Regional tidal ventilation and compliance during a stepwise vital capacity manoeuvre. *Intensive Care Medicine,* 36**,** 1953-1961.
82. DAVALOS, R. & RUBINSKY, B. 2004. Electrical impedance tomography of cell viability in tissue with application to cryosurgery. *J Biomech Eng.,* 126**,** 5.
83. DAVIDSON, J. L., WRIGHT, P., AHSAN, S. T., ROBINSON, R. L., POMFRETT, C. J. D. & MCCANN, H. 2010. fEITER – a new EIT instrument for functional brain imaging. *Journal of Physics: Conference Series,* 224**,** 012025.
84. DAVIES, H. E., WATHEN, C. G. & GLEESON, F. V. 2011. *The risks of radiation exposure related to diagnostic imaging and how to minimise them*.
85. DAWSON, P. 2004. Patient dose in multislice CT: why is it increasing and does it matter? *British Journal of Radiology,* 77**,** S10-S13.
86. DEVOUS SR, M. D. 2005. Single-Photon Emission Computed Tomography in Neurotherapeutics. *NeuroRX,* 2**,** 237-249.

87. DI RUSSO, F., MARTÍNEZ, A., SERENO, M. I., PITZALIS, S. & HILLYARD, S. A. 2002. Cortical sources of the early components of the visual evoked potential. *Human Brain Mapping,* 15**,** 95-111.
88. DIRUSSO, F., MARTINEZ, A., SERENO, M. I., PITZALIS, S. & HILLYARD, S. 2001. Cortical sources of the early components of the visual evoked potential. *Human Brain Mapping,* 15**,** 95-111.
89. DIRUSSO, F., PITZALIS, S., SPITONI, G., APRILE, T., PATRIA, F., SPINELLI, D. & HILLYARD, S. A. 2005. Identification of the neural sources of the pattern-reversal VEP. *NeuroImage,* 24**,** 874-86.
90. DOU, L., GAO, H.-M., LU, L. & CHANG, W.-X. 2014. Bispectral index in predicting the prognosis of patients with coma in intensive care unit. *World Journal of Emergency Medicine,* 5**,** 53-56.
91. DOWRICK, T., BLOCHET, C. & HOLDER, D. 2016. In vivo bioimpedance changes during haemorrhagic and ischaemic stroke in rats: towards 3D stroke imaging using electrical impedance tomography. *Physiological Measurement,* 37**,** 765.
92. DRESSLER, O., SCHNEIDER, G., STOCKMANNS, G. & KOCHS, E. F. 2004. Awareness and the EEG power spectrum: analysis of frequencies. *British Journal of Anaesthesia,* 93**,** 806-809.
93. DUCATI, A., FAVA, E. & MOTTI, E. D. F. 1988. Neuronal generators of the visual evoked potentials: intracerebral recording in awake humans. *Electroencephalography and Clinical Neurophysiology/Evoked Potentials Section,* 71**,** 89-99.
94. DUECK, M. H., PETZKE, F., GERBERSHAGEN, H. J., PAUL, M., HEßELMANN, V., GIRNUS, R., KRUG, B., SORGER, B., GOEBEL, R., LEHRKE, R., STURM, V. & BOERNER, U. 2005. Propofol attenuates responses of the auditory cortex to acoustic stimulation in a dose-dependent manner: A FMRI study. *Acta Anaesthesiologica Scandinavica,* 49**,** 784-791.
95. DUNN, K. & NELSON, M. 2014. Neurovascular signaling in the brain and the pathological consequences of hypertension. *Am J Physiol Heart Circ Physiol.*, 306**,** H1-14. doi: 10.1152/ajpheart.00364.2013. Epub 2013 Oct 25.
96. DUYN, J. H. & KORETSKY, A. P. 2011. Novel frontiers in ultra-structural and molecular MRI of the brain. *Current Opinion in Neurology,* 24**,** 386-393.
97. ECKERT, T., BARNES, A., DHAWAN, V., FRUCHT, S., GORDON, M. F., FEIGIN, A. S. & EIDELBERG, D. 2005. FDG PET in the differential diagnosis of parkinsonian disorders. *NeuroImage,* 26**,** 912-921.
98. EKMAN, A., LINDHOLM, M. L., LENNMARKEN, C. & SANDIN, R. 2004. Reduction in the incidence of awareness using BIS monitoring. *Acta Anaesthesiologica Scandinavica,* 48**,** 20-26.
99. ELISBERG, E. I. 1963. Heart rate response to the valsalva maneuver as a test of circulatory integrity. *JAMA,* 186**,** 200-205.
100. EROL, R. A., CHERIAN, P., SMALLWOOD, R. H., BROWN, B. H. & BARDHAN, K. D. 1996a. Can electrical impedance tomography be used to detect gastro-oesophageal reflux? *Physiological Measurement,* 17**,** A141.
101. EROL, R. A., CHERIAN, P., SMALLWOOD, R. H., BROWN, B. H. & BARDHAN, K. D. 1996b. Can electrical impedance tomography be used to detect gastro-oesophageal reflux? *Physiol Meas,* 17 Suppl 4A**,** A141-7.
102. ESLER, B., LYONS, T., TUROVETS, S. & TUCKER, D. 2010. Instrumentation for low frequency EIT studies of the human head and its

validation in phantom experiments. *Journal of Physics: Conference Series,* 224**,** 012007.
103. EYUBOGLU, B. M. & BROWN, B. H. 1988. Methods of cardiac gating applied potential tomography. *Clin Phys Physiol Meas,* 9**,** 43-8.
104. EYUBOGLU, B. M., BROWN, B. H. & BARBER, D. C. 1989. In vivo imaging of cardiac related impedance changes. *Engineering in Medicine and Biology Magazine, IEEE,* 8**,** 39-45.
105. FABRIZI, L., MCEWAN, A., WOO, E. & HOLDER, D. S. 2007. Analysis of resting noise characteristics of three EIT systems in order to compare suitability for time difference imaging with scalp electrodes during epileptic seizures. *Physiological Measurement,* 28**,** S217.
106. FAGERBERG, A., SÖNDERGAARD, S., KARASON, S. & ÅNEMAN, A. 2009. Electrical impedence tomography and heterogeneity of pulmonary perfusion and ventilation in porcine acute lung injury. *Acta Anaesthesiologica Scandinavica,* 53**,** 1300-1309.
107. FAN, S.-Z., YEH, J.-R., CHEN, B.-C. & SHIEH, J.-S. 2010. Comparison of EEG Approximate Entropy and complexity measures of depth of anaesthesia during inhalational general anaesthesia. *Journal of Medical and Biological Engineering,* 31**,** 8.
108. FAN, S., YEH, J., CHEN, B. & SHIEH, J. 2011. Comparison of eeg approximate entropy and complexity measures of depth of anaesthesia during inhalational general anaesthesia. *Journal of Medical and Biological Engineering,* 31.
109. FARKAS, E. & LUITEN, P. G. M. 2001. Cerebral microvascular pathology in aging and Alzheimer's disease. *Progress in Neurobiology,* 64**,** 575-611.
110. FAWCETT, T. 2006a. An introduction to ROC analysis. *Pattern Recogn. Lett.,* 27**,** 861-874.
111. FAWCETT, T. 2006b. An introduction to ROC analysis. *Pattern Recognition Letters,* 27**,** 861-874.
112. FELKER, G. M., CUCULICH, P. S. & GHEORGHIADE, M. 2006. The Valsalva Maneuver: A Bedside "Biomarker" for Heart Failure. *The American Journal of Medicine,* 119**,** 117-122.
113. FERNÁNDEZ, T., HARMONY, T., SILVA-PEREYRA, J., FERNÁNDEZ-BOUZAS, A., GERSENOWIES, J., GALÁN, L., CARBONELL, F., MAROSI, E., OTERO, G. & VALDÉS, S. I. 2000. Specific EEG frequencies at specific brain areas and performance. *Neuroreport.,* 11**,** 2663-8.
114. FISET, P., PAUS, T., DALOZE, T., PLOURDE, G., MEURET, P., BONHOMME, V., HAJJ-ALI, N., BACKMAN, S. B. & EVANS, A. C. 1999. Brain Mechanisms of Propofol-Induced Loss of Consciousness in Humans: a Positron Emission Tomographic Study. *The Journal of Neuroscience,* 19**,** 5506-5513.
115. FLEISHER, L. A. M. D., PINCUS, S. M. P. D. & ROSENBAUM, S. H. M. D. 1993. Approximate Entropy of Heart Rate as a Correlate of Postoperative Ventricular Dysfunction. *Anesthesiology,* 78**,** 683-692.
116. FLORKOWSKI, C. M. 2008. Sensitivity, Specificity, Receiver-Operating Characteristic (ROC) Curves and Likelihood Ratios: Communicating the Performance of Diagnostic Tests. *The Clinical Biochemist Reviews,* 29**,** S83-S87.
117. FORSYTH, J., BORSIC, A., HALTER, R. J., HARTOV, A. & PAULSEN, K. D. 2011. Optical breast shape capture and finite-element mesh generation

for electrical impedance tomography. *Physiological Measurement,* 32**,** 797-809.
118. FRANKS, N. P. 2008. General anaesthesia: from molecular targets to neuronal pathways of sleep and arousal. *Nat Rev Neurosci,* 9**,** 370-386.
119. FREEMAN, R. 2006. Assessment of cardiovascular autonomic function. *Clinical Neurophysiology,* 117**,** 716-730.
120. FRERICHS, I. 2000. Electrical impedance tomography (EIT) in applications related to lung and ventilation: a review of experimental and clinical activities. *Physiological Measurement,* 21**,** R1.
121. FRERICHS, I., BECHER, T. & WEILER, N. 2014. Electrical impedance tomography imaging of the cardiopulmonary system. *Current Opinion in Critical Care,* 20**,** 323-332.
122. FRERICHS, I., PULLETZ, S., ELKE, G., REIFFERSCHEID, F., SCHÄDLER, D., SCHOLZ, J. & WEILER, N. 2009. Assessment of Changes in Distribution of Lung Perfusion by Electrical Impedance Tomography. *Respiration,* 77**,** 282-291.
123. FRYER, M. 2004. Intravenous induction agents. *Anaesthesia & Intensive Care Medicine,* 5**,** 317-321.
124. GABRIEL, C., GABRIEL, S. & CORTHOUT, E. 1996. The dielectric properties of biological tissues: I. Literature survey. *Phys Med Biol.,* 41**,** 2231-49.
125. GAGNON, H., GUARDO, R., KOKTA, V. & HARTINGER, A. E. 2010. A hybrid FEM model to simulate the electrical characteristics of biological tissues at the cellular level. *Journal of Physics: Conference Series,* 224**,** 012084.
126. GAO, J., YUE, S., CHEN, J. & WANG, H. 2014. Classification of normal and cancerous lung tissues by electrical impendence tomography. *Biomed Mater Eng,* 24**,** 2229-41. doi: 10.3233/BME-141035.
127. GARCIA, P. S., KOLESKY, S. E. & JENKINS, A. 2010. General Anesthetic Actions on GABA(A) Receptors. *Current Neuropharmacology,* 8**,** 2-9.
128. GARVEY, C. J. & HANLON, R. 2002. Computed tomography in clinical practice. *British Medical Journal,* 324**,** 4.
129. GATTINONI, L. M. D. F., PROTTI, A. M. D., CAIRONI, P. M. D. & CARLESSO, E. M. 2010. Ventilator-induced lung injury: The anatomical and physiological framework. *Critical Care Medicine,* 38(10) Supplement, Thinking Outside the**,** Proceedings of a Round Table Conference in Brussels, Belgium, March 2010:S539-S548.
130. GERSING, E. 1999. Monitoring Temperature-Induced Changes in Tissue during Hyperthermia by Impedance Methods. *Annals of the New York Academy of Sciences,* 873**,** 13-20.
131. GERTLER, R., BROWN, H. C., MITCHELL, D. H. & SILVIUS, E. N. 2001. Dexmedetomidine: a novel sedative-analgesic agent. *Proceedings (Baylor University. Medical Center),* 14**,** 13-21.
132. GIBSON, A., BAYFORD, R. H. & HOLDER, D. S. 2000. Two-dimensional finite element modelling of the neonatal head. *Physiological Measurement,* 21**,** 45.
133. GILAD, O. & HOLDER, D. S. 2009b. Impedance changes recorded with scalp electrodes during visual evoked responses: Implications for Electrical Impedance Tomography of fast neural activity. *NeuroImage,* 47**,** 514-522.

134. GILAD, O., HORESH, L. & HOLDER, D. S. 2007. Design of electrodes and current limits for low frequency electrical impedance tomography of the brain. *Medical & Biological Engineering & Computing,* 45**,** 621-633.
135. GILAD, O., HORESH, L. & HOLDER, D. S. 2009. A modelling study to inform specification and optimal electrode placement for imaging of neuronal depolarization during visual evoked responses by electrical and magnetic detection impedance tomography. *Physiological Measurement,* 30**,** S201.
136. GIROUARD, H. & IADECOLA, C. 2006. *Neurovascular coupling in the normal brain and in hypertension, stroke, and Alzheimer disease*.
137. GRANT, C., PHAM, T., HOUGH, J., RIEDEL, T., STOCKER, C. & SCHIBLER, A. 2011. Measurement of ventilation and cardiac related impedance changes with electrical impedance tomography. *Critical Care,* 15**,** R37.
138. GREENFIELD, S. A. & COLLINS, T. F. T. 2005. A neuroscientific approach to consciousness. *Prog Brain Res,* 150**,** 11-23.
139. GREGORI, B., PRO, S., BOMBELLI, F., RICCIA, M. L. & ACCORNERO, N. 2006. Vep latency: Sex and head size. *Clinical Neurophysiology,* 117**,** 1154-1157.
140. GRIFFITHS, H. 1988. A phantom for electrical impedance tomography. *Clinical Physics and Physiological Measurement,* 9**,** 15.
141. GRIFFITHS, H. 1995. A Cole phantom for EIT. *Physiol Meas.,* 16**,** A29-38.
142. GRONLUND, J., JALONEN, J. & VALIMAKI, I. 1997. Transcephalic electrical impedance provides a means for quantifying pulsatile cerebral blood volume changes following head-up tilt. *Early Human Development,* 47**,** 11-18.
143. GRONLUND, J. U., KERO, P., KORVENRANTA, H., AARIMAA, T., JALONEN, J., TUOMINEN, J. & VALIMAKI, I. A. T. 1995. Cerebral circulation assessed by transcephalic electrical impedance during the first day of life â€" a potential predictor of outcome? *Early Human Development,* 41**,** 129-145.
144. GROSWASSER, Z., KRISS, A., HALLIDAY, A. M. & MCDONALD, W. I. 1985. Pattern- and flash-evoked potentials in the assessment and management of optic nerve gliomas. *Journal of neurology, neurosurgery, and psychiatry,* 48**,** 1125-1134.
145. GUEDEL, A. E. 1937. *Inhalational anesthesia,* New York, Macmillan.
146. GUSENOFF, J. A., HARMAN, S. M., VELDHUIS, J. D., JAYME, J. J., ST. CLAIR, C., MÜNZER, T., CHRISTMAS, C., O'CONNOR, K. G., STEVENS, T. E., BELLANTONI, M. F., PABST, K. & BLACKMAN, M. R. 2001. *Cortisol and GH secretory dynamics, and their interrelationships, in healthy aged women and men*.
147. GUTTIKONDA, R., HERTS, B. R., DONG, F., BAKER, M. E., FENNER, K. B. & POHLMAN, B. 2014. Estimated radiation exposure and cancer risk from CT and PET/CT scans in patients with lymphoma. *European Journal of Radiology,* 83**,** 1011-1015.
148. HAGLER, D. J., HALGREN, E., MARTINEZ, A., HUANG, M., HILLYARD, S. A. & DALE, A. M. 2009. Source estimates for MEG/EEG visual evoked responses constrained by multiple, retinotopically-mapped stimulus locations. *Human Brain Mapping,* 30**,** 32.
149. HAHN, G., BEER, M., FRERICHS, I., DUDYKEVYCH, T., SCHRODER, T. & HELLIGE, G. 2000. A simple method to check the dynamic

performance of electrical impedance tomography systems. *Physiol Meas.,* 21**,** 53-60.
150. HAHN, G., JUST, A., DITTMAR, J. & HELLIGE, G. 2008. Systematic errors of EIT systems determined by easily-scalable resistive phantoms. *Physiol Meas.,* 29**,** S163-72. doi: 10.1088/0967-3334/29/6/S14. Epub 2008 Jun 10.
151. HAJIAN-TILAKI, K. 2013. Receiver Operating Characteristic (ROC) Curve Analysis for Medical Diagnostic Test Evaluation. *Caspian Journal of Internal Medicine,* 4**,** 627-635.
152. HALLIDAY, A. M., MCDONALD, W. I. & MUSHIN, J. 1973. *Visual Evoked Response in Diagnosis of Multiple Sclerosis*.
153. HANLEY, J. A. & MCNEIL, B. J. 1982. The meaning and use of the area under a receiver operating characteristic (ROC) curve. *Radiology,* 143**,** 29-36.
154. HARDING, G. F. A., ODOM, J. V., SPILEERS, W. & SPEKREIJSE, H. 1996. Standard for visual evoked potentials 1995. *Vision Research,* 36**,** 3567-72.
155. HARI, R. & LOUNASMAA, O. 1989. Recording and interpretation of cerebral magnetic fields. *Science,* 244**,** 432-436.
156. HARI, R. & SALMELIN, R. 2012. Magnetoencephalography: From SQUIDs to neuroscience: Neuroimage 20th Anniversary Special Edition. *NeuroImage,* 61**,** 386-396.
157. HARRIS, N. D., SUGGETT, A. J., BARBER, D. C. & BROWN, B. H. 1987. Applications of applied potential tomography (APT) in respiratory medicine. *Clin Phys Physiol Meas,* 8**,** 155-65.
158. HASHIMOTO, T., KASHII, S., KIKUCHI, M., HONDA, Y., NAGAMINE, T. & SHIBASAKI, H. 1999. Temporal profile of visual evoked responses to pattern-reversal stimulation analyzed with a whole-head magnetometer. *Exp Brain Res.,* 125**,** 375-82.
159. HEISZ, J. J. & MCINTOSH, A. R. 2013. Applications of EEG Neuroimaging Data: Event-related Potentials, Spectral Power, and Multiscale Entropy. *Journal of Visualized Experiments : JoVE***,** 50131.
160. HENDERSON, L. A., MACEY, P. M., MACEY, K. E., FRYSINGER, R. C., WOO, M. A., HARPER, R. K., ALGER, J. R., YAN-GO, F. L. & HARPER, R. M. 2002. Brain Responses Associated With the Valsalva Maneuver Revealed by Functional Magnetic Resonance Imaging. *Journal of Neurophysiology,* 88**,** 3477-3486.
161. HENDERSON, R. P. & WEBSTER, J. G. 1978. An impedance camera for spatially specific measurements of the thorax. *IEEE TRANSACTIONS ON BIOMEDICAL ENGINEERING,* 25**,** 250-4.
162. HILL, T. C. 1980. Single-Photon Emission Computed Tomography to Study Cerebral Function in Man. *Journal of Nuclear Medicine,* 21**,** 1197-1199.
163. HINER, B. C. 2005. Valsalva Maneuver. *Clinical Medicine & Research,* 3**,** 55.
164. HIROFUMI, O., OTONE, E., HIROSHI, I., SATOSI, I., SHIGEO, I., YASUHIRO, N. & MASATO, S. 2003. The effectiveness of regional cerebral oxygen saturation monitoring using near-infrared spectroscopy in carotid endarterectomy. *Journal of Clinical Neuroscience,* 10**,** 79-83.
165. HIROTA, K. 2006. Special cases: ketamine, nitrous oxide and xenon. *Best Pract Res Clin Anaesthesiol.,* 20**,** 69-79.

166. HODGKIN, A. L. & HUXLEY, A. F. 1939. Action potentials recorded from inside a nerve fibre. *Nature,* 144**,** 2.
167. HOLDER, D. 2004. Brief introduction to bioimpedance. *Electrical Impedance Tomography.* Taylor & Francis.
168. HOLDER, D. S. 1987. Feasibility of developing a method of imaging neuronal activity in the human brain: a theoretical review. *Medical and Biological Engineering and Computing,* 25**,** 2.
169. HOLDER, D. S. 1992a. Electrical impedance tomography (EIT) of brain function. *Brain Topography,* 5**,** 87-93.
170. HOLDER, D. S. 1992b. Electrical impedance tomography with cortical or scalp electrodes during global cerebral ischaemia in the anaesthetised rat. *Clin Phys Physiol Meas,* 13**,** 87-98.
171. HOLDER, D. S. 2005. *Electrical Impedance Tomography of brain function* [Online]. Available: http://www.ucl.ac.uk/medphys/research/eit/pubs/brain_EIT_overview.pdf.
172. HOLDER, D. S., GONZÁLEZ-CORREA, C. A., TIDSWELL, T., GIBSON, A., CUSICK, G. & BAYFORD, R. H. 1999. Assessment and Calibration of a Low-Frequency System for Electrical Impedance Tomography (EIT), Optimized for Use in Imaging Brain Function in Ambulant Human Subjects. *Annals of the New York Academy of Sciences,* 873**,** 512-519.
173. HOLDER, D. S., RAO, A. & HANQUAN, Y. 1996. Imaging of physiologically evoked responses by electrical impedance tomography with cortical electrodes in the anaesthetized rabbit. *Physiological Measurement,* 17**,** A179.
174. HOLDER, D. S. & TIDSWELL, T. 2005. Electrical impedance tomography of brain function. *In:* HOLDER, D. S. (ed.) *Electrical impedance tomography. Methods, history and applications.* Bristol and Philadelphia: Institute of Physics Publishing.
175. HOLMAN B & S., T. S. 1990. Single-photon emission computed tomography (spect): Applications and potential. *JAMA: The Journal of the American Medical Association,* 263**,** 561-564.
176. HONAN, W. P., HERON, J. R., FOSTER, D. H., EDGAR, G. K. & SCASE, M. O. 1993. Abnormalities of visual function in hereditary motor and sensory neuropathy. *Journal of the Neurological Sciences,* 114**,** 5.
177. HORKY, L. L. & TREVES, S. T. 2011. PET and SPECT in Brain Tumors and Epilepsy. *Neurosurgery clinics of North America,* 22**,** 169-184.
178. HORNERO, R., ABOY, M., ABASOLO, D., MCNAMES, J. & GOLDSTEIN, B. 2005. Interpretation of approximate entropy: analysis of intracranial pressure approximate entropy during acute intracranial hypertension. *Biomedical Engineering, IEEE Transactions on,* 52**,** 1671-1680.
179. HOUNSFIELD, G. N. 1973. Computerized transverse axial scanning (tomography) 1. Description of system. *Br J Radiol,* 46**,** 7.
180. HU, Z., YANG, W., LIU, H., WANG, K., BAO, C., SONG, T., WANG, J. & TIAN, J. 2014. From PET/CT to PET/MRI: Advances in Instrumentation and Clinical Applications. *Molecular Pharmaceutics,* 11**,** 3798-3809.
181. HUANG, B., LAW, M. W.-M. & KHONG, P.-L. 2009. Whole-Body PET/CT Scanning: Estimation of Radiation Dose and Cancer Risk. *Radiology,* 251**,** 166-174.

182. HUDETZ, A. G. 2012. General anesthesia and human brain connectivity. *Brain Connect,* 2**,** 291-302. doi: 10.1089/brain.2012.0107.
183. HYNDMAN, R. & ATHANASOPOULOS, G. 2013. Forecasting: principles and practice.
184. IADECOLA, C. 2004. Neurovascular regulation in the normal brain and in Alzheimer's disease. *Nat Rev Neurosci,* 5**,** 347-360.
185. JACQUES, S. L. 2013. Optical properties of biological tissues: a review. *Phys Med Biol,* 58**,** R37-61.
186. JAGADEESAN, N., WOLFSON, M., CHEN, Y., WILLINGHAM, M. & AVIDAN, M. S. 2013. Brain monitoring during general anesthesia. *Trends in Anaesthesia and Critical Care,* 3**,** 13-18.
187. JASPER, H. 1949. Diffuse projection systems: the integrative action of the thalamic reticular system. *Electroencephalogr Clin Neurophysiol.,* 1**,** 405-19; discussion 419-20.
188. JEHL, M. & HOLDER, D. 2016. Correction of electrode modelling errors in multi-frequency EIT imaging. *Physiological Measurement,* 37**,** 893-903.
189. JENKNER, F. L. 1957. [The diagnostic value of cranial rheography in cerebral vascular disorders]. *Wien Klin Wochenschr,* 69**,** 619-20.
190. JOBSIS, F. 1977. Noninvasive, infrared monitoring of cerebral and myocardial oxygen sufficiency and circulatory parameters. *Science,* 198**,** 1264-1267.
191. JOHANSEN, M. D. P. D. JAY W. & SEBEL, M. B. B. S. P. D. M. B. A. PETER S. 2000. Development and Clinical Application of Electroencephalographic Bispectrum Monitoring. *Anesthesiology,* 93**,** 1336-1344.
192. JONES, D. C. & BLUME, W. T. 2000. Pattern-Evoked Potential Latencies From Central and Peripheral Visual Fields. *Journal of Clinical Neurophysiology,* 17**,** 68-76.
193. JOSSINET, J. 1998. The impedivity of freshly excised human breast tissue. *Physiological Measurement,* 19**,** 61.
194. KANDEL, E. R., SCHWARTZ, J. H. & JESSELL, T. M. 2000. *Principles of neural science,* New York, McGraw-Hill, Health Professions Division.
195. KAPLAN, D. T., FURMAN, M. I., PINCUS, S. M., RYAN, S. M., LIPSITZ, L. A. & GOLDBERGER, A. L. 1991. Aging and the complexity of cardiovascular dynamics. *Biophysical Journal,* 59**,** 945-949.
196. KARSTEN, J., LUEPSCHEN, H., GROSSHERR, M., BRUCH, H. P., LEONHARDT, S., GEHRING, H. & MEIER, T. 2011. Effect of PEEP on regional ventilation during laparoscopic surgery monitored by electrical impedance tomography. *Acta Anaesthesiologica Scandinavica,* 55**,** 878-886.
197. KENNETT, R. 2012. Modern electroencephalography. *Journal of Neurology,* 259**,** 783-789.
198. KERROUCHE, N., MCLEOD, C. N. & LIONHEART, W. R. B. 2001. Time series of EIT chest images using singular value decomposition and Fourier transform. *Physiological Measurement,* 22**,** 147.
199. KHAN, K. S., HAYES, I. & BUGGY, D. J. 2014. Pharmacology of anaesthetic agents I: intravenous anaesthetic agents. *Continuing Education in Anaesthesia, Critical Care & Pain,* 14**,** 100-105.
200. KORTH, M. & NGUYEN, N. X. 1997. The effects of stimulus size on human cortical potentials evoked by chromatic patterns. *Vision Research,* 37**,** 9.

201. KOTHARI, R., SINGH, S., SINGH, R., SHUKLA, A. K. & BOKARIYA, P. 2014. Influence of visual angle on pattern reversal visual evoked potentials. *Oman Journal of Ophthalmology,* 7**,** 120-125.
202. KRAINIK, A. M. D. P., HUND-GEORGIADIS, M. M. D., ZYSSET, S. P. & VON CRAMON, D. Y. M. D. P. 2005. Regional Impairment of Cerebrovascular Reactivity and BOLD Signal in Adults After Stroke. *Stroke,* 36**,** 1146-1152.
203. KUC, R. 1988. *Introduction to Digital Signal Processing*, McGraw-Hill Inc.,US.
204. KUIPER, J. W. M. D., GROENEVELD, A. B. J. M. D. P. F. F., SLUTSKY, A. S. M. D. & PLOTZ, F. B. M. D. P. 2005. Mechanical ventilation and acute renal failure *. *Critical Care Medicine,* 33**,** 1408-1415.
205. KUMAR, S., PANDEY, A., SHARMA, P., SHAMIM, S., MALHOTRA, A. & KUMAR, R. 2012. Instantaneous exposure to nuclear medicine staff involved in PET–CT imaging in developing countries: experience from a tertiary care centre in India. *Japanese Journal of Radiology***,** 1-5.
206. LA FOUGÈRE, C., ROMINGER, A., FÖRSTER, S., GEISLER, J. & BARTENSTEIN, P. 2009. PET and SPECT in epilepsy: A critical review. *Epilepsy & Behavior,* 15**,** 50-55.
207. LAITINEN, L. V. 1968. A comparative study on pulsatile intracerebral impedance and rheoencephalography. *Electroencephalography and clinical neurophysiology,* 25**,** 197-202.
208. LÅNGSJÖ, J. W., ALKIRE, M. T., KASKINORO, K., HAYAMA, H., MAKSIMOW, A., KAISTI, K. K., AALTO, S., AANTAA, R., JÄÄSKELÄINEN, S. K., REVONSUO, A. & SCHEININ, H. 2012. Returning from Oblivion: Imaging the Neural Core of Consciousness. *The Journal of Neuroscience,* 32**,** 4935-4943.
209. LAUREYS, S., MAJERUS, S. & MOONEN, G. 2002. Assessing Consciousness in Critically Ill Patients. *In:* VINCENT, J.-L. (ed.) *Intensive Care Medicine.* Springer New York.
210. LE BIHAN, D., JEZZARD, P., HAXBY, J., SADATO, N., RUECKERT, L. & MATTAY, V. 1995. Functional Magnetic Resonance Imaging of the Brain. *Annals of Internal Medicine,* 122**,** 296-303.
211. LEATHARD, A. D., BROWN, B. H., CAMPBELL, J., ZHANG, F., MORICE, A. H. & TAYLER, D. 1994. A comparison of ventilatory and cardiac related changes in EIT images of normal human lungs and of lungs with pulmonary emboli. *Physiological Measurement,* 15**,** A137.
212. LEBLHUBER, F., REISECKER, F., MAYR, W. R. & DEISENHAMMER, E. 1986. Heterogeneity of hereditary motor and sensory neuropathy type I (HMSN I): electroneurographical findings, visual evoked potentials and blood group markers in a family with Charcot-Marie-Tooth disease (CMT). *Acta Neurol Scand.,* 74**,** 145-9.
213. LEE, K. H., HASHIMOTO, S. A., HOOGE, J. P., KASTRUKOFF, L. F., OGER, J. J. F., LI, D. K. B. & PATY, D. W. 1991. Magnetic resonance imaging of the head in the diagnosis of multiple sclerosis: A prospective 2-year follow-up with comparison of clinical evaluation, evoked potentials, oligoclonal banding, and CT. *Neurology,* 41**,** 657-660.
214. LEIDE-SVEGBORN, S. 2010. Radiation exposure of patients and personnel from a PET/CT procedure with 18F-FDG. *Radiation Protection Dosimetry,* 139**,** 208-213.

215. LEMIEUX, L. 2004. Electroencephalography-correlated functional MR imaging studies of epileptic activity. *Neuroimaging clinics of North America,* 14**,** 487-506.
216. LESLIE, K., MYLES, P. S., FORBES, A., CHAN, M. T., SHORT, T. G. & SWALLOW, S. K. 2005. Recovery from bispectral index-guided anaesthesia in a large randomized controlled trial of patients at high risk of awareness. *Anaesth Intensive Care.,* 33**,** 443-51.
217. LEUTHOLD, A. C., LANGHEIM, F. J. P., LEWIS, S. M. & GEORGOPOULOS, A. P. 2005. Time series analysis of magnetoencephalographic data during copying. *Experimental Brain Research,* 164**,** 411-422.
218. LEVIN, A. B. 1966. A simple test of cardiac function based upon the heart rate changes induced by the valsalva maneuver. *The American Journal of Cardiology,* 18**,** 90-99.
219. LI, T.-N. & LI, Y. 2014. Depth of anaesthesia monitors and the latest algorithms. *Asian Pacific Journal of Tropical Medicine,* 7**,** 429-437.
220. LIONHEART, W., POLYDORIDES, N. & BORSIC, A. 2005. The reconstruction problem. *In:* HOLDER, D. S. (ed.) *Electrical Impedance Tomography. Mthods, history and applications.* Briston and Philadelphia: Institute of Physics Publishing.
221. LIONHEART, W. R. 2004. EIT reconstruction algorithms: pitfalls, challenges and recent developments. *Physiological measurement,* 25**,** 125-42.
222. LIPSITZ, L. A. 2002. Dynamics of Stability: The Physiologic Basis of Functional Health and Frailty. *The Journals of Gerontology Series A: Biological Sciences and Medical Sciences,* 57**,** B115-B125.
223. LIPSITZ, L. A. & GOLDBERGER, A. L. 1992. Loss of "complexity" and aging: Potential applications of fractals and chaos theory to senescence. *JAMA,* 267**,** 1806-1809.
224. LISTON, A. D., BAYFORD, R. H. & HOLDER, D. S. 2004. The effect of layers in imaging brain function using electrical impedance tomograghy. *Physiological Measurement,* 25**,** 143.
225. LIU, P. D. X., LAUER, M. D. KATHRYN K., WARD, M. S. B. D., LI, P. D. S.-J. & HUDETZ, D. B. M. P. D. ANTHONY G. 2013. Differential Effects of Deep Sedation with Propofol on the Specific and Nonspecific Thalamocortical SystemsA Functional Magnetic Resonance Imaging Study. *Anesthesiology,* 118**,** 59-69.
226. LIVINGSTONE, I. R., MASTAGLIA, F. L., EDIS, R. & HOWE, J. W. 1981. Visual involvement in friedreich's ataxia and hereditary spastic ataxia: A clinical and visual evoked response study. *Archives of Neurology,* 38**,** 75-79.
227. LU, L. 1995. *Aspects of an electrical impedance tomography spectroscopy (EITS) system PhD Thesis* Doctorate of Philosophy, University of Sheffield.
228. LUEBBEHUSEN, M. 2005. Bispectral Index Monitoring: No longer used only in the OR, Bispectral Index Monitoring can now be used to help ensure that a patient is sedated safely and effectively. *Technol Today***,** 6.
229. MACEY, P. M., WU, P., KUMAR, R., OGREN, J. A., RICHARDSON, H. L., WOO, M. A. & HARPER, R. M. 2012. Differential responses of the insular cortex gyri to autonomic challenges. *Autonomic Neuroscience,* 168**,** 72-81.

230. MAIER, J., DAGNELIE, G., SPEKREIJSE, H. & VAN DIJK, B. W. 1987. Principal components analysis for source localization of VEPs in man. *Vision Research,* 27**,** 165-177.
231. MAKSIMOW, A., SNAPIR, A., SÄRKELÄ, M., KENTALA, E., KOSKENVUO, J., POSTI, J., JÄÄSKELÄINEN, S. K., HINKKA-YLI-SALOMÄKI, S., SCHEININ, M. & SCHEININ, H. 2007. Assessing the depth of dexmedetomidine-induced sedation with electroencephalogram (EEG)-based spectral entropy. *Acta Anaesthesiologica Scandinavica,* 51**,** 22-30.
232. MALONE, E., JEHL, M., ARRIDGE, S., BETCKE, T. & HOLDER, D. 2014a. Stroke type differentiation using spectrally constrained multifrequency EIT: evaluation of feasibility in a realistic head model. *Physiol Meas.,* 35**,** 1051-66. doi: 10.1088/0967-3334/35/6/1051. Epub 2014 May 20.
233. MALONE, E., JEHL, M., ARRIDGE, S., BETCKE, T. & HOLDER, D. 2014b. Stroke type differentiation using spectrally constrained multifrequency EIT: evaluation of feasibility in a realistic head model. *Physiological Measurement,* 35**,** 1051.
234. MALONE, E., SATO DOS SANTOS, G., HOLDER, D. & ARRIDGE, S. 2014c. Multifrequency electrical impedance tomography using spectral constraints. *IEEE Trans Med Imaging.,* 33**,** 340-50. doi: 10.1109/TMI.2013.2284966. Epub 2013 Oct 9.
235. MARKUS, H. S. 2000. Transcranial Doppler ultrasound. *British Medical Bulletin,* 56**,** 378-388.
236. MASHOUR, G. A., SHANKS, A., TREMPER, K. K., KHETERPAL, S., TURNER, C. R., RAMACHANDRAN, S. K., PICTON, P., SCHUELLER, C., MORRIS, M., VANDERVEST, J. C., LIN, N. & AVIDAN, M. S. 2012. Prevention of Intraoperative Awareness with Explicit Recall in an Unselected Surgical PopulationA Randomized Comparative Effectiveness Trial. *Anesthesiology,* 117**,** 717-725.
237. MASUCCI, E. F., SEIPEL, J. H. & KURTZKE, J. F. 1970. Clinical evaluation of "quantitative" rheoencephalography. *Neurology,* 20**,** 642-8.
238. MATTHEWS, P. M., HONEY, G. D. & BULLMORE, E. T. 2006. Applications of fMRI in translational medicine and clinical practice. *Nat Rev Neurosci,* 7**,** 732-744.
239. MAYBERG, H. S., ROBINSON, R. G., WONG, D. F., PARIKH, R., BOLDUC, P., STARKSTEIN, S. E., PRICE, T., DANNALS, R. F., LINKS, J. M., WILSON, A. A. & ET AL. 1988. PET imaging of cortical S2 serotonin receptors after stroke: lateralized changes and relationship to depression. *The American journal of psychiatry,* 145**,** 937-43.
240. MCARTHUR, C., JAMPANA, R., PATTERSON, J. & HADLEY, D. 2011. Applications of cerebral SPECT. *Clinical Radiology,* 66**,** 651-661.
241. MCCANN, H., AHSAN, S. T., DAVIDSON, J. L., ROBINSON, R. L., WRIGHT, P. & POMFRETT, C. J. D. A portable instrument for high-speed brain function imaging: FEITER. Engineering in Medicine and Biology Society,EMBC, 2011 Annual International Conference of the IEEE, Aug. 30 2011-Sept. 3 2011 2011. 7029-7032.
242. MCCANN, H., POLYDORIDES, N., MURRIETA-LEE, J. C., KOU, G., BEATTY, P. & POMFRETT, C. J. D. Sub-second functional imaging by Electrical Impedance Tomography. Engineering in Medicine and Biology

Society, 2006. EMBS '06. 28th Annual International Conference of the IEEE, Aug. 30 2006-Sept. 3 2006 2006. 4269-4272.
243. MCEWAN, A., CUSICK, G. & HOLDER, D. S. 2007. A review of errors in multi-frequency EIT instrumentation. *Physiological Measurement,* 28**,** S197.
244. MCEWAN, A., ROMSAUEROVA, A., YERWORTH, R., HORESH, L., BAYFORD, R. & HOLDER, D. 2006. Design and calibration of a compact multi-frequency EIT system for acute stroke imaging. *Physiological Measurement,* 27**,** S199.
245. MCGEER, P. L., KAMO, H., HARROP, R., LI, D. K., TUOKKO, H., MCGEER, E. G., ADAM, M. J., AMMANN, W., BEATTIE, B. L., CALNE, D. B. & ET AL. 1986. Positron emission tomography in patients with clinically diagnosed Alzheimer's disease. *Canadian Medical Association journal = journal de l'Association medicale canadienne,* 134**,** 597-607.
246. MENDELOWITZ, D. 1999. Advances in Parasympathetic Control of Heart Rate and Cardiac Function. *Physiology,* 14**,** 155-161.
247. MENEILLY, G. S., RYAN, A. S., VELDHUIS, J. D. & ELAHI, D. 1997. Increased Disorderliness of Basal Insulin Release, Attenuated Insulin Secretory Burst Mass, and Reduced Ultradian Rhythmicity of Insulin Secretion in Older Individuals. *The Journal of Clinical Endocrinology & Metabolism,* 82**,** 4088-4093.
248. METHERALL, P., BARBER, D. C., SMALLWOOD, R. H. & BROWN, B. H. 1996. Three-dimensional electrical impedance tomography. *Nature,* 380**,** 509-512.
249. MEYER, J. H., KAPUR, S., HOULE, S., DASILVA, J., OWCZAREK, B., BROWN, G. M., WILSON, A. A. & KENNEDY, S. H. 1999. Prefrontal cortex 5-HT2 receptors in depression: an [18F]setoperone PET imaging study. *The American journal of psychiatry,* 156**,** 1029-34.
250. MILES, K. A. 2004. Brain perfusion: computed tomography applications. *Neuroradiology,* 46**,** s194-s200.
251. MILLER, J. W. & FERRENDELLI, J. A. 1990. Characterization of GABAergic seizure regulation in the midline thalamus. *Neuropharmacology.,* 29**,** 649-55.
252. MISHRA, V., BOUAYAD, H., SCHNED, A., HEANEY, J. & HALTER, R. J. Electrical impedance spectroscopy for prostate cancer diagnosis. Engineering in Medicine and Biology Society (EMBC), 2012 Annual International Conference of the IEEE, Aug. 28 2012-Sept. 1 2012 2012. 3258-3261.
253. MOMOSE, K., YUICHI, K., KIYOSAWA, M., SENDA, M. & KOMIYA, K. Measurement of temporal frequency characteristics of VEP using pseudorandom binary sequence and their correlation with cerebral blood flow in human visual cortex. Engineering in Medicine and Biology Society, 1997. Proceedings of the 19th Annual International Conference of the IEEE, 30 Oct-2 Nov 1997 1997. 1518-1521 vol.4.
254. MUDERS, T., LUEPSCHEN, H. & PUTENSEN, C. 2009. Regional Ventilation Delay Index: Detection of Tidal Recruitment using Electrical Impedance Tomography. *In:* VINCENT, J.-L. (ed.) *Intensive Care Medicine.* Springer New York.
255. MULLINGER, K. & BOWTELL, R. 2011. Combining EEG and fMRI. *In:* MODO, M. & BULTE, J. W. M. (eds.) *Magnetic Resonance Neuroimaging.* Humana Press.

256. MURKIN, J. M. & ARANGO, M. 2009. Near-infrared spectroscopy as an index of brain and tissue oxygenation. *British Journal of Anaesthesia,* 103**,** i3-i13.
257. MURPHY, D., BURTON, P., COOMBS, R., TARASSENKO, L. & ROLFE, P. 1987. Impedance imaging in the newborn. *Clinical Physics and Physiological Measurement,* 8**,** 131.
258. MURRIETA-LEE, J. C., POMFRETT, C. J. D., BEATTY, P. C. W., POLYDORIDES, N., MUSSEL, C. B., WATERFALL, R. C. & MCCANN, H. Subsecond observations of EIT voltage changes on the human scalp due to brain stimulus. Engineering in Medicine and Biology Society, 2004. IEMBS '04. 26th Annual International Conference of the IEEE, 1-5 Sept. 2004 2004. 1317-1320.
259. MYLES, P. S., LESLIE, K., MCNEIL, J., FORBES, A. & CHAN, M. T. V. 2004. Bispectral index monitoring to prevent awareness during anaesthesia: the B-Aware randomised controlled trial. *The Lancet,* 363**,** 1757-1763.
260. NAGAI, M., HOSHIDE, S. & KARIO, K. 2010. The insular cortex and cardiovascular system: a new insight into the brain-heart axis. *Journal of the American Society of Hypertension,* 4**,** 174-182.
261. NASON, G. P. 2006. Stationary and non-stationary time series. *In:* MADER, H. & COLES, S. C. (eds.) *Statistics in Volcanology.* Geological society of London.
262. NEWELL, D. W., AASLID, R., LAM, A., MAYBERG, T. S. & WINN, H. R. 1994. Comparison of flow and velocity during dynamic autoregulation testing in humans. *Stroke.,* 25**,** 793-7.
263. NGUYEN, P. K. & WU, J. C. 2011. Radiation exposure from imaging tests: is there an increased cancer risk? *Expert review of cardiovascular therapy,* 9**,** 177-183.
264. NICOLL, R. A. & MADISON, D. V. 1982. General anesthetics hyperpolarize neurons in the vertebrate central nervous system. *Science.,* 217**,** 1055-7.
265. NOACHTAR, S., HASHIMOTO, T. & LÜDERS, H. 1993. Pattern visual evoked potentials recorded from human occipital cortex with chronic subdural electrodes. *Electroencephalography and Clinical Neurophysiology/Evoked Potentials Section,* 88**,** 435-446.
266. NORDBERG, A. 2011. Molecular imaging in Alzheimer's disease: new perspectives on biomarkers for early diagnosis and drug development. *Alzheimer's research & therapy,* 3**,** 34.
267. NORKIENE, I., SAMALAVICIUS, R., MISIURIENE, I., PAULAUSKIENE, K., BUDRYS, V. & IVASKEVICIUS, J. 2010. Incidence and risk factors for early postoperative cognitive decline after coronary artery bypass grafting. *Medicina (Kaunas),* 46**,** 460-4.
268. ODOM, J. V., BACH, M., BRIGELL, M., HOLDER, G. E., MCCULLOCH, D. L., TORMENE, A. P. & VAEGAN 2010. ISCEV standard for clinical visual evoked potentials (2009 update). *Doc Opthalmol,* 120**,** 111-9.
269. OH, T., GILAD, O., GHOSH, A., SCHUETTLER, M. & HOLDER, D. S. 2011. A novel method for recording neuronal depolarization with recording at 125–825 Hz: implications for imaging fast neural activity in the brain with electrical impedance tomography. *Medical & Biological Engineering & Computing,* 49**,** 593-604.

270. OH, T. I., KOO, H., LEE, K. H., KIM, S. M., LEE, J., KIM, S. W., SEO, J. K. & WOO, E. J. 2008. Validation of a multi-frequency electrical impedance tomography (mfEIT) system KHU Mark1: impedance spectroscopy and time-difference imaging. *Physiol Meas.*, 29**,** 295-307. doi: 10.1088/0967-3334/29/3/002. Epub 2008 Feb 11.
271. OLEJNICZAK, P. 2006. Neurophysiologic Basis of EEG. *Journal of Clinical Neurophysiology,* 23**,** 186-189.
272. ONOFRJ, M., FULGENTE, T., THOMAS, A., CURATOLA, L., PERESSON, M., LOPEZ, L., LOCATELLI, T., MARTINELLI, V. & COMI, G. 1995. Visual Evoked Potentials Generator Model Derived from Different Spatial Frequency Stimuli of Visual Field Regions and Magnetic Resonance Imaging Coordinates of V1, V2, V3 Areas in Man. *International Journal of Neuroscience,* 83**,** 213-239.
273. OTSUKA, M., ICHIYA, Y., KUWABARA, Y., HOSOKAWA, S., SASAKI, M., YOSHIDA, T., FUKUMURA, T., KATO, M. & MASUDA, K. 1996. Glucose metabolism in the cortical and subcortical brain structures in multiple system atrophy and Parkinson's disease: a positron emission tomographic study. *Journal of the Neurological Sciences,* 144**,** 77-83.
274. PACKHAM, B., KOO, H., ROMSAUEROVA, A., AHN, S., MCEWAN, A., JUN, S. C. & HOLDER, D. S. 2012. Comparison of frequency difference reconstruction algorithms for the detection of acute stroke using EIT in a realistic head-shaped tank. *Physiological Measurement,* 33**,** 767.
275. PANERAI, R. 2009. Transcranial Doppler for evaluation of cerebral autoregulation. *Clinical Autonomic Research,* 19**,** 197-211.
276. PAPOULIS, A. 1962. The Fourier Integral and its Applications. New York: McGraw-Hill Co.
277. PARRA, J., KALITZIN, S. N. & LOPES DA SILVA, F. H. 2004. Magnetoencephalography: an investigational tool or a routine clinical technique? *Epilepsy & Behavior,* 5**,** 277-285.
278. PATY, D. W., OGER, J. J. F., KASTRUKOFF, L. F., HASHIMOTO, S. A., HOOGE, J. P., EISEN, A. A., EISEN, K. A., PURVES, S. J., LOW, M. D., BRANDEJS, V., ROBERTSON, W. D. & B. LI, D. K. 1988. MRI in the diagnosis of MS: A prospective study with comparison of clinical evaluation, evoked potentials, oligoclonal banding, and CT. *Neurology,* 38**,** 180.
279. PEARCE, M. S., SALOTTI, J. A., LITTLE, M. P., MCHUGH, K., LEE, C., KIM, K. P., HOWE, N. L., RONCKERS, C. M., RAJARAMAN, P., CRAFT, A. W., PARKER, L. & BERRINGTON DE GONZÁLEZ, A. 2012. Radiation exposure from CT scans in childhood and subsequent risk of leukaemia and brain tumours: a retrospective cohort study. *The Lancet,* 380**,** 499-505.
280. PEREZ-BORJA, C. & MEYER, J. S. 1964. A CRITICAL EVALUATION OF RHEOENCEPHALOGRAPHY IN CONTROL SUBJECTS AND IN PROVEN CASES OF CEREBROVASCULAR DISEASE. *Journal of neurology, neurosurgery, and psychiatry,* 27**,** 66-72.
281. PEREZ, J. J. 2014. To what extent is the bipolar rheoencephalographic signal contaminated by scalp blood flow? A clinical study to quantify its extra and non-extracranial components. *BioMedical Engineering OnLine,* 13**,** 131.
282. PEREZ, J. J., GUIJARRO, E. & BARCIA, J. A. 2004. Influence of the scalp thickness on the intracranial contribution to rheoencephalography. *Physics in medicine and biology,* 49**,** 4383-94.

283. PEROUANSKY, M. A. & HEMMINGS JR, H. C. 2006. Chapter 25 - Intravenous anesthetic agents. *In:* HOPKINS, H. C. H. M. (ed.) *Foundations of Anesthesia (Second Edition).* Edinburgh: Mosby.
284. PIKKEMAAT, R. & LEONHARDT, S. 2010. Separation of ventilation and perfusion related signals within EIT-data streams. *Journal of Physics: Conference Series,* 224**,** 012028.
285. PINCUS, S. 1995. Approximate entropy (ApEn) as a complexity measure. *Chaos.,* 5**,** 110-117.
286. PINCUS, S. M. 1991. Approximate entropy as a measure of system complexity. *Proceedings of the National Academy of Sciences,* 88**,** 2297-2301.
287. PINCUS, S. M., CUMMINS, T. R. & HADDAD, G. G. 1993. Heart rate control in normal and aborted-SIDS infants. *Am J Physiol.,* 264**,** R638-46.
288. PINCUS, S. M. & GOLDBERGER, A. L. 1994a. *Physiological time-series analysis: what does regularity quantify?*
289. PINCUS, S. M. & GOLDBERGER, A. L. 1994b. Physiological time-series analysis: what does regularity quantify? *Am J Physiol.,* 266**,** H1643-56.
290. POLZER, K. & SCHUHFRIED, F. 1950. [Experimental interpretation of the rheocardiogram]. *Wien Med Wochenschr,* 100**,** 789-91.
291. POMFRETT, C. J., DOLLING, S., ANDERS, N. R., GLOVER, D. G., BRYAN, A. & POLLARD, B. J. P. 2009. Delta sleep-inducing peptide alters bispectral index, the electroencephalogram and heart rate variability when used as an adjunct to isoflurane anaesthesia. *Eur J Anaesthesiol.,* 26**,** 128-34. doi: 10.1097/EJA.0b013e32831c8644.
292. POMFRETT, C. J. & POLLARD, B. J. 2009. EUROANAESTHESIA 2009: The European Anaesthesiology Congress. *European Journal of Anaesthesiology (EJA),* 26; (Suppl 45).
293. PRABHAKAR, H., BITHAL, P. K., SURI, A., RATH, G. P. & DASH, H. H. 2007. Intracranial Pressure Changes During Valsalva Manoeuvre in Patients Undergoing a Neuroendoscopic Procedure. *Minim Invasive Neurosurg,* 50**,** 98-101.
294. PRASAD, S., HOUSERKOVA, D. & CAMPBELL, J. 2008. Breast imaging using 3D electrical impedance tomography. *Biomed Pap Med Fac Univ Palacky Olomouc Czech Repub,* 152**,** 151-154.
295. PRESTON, D. L., RON, E., TOKUOKA, S., FUNAMOTO, S., NISHI, N., SODA, M., MABUCHI, K. & KODAMA, K. 2007. Solid Cancer Incidence in Atomic Bomb Survivors: 1958–1998. *Radiation Research,* 168**,** 1-64.
296. PULLETZ, S., ELKE, G., ZICK, G., SCHÄDLER, D., SCHOLZ, J., WEILER, N. & FRERICHS, I. 2008. Performance of electrical impedance tomography in detecting regional tidal volumes during one-lung ventilation. *Acta Anaesthesiologica Scandinavica,* 52**,** 1131-1139.
297. PUNJASAWADWONG, Y., BOONJEUNGMONKOL, N. & PHONGCHIEWBOOK, A. 2007. Bispectral index for improving anaesthetic delivery and postoperative recovery. *Cochrane Database Syst Rev.***,** CD003843.
298. PURDON, P. L., PIERCE, E. T., BONMASSAR, G., WALSH, J., HARRELL, P. G., KWO, J., DESCHLER, D., BARLOW, M., MERHAR, R. C., LAMUS, C., MULLALY, C. M., SULLIVAN, M., MAGINNIS, S., SKONIECKI, D., HIGGINS, H.-A. & BROWN, E. N. 2009. Simultaneous Electroencephalography and Functional Magnetic Resonance Imaging of

General Anesthesia. *Annals of the New York Academy of Sciences,* 1157**,** 61-70.
299. QURAISHI, T., BRYAN, A., DAVIDSON, J., POMFRETT, C. J. D., WRIGHT, P., MCCANN, H. & POLLARD, B. J. 2013. Functional EIT with evoked response images reveal areas of changing conductivity in the brain during the Valsalva manoeuvre. *British Journal of Anaesthesia,* 5**,** 870-870.
300. QURAISHI, T., POMFRETT, C. J. D., DAVIDSON, J. L., ROBINSON, R., WRIGHT, P., AHSAN, S. T., BRYAN, A., POLLARD, B. J. P. & MCCANN, H. 2011. Functional Electrical Impedance Tomography by Evoked Response (fEITER): monitoring cerebral auto-regulation during the Valsalva manoeuvre. *British Journal of Anaesthesia,* 106**,** 441-442.
301. RADHAKRISHNAN, N. & GANGADHAR, B. N. 1998. Estimating regularity in epileptic seizure time-series data. *Engineering in Medicine and Biology Magazine, IEEE,* 17**,** 89-94.
302. RADIOGRAPHERS, S. O. 2011. The Ionising Radiation (Medical Exposure) (Amendment) Regulations 2011. *In:* SAFETY, H. A. (ed.) *2011 No. 1567; HEALTH AND SAFETY.* Society of Radiographers.
303. RAMPIL, M. S. M. D. IRA J. 1998. A Primer for EEG Signal Processing in Anesthesia *Anesthesiology,* 89**,** 980-1002.
304. RANETA, O., ONDRUS, D. & BELLA, V. 2012. Utilisation of electrical impedance tomography in breast cancer diagnosis. *Klin Onkol,* 25**,** 36-41.
305. RANI, D. D. & HARSOOR, S. S. 2012. Depth of general anaesthesia monitors. *Indian Journal of Anaesthesia,* 56**,** 437-441.
306. RANIERI, V., SUTER, P. M., TORTORELLA, C. & ET AL. 1999. Effect of mechanical ventilation on inflammatory mediators in patients with acute respiratory distress syndrome: A randomized controlled trial. *JAMA,* 282**,** 54-61.
307. RAO, A., GIBSON, A. & HOLDER, D. S. 1997. EIT images of electrically induced epileptic activity in anaesthetised rabbits. *Medical & Biological Engineering & Computing,* 35.
308. RAVN, S., HOLMBERG, M., SØRENSEN, P., FROKJAER, J. B. & CARL, J. 2014. Presurgical functional magnetic resonance imaging in patients with brain tumors. *Acta Radiologica*.
309. REED, S. J. & PLOURDE, G. 2015. Attenuation of High-Frequency (50-200 Hz) Thalamocortical EEG Rhythms by Propofol in Rats Is More Pronounced for the Thalamus than for the Cortex. *PLoS ONE,* 10**,** e0123287.
310. REINHARD, HETZEL, HINKOV & LÜCKING 2000. Cerebral haemodynamics during the Mueller manoeuvre in humans. *Clinical Physiology,* 20**,** 292-303.
311. RENNA, M., WIGMORE, T., MOFEEZ, A. & GILLBE, C. 2002. Biasing Effect Of The Electromyogram On Bis: A Controlled Study During High-Dose Fentanyl Induction. *Journal of Clinical Monitoring and Computing,* 17**,** 377-381.
312. RIU, P. J. & ANTON, D. 2010. Performance assessment of EIT measurement systems. *Journal of Physics: Conference Series,* 224**,** 012015.
313. ROBINSON, R. 2011. *Experimental study of electrophysiology using the fEITER system.* Doctor of Philosophy, The University of Manchester.
314. ROCCO, P. R. M. A., DOS SANTOS, C. B. C. & PELOSI, P. D. 2012. Pathophysiology of ventilator-associated lung injury. *Current Opinion in Anaesthesiology,* 25**,** 123-130.

315. ROMSAUEROVA, A., MCEWAN, A., HORESH, L., YERWORTH, R., BAYFORD, R. H. & HOLDER, D. S. 2006b. Multi-frequency electrical impedance tomography (EIT) of the adult human head: initial findings in brain tumours, arteriovenous malformations and chronic stroke, development of an analysis method and calibration. *Physiological Measurement,* 27**,** S147.
316. RUSSELL, I. F. 2013. The ability of bispectral index to detect intra-operative wakefulness during total intravenous anaesthesia compared with the isolated forearm technique. *Anaesthesia,* 68**,** 502-511.
317. SAMRA, S. K., DORJE, P., ZELENOCK, G. B. & STANLEY, J. C. 1996. Cerebral Oximetry in Patients Undergoing Carotid Endarterectomy Under Regional Anesthesia. *Stroke,* 27**,** 49-55.
318. SATO, S. & SMITH, P. D. 1985. Magnetoencephalography. *Journal of Clinical Neurophysiology,* 2**,** 173-192.
319. SCHAEFER, M., GROSS, W., ACKEMANN, J. & GEBHARD, M. M. 2002. The complex dielectric spectrum of heart tissue during ischemia. *Bioelectrochemistry,* 58**,** 171-180.
320. SCHAEFER, M., WANIA, V., BASTIN, B., SCHMALZ, U., KIENBAUM, P., BEIDERLINDEN, M. & TRESCHAN, T. 2014. Electrical impedance tomography during major open upper abdominal surgery: a pilot-study. *BMC Anesthesiology,* 14**,** 51.
321. SCHEEREN, T. W. L., SCHOBER, P. & SCHWARTE, L. A. 2012. Monitoring tissue oxygenation by near infrared spectroscopy (NIRS): background and current applications. *Journal of Clinical Monitoring and Computing,* 26**,** 279-287.
322. SCHIFF, N. D. 2008. Central Thalamic Contributions to Arousal Regulation and Neurological Disorders of Consciousness. *Annals of the New York Academy of Sciences,* 1129**,** 105-118.
323. SCHRÖTER, M. S., SPOORMAKER, V. I., SCHORER, A., WOHLSCHLÄGER, A., CZISCH, M., KOCHS, E. F., ZIMMER, C., HEMMER, B., SCHNEIDER, G., JORDAN, D. & ILG, R. 2012. Spatiotemporal Reconfiguration of Large-Scale Brain Functional Networks during Propofol-Induced Loss of Consciousness. *The Journal of Neuroscience,* 32**,** 12832-12840.
324. SCHWAN, H. P. & KAY, C. F. 1957. THE CONDUCTIVITY OF LIVING TISSUES. *Annals of the New York Academy of Sciences,* 65**,** 1007-1013.
325. SCHWENDER, D., DAUNDERER, M., MULZER, S., KLASING, S., FINSTERER, U. & PETER, K. 1996. Spectral edge frequency of the electroencephalogram to monitor "depth" of anaesthesia with isoflurane or propofol. *British Journal of Anaesthesia,* 77**,** 179-184.
326. SCHWILDEN, H., SCHÜTTLER, J. & STOECKEL, H. 1985. Quantitation of the EEG and pharmacodynamic modelling of hypnotic drugs: etomidate as an example. *European journal of anaesthesiology,* 2**,** 121-131.
327. SELNES, O. A., GOTTESMAN, R. F., GREGA, M. A., BAUMGARTNER, W. A., ZEGER, S. L. & MCKHANN, G. M. 2012. Cognitive and Neurologic Outcomes after Coronary-Artery Bypass Surgery. *New England Journal of Medicine,* 366**,** 250-257.
328. SEYMEN, P., SELAMET, U., AYTAC, E., TRABULUS, S. & SEYMEN, H. O. 2010. Evaluation of visual evoked potentials in chronic renal failure patients with different treatment modalities. *J Nephrol,* 23**,** 6.

329. SHENTON, M. E., HAMODA, H. M., SCHNEIDERMAN, J. S., BOUIX, S., PASTERNAK, O., RATHI, Y., VU, M. A., PUROHIT, M. P., HELMER, K., KOERTE, I., LIN, A. P., WESTIN, C. F., KIKINIS, R., KUBICKI, M., STERN, R. A. & ZAFONTE, R. 2012. A review of magnetic resonance imaging and diffusion tensor imaging findings in mild traumatic brain injury. *Brain Imaging and Behavior,* 6**,** 137-192.
330. SHIBASAKI, H. 2008. Human brain mapping: Hemodynamic response and electrophysiology. *Clinical Neurophysiology,* 119**,** 731-743.
331. SHIGETO, H., TOBIMATSU, S., YAMAMOTO, T., KOBAYASHI, T. & KATO, M. 1998. Visual evoked cortical magnetic responses to checkerboard pattern reversal stimulation: A study on the neural generators of N75, P100 and N145. *Journal of the Neurological Sciences,* 156**,** 186-194.
332. SHRESTHA, S., HIRVONEN, J., HINES, C. S., HENTER, I. D., SVENNINGSSON, P., PIKE, V. W. & INNIS, R. B. 2011. Serotonin-1A receptors in major depression quantified using PET: Controversies, confounds, and recommendations. *NeuroImage,* 59**,** 3243-3251.
333. SHUSHTARIAN, S. M., VALIOLLAHI, P. & YAHYABEK, A. 2009. Effect of Distance between Monitor & Patient in Recording Visual Evoked Potential Using Pattern Reversal Checker Board Stimulation. *In:* DÖSSEL, O. & SCHLEGEL, W. (eds.) *World Congress on Medical Physics and Biomedical Engineering, September 7 - 12, 2009, Munich, Germany.* Springer Berlin Heidelberg.
334. SIGL, J. & CHAMOUN, N. 1994. An introduction to bispectral analysis for the electroencephalogram. *Journal of Clinical Monitoring,* 10**,** 392-404.
335. SILVA, A. C., LEE, S.-P., IADECOLA, C. & KIM, S.-G. 2000. Early Temporal Characteristics of Cerebral Blood Flow and Deoxyhemoglobin Changes During Somatosensory Stimulation. *J Cereb Blood Flow Metab,* 20**,** 201-206.
336. SINHA, P. 2010. Speech Processing in Embedded Systems. Springer US.
337. SLUTSKY, A. S. & TREMBLAY, L. N. 1998. Multiple System Organ Failure. *American Journal of Respiratory and Critical Care Medicine,* 157**,** 1721-1725.
338. SMALLWOOD, R. H., HAMPSHIRE, A. R., BROWN, B. H., PRIMHAK, R. A., MARVEN, S. & NOPP, P. 1999. A comparison of neonatal and adult lung impedances derived from EIT images. *Physiological Measurement,* 20**,** 401.
339. SMALLWOOD, R. H., MANGNALL, Y. F. & LEATHARD, A. D. 1994. Transport of gastric contents (electric impedance imaging). *Physiological Measurement,* 15**,** A175.
340. SMIT, H., VONK NOORDEGRAAF, A., MARCUS, J. T., BOONSTRA, A., VRIES, P. & POSTMUS, P. 2004. Determinants of pulmonary perfusion measured by electrical impedance tomography. *European Journal of Applied Physiology,* 92**,** 45-49.
341. SOBOL, W. T. 2012. Recent advances in MRI technology: Implications for image quality and patient safety. *Saudi Journal of Ophthalmology,* 26**,** 393-399.
342. SOBOTA, V. & SUCHOMEL, J. Monitoring of pulmonary embolism using electrical impedance tomography: A case study. E-Health and Bioengineering Conference (EHB), 2013, 21-23 Nov. 2013 2013. 1-4.

343. SOCIETY OF RADIOGRAPHERS 2011. The Ionising Radiation (Medical Exposure) Regulations 2000. *In:* SAFETY, H. A. (ed.) *2000 No. 1059; HEALTH AND SAFETY.*
344. SRINIVASAN, V., ESWARAN, C. & SRIRAAM, N. 2007. Approximate Entropy-Based Epileptic EEG Detection Using Artificial Neural Networks. *Information Technology in Biomedicine, IEEE Transactions on,* 11**,** 288-295.
345. STAM, C. J. 2010. Use of magnetoencephalography (MEG) to study functional brain networks in neurodegenerative disorders. *Journal of the Neurological Sciences,* 289**,** 128-134.
346. STEARNS, S. D. 1990. *Digital Signal Analysis,* Prentice-Hall; 2nd Revised edition.
347. STERIADE, M. 1993. Central core modulation of spontaneous oscillations and sensory transmission in thalamocortical systems. *Current Opinion in Neurobiology,* 3**,** 619-625.
348. STUCHLY, M. A. & STUCHLY, S. S. 1980. Dielectric properties of biological substances—tabulated. *Journal of Microwave Power & Electromagnetic Energy,* 15**,** 8.
349. STURZENEGGER, M., NEWELL, D. W. & AASLID, R. 1996. Visually Evoked Blood Flow Response Assessed by Simultaneous Two-Channel Transcranial Doppler Using Flow Velocity Averaging. *Stroke,* 27**,** 2256-2261.
350. SUCHOMEL, J. & SOBOTA, V. 2013. A model of end-expiratory lung impedance dependency on total extracellular body water. *Journal of Physics: Conference Series,* 434**,** 012011.
351. SUROWIEC, A. J., STUCHLY, S. S., BARR, J. R. & SWARUP, A. 1988. Dielectric properties of breast carcinoma and the surrounding tissues. *Biomedical Engineering, IEEE Transactions on,* 35**,** 257-263.
352. SWISSTOM 2014. Swisstom EIT inside. Landquart.
353. TACKMANN, W. & RADU, E. W. 1980. Pattern shift visual evoked potentials in Charcot-Marie-Tooth disease, HMSN type I. *J Neurol,* 224**,** 71-4.
354. TANG, T., OH, S. & SADLEIR, R. J. 2010. A robust current pattern for the detection of intraventricular hemorrhage in neonates using electrical impedance tomography. *Annals of Biomedical Engineering,* 38**,** 2733-2747.
355. TEXAS-INSTRUMENTS 1980. Power Spectra Estimation - Application Note 255.
356. TIDSWELL, A., BAGSHAW, A., HOLDER, D., YERWORTH, R., EADIE, L., MURRAY, S., MORGAN, L. & BAYFORD, R. 2003. A comparison of headnet electrode arrays for electrical impedance tomography of the human head. *Physiological Measurement,* 24**,** 527.
357. TIDSWELL, A., GIBSON, A., BAYFORD, R. & HOLDER, D. 2001a. Validation of a 3D reconstruction algorithm for EIT of human brain function in a realistic head-shaped tank. *Physiological Measurement,* 22**,** 177.
358. TIDSWELL, T., GIBSON, A., BAYFORD, R. H. & HOLDER, D. S. 2001b. Three-Dimensional Electrical Impedance Tomography of Human Brain Activity. *NeuroImage,* 13**,** 283-294.
359. TIECKS, F. P., DOUVILLE, C., BYRD, S., LAM, A. M. & NEWELL, D. W. 1996. Evaluation of Impaired Cerebral Autoregulation by the Valsalva Maneuver. *Stroke,* 27**,** 1177-1182.

360. TIECKS, F. P., LAM, A. M., MATTA, B. F., STREBEL, S., DOUVILLE, C. & NEWELL, D. W. 1995. Effects of the Valsalva Maneuver on Cerebral Circulation in Healthy Adults : A Transcranial Doppler Study. *Stroke,* 26**,** 1386-1392.
361. TORT, A. B. L., KOMOROWSKI, R., EICHENBAUM, H. & KOPELL, N. 2010. *Measuring Phase-Amplitude Coupling Between Neuronal Oscillations of Different Frequencies*.
362. TOWERS, C. M., MCCANN, H., WANG, M., BEATTY, P. C., POMFRETT, C. J. D. & BECK, M. S. 2000. 3D simulation of EIT for monitoring impedance variations within the human head. *Physiological Measurement,* 21**,** 119.
363. UHRIG, L., DEHAENE, S. & JARRAYA, B. 2014. Cerebral mechanisms of general anesthesia. *Annales Françaises d'Anesthésie et de Réanimation,* 33**,** 72-82.
364. UMUTLU, L., LADD, M. E., FORSTING, M. & LAUENSTEIN, T. 2014. 7 Tesla MR Imaging: Opportunities and Challenges. *Fortschr Röntgenstr,* 186**,** 121-129.
365. VANNI, S., TANSKANEN, T., SEPPÄ, M., UUTELA, K. & HARI, R. 2001. Coinciding early activation of the human primary visual cortex and anteromedial cuneus. *Proceedings of the National Academy of Sciences,* 98**,** 2776-2780.
366. VELLY, M. D. LIONEL J., REY, M. D. P. D. MARC F., BRUDER, M. D. NICOLAS J., GOUVITSOS, M. D. FRANÇOIS A., WITJAS, M. D. T., REGIS, M. D. JEAN M., PERAGUT, M. D. JEAN C. & GOUIN, M. D. FRANÇOIS M. 2007. Differential Dynamic of Action on Cortical and Subcortical Structures of Anesthetic Agents during Induction of Anesthesia. *Anesthesiology,* 107**,** 202-212.
367. VESELIS, R. A. M. D., FESHCHENKO, V. A. P., REINSEL, R. A. P., DNISTRIAN, A. M. P., BEATTIE, B. B. S. & AKHURST, T. J. M. F. 2004. Thiopental and Propofol Affect Different Regions of the Brain at Similar Pharmacologic Effects. *Anesthesia & Analgesia,* 99**,** 399-408.
368. VETS, P., TEN BROECKE, P., ADRIAENSEN, H., VAN SCHIL, P. & DE HERT, S. 2004. Cerebral oximetry in patients undergoing carotid endarterectomy: preliminary results. *Acta Anaesthesiol Belg,* 55**,** 215-20.
369. VIALATTE, F.-B., MAURICE, M., DAUWELS, J. & CICHOCKI, A. 2010. Steady-state visually evoked potentials: Focus on essential paradigms and future perspectives. *Progress in Neurobiology,* 90**,** 418-438.
370. WALSH, P., KANE, N. & BUTLER, S. 2005. The clinical role of evoked potentials. *Journal of Neurology, Neurosurgery & Psychiatry,* 76**,** ii16-ii22.
371. WEIR, C. J. 2006. The molecular mechanisms of general anaesthesia: dissecting the GABAA receptor. *Continuing Education in Anaesthesia, Critical Care & Pain,* 6**,** 49-53.
372. WHELESS, J. W. M. D., CASTILLO, E. P., MAGGIO, V. M. D., KIM, H. L. M. D., BREIER, J. I. P., SIMOS, P. G. P. & PAPANICOLAOU, A. C. P. 2004. Magnetoencephalography (MEG) and Magnetic Source Imaging (MSI). *Neurologist,* 10**,** 138-153.
373. WILLIAMSON, J. W., MCCOLL, R. & MATHEWS, D. 2003. Evidence for central command activation of the human insular cortex during exercise. *Journal of Applied Physiology,* 94**,** 1726-1734.

374. WILLIAMSON, J. W., MCCOLL, R., MATHEWS, D., MITCHELL, J. H., RAVEN, P. B. & MORGAN, W. P. 2002. Brain activation by central command during actual and imagined handgrip under hypnosis. *Journal of Applied Physiology,* 92**,** 1317-1324.
375. WILSON, A. J., MILNES, P., WATERWORTH, A. R., SMALLWOOD, R. H. & BROWN, B. H. 2001. Mk3.5: a modular, multi-frequency successor to the Mk3a EIS/EIT system. *Physiological Measurement,* 22**,** 49.
376. WIPPOLD, F. J. 2007. Head and neck imaging: The role of CT and MRI. *Journal of Magnetic Resonance Imaging,* 25**,** 453-465.
377. WOO, E. J. Functional brain imaging using MREIT and EIT: Requirements and feasibility. 2011 8th International Symposium on Noninvasive Functional Source Imaging of the Brain and Heart and the 2011 8th International Conference on Bioelectromagnetism, 13-16 May 2011 2011. 131-134.
378. YALE, S. H. 2005. Antonio Maria Valsalva (1666 – 1723). *Clinical Medicine and Research,* 3**,** 35-38.
379. YASIN, M., BÖHM, S., GAGGERO, P. O. & ADLER, A. 2011. Evaluation of EIT system performance. *Physiological Measurement,* 32**,** 851.
380. YEN, C. C.-C., FUKUDA, M. & KIM, S.-G. 2011. BOLD responses to different temporal frequency stimuli in the lateral geniculate nucleus and visual cortex: Insights into the neural basis of fMRI. *NeuroImage,* 58**,** 82-90.
381. YENTES, J., HUNT, N., SCHMID, K., KAIPUST, J., MCGRATH, D. & STERGIOU, N. 2013. The Appropriate Use of Approximate Entropy and Sample Entropy with Short Data Sets. *Annals of Biomedical Engineering,* 41**,** 349-365.
382. YERWORTH, R., BAYFORD, R., CUSICK, G., CONWAY, M. & HOLDER, D. 2002. Design and performance of the UCLH Mark 1b 64 channel electrical impedance tomography (EIT) system, optimized for imaging brain function. *Physiological Measurement,* 23**,** 149.
383. YERWORTH, R. J., BAYFORD, R. H., BROWN, B., MILNES, P., CONWAY, M. & HOLDER, D. S. 2003. Electrical impedance tomography spectroscopy (EITS) for human head imaging. *Physiol Meas,* 24**,** 477-89.
384. ZALETEL, M., ŠTRUCL, M., RODI, Z. & ZVAN, B. 2004. The relationship between visually evoked cerebral blood flow velocity responses and visual-evoked potentials. *NeuroImage,* 22**,** 1784-1789.
385. ZHANG, H., WANG, W., ZHAO, Z., GE, Y., ZHANG, J., YU, D., CHAI, W., WU, S. & XU, L. 2010. The Action Sites of Propofol in the Normal Human Brain Revealed by Functional Magnetic Resonance Imaging. *The Anatomical Record: Advances in Integrative Anatomy and Evolutionary Biology,* 293**,** 1985-1990.
386. ZHANG, R., CRANDALL, C. G. & LEVINE, B. D. 2004. Cerebral Hemodynamics During the Valsalva Maneuver. *Stroke,* 35**,** 843-847.
387. ZHENG, B., ZULEY, M. L., SUMKIN, J. H., CATULLO, V. J., ABRAMS, G. S., RATHFON, G. Y., CHOUGH, D. M., GRUSS, M. Z. & GUR, D. 2008. Detection of breast abnormalities using a prototype resonance electrical impedance spectroscopy system: A preliminary study. *Medical Physics,* 35**,** 3041-3048.

APPENDIX 1: fEITER Measurement Index

Measurement index	Current electrode pair	Electrode measurement pairs
1-28	1-30	2-3, 3-4, 4-5, 5-6, 6-7, 7-8, 8-9, 9-10, 10-11, 11-12, 12-13, 13- 14, 14-15, 15-16, 16-17, 17-18, 18-19, 19-20, 20-21, 21-22, 22- 23, 23-24, 24-25, 25-26, 26-27, 27-28, 28-29, 31-32
29-56	1-27	2-3, 3-4, 4-5, 5-6, 6-7, 7-8, 8-9, 9-10, 10-11, 11-12, 12-13, 13- 14, 14-15, 15-16, 16-17, 17-18, 18-19, 19-20, 20-21, 21-22, 22- 23, 23-24, 24-25, 25-26, 28-29, 29-30, 30-31, 31-32
57-83	22-26	1-2, 2-3, 3-4, 4-5, 5-6, 6-7, 7-8, 8-9, 9-10, 10-11, 11-12, 12-13, 13-14, 14-15, 15-16, 16-17, 17-18, 18-19, 19-20, 20-21, 23-24, 24-25, 27-28, 28-29, 29-30, 30-31, 31-32
84-110	9-18	1-2, 2-3, 3-4, 4-5, 5-6, 6-7, 7-8, 10-11, 11-12, 12-13, 13-14, 14- 15, 15-16, 16-17, 19-20, 20-21, 21-22, 22-23, 23-24, 24-25, 25- 26, 26-27, 27-28, 28-29, 29-30, 30-31, 31-32
111-137	7-16	1-2, 2-3, 3-4, 4-5, 5-6, 8-9, 9-10, 10-11, 11-12, 12-13, 13-14, 14- 15, 17-18, 18-19, 19-20, 20-21, 21-22, 22-23, 23-24, 24-25, 25- 26, 26-27, 27-28, 28-29, 29-30, 30-31, 31-32
138-164	3-12	1-2, 4-5, 5-6, 6-7, 7-8, 8-9, 9-10, 10-11, 13-14, 14-15, 15-16, 16-17, 17-18, 18-19, 19-20, 20-21, 21-22, 22-23, 23-24, 24-25, 25-26, 26-27, 27-28, 28-29, 29-30, 30-31, 31-32
165-192	1-28	2-3, 3-4, 4-5, 5-6, 6-7, 7-8, 8-9, 9-10, 10-11, 11-12, 12-13, 13- 14, 14-15, 15-16, 16-17, 17-18, 18-19, 19-20, 20-21, 21-22, 22- 23, 23-24, 24-25, 25-26, 26-27, 29-30, 30-31, 31-32
193-219	8-12	1-2, 2-3, 3-4, 4-5, 5-6, 6-7, 9-10, 10-11, 13-14, 14-15, 15-16, 16-17, 17-18, 18-19, 19-20, 20-21, 21-22, 22-23, 23-24, 24-25, 25-26, 26-27, 27-28, 28-29, 29-30, 30-31, 31-32
220-246	5-15	1-2, 2-3, 3-4, 6-7, 7-8, 8-9, 9-10, 10-11, 11-12, 12-13, 13-14, 16- 17, 17-18, 18-19, 19-20, 20-21, 21-22, 22-23, 23-24, 24-25, 25- 26, 26-27, 27-28, 28-29, 29-30, 30-31, 31-32
247-274	1-29	2-3, 3-4, 4-5, 5-6, 6-7, 7-8, 8-9, 9-10, 10-11, 11-12, 12-13, 13-14, 14 -15, 15-16, 16-17, 17-18, 18-19, 19-20, 20-21, 21-22, 22- 23, 23-24, 24-25, 25-26, 26-27, 27-28, 30-31, 31-32

375-301	4-13	1-2, 2-3, 5-6, 6-7,7-8, 8-9, 9-10, 10-11, 11-12, 14-15, 15-16, 16-17, 17-18, 18-19, 19-20, 20-21, 21-22, 22-23, 23-24, 24-25, 25-26, 26-27, 27-28, 28-29, 29-30, 30-31, 31-32
302-328	8-17	1-2, 2-3, 3-4, 4-5, 5-6, 6-7, 9-10, 10-11, 11-12, 12-13, 13-14, 14- 15, 15-16, 18-19, 19-20, 20-21, 21-22, 22-23, 23-24, 24-25, 25- 26, 26-27, 27-28, 28-29, 29-30, 30-31, 31-32
329-355	7-13	1-2, 2-3, 3-4, 4-5, 5-6, 8-9, 9-10, 10-11, 11-12, 14-15, 15-16, 16- 17, 17-18, 18-19, 19-20, 20-21, 21-22, 22-23, 23-24, 24-25, 25- 26, 26-27, 27-28, 28-29, 29-30, 30-31, 31-32
356-382	20-24	1-2, 2-3, 3-4, 4-5, 5-6, 6-7, 7-8, 8-9, 9-10, 10-11, 11-12, 12-13, 13-14, 14-15, 15-16, 16-17, 17-18, 18-19, 19-20, 22-23, 25-26, 26-27, 27-28, 28-29, 29-30, 30-31, 31-32
383-409	6-14	1-2, 2-3, 3-4, 4-5, 7-8, 8-9, 9-10, 10-11, 11-12, 12-13, 15-16, 16-17, 17-18, 18-19, 19-20, 20-21, 21-22, 22-23, 23-24, 24-25, 25-26, 26-27, 27-28, 28-29, 29-30, 30-31, 31-32
410-437	1-31	2-3, 3-4, 4-5, 5-6, 6-7, 7-8, 8-9, 9-10, 10-11, 11-12, 12-13, 13- 14, 14-15, 15-16, 16-17, 17-18, 18-19, 19-20, 20-21, 21-22, 22- 23, 23-24, 24-25, 25-26, 26-27, 27-28, 28-29, 29-30
438-465	1-10	2-3, 3-4, 4-5, 5-6, 6-7, 7-8, 8-9, 11-12, 12-13, 13-14, 14-15, 15- 16, 16-17, 17-18, 18-19, 19-20, 20-21, 21-22, 22-23, 23-24, 24- 25, 25-26, 26-27, 27-28, 28-29, 29-30, 30-31
466-492	2-11	3-4, 4-5, 5-6, 6-7, 7-8, 8-9, 9-10, 12-13, 13-14, 14-15, 15-16, 16- 17, 17-18, 18-19, 19-20, 20-21, 21-22, 22-23, 23-24, 24-25, 25- 26, 26-27, 27-28, 28-29, 29-30, 30-31
493-519	21-25	1-2, 2-3, 3-4, 4-5, 5-6, 6-7, 7-8, 8-9, 9-10, 10-11, 11-12, 12-13, 13-14, 14-15, 15-16, 16-17, 17-18, 18-19, 19-20, 22-23, 23-24, 26-27, 27-28, 28-29, 29-30, 30-31
520-546	19-23	1-2, 2-3, 3-4, 4-5, 5-6, 6-7, 7-8, 8-9, 9-10, 10-11, 11-12, 12-13, 13-14, 14-15, 15-16, 16-17, 17-18, 20-21, 21-22, 24-25, 25-26, 26-27, 27-28, 28-29, 29-30, 30-31

APPENDIX 2: Software Scripts

(A) MatLab script to import fEITER data and reshape into a single matrix
Provided by Dr. John Davidson – University of Manchester

```
%read in data
[Vm,Im,BadSine,Idrv_chk,st_marker,sync_word,CP_id,ADC_sat,first_byte,d_type]
=read_fEITER_datfile_v2('file_A.dat','{magn}');
%perform Current Pattern Identification check
[CPid_chck]=CPid_check(CP_id);
%remove the 1st and last column from the Vm and ADC_sat data (these refer to ref-1
and 32-ref data)
red_Vm = Vm(:,2:32); red_ADC_sat = ADC_sat(:,2:32);
%load the 'excluded data' matrix from file for the head strategy
load head_excluded_meas_matrix
%generate the measurement vector for a frame of data – for the fEITER HEAD
STRATEGY
%where ind_meas is for m_3d_fields_v2 and df is for jacobian_3d  - 546
measurements
[meas_vector,ind_meas,df]=head_strategy_vector(ex_1);
%reshape the data for the 546 measurement head strategy     LOGICAL AND to the
2 current sources
[rs_Vm,rs_Im,rs_sm,rs_ADC_sat,rs_Idrv_chk]=data_reshaping_head(CP_id,
red_Vm,Im,st_marker,red_ADC_sat,Idrv_chk,'{y}',ex_1);
%extract data from the FIRST and LAST 100 frames
rs_Im_1_100 = rs_Im(:,1:100); rs_Vm_1_100 = rs_Vm(:,1:100);
rs_Vm_5892_5991 = rs_Vm(:,5892:5991); rs_Im_5892_5991 = rs_Im(:,5892:5991);
%find problem data (for ALL frames) based on the ADC saturation flag
[meas_problems]=find_flag_indices(rs_ADC_sat,meas_vector);
%find problem data (for ALL frames) based on the current drive flag
[drive_problems]=find_flag_indices(1-rs_Idrv_chk,meas_vector);

%single voltage measurement across all frames
Vm_1_30_2_3 = rs_Vm(1,:)';
%normalise voltages to 1 mA current
norm_Vm = (0.001 ./ rs_Im) .* rs_Vm;

norm_Vm_1_30_2_3 = norm_Vm(1,:)';
norm_Vm_1_30_3_4 = norm_Vm(2,:)';
norm_Vm_1_30_4_5 = norm_Vm(3,:)';
norm_Vm_1_30_5_6 = norm_Vm(4,:)';
% Above script was continued for all measurements until:
"norm_Vm_19_23_30_31 = norm_Vm(546,:)';"
```

(B) Spike2 script to display multiple, normalised fEITER data on a single trace
Provided by Dr. Chris Pomfrett

```
var test[5998];
var stmarker[119960][2];
var thisCh%;
var fileindex%;
var file$;
var file%;
var path%;
var path$;
var retry%;
var check%;
var sum;
var mean;
var smrfile%;                    'id for filename
var stmarker$ := "st_marker";    'st_marker variable
var vpairno%;                    'counter for names of Matlab variables
var vpairs$[109][2];             'string array for names of Matlab variables
'injection - voltage pair variables called from Matlab follow;
vpairs$[0][0] := "norm_Vm_1_10_2_3" ;'   current injection 1-10, voltage
    measurement 2-3;
vpairs$[1][0] := "norm_Vm_1_10_3_4" ;
vpairs$[2][0] := "norm_Vm_1_10_4_5" ;
vpairs$[3][0] := "norm_Vm_1_10_5_6" ;
vpairs$[4][0] := "norm_Vm_1_10_6_7" ;
vpairs$[5][0] := "norm_Vm_1_10_7_8" ;
vpairs$[6][0] := "norm_Vm_1_10_8_9" ;
```

Continued for remaining injection pairs:

```
'shortened injection - voltage pair channel labels follow;
vpairs$[0][1] := "01100203" ;' injection 01-10, measurement 02-03;
vpairs$[1][1] := "01100304" ;
vpairs$[2][1] := "01100405" ;
vpairs$[3][1] := "01100506" ;
vpairs$[4][1] := "01100607" ;
vpairs$[5][1] := "01100708" ;
vpairs$[6][1] := "01100809" ;
vpairs$[7][1] := "01101112" ;

var ml%;
var ml$[121];
ml$[0] :=
    "[Vm,Im,BadSine,Idrv_chk,st_marker,sync_word,CP_id,ADC_sat,first_byte,
    d_type]=read_fEITER_datfile_v2('aud_seq10_14-20.dat','{magn}');";
ml$[1] := "[CPid_chck]=CPid_check(CP_id);";
ml$[2] := "red_Vm = Vm(:,2:32); red_ADC_sat = ADC_sat(:,2:32);";
```

```
ml$[3] := "load head_excluded_meas_matrix;";
ml$[4] := "[meas_vector,ind_meas,df]=head_strategy_vector(ex_1);";
ml$[5] := "
        [rs_Vm,rs_Im,rs_sm,rs_ADC_sat,rs_Idrv_chk]=data_reshaping_head(CP_id,
        red_Vm,Im,st_marker,red_ADC_sat,Idrv_chk,'{y}',ex_1);";
ml$[6] := "rs_Im_1_100 = rs_Im(:,1:100); rs_Vm_1_100 = rs_Vm(:,1:100);";
ml$[7] := "rs_Vm_5892_5991 = rs_Vm(:,5892:5991); rs_Im_5892_5991 =
        rs_Im(:,5892:5991);";
ml$[8] := "[meas_problems]=find_flag_indices(rs_ADC_sat,meas_vector);";
ml$[9] := "[drive_problems]=find_flag_indices(1-rs_Idrv_chk,meas_vector);";
ml$[10] := "Vm_1_30_2_3 = rs_Vm(1,:)';";
ml$[11] := "norm_Vm = (0.001 ./ rs_Im) .* rs_Vm;";
ml$[12] := "norm_Vm_1_10_2_3 = norm_Vm(438,:)';";
ml$[13] := "norm_Vm_1_10_3_4 = norm_Vm(439,:)';";
ml$[14] := "norm_Vm_1_10_4_5 = norm_Vm(440,:)';";
ml$[15] := "norm_Vm_1_10_5_6 = norm_Vm(441,:)';";
ml$[16] := "norm_Vm_1_10_6_7 = norm_Vm(442,:)';";
ml$[17] := "norm_Vm_1_10_7_8 = norm_Vm(443,:)';";
ml$[18] := "norm_Vm_1_10_8_9 = norm_Vm(444,:)';";
ml$[19] := "norm_Vm_1_10_11_12 = norm_Vm(445,:)';";
ml$[20] := "norm_Vm_1_10_12_13 = norm_Vm(446,:)';";
```

Continued for remaining injection pairs, last function will read:

```
ml$[120] := "norm_Vm_19_23_31_32 = norm_Vm(546,:)';";
```

```
path% := FilePathSet("",0,"Location of data files",0);
path$ := FilePath$(0);
file% := FileOpen("",9,0,"Load fEITER data file");
if file% <= 0 then
                'Check to see if it opens. If not, give
    retry%:=Query("Failed to open data file\nor user pressed
    cancel","Retry","Quit");
    if retry% then
  else Halt;
  endif;
endif;
file$ := FileName$(3)+FileName$(4);
check% := MatLabOpen(1);
check% := MatLabEval("cd ('"+path$+"');");      'set the Matlab working directory to
    the directory we want to work in
PrintLog("Data directory = "+path$+"\n");
                                'load the fEITER Labview data into Matlab
check% :=
    MatLabEval("[Vm,Im,BadSine,Idrv_chk,st_marker,sync_word,CP_id,ADC_
    sat,first_byte,d_type]=read_fEITER_datfile_v2('"+file$+".dat','{magn}');");
Message("loading file ",file$);
PrintLog("fEITER file = "+file$+"\n");
for ml% := 1 to 120 step 1 do
check% := MatLabEval(ml$[ml%]);
```

```
next;
'check% := MatLabEval("save ('"+file$+"';");     'save the Matlab workspace
'PrintLog("Matlab workspace = "+file$+"\n");
check% := FileNew(7,1,10,100,60,120);          'make a new Spike2 file
for vpairno% := 0 to 108 step 1 do
check% := MatLabGet(vpairs$[vpairno%][0],test[]);'get the variable from Matlab
   if check% = 0 then
   PrintLog("Variable "+vpairs$[vpairno%][0]+" loaded OK\n");
   else
   PrintLog("Variable "+vpairs$[vpairno%][0]+" fail\n");
   endif;
sum := ArrSum(test[]);                    'find sum of data
mean := sum/5998;                         'calculate mean data within sampling epoch
check% := ArrSub(test[],mean);               'shifts DC baseline to mean of epoch
check% := ArrMul(test[],5000);               'amplify to preserve LSB when channel
        copied
thisCh% := MemChan(1,0,0.01);                'make a new memory channel
MemSetItem(thisCh%, 0, 0, test[]);           'copy data array into memory channel
ChanTitle$(thisCh%,vpairs$[vpairno%][1]);      'label the channel with shortened
        pair id
ChanUnits$(thisCh%,"mV");                    'set units
ChanScale(thisCh%,0.1);                   'scale the channel
MemSave(thisCh%,vpairno%+5,1);               'copy to new real channel
ChanDelete(thisCh%);                      'delete memory channel
ChanShow(vpairno%+5);                        'display the channel
next
check% := MatLabGet(stmarker$,stmarker[][]);   'get the stimulus marker from
        Matlab
thisCh% := MemChan(1,0,0.0005);              'stimulus marker is sampled at 2KHz
MemSetItem(thisCh%, 0, 0, stmarker[][0]);      'extract first column of stimulus
        marker and save as a memory channel
ChanTitle$(thisCh%,"Stim");                  'name the channel
MemSave(thisCh%,4);                       'save the temporary memory channel to
        permanent channel 4
ChanDelete(thisCh%);                         'delete the memory channel
ChanShow(4);                              'show the stimulus mark
XRange(0.0,60.0);                         'show all 60s of x axis
Optimise();                               'optimise all y axes
FontSet("Arial",6,0);                        'set font to Arial
MatLabClose();                            'closedown matlab
```

(C) MatLab scrip for PSD estimation, REG and HFN filtering Provided by Dr. Tom Marchant – The Christie NHS Foundation Trust

```
>> Ref = ABVM(1:1000);

% Autocovariance was applied to reference signal named 'Ref'
% Ref data was duplicated
>> Auto_cov = xcov(Ref,RefCopy);

% Apply hanning window
>> Hanwin = Auto_cov.*hanning(length(Auto_cov));

% PSD estimate
>> N = length(Hanwin)
fs = 100
X_mags = abs(fft(Hanwin));
X_mags_mean = mean(X_mags);
X_mags_new = [X_mags-X_mags_mean];
bin_vals = [0 : N-1];
fax_Hz = bin_vals*fs/N;
N_2 = ceil(N/2);
plot(fax_Hz(1:N_2), X_mags_new(1:N_2))
xlabel('Frequency (Hz)')
ylabel('Magnitude');
title('Single-sided Magnitude spectrum (Hertz)');

% Apply first order differencing to the data
>> diff_data = diff(data_signal);

% Apply Hanning window to the first 100 data points of the differenced data
>> hw = hann(200);          % symmetric Hann window
hw = hw(1:100);             % take first half of the window
hw2 = ones(5997,1);         % create vector of ones to multiply signal by
hw2(1:100) = hw;            % place the Hann roll off at the beginning

% Apply the hann window of 100 to the beginning of the differenced data signal
>> Hanwin = diff_data.*hw2;

% Filter the REG signal occurring at a frequency of approximately 1Hz using a band
stop filter. Divide frequency by half the total sampling rate (100).
% Design stop band butterworth filter for REG frequency between 0.85 and 4.5
>> [b_stop a_stop] = butter(5, [0.012  0.04], 'stop');

% Apply filter to difference and windowed data named:
>> X_filteredREG = filter(b_stop, a_stop, Hanwin);

% Plot original and filtered signal
>> subplot(2,1,1)
```

```
plot(VM1)
Subplot(2,1,2)
Plot(X_filtered)

% PSD estimate of REG filtered signal to identify high frequency noise components of the signal. Duplicate the filtered signal then apply auto covariance function and estimate the PSD

>> Auto_cov = xcov(X_filteredREG,X_filteredREGCopy);

% Apply hanning window
>> Hanwin = Auto_cov.*hanning(length(Auto_cov));

% PSD estimate
>> N = length(Hanwin)
fs = 100
X_mags = abs(fft(Hanwin));
X_mags_mean = mean(X_mags);
X_mags_new = [X_mags-X_mags_mean];
bin_vals = [0 : N-1];
fax_Hz = bin_vals*fs/N;
N_2 = ceil(N/2);
plot(fax_Hz(1:N_2), X_mags_new(1:N_2))
xlabel('Frequency (Hz)')
ylabel('Magnitude');
title('Single-sided Magnitude spectrum (Hertz)');


% Apply a low pass filter to remove high frequency components of the previously filtered data for REG, using a cut-off frequency from the PSD estimate
>>  [b a] = butter(m,n,'low');

m = filter order for example 2
n = cut off frequency for example 0.1 (will filter frequencies above this)
'low' low pass filter

>> X_filteredHFN = filter(b,a,X_filteredREG);
```

The first 100 data points must be excluded from further analysis due to windowing the first 100 data points

```
hist_values = (hist_stim,n_ref);
```

FOR DATA WHERE NO REG IS IDENTIFIED, ONLY APPLY HFN FILTERING

```
%PSD of the data signal to identify high frequency noise, difference the data then duplicate before applying apply autocovariance
>> diff_data = diff(data_signal);
Auto_cov = xcov(diff_data,diff_dataCopy);

% Apply hanning window
>> Hanwin = Auto_cov.*hanning(length(Auto_cov));

% PSD estimate
>> N = length(Hanwin)
fs = 100
X_mags = abs(fft(Hanwin));
X_mags_mean = mean(X_mags);
X_mags_new = [X_mags-X_mags_mean];
bin_vals = [0 : N-1];
fax_Hz = bin_vals*fs/N;
N_2 = ceil(N/2);
plot(fax_Hz(1:N_2), X_mags_new(1:N_2))
xlabel('Frequency (Hz)')
ylabel('Magnitude');
title('Single-sided Magnitude spectrum (Hertz)');


% Apply Hanning window to the first 100 data points of the differenced data
>> hw = hann(200);          % symmetric Hann window
hw = hw(1:100);             % take first half of the window
hw2 = ones(5997,1);         % create vector of ones to multiply signal by
hw2(1:100) = hw;            % place the Hann roll off at the beginning

% Apply the hann window of 100 to the beginning of the differenced data signal
>> Hanwin = diff_data.*hw2;

% Apply a low pass filter to remove high frequency components of the differenced data using a cut-off frequency from the PSD estimate
>> [b a] = butter(m,n,'low');

m = filter order for example 2
n = cut off frequency for example 0.1 (will filter frequencies above this)
'low' low pass filter

>> X_filteredHFN = filter(b,a,Hanwin);
```

(D) MatLab script to produce histograms and ROC curves Provided by Dr. Tom Marchant – The Christie NHS Foundation trust

```
% read data from csv file
data = csvread('H:\IGRT\FeasibilityAccount\fEITER\test_data.csv');
vals = data(:,2);

% plot data
figure();
plot(vals);

% Define number of times to repeat random sampling
N = 5000;

% Define length of samples to compare
len = 50;

% Define reference period start and end
ref_start = 1;
ref_end = 1000;

% Define stimulus period start and end
stim_start = 1001;
stim_end = 3001;

% First test consistency of data samples in reference region.

% initialize array to hold t-values for N comparisons of samples from
% reference period
tvals_ref = zeros(N, 1);

% for loop to repeat N times
for i = 1:N
    % select first sample from reference period
    % select random number from ref_start to (ref_end-len)
    i1 = round(ref_start + rand(1)*(ref_end - len - ref_start));
    samp1 = vals(i1:i1+len-1);
    % compute first sample mean and SD
    samp1_mean = mean(samp1);
    samp1_sd = std(samp1);

    % select second sample from reference period
    % select random number from ref_start to (ref_end-len)
    i2 = round(ref_start + rand(1)*(ref_end - len - ref_start));
    samp2 = vals(i2:i2+len-1);
    % compute second sample mean and SD
    samp2_mean = mean(samp2);
```

```
    samp2_sd = std(samp2);

% calculate t-statistic for these two distributions
tval = (samp1_mean - samp2_mean) / sqrt(((samp1_sd^2)/len) +
          ((samp2_sd^2)/len));
% put the t-value into the tvals_ref array (take abs value as we don't
% care if diff is positive or negative)
tvals_ref(i) = abs(tval);
end

% generate histogram of tvals_ref (150 bins from 0 to 300)
[n_ref, centres] = hist(tvals_ref, [0:150]*2);
figure();
%hist(tvals_ref, [0:150]*2);
bar(centres, n_ref, 1.0, 'g', 'LineStyle', 'none');  % plot as bar chart
patch1 = findobj(gca,'type','Patch'); % The child object of axes is a Patch Object
set(patch1,'FaceAlpha',0.4);  % make chart slightly transparent

% Now test consistency of data samples in reference vs stimulus regions.

% initialize array to hold t-values for N comparisons of samples from
% reference period
tvals_stim = zeros(N, 1);

% for loop to repeat N times
for i = 1:N
% select first sample from reference period
% select random number from ref_start to (ref_end-len)
i1 = round(ref_start + rand(1)*(ref_end - len - ref_start));
samp1 = vals(i1:i1+len-1);
% compute first sample mean and SD
samp1_mean = mean(samp1);
samp1_sd = std(samp1);

% select second sample from stimulus period
% select random number from stim_start to (stim_end-len)
i2 = round(stim_start + rand(1)*(stim_end - len - stim_start));
samp2 = vals(i2:i2+len-1);
% compute second sample mean and SD
samp2_mean = mean(samp2);
samp2_sd = std(samp2);

% calculate t-statistic for these two distributions
tval = (samp1_mean - samp2_mean) / sqrt(((samp1_sd^2)/len) +
          ((samp2_sd^2)/len));
% put the t-value into the tvals_ref array
tvals_stim(i) = abs(tval);
end

% generate histogram of tvals_ref
```

```
[hist_stim, centres] = hist(tvals_stim, [0:150]*2);
hold on
%hist(tvals_stim, [0:150]*2);
bar(centres, hist_stim, 1.0, 'r', 'LineStyle', 'none'); % plot as bar chart
patch1 = findobj(gca,'type','Patch'); % The child object of axes is a Patch Object
set(patch1,'FaceAlpha',0.4); % make chart slightly transparent
hold off

%% test classifier based on t threshold. Classifier says signal is stimulus
%% if t > thresh. Test thresh for each histogram bin and work out how good
%% the classifier is. Sensitivity = true positive rate (i.e. what
%% proportion of the stimulus points have t >= thresh).
%% Specificity is the true negative rate (i.e. what proportion of reference
%% points have t < thresh).

sens = hist_stim * 0.0;
spec = hist_stim * 0.0; % initialise arrays

for i=1:151
   sens(i) = sum(tvals_stim >= centres(i))/N;
   spec(i) = sum(tvals_ref < centres(i))/N;
end

% plot ROC curve, sens against 1-spec
figure;
plot(1-spec, sens)
xlabel('1-specificity')
ylabel('sensitivity')
title('ROC curve')

% plot sensitivity + specificity against cut value. This is the Youden Index. The
        maximum can
% be used as the optimum cut.
figure;
YI = sens+spec;
plot(centres,sens+spec)
xlabel('cut value')
ylabel('sensitivity + specificity')

iopt = find(YI == max(YI));
cutopt = centres(iopt);
disp(['Optimum cut is at t = ', num2str(cutopt)])
```

(E) MatLab Approximate entropy (ApEn) function Provided by Avinash Parnandi – University of Southern California

```
function [apen] = approx_entropy(n,r,a)

data =a;

for m=n:n+1; % run it twice, with window size differing by 1

set = 0;
count = 0;
counter = 0;
window_correlation = zeros(1,(length(data)-m+1));

for i=1:(length(data))-m+1,
current_window = data(i:i+m-1); % current window stores the sequence
to be compared with other sequences

for j=1:length(data)-m+1,
sliding_window = data(j:j+m-1); % get a window for comparision with
the current_window

% compare two windows, element by element
% can also use some kind of norm measure; that will perform better
for k=1:m,
if((abs(current_window(k)-sliding_window(k))>r) && set == 0)
set = 1; % i.e. the difference between the two sequence is greater
than the given value
end
end
if(set==0)
count = count+1; % this measures how many sliding_windows are
similar to the current_window
end
set = 0; % reseting 'set'

end
counter(i)=count/(length(data)-m+1); % we need the number of similar
windows for every cuurent_window
count=0;
i;
end  %  for i=1:(length(data))-m+1, ends here

counter;  % this tells how many similar windows are present for each
window of length m
%total_similar_windows = sum(counter);

%window_correlation = counter/(length(data)-m+1);
correlation(m-n+1) = ((sum(counter))/(length(data)-m+1));

end % for m=n:n+1; % run it twice
correlation(1);
correlation(2);
apen = log(correlation(1)/correlation(2));
```

APPENDIX 3: Study Documents

(A) fEITER Volunteer and patient study documents

fEITER Clinical Trial Protocol

Version 1.0, 1 August 2007, CJDP

General Information

Sponsor:
The University of Manchester
Oxford Road, Manchester M13 9PL

Principal Investigator:
Dr Chris Pomfrett Ph.D.
Lecturer in Neurophysiology applied to Anaesthesia
Manchester Royal Infirmary
Oxford Road, Manchester M13 9WL
chris.pomfrett@manchester.ac.uk
Office phone: 0161 276 8582; Mobile & voicemail: 07885 202017.

Senior Physician:
Professor Brian Pollard FRCA.
Department of Anaesthesia,
Manchester Royal Infirmary,
Oxford Road, Manchester M13 9WL
brian.pollard@manchester.ac.uk
Office phone: 0161 276 4553

Background Information

The new device under investigation is called fEITER (functional Electrical Impedance Tomography by Evoked Response). EIT (Electrical Impedance Tomography) is a brain imaging technique that works by measuring changes in electrical conductivity of the head in response to minute levels of current injected through the head.

Summary of previous findings
In earlier studies on animals and humans (Holder et al), slow changes in brain conductivity were observed using EIT, which were believed to correspond to changes in neuronal osmotic gradients during normal brain function; EIT had no effect on brain function itself. fEITER is an enhancement of this EIT measuring technique; by including sensory stimuli, fast (sub-second) changes in electrical impedance will be detected as the brain processes the sensory information.

Known and potential risks & benefits to human subjects
There is no direct risk to brain function from the use of low-level current injection through the human brain. Much higher currents are used therapeutically in electro-convulsive therapy and induced within the brain during trans-cranial magnetic stimulation. Indirect risk of discomfort and neuralgia arises in the event that cranial nerves i.e. the facial and trigeminal nerves, are stimulated by inappropriate placement of electrodes and by a stimulus pattern that induces neural action potentials in the nerves as a result of physiological integration of short pulses of injected current into longer pulses.

There will be no direct benefits arising from the use of fEITER to human subjects until it has been evaluated as an imaging modality.

Statement of compliance
The trial will be conducted in compliance with the protocol, good clinical practice and applicable statutory requirements.

Population to be studied
Two groups will be studied. The first group will be volunteers drawn from the experimenter team. The second group will be fit and healthy (ASA I-II) patients scheduled for elective surgery facilitated with the volatile anaesthetic isoflurane, who will be tested with fEITER before and during anaesthesia.

Trial objectives and purpose
Functional brain imaging using positron emission tomography has shown that general anaesthesia reduces brain function in a dose-related manner. It is hypothesised that fEITER will derive similar images of human brain function arising from the normal changes in synaptic impedance that occur during cerebral processing of sensory information, but much faster than existing scanning methods and with a suitcase-sized device. We expect fEITER to visualise the reduction in cerebral sensory processing during anaesthesia, and this study will allow the preparation of a dose-response curve indicating the level of anaesthesia with fEITER. Deep surgical anaesthesia has a maximal effect on reducing brain metabolism, so such measurement will permit calibration of the 100% level for sensitivity of fEITER. The null hypothesis is that fEITER will visualise no effect of anaesthesia on brain function.

Trial methods
fEITER measures voltage, and derives impedance, using simultaneous recordings made from many scalp electrodes at the same time as minute levels of current are injected through the head using two of the same electrodes. The active recording and current injection electrodes alternate function rapidly so that many thousands of measurements can be made during a sub-second (fEITER) scan of the brain.

Commercially-available low contact impedance physiological recording electrodes (ZipPrep, Aspect Medical Systems) will be affixed to the scalp of volunteers and patients before commencing the trial. Several different standard placements (10-20 montage) of up to 32 electrodes will be trialled. Electrode to skin contact impedance will be checked by fEITER continuously during the trial, and fEITER will alert the experimenters should electrodes need to be reapplied.

Volunteers and patients will be asked to look at flashes of red light (via LED-equipped safety goggles) and to listen to clicks and tones (via infra red headphones). The order of the visual and auditory stimuli will be randomised and coded by computer. The impedance map of the brain in response to each of stimuli, or non-stimulus controls, will be measured and coded for off-line analysis by fEITER. The patients will be first tested with fEITER whilst awake i.e. before any pharmacological intervention. This stage will act as a tolerance test for fEITER to ensure that there is absolutely no sensation associated with its use, and no discomfort from the sensory stimuli. Patients will then be anaesthetised and any change in fEITER's measurement of electrical impedance will be automatically recorded for subsequent off-line analysis and reconstruction of impedance maps.

Trial Design

The primary endpoint of this trial will be the off-line reconstruction of brain electrical impedance images obtained in awake and anaesthetised human subjects.

The design of the study is an evaluation trial of a new medical device, measuring the sensitivity of the monitor to changes in brain impedance caused by hypnotic general anaesthesia. All blinding will be performed automatically on-line during data acquisition. Randomisation will be within each trial i.e. as a crossover with the patients acting as their own control; whether auditory or visual stimuli are presented will be randomly selected and coding of the computer- selected modality along with the end-tidal volatile anaesthetic concentration will be coded on-line and only decoded after analysis has been completed. Data will be automatically logged onto computer hard disc continuously during the trial and will be manually archived onto write once optical media after each trial.

Standard clinically appropriate and routine levels of anaesthesia and analgesia with be used in patients; there will be no change in the normal clinical procedure.

Information sheet for the fEITER research project (Version 2.0 Awake volunteers)

We would like to invite you to take part in a research study. Before you decide you need to understand why the research is being done and what it would involve for you. Please take time to read the following information carefully. Talk to others about the study if you wish.
(Part 1 tells you the purpose of this study and what will happen to you if you take part. Part 2 gives you more detailed information about the conduct of the study).
Ask us if there is anything that is not clear or if you would like more information.
Take time to decide whether or not you wish to take part.

Part 1 of the information sheet

What is the purpose of the study?

Functional electrical impedance tomography by evoked response (fEITER) is a new technique for creating an image of brain activity. fEITER is designed to be used at the bedside by a range of healthcare professionals, unlike other brain imaging techniques that require the patient to visit a large scanner needing specialised staff. fEITER has been invented at Manchester University, and it is hoped that it will become a useful clinical tool allowing brain imaging on more people and in places where other techniques cannot currently be used, such as clinics and the operating room during surgery.

Why have I been invited?

We are interested in the images that fEITER gives in awake volunteers.

Do I have to take part?

You do not have to take part in this trial. Your participation is voluntary.

What will happen to me if I take part?

We will stick some pads on your scalp. The pads are medically-approved and widely used around the world. The number may vary, but will not exceed 32. These pads will allow us to measure the electrical activity at the surface of your head. We will also ask you to wear goggles and/or headphones. These will allow you to see flashes of light and hear clicks of sound.

What will I have to do?

We will ask you to relax and watch the flashes and/or listen to the clicks in your ear.

What is the device that is being tested?

The device is called fEITER, and works by measuring how your brain conducts a minute electric current (electrical impedance tomography). This current is altered by the much larger changes naturally present in your brain as it thinks. By making many thousands of measurements, we will be able to see your brain responding to standard stimuli, such as flashes of light or noise. We wish to test whether your response changes during sedation or anaesthesia.

What are the possible disadvantages and risks of taking part?

There are no disadvantages in taking part in this study.

There are some slight risks that you need to know about:

Flashes used during the trial might be a problem if you have a history of epilepsy, so it is important that you tell us if you have ever suffered from epilepsy.

The research involves the injection of a small electrical current through the skin. The size of this electrical current is up to 1 milliamp, which is within international safety limits. However, it is possible that even this small current may cause temporary discomfort or pain (neuralgia). If such neuralgia is present, we will stop the trial immediately.

What are the side effects of any treatment received when taking part?

There will be no side effects arising from the trial.

What are the possible benefits of taking part?

We do not expect that the study will help you but the information we get from this study will help improve the availability of brain imaging techniques.

What happens when the research study stops?

The results of this study will be published in a medical scientific journal and presented at a scientific conference.

What if there is a problem?

Any complaint about the way you have been dealt with during the study or any possible harm you might suffer will be addressed. The detailed information on this is given in Part 2 of the information sheet.

Part 2 of the information sheet

What if relevant new information becomes available?

Sometimes we get new information about the treatment being studied. If this happens, your research doctor will tell you and discuss whether you should continue in the study. If you decide not to carry on, your research doctor will make arrangements for your care to continue. If you decide to continue in the study he may ask you to sign an updated consent form.

What will happen if I don't want to carry on with the study? What if there is a problem?

If you have a concern about any aspect of this study, you should ask to speak to the researchers who will do their best to answer your questions (Dr Bryan, contact number 0161 276 4537/ 4551/4552). If you remain unhappy and wish to complain formally, you can do this through the University of Manchester. Details can be obtained from Professor Pollard.
In the event that something does go wrong and you are harmed during the research and this is due to someone's negligence then you may have grounds for a legal action for compensation against (The University of Manchester) but you may have to pay your legal costs. The normal National Health Service complaints mechanisms will still be available to you (if appropriate).
We will provide compensation for any injury caused by taking part in this study in accordance with the guidelines of the Association of the British Pharmaceutical Industry (ABPI).
We will pay compensation where the injury probably resulted from:
A drug being tested or administered as part of the trial protocol
Any test or procedure you received as part of the trial
Any payment would be without legal commitment. (Please ask if you wish more information on this)
We would not be bound by these guidelines to pay compensation where:
The injury resulted from a drug or procedure outside the trial protocol
The protocol was not followed.

Will my taking part in this study be kept confidential?

All information which is collected about you during the course of the research will be kept strictly confidential, and any information about you which leaves the hospital/surgery will have your name and address removed so that you cannot be recognised (if it is applicable to your research).

Involvement of the General Practitioner/Family doctor (GP)

Your GP will be advised that you have taken part in this trial.

What will happen to the results of the research study?

The results from this study will be archived onto computer media, encrypted and stored securely for fifteen years.

Who is organising and funding the research?

The Wellcome Trust have funded this study, which has been organised by the University of Manchester.

Who has reviewed the study?

All research in the NHS is looked at by independent group of people, called a Research Ethics Committee to protect your safety, rights, wellbeing and dignity. This study has been reviewed and given favourable opinion by South Manchester Research Ethics Committee.

Procedure

We will stick up to 32 standard pads to your scalp. These are attached to fEITER by wires, and allow it to measure the electrical activity of your brain. We will also ask you to listen to sounds using headphones and look at pictures produced in goggles. This is so that we can test whether fEITER can measure your brain's response to these stimuli

It is important that you report any discomfort that you may feel. We do not expect you to feel anything unusual, but this trial is partially to test this. In an earlier trial of fEITER on staff, one person felt pain on the forehead and the trial was stopped. We believe that we have eliminated the reason this happened.

Further information and contact details

Should you want further information regarding this research, please ask Dr Angella Bryan, who is a Clinical Scientist. If you want to contact the Senior Medical Doctor responsible for this project, please contact Professor Brian Pollard.

Thank you.

Contact Details:

Professor Brian Pollard [Tel: 0161 276 8651 / 4551/ 4552]
Professor of Anaesthesia

Dr Angella Bryan [Tel: 0161 276 4537/ 4551/4552]
Clinical Scientist

Participant information sheet for the fEITER research project
version 2.0 (Patient)

We would like to invite you to take part in a research study. Before you decide you need to understand why the research is being done and what it would involve for you. Please take time to read the following information carefully. Talk to others about the study if you wish.
(Part 1 tells you the purpose of this study and what will happen to you if you take part. Part 2 gives you more detailed information about the conduct of the study).
Ask us if there is anything that is not clear or if you would like more information.
Take time to decide whether or not you wish to take part.

Part 1 of the information sheet

What is the purpose of the study?

Functional electrical impedance tomography by evoked response (fEITER) is a new technique for creating an image of brain activity. fEITER is designed to be used at the bedside by a range of healthcare professionals, unlike other brain imaging techniques that require the patient to visit a large scanner needing specialised staff. fEITER has been invented at Manchester University, and it is hoped that it will become a useful clinical tool allowing brain imaging on more people and in places where other techniques cannot currently be used, such as clinics and the operating room during surgery.

Why have I been invited?

You have been invited because you are about to be anaesthetised. We are interested in the images that fEITER gives in both anaesthetised and awake individuals. The equipment has already been tested on awake volunteers.

Do I have to take part?

You do not have to take part in this trial. Your participation is completely voluntary and will not affect your normal clinical care.

What will happen to me if I take part?

We will stick some pads on your scalp. The pads are medically-approved and widely used around the world. The number may vary, but will not exceed 32. These pads will allow us to measure the electrical activity at the surface of your head. We will also ask you to wear goggles and/or headphones. These will allow you to see flashes of light and hear clicks of sound.

What will I have to do?

We will ask you to relax and watch the flashes and/or listen to the clicks in your ear.

What is the device that is being tested?

The device is called fEITER, and works by measuring how your brain conducts a minute electric current (electrical impedance tomography). This current is altered by the much larger changes naturally present in your brain as it thinks. By making many thousands of measurements, we will be able to see your brain responding to standard stimuli, such as flashes of light or noise. We wish to test whether your response changes during anaesthesia.

What are the possible disadvantages and risks of taking part?

There are no disadvantages in taking part in this study.
There are some slight risks that you need to know about:
Flashes used during the trial might be a problem if you have a history of epilepsy, so it is important that you tell us if you have ever suffered from epilepsy.
The research involves the injection of a small electrical current through the skin. The size of this electrical current is up to 1 milliamp, which is within international safety limits. However, it is possible that even this small current may cause temporary discomfort or pain (neuralgia). If such neuralgia is present, we will stop the trial immediately.

What are the side effects of any treatment received when taking part?

There will be no side effects arising from the trial.

What are the possible benefits of taking part?

We do not expect that the study will help you but the information we get from this study will help improve the availability of brain imaging techniques.

What happens when the research study stops?

The results of this study will be published in a medical scientific journal and presented at a scientific conference.

What if there is a problem?

Any complaint about the way you have been dealt with during the study or any possible harm you might suffer will be addressed. The detailed information on this is given in Part 2 of the information sheet.

Part 2 of the information sheet

What if relevant new information becomes available?

Sometimes we get new information about the treatment being studied. If this happens, your research doctor will tell you and discuss whether you should continue in the study. If you decide not to carry on, your research doctor will make arrangements for your care to continue. If you decide to continue in the study he may ask you to sign an updated consent form.
If this happens, your research doctor might consider you should withdraw from the study. He/she will explain the reasons and arrange for your care to continue.

If the study is stopped for any other reason, we will tell you and arrange your continuing care.

What will happen if I don't want to carry on with the study?
What if there is a problem?

If you have a concern about any aspect of this study, you should ask to speak to the researchers who will do their best to answer your questions (Dr Bryan, contact number 0161 276 4537/ 4551/4552). If you remain unhappy and wish to complain formally, you can do this through the NHS Complaints Procedure. Details can be obtained from the hospital.
In the event that something does go wrong and you are harmed during the research and this is due to someone's negligence then you may have grounds for a legal action for compensation against The University of Manchester but you may have to pay your legal costs. The normal National Health Service complaints mechanisms will still be available to you (if appropriate).
We will provide compensation for any injury caused by taking part in this study in accordance with the guidelines of the Association of the British Pharmaceutical Industry (ABPI).
We will pay compensation where the injury probably resulted from:
A drug being tested or administered as part of the trial protocol
Any test or procedure you received as part of the trial
Any payment would be without legal commitment. (Please ask if you wish more information on this)
We would not be bound by these guidelines to pay compensation where:
The injury resulted from a drug or procedure outside the trial protocol
The protocol was not followed.

Will my taking part in this study be kept confidential?

All information which is collected about you during the course of the research will be kept strictly confidential, and any information about you which leaves the hospital will have your name and address removed so that you cannot be recognised.

Involvement of the General Practitioner/Family doctor (GP)

Your GP will be advised that you have taken part in this trial.

What will happen to the results of the research study?

The results from this study will be archived onto computer media, encrypted and stored securely for fifteen years.

Who is organising and funding the research?

The Wellcome Trust have funded this study, which has been organised by the University of Manchester.

Who has reviewed the study?

All research in the NHS is looked at by independent group of people, called a Research Ethics Committee, to protect your safety, rights, wellbeing and dignity. This study has been reviewed and given favourable opinion by the South Manchester Research Ethics Committee.

Procedure

We will stick up to 32 standard pads to your scalp. These are attached to fEITER by wires, and allow it to measure the electrical activity of your brain. We will also ask you to listen to sounds using headphones and look at flashes of light produced in goggles. This is so that we can test whether fEITER can measure your brain's response to these stimuli. The test will last up to fifteen minutes while you are awake. While you are anaesthetised as part of your clinical care, we will repeat the test to measure the effects of anaesthesia.

It is important that you report any discomfort that you may feel. We do not expect you to feel anything unusual, but this trial is partially to test this. In an earlier trial of fEITER on research scientists, one person felt pain on the forehead and the trial was stopped. We believe that we have eliminated the reason this happened.

Further information and contact details

Should you want further information regarding this research, please ask Dr Angella Bryan, who is a Clinical Scientist. If you want to contact the Senior Medical Doctor responsible for this project, please contact Professor Brian Pollard.

Thank you.

Contact Details:

Professor Brian Pollard [Tel: 0161 276 8651 / 4551/ 4552]
Professor of Anaesthesia

Dr Angella Bryan [Tel: 0161 276 4537/ 4551/4552]
Clinical Scientist

(B) fEITER volunteer trial testing autonomic challenges

Monitoring the brain during autonomic challenges using Electrical Impedance Tomography (EIT)

Staff volunteer study – Protocol Version 1.4

Department of Anaesthesia
5th Floor - St Mary's Hospital
Oxford Road, Manchester M13 9WL
brian.pollard@manchester.ac.uk

Sponsor:
The University of Manchester
Oxford Road, Manchester M13 9PL

Principal Investigator:
Professor Brian Pollard FRCA

Consultant Clinical Scientist:
Dr. Angella Bryan

Education purpose of the study to be undertaken

This study will be undertaken as part of PhD programme for Tanviha Quraishi who is a PhD student registered with the University of Manchester. The student is a full time member of staff at Central Manchester NHS Foundation Trust (CMFT). The student's role within this study will involve data collection using the fEITER system, time management of the challenges undertaken and assistance to Dr. Angella Bryan (Clinical Scientist of the research group) during the study. Following completion of the study, the student will be responsible for data analysis which will form part of the PhD thesis.

The student will be supervised by Dr. Angella Bryan and Professor Pollard who will be present throughout the study.

As an employee at CMFT and a member of the research group, the student has undertaken GCP training and is fully aware of the guidelines concerning data collection and storage.

Background information

Functional Electrical Impedance Tomography with Evoked Response (fEITER) is a brain imaging device invented at the University of Manchester. The device passes multiple current flows of low amplitude (1 mA) and high frequency (10 kHz) across pairs of diametrically opposed electrodes on the scalp. Resulting potentials are measured from other pairs of electrodes and reconstructed to form a tomographic conductivity map of activity within the brain (McCann et al., 2011, Towers et al., 2000). It is known that changes in conductivity in the brain monitored by EIT arise from ionic and haemodynamic changes in brain tissue (Brown, 2003, Holder, 2005).

To date EIT in the brain has successfully been used to locate epileptic foci, cortical spreading depression and evoked responses from visual, somatosensory and motor stimuli in animal (Bodo et al., 2003, Holder, 1992a, Holder et al., 1996) and tank

studies(Holder et al., 1999). Changes in cerebral blood flow can be monitored using EIT using a measurement technique more commonly known as Rheoencephalography (REG) (Perez-Borja and Meyer, 1964, Polzer and Schuhfried, 1950). Direct imaging of neuronal activity isn't currently possible as no such imaging modality exists which has a sub-second temporal resolution commensurate with neuronal processing activity. Alternatively, conventional brain imaging devices such as fMRI and PET couple neuronal activity to secondary physiological mechanisms such as changes in cerebral blood flow and metabolic rates. EIT proposes a solution to directly capture neuronal activity using a sub-second temporal resolution. Currently there exists no commercial EIT device adapted for imaging the brain. Volunteer and clinical trials carried out previously at CMFT utilised a non-commercial EIT device known as fEITER. fEITER will be used in the proposed study for convenience.

fEITER captures data using a sub-second resolution of 100 frames per second (10 ms temporal resolution) and therefore has the temporal capacity to monitor neuronal activity within the brain. Furthermore, multiple high frequency current injections across diametrically opposed electrodes maximises current density within the brain. This allows global activity at all levels of the brain to be captured.

Safety/Efficacy of fEITER

To date, fEITER has been utilised on 40 individuals with no adverse effects. It is MEAM electrical safety checked and maintained by the University of Manchester. It is a non-CE Marked Device. A preliminary study consisting of 15 volunteers was conducted at CMFT whereby fEITER was used successfully to monitor the brain of individuals whilst they were presented with audio and visual stimuli. Following the volunteer study a patient clinical trial was undertaken. During anaesthetic induction with propofol, fEITER was successfully used to monitor the brain of 15 patients scheduled for abdominal surgery during induction of anaesthesia (Bryan et al., 2011) and during surgery.

Aims

The proposed study will further evaluate the ability of EIT to capture sub-second changes in conductivity relating to neuronal activity. This study is not intended to generate data to further develop the fEITER device for CE Marking. It is to be used in this study purely for convenience to provide EIT in combination with the use of commercially available, low contact impedance, physiological recording electrodes.

Population to be studied

20 healthy adult members of staff at Central Manchester Foundation Trust will be recruited as volunteers for the study following poster advertisement within the Trust; these will predominantly be Anaesthetists or Scientists.

Details of the volunteer study will be advertised to staff members within the Department of Anaesthesia. The names and contact details of the research group will also be provided allowing volunteers to contact members of the research group for more details regarding the study. Following an expression of interest, the volunteers will be provided with a participant information sheet by Dr Angella Bryan, a

Consultant Clinical Scientist. The study and project details will be explained fully to the potential volunteers by Dr Bryan. Records of consent or refusal to consent will be kept confidential to avoid any opportunity for coercion to participate in the study. Volunteers who are happy to participate will be requested to sign a consent form at least 24 hours before the study.

Autonomic challenges

In the proposed study, volunteers will be asked to perform firstly a Valsalva manoeuvre (VM) and then after a period of rest, an inverse of the VM: the Mueller's (also spelt Muller's and Müller's) manoeuvre (MM).

The VM is a physiological test frequently used to evaluate the integrity of the autonomic nervous system. It causes characteristic changes in cerebral and systemic circulatory systems which have been monitored using ECG, MABP monitors and transcranial Doppler. Imaging techniques such as fMRI have since been employed to identify precise neural sites responsible for eliciting autonomic outflow associated with performing the manoeuvre correctly. These studies have identified various regions within the brain associated with autonomic outflow occurring during early stages of the manoeuvre.

Unlike the VM the MM is performed by forced inspiration against a closed airway. A correctly performed MM generates a collapsed airway and sub atmospheric intrathoracic pressure. The manoeuvre has been used as a clinical test to evaluate physiology of the upper airway and also to simulate effects of obstructive sleep apnoea. Recent studies have compared the characteristic changes in MABP and heart rate intervals observed during the VM, with changes observed during the MM. The results demonstrated changes in heart rate intervals and systemic blood pressure were temporally consistent during both manoeuvres although the direction of changes were opposite during some phases of the MM. Despite observed changes during the MM being smaller than those observed during phases of the VM, the authors concluded similar autonomic and neural mechanisms were responsible for generating the observed cardiovascular responses to both manoeuvres (Carrasco-Sosa and Guillen-Mandujano, 2011, Carrasco-Sosa and Guillén-Mandujano, 2012) . Similar to the VM, cerebral blood flow changes during the MM have also been evaluated using transcranial Doppler (Reinhard et al., 2000).

Volunteers will also be asked to perform the hand grip test using a hand held dynamometer to determine levels of applied grip. Similar to early stages of the VM, the hand grip test is known to activate sympathetic outflow. It can also be used as a physiological test to evaluate sympathetic function, as it evokes an increase in heart rate and systolic blood pressure which are proportional to the intensity of the hand grip test (Williamson et al., 2003, Williamson et al., 2002). fMRI responses have shown activation of the insular cortex in response to this autonomic challenge, providing further evidence for a neural mechanism mediating autonomic outflow (Macey et al., 2012).

Study objectives and purpose

fMRI trials have identified areas of the brain thought to be responsible for autonomic outflow caused by the VM (Nagai et al., 2010). The volunteer study we propose to execute will further our understanding of precise neural sites involved in mediating autonomic outflow. Furthermore, the use of other autonomic challenges will further

evaluate the ability of EIT to capture genuine neuronal responses which have previously been correlated to the BOLD signal using fMRI.

Study methods

fEITER injects multiple low amplitude and high frequency currents across diametrically opposed electrodes placed on the scalp. Simultaneous voltage measurements are captured by fEITER from pairs of non-injecting electrodes. Voltage measurements are made 100 times every second resulting in almost 6000 measurements during one minutes worth of fEITER monitoring time. A total of 21 random sequences of current injections occur during each second therefore the combination and location of non-injecting electrode pairs from which voltages are measured is continuously changing. This method effectively maximises current density within the head, resulting in a global scan of the brain at varying depths.

Commercially available, low contact impedance, physiological recording electrodes will be affixed to the scalp of volunteers before commencing the study. The electrodes will be placed at landmarks around the scalp which will be identified using a modified version of the international 10-20 EEG electrode placement montage. A total of 32 electrodes will be attached to each volunteer.

The study will take place in the Department of Anaesthesia, 5th Floor St Mary's Hospital in an area designated for physiological measurements. During one minute of monitoring with fEITER, volunteers will be asked to perform one of the test scenarios (VM, MM, hand grip with periods of reference prior to and following the tests. Each volunteer will be asked to repeat each challenge 3 times in a randomised fashion and with sufficient recovery time before performing the next challenge. Volunteers will also be asked to remain still and silent for a complete minute of fEITER recordings where no autonomic challenges are being undertaken; these data will also be referred to as references.

Continuous ECG monitoring will be undertaken to monitor expected cardiovascular changes during the autonomic challenges.

Study Design

The endpoint of this study will be the off-line reconstruction of brain electrical impedance images obtained in volunteers performing the VM, the MM and handgrip test.

This evaluation study will assess the ability of EIT to capture sub-second changes in brain impedance elicited by autonomic challenges: the VM, MM and the hand grip test. Sub-second changes in brain impedance have been observed in the preliminary volunteer study.

Randomisation will be within each study i.e. as a crossover with the patients acting as their own control. Data will be automatically logged onto a computer hard disc continuously during the study and will be manually archived onto write once optical media after each study.

Duration
Previous volunteer studies undertaken using fEITER lasted for 8 weeks in which 20 volunteers were recruited. We therefore anticipate that the proposed study involving 20 volunteers will be completed within 8 weeks from the first volunteer.

Inclusion/Exclusion
Individuals who have suffered a recent heart attack, individuals who have been diagnosed with coronary artery disease and those who may have had a recent reduction in blood volume will be excluded. None of the experimenter volunteers will be paid. Potential volunteers who respond to the advertisement poster will be approached at least 24 hours before the study by Dr Angella Bryan, Clinical Scientist on the team. Potential volunteers will be given an information sheet and told what the project will entail and asked to sign a consent form.

Analysis
Waveform raw EIT waveforms will exported into SPIKE and IDL software for further signal processing analysis involving approximate entropy (ApEn). A paired t test or Wilcoxon signed ranks test will be used to temporally compare raw baseline data with autonomic challenge data to determine whether or not fast, neuronal changes can be captured using EIT.
Following reconstruction of the EIT data we intend to identify areas of the brain activated during the autonomic challenge. Isolation of EIT voltage data of specific areas will be undertaken using MatLab and Mayavi. Once raw data has been extracted during different time points of the challenge, we aim to determine statistical significance compared to baseline measurements using a paired t test or Wilcoxon signed rank test.

Confidentiality
Records of consent or refusal to consent will be kept confidential so that there is no chance for coercion of staff or volunteers to participate in the study.
Data will be anonymised, encrypted and stored according to Good Clinical Practice guidelines.

Staff Volunteer Information sheet: Monitoring the brain of awake volunteers during autonomic challenges using Electrical Impedance Tomography (EIT) (Version 1.5 Awake volunteers)

We would like to invite you to participate in a research study. Before you decide whether or not to take part you need to understand why this research is being undertaken and what you would be required to do. Please take some time to read the following information carefully before deciding whether or not you would like to participate. Part 1 of this information sheet will inform you of the purpose of this study being conducted. Part 2 will give you more detail about the conduct of the

study. Do not hesitate to ask a member of the research team if anything is unclear or if you would like more information. Take time to decide whether or not you wish to take part in the study.

Part 1 of the information sheet

What is the purpose of the study?

The purpose of this study is to help determine whether Electrical Impedance Tomography (EIT) can be reliably used as a functional brain imaging device. The EIT device that will be used for this study is known as Functinal EIT with Evoked Response (fEITER). fEITER is an imaging device which is capable of monitoring fast electrical activity of the brain at all depths. This activity can be reconstructed to form an image of brain activity. Functional brain imaging techniques used within clinical practice are expensive, fixed facilities which require individuals to be transported to them. Results from this study would provide supporting evidence for EIT to be used as a clinical brain imaging technique within medicine. fEITER is a portable device which can be used at the bedside. It works by injecting multiple, small currents through the brain via sticky electrodes attached onto the scalp. The current measures 1mA in amplitude and cannot be felt. The injected current is altered as it passes through the functioning brain and this alteration is measured at the same time by other electrodes also attached onto the scalp. fEITER captures multiple measurements 100 times every second allowing fast electrical activity occurring over milliseconds to be captured. The voltage measurements are then used to reconstruct images of electrical activity in the brain representing activity during the time of measurements.

Alterations in the passing current are caused by normal physiology of the brain including electrical activity and blood flow. We aim to induce changes in the normal physiology of the brain by asking volunteers to perform certain actions known to alter electrical activity and blood flow within the brain. By monitoring the brain using fEITER we hope to capture fast electrical activity and slower blood flow changes in the brain known to be caused by the voluntary actions. Results from this study would support the use of EIT as an imaging technology which is capable of capturing fast electrical changes within the brain.

This study will be undertaken as part of PhD programme for Tanviha Quraishi who is a PhD student registered with the University of Manchester. The student is a full time member of staff at Central Manchester NHS Foundation Trust (CMFT). The student's role within this study will involve data collection using the fEITER system, time management of the challenges undertaken and assistance to Dr. Angella Bryan (Clinical Scientist of the research group) during the study. Following completion of the study, the student will be responsible for data analysis which will form part of the PhD thesis.

The student will be supervised by Dr. Angella Bryan and Professor Pollard who will be present throughout the study.

As an employee at CMFT and a member of the research group, the student has undertaken GCP training and is fully aware of the guidelines concerning data collection and storage.

Why have I been invited?

We are interested in monitoring the brains of healthy, awake volunteers.

Do I have to take part?

You do not have to take part in this study. Your participation is voluntary.

What will happen to me if I take part?

We will stick some pads on your scalp which will be connected to cables attached to fEITER. The pads are medically approved and used around the world. The number of pads used may vary but will not exceed 32 in total. The hair on your head will not be shaved/removed, it will be parted to ensure the pads touch the scalp. These pads will allow electrical activity of the brain to be measured at the surface. We will ask you to
perform the following 3 autonomic actions during which we will record activity in your brain:

The Valsalva manoeuvre
Forcibly breathing out with your mouth closed and your nostrils pinched.

The Muller's manoeuvre
Forcibly breathing in with your mouth closed and your nostrils pinched.

The hand grip test
Applying as much grip pressure as possible using a device to measure grip strength.

What will I have to do?

You will be asked to remain in a sitting position and perform the 3 named actions above with interval times in between each action. You will be asked to perform the actions three times.

What is the technology that is being tested?

fEITER is an EIT brain imaging device which was invented at the University of Manchester by Professor Hugh McCann and Dr. Christopher Pomfrett. It is a non-CE marked device. fEITER injects a very small current (1mA) multiple times across pairs of electrodes attached to the scalp. The current cannot be felt by subjects and fEITER poses no harm to participants. The voltage of the injected current changes as it passes through the different tissues and contents of the head including the scalp, skull, brain tissue and blood. The change in voltage is detected by multiple electrodes pairs across the scalp which is the process of acquiring fEITER data. The data can be reconstructed to form an image of the brain and show varying levels of activity in different areas of the brain. The actions you will be asked to perform in the study are known to cause changes in the electrical activity of specific areas in the brain and also in the brain's blood flow. We are hoping to detect these changes using fEITER and relate the changes to areas of the brain.
fEITER as a whole is constructed to meet the standard BS EN 6060-1-1. It is a medical device, Class II, Type BF applied part and the system as an assemblage has been tested for electrical safety appropriate for such a device by Medical Engineering and Maintenance (MEAM) at Central Manchester University Hospitals NHS Trust.

What are the possible disadvantages and risks of taking part?

There are no disadvantages in taking part in this study.
There are some risks that you need to know about:

Repeatedly performing the Valsalva manoeuvre carries a risk for individuals who have a history of heart disease or have had a heart attack. It is important that you tell a member of the research team if you have a history of heart disease or have suffered a heart attack.

What are the side effects of any treatment received when taking part?

There will be no side effects arising from the study. fEITER has been successfully used at the Manchester Royal Infirmary to monitor the brain of 20 awake volunteers and 20 patients during awake and anaesthetised states (Bryan et al., 2011, Quraishi et al., 2011). No sensations or adverse effects were reported by participants.

What are the possible benefits of taking part?

We do not expect this study to benefit you but the information we get from this study will help improve the availability of brain imaging techniques within healthcare.

What happens when the research study stops?

The results of this study will be published in a medical scientific journal and presented at a scientific conference.

What if there is a problem?

Any complaint about the way you have been treated during the study or any possible harm you might suffer will be addressed. There is more detail provided on this question in Part 2 of the information sheet.

Part 2 of the information sheet.

What if relevant new information becomes available?

Sometimes we get new information about the treatment being studied. If this happens, your research doctor will tell you and discuss whether you should continue in the study. If you decide not to carry on, your research doctor will make arrangements for your care to continue. If you decide to continue in the study he may ask you to sign an updated consent form.

If this happens, your research doctor might consider you should withdraw from the study. He/she will explain the reasons and arrange for your care to continue.

If the study is stopped for any other reason, we will tell you and arrange your continuing care.

What will happen if I don't want to carry on with the study? What if there is a problem?

If you have a concern about any aspect of this study, you should ask to speak to the researchers who will do their best to answer your questions. If they are unable to resolve your concern or you wish to make a complaint regarding the study, please contact a University Research Practice and Governance Co-ordinator on 0161 275 7583 or 0161 275 8093 or by email to research.complaints@manchester.ac.uk

Will my taking part in this study be kept confidential?

All information which is collected about you during the course of the research will be kept strictly confidential, and any information about you which leaves the hospital/surgery will have your name and address removed so that you cannot be recognised (if it is applicable to your research).

Involvement of the General Practitioner/Family doctor (GP)

Your GP will be advised that you have taken part in this study.

What will happen to the results of the research study?

The results from this study will be archived onto computer media, encrypted and stored securely for fifteen years.

Who is sponsoring the research and who is responsible for the technology being used?

The research is being sponsored by the University of Manchester and the measurements will be undertaken at CMFT. The University of Manchester will be taking full responsibility for the use of the non CE marked device. Results from the study will also form part of a PhD project through the University of Manchester.

Who has reviewed the study?

All research in the NHS is looked at by independent group of people, called a Research Ethics Committee to protect your safety, rights, wellbeing and dignity. This study has been reviewed and given favourable opinion by the Research Ethics Committee; REC reference: 13/NW/0751, IRAS project ID: 130538

Procedure

We will stick up to 32 standard pads to your scalp. These are attached to fEITER system by wires, and allow it to measure the electrical activity of your brain. We will also ask you to perform the following 3 separate actions:

1. The Valsalva manoeuvre
2. The Muller's manoeuvre
3. The hand grip test

This is so that we can test whether fEITER is capable of measuring well known changes in the brain in response to these actions. You will be asked to repeat each action twice more; this means that you will undertake each challenge a total of 3 times. The study in total will last up to 1.5 hours including electrode application and removal.

It is important that you report any discomfort that you may feel. We do not expect you to feel anything unusual, but this study is partially to test this.

Further information and contact details

Should you want further information regarding this research, please ask Dr Angella Bryan, who is a Consultant Clinical Scientist. If you want to contact the Chief Investigator for this study, please contact Professor Brian Pollard.
Thank you.

Contact Details:

Professor Brian Pollard [Tel: 0161 276 8561]
Professor of Anaesthesia

Dr. Angella Bryan [Tel: 0161 276 4537]
Consultant Clinical Scientist

APPENDIX 4: fEITER Image Reconstructions

fEITER image reconstructions presented in this appendix have been undertaken by a dedicated team at the School of Electrical and Electronic Engineering at the University of Manchester. Forward calculations were performed and compared to EIDORS 3D. A 7-tissue head model consisting of 53,336 tetrahedral elements was employed for reconstructions. For each minute of monitoring, captured fEITER frames totalled 5998. For reconstruction purposes, frames of data were averaged over 50ms. The first 5s were utilised as a reference period to generate subsequent reconstruction frames showing a change in conductivity relative to the reference. As a result, a total of 1100 image frames were generated over 60 s of fEITER monitoring time for each volunteer and patient. A sub-set of images reconstructed from a single volunteer for the VM and from a single patient during induction of anaesthesia are presented below.

(A) The Valsalva manoeuvre

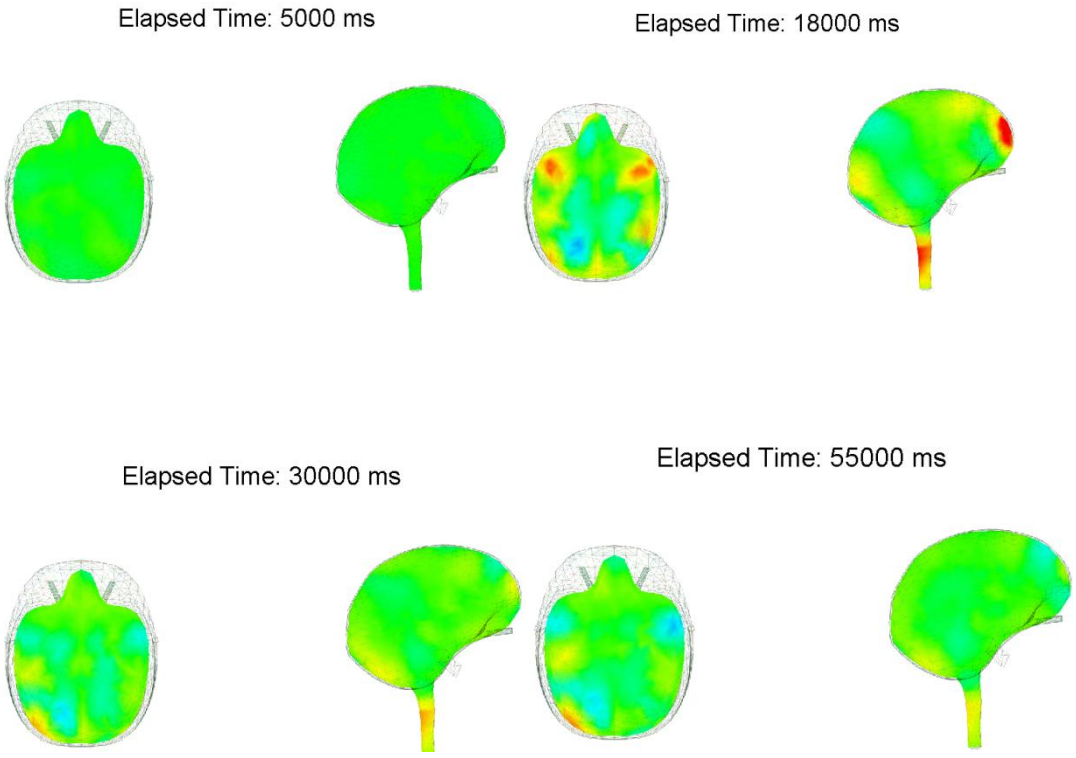

Figure 1. **Reconstructed fEITER data from a single volunteer during the VM.** Sub-set of fEITER reconstructions for a single volunteer during the VM trial. Conductivity changes from the reference (green) can be visualised by areas of yellow and blue. Each image is an average of 5 frames of data. Conductivity changes are relative to a 5s reference period at the beginning of fEITER monitoring time before the manoeuvre was initiated at 10s.

(B) **Induction of anaesthesia**

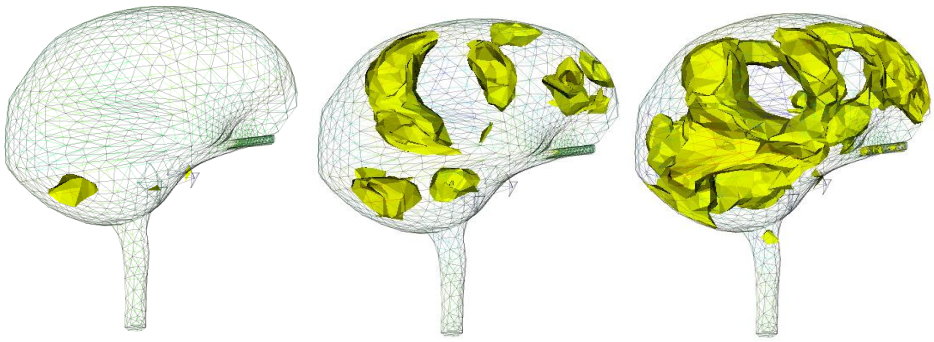

Figure 2. **Reconstructed fEITER data from a single patient during induction of anaesthesia.** Sub-set of fEITER reconstructions for a single patient during stages of anaesthetic induction. All images have been produced in reference to a baseline (shown in the left image). The right image represents the brain of an anaesthetised individual.

There are many known problems which have been described in literature concerning EIT measurements of the brain. Firstly, imaging the small impedance changes of the brain encased in a highly resistive skull poses a major technical challenge as this provides a resistive barrier to current injection. EIT systems which have been developed to image the brain have optimised the amplitude, frequency and the pattern of current injected to overcome the challenge of maximising current density in the brain by penetrating the resistive skull (Wilson et al., 2001, Yerworth et al., 2002). The fEITER system has been developed for high-speed brain imaging by utilising a high frequency (10 kHz), low amplitude (1 mA peak-peak) current which is injected in a diametrically opposed pattern to penetrate the skull whilst also being electrically safe for continuous and repetitive measurements. The system is also able to capture data using a sub-second temporal resolution (100 fps), commensurate with neuronal activity.

EIT systems such as fEITER which are specifically developed for brain imaging have excellent temporal resolution but they often lack high spatial resolution. fEITER reconstructions of the brain are based on a FEM of the head consisting of 53,336 tetrahedral elements, representing 7 tissues of the head (McCann et al., 2011). Each element has a particular resistance value depending on the tissue type it is implicated for at a specified injection frequency (Brown, 2003). The spatial resolution of fEITER is approximately 8mm which cannot compete with the high resolution imaging modalities such as MRI and CT. This also makes it difficult to localise precise areas of the brain demonstrating changes in conductivity. In addition, global haemodynamic effects cannot be eliminated as the spatial resolution of fEITER will incorporate the diameter of major cerebral vessels such as the middle cerebral artery.

Furthermore, although accuracy of the forward model has been improved by use of a head model rather than a spherical shape consisting of elements, the head model still deviates from individual head shape and individual differences in tissue components such as variations of skull and skin thickness. A poor spatial resolution combined with inaccuracies in the forward model for each individual ultimately means anatomical areas of interest implicated in the mediating autonomic outflow during the VM or areas which are activated during induction of anaesthesia be in a variable position for each individual.

APPENDIX 5: EIT Publications by The Author

(A) Proceedings of the Anaesthetic Research Society: British Journal of Anaesthesia. 2011;106:428-9.

Functional Electrical Impedance Tomography by Evoked Response (fEITER): monitoring cerebral auto-regulation during the Valsalva manoeuvre

*T Quraishi[1], CJD Pomfrett[2], *J Davidson[3], *R Robinson[3], *P Wright[3], *ST Ahsan[3], A Bryan[1], *BJ Pollard[1], H McCann[3]

1. Department of Anaesthesia, Division of Clinical & Scientific Services, CMFT
2. Cardiovascular Research Group, School of Biomedicine, University of Manchester
3. School of Electrical & Electronic Engineering, University of Manchester

fEITER is a novel imaging device which monitors changes in cerebral impedance across the whole brain. We aimed to evaluate haemodynamic and electrophysiological changes across the brain in response to volunteers performing the Valsalva manoeuvre (VM).

Each volunteer had 32 Zipprep™ (Covidien, UK) electrodes placed on the scalp using the 10-20 system. The VM was initiated at 10 s and released at 25 s. Sinusoidal current of 1 mA pk-pk was injected at 10 kHz; continuous voltage data were recorded from all electrodes excluding the current injection pair, for 60 s at a temporal resolution of 10ms. The VM was performed by 15 volunteers at CMFT.

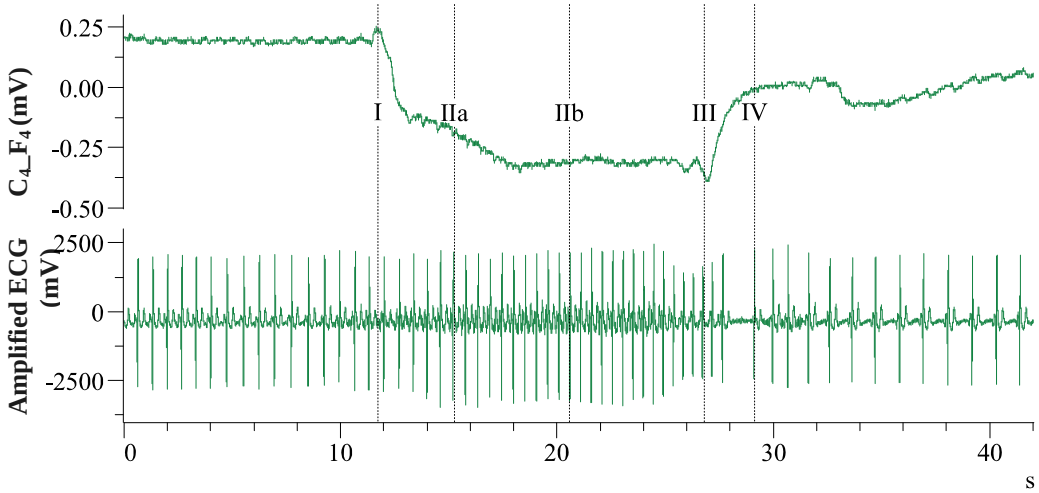

Figure 1. Voltage data from a single volunteer for injection pair F_{PZ}_O_Z; voltage measurement pair C_4_F_4 (upper trace) and simultaneous chest recording of ECG (lower trace). Phases I – IV of the VM are shown across both traces.

Figure 1 (upper trace) shows sub-second cerebral transimpedance changes in response to the VM. Pooled voltage measurements beginning at 5 s were compared to measurements at 8 s for an epoch of 40 ms; no significant differences were observed during this reference period prior to the VM being initiated. Voltage measurements during the VM at 20 s were significantly different to those taken at 5 s for an epoch of 40 ms (Wilcoxon Signed Ranks test, $p = < 0.05$).

Sub-second transimpedance changes signify neural mechanisms involved in cerebral auto-regulation during the most distinct phases of the VM (I and III). The cerebral transimpedance waveform (Figure 1) is similar to those obtained from middle cerebral artery recordings previously performed using transcranial Doppler[1]. These findings show fEITER has the potential to monitor haemodynamic regulation across the brain.

References: 1. Zhang R et al. *Stroke* 2004;35:843-847

(B) Proceedings of the Anaesthetic Research Society: British Journal of Anaesthesia. 2011;106:428-9.

Functional electrical impedance tomography by evoked response (fEITER): a new device for the study of human brain function during anaesthesia

A Bryan[1], CJD Pomfrett[12], J Davidson[3*], BJ Pollard[1], T Quraishi[1*], P Wright[3*], R Robinson[3*], ST Ahsan[3*], H McCann[3*]*1. Department of Anaesthesia, Division of Clinical & Scientific Services, CMFT; 2. School of Biomedicine 3. School of Electrical & Electronic Engineering, University of Manchester M13 9PL*

The objective of this project was to develop a non-invasive and portable brain imager, based on electrical impedance tomography, for use by anaesthetists. fEITER gives the 100 frames per second resolution needed to study sub-second mechanisms underlying consciousness[1].

fEITER met the requirements of the Medical Device Directive, received MHRA "no objection", and a favourable ethical opinion from S.Manchester LREC (ISRCTN 93596854). All subjects gave written, informed consent. fEITER injected a sinusoidal current (1mA pk-pk, 10kHz) between opposite electrode pairs (ZipPrep, Covidien,UK), pseudo-randomly selected from 32 electrodes positioned using the 10-20 montage. Non-current injection electrodes were used for >500 voltage measurements during each 10ms measurement frame. Flash stimuli were presented using fEITER. Stage 1 of the study (awake, completed) required the recruitment of twenty ASA I volunteers. Twenty ASA I or II patients scheduled for elective surgery with BIS monitoring are being recruited now for stage 2 (anaesthetised).

The rheoencephalograph[2] was time-locked to the ECG but with different latencies depending on the position of the recording on the head. Sub-second responses to single flashes were of sufficient magnitude to reconstruct as 3D maps of conductivity change that highlighted the visual cortex and frontal lobes in temporal ranges expected for visual processing. Large, sub-second changes in trans-cerebral impedance were noted during propofol induction (Figure 1).

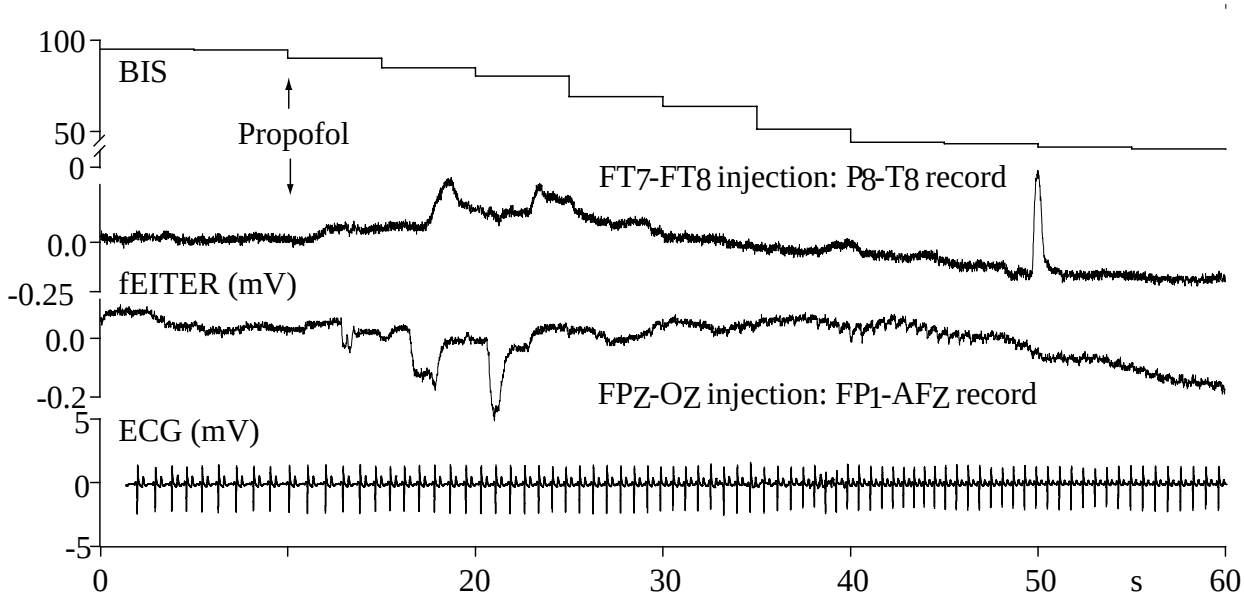

Figure 1. BIS, ECG and fEITER traces describing induction of anaesthesia

References: 1. Koch C, Greenfield S. Scientific American 2007; 297: 76-83; 2. Bodo M et al J. Physics 2010; doi:10.1088/1742-6596/224/1/012088.
Acknowledgements: This study was supported by the NIHR Manchester Biomedical Research Centre, and funded by the Wellcome Trust.

(C) Proceedings of the Anaesthetic Research Society: British Journal of Anaesthesia. 2011:107;827-8.

Functional Electrical Impedance Tomography by Evoked Response (fEITER): monitoring for asymmetry in awake and anaesthetised patients

B O'Neill[1,2]*, A Bryan[1], T Quraishi[1]*, J Davidson[3]*, P Wright[3]*, H McCann[3]*, BJ Pollard[1,2]*

1. Department of Anaesthesia, Division of Clinical & Scientific Services, CMFT
2. School of Medicine, University of Manchester
3. School of Electrical & Electronic Engineering, University of Manchester

fEITER is a novel imaging device which monitors changes in cerebral conductivity at 100 frames per second across the whole brain. We aimed to evaluate cerebral asymmetry using fEITER in relation to the depth of anaesthesia, as measured with bispectral index (BIS).

ASA I or II patients scheduled for elective surgery gave written, informed consent. 32 Zipprep^{TM} (Covidien, UK) electrodes were placed on the patient's scalp using the 10-20 system. fEITER injected sinusoidal current of 1mA pk-pk at 10kHz. Continuous voltage data were recorded from non-injecting electrodes for 60s; during awake and anaesthetised conditions. BIS was simultaneously recorded with the BIS Vista monitor (Covidien, UK).

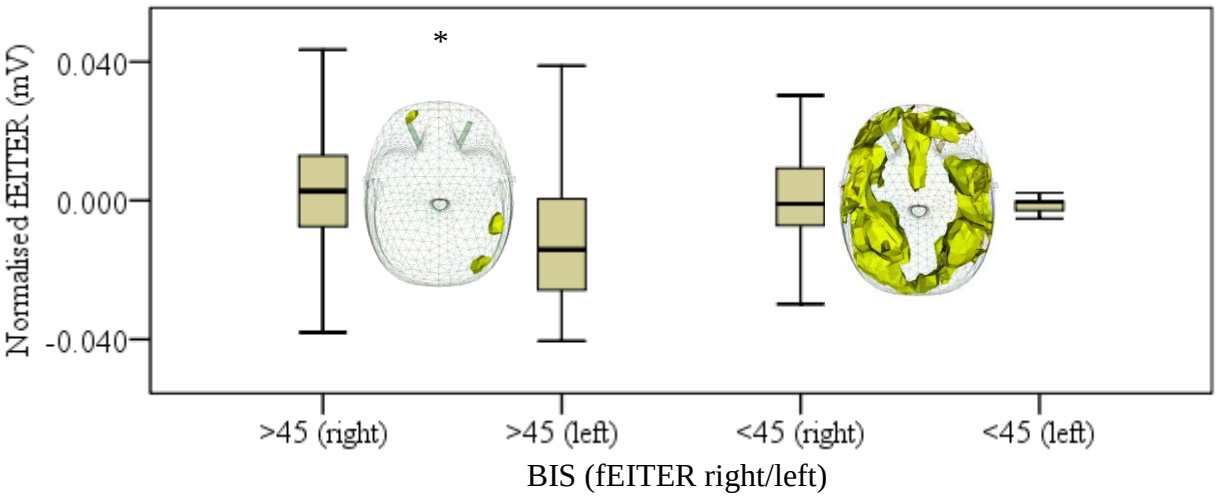

Figure 1. Single subject data (adult male). Box and whisker plots of fEITER conductivity changes at BIS >45 and <45, for measurement pairs: FT_8-T_8 (right) and FT_7-T_8 (left). * indicates significant differences between fEITER right and left ($p<0.05$). Reconstructed awake and anaesthetised fEITER images are also shown.

fEITER right and left normalised conductivity values were compared for a central current injection at FP_Z-O_Z. We observed a significant difference ($p<0.05$) between right and left hemispherical fEITER measurements at higher BIS levels (BIS>45 (fig.1).

Previous findings demonstrated laterality during anaesthesia with bilateral BIS[1]. fEITER measures sub-second conductivity changes during anaesthetic induction[2]; current results demonstrate cerebral laterality between the awake and anaesthetised state using fEITER.

References: 1. Pomfrett CJD et al. Delta sleep-inducing peptide alters bispectral index, the electroencephalogram and heart rate variability when used as an adjunct to isoflurane anaesthesia. *Eur J Anaesthesiol.* 2009;26:128-134; 2. Bryan A et al. Functional electrical impedance tomography by evoked response: a new device for the study of human brain function during anaesthesia. *Br J Anaesth.* 2011;106:428-9.

Acknowledgements: This study was funded by the Wellcome Trust.

(D) BJ Pollard, CJD Pomfrett, A Bryan, T Quraishi, J Davidson, H McCann. Functional Electrical Impedance Tomography by Evoked Response (fEITER): Sub-second changes in brain function during induction of anaesthesia with propofol. European Journal of Anaesthesia. 2011; 28:97-8. (Poster)

(E) Proceedings of the Anaesthetic Research Society: British Journal of Anaesthesia. 2013:110;870.

Functional EIT with Evoked Response (fEITER) images reveal areas of changing conductivity in the brain during the Valsalva manoeuvre (VM)

T Quraishi[1], A Bryan[1], *J Davidson[2], CJD Pomfrett[3], *P Wright[2], *H McCann[2], *BJ Pollard[1]

1. Department of Anaesthesia, Division of Clinical & Scientific Services, CMFT
2. School of Electrical & Electronic Engineering, University of Manchester
3. National Institute for Health and Clinical Excellence, Manchester

fEITER is a functional neuroimaging device which has been used to monitor the brain of 15 volunteers performing the VM. Preliminary analysis of fEITER waveforms revealed conductivity changes in response to the VM [1, 2]. Slower changes were attributed to haemodynamic changes in the brain whereas sub-second changes were attributed to neuronal activity resulting in autonomic outflow (Bryan et al., 2011). Reconstructed images have demonstrated sub-second conductivity changes in areas of the brain associated with autonomic responses to the VM. Voxel data relating to the insular and pre-frontal cortex were extracted and analysed.

32 Zipprep™ (Covidien, UK) electrodes were placed on the scalp of each volunteer according to the international 10-20 system of EEG electrode placement. Monitoring with fEITER was undertaken for 60s; the VM was initiated at 10s and released at 25s. Voxel data relating to the insular and pre-frontal cortex were extracted from the images using MatLab and MayaVi software. Voxel data across all volunteers were pooled, normalised and statistically analysed using the Wilcoxon Signed Rank test.

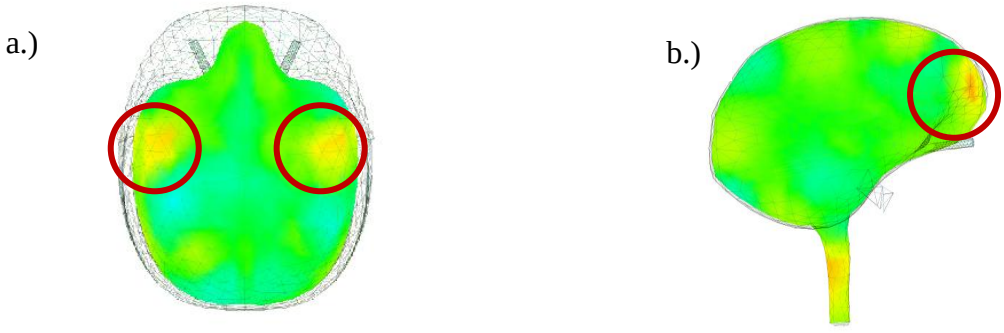

Figure 1. Single subject images of the brain during the VM. Conductivity changes are visible in circled areas relating to the insular (a), and pre-frontal cortex (b) following onset of the VM.

Prior to VM onset, pooled voxel data for the insular and pre-frontal cortex were statistically compared with pooled voxel data for the same areas of the brain following onset of the VM using a sub-second epoch of 500ms. Results demonstrated significant differences in conductivity at the insular and pre-frontal cortex following initiation of the VM (Wilcoxon Signed Rank test, $p < 0.005$). The insular and pre-frontal cortex have previously been identified as neural components of initiating autonomic outflow in response to the VM using functional MRI (Nagai et al., 2010).

(E) Proceedings of the Anaesthetic Research Society: British Journal of Anaesthesia. 2014: 113;327-8.

Measuring impedance changes in the brain using Electrical Impedance Tomography (EIT) in response to visual stimulation

Quraishi T [a], *Bryan A* [a], *Pomfrett CJD* [b], *Davidson J* [c], *Wright P* [c], *Pollard BJ* [c]
[a] Department of Anaesthesia, Central Manchester NHS Foundation Trust, [b] National Institute for Health and Clinical Excellence, Manchester, [c] The University of Manchester

Visually evoked blood flow responses (VEFR) and regional cerebral blood flow (rCBF) in the brain have previously been measured using functional imaging techniques[1] and TCD[2]. Our study aimed to show whether EIT is capable of detecting impedance changes during functional activity in the brain evoked by a visual stimulus.

32 ZipprepTM (Covidien, UK) electrodes were placed on the scalp of 20 volunteers. Functional EIT with Evoked Response (fEITER) was used to inject sinusoidal current of 1mA pk-pk at 10kHz; EIT data was captured every 10ms, for 60s. Volunteers kept their eyes closed at all times. A sequence of 20 flashes starting from 21s to 41s at 1kHz was presented to volunteers using goggles containing a grid of LED lights. Percentage differences from baseline (initial 15s) was calculated for 7 volunteers then pooled.

Pooled EIT data prior to visual stimulation for an epoch of 15s, beginning at 0s, was statistically compared to a 15s epoch of data during visual stimulation beginning at 25s. Results demonstrated significant differences in percentage impedance changes following the onset of visual stimulation (Wilcoxon Signed Rank test, $P<0.005$). The magnitude of percentage impedance changes shown in Figure 1, is reflective of results collected by other EIT groups[3]. These results demonstrate the ability of EIT to capture functional changes in the brain.

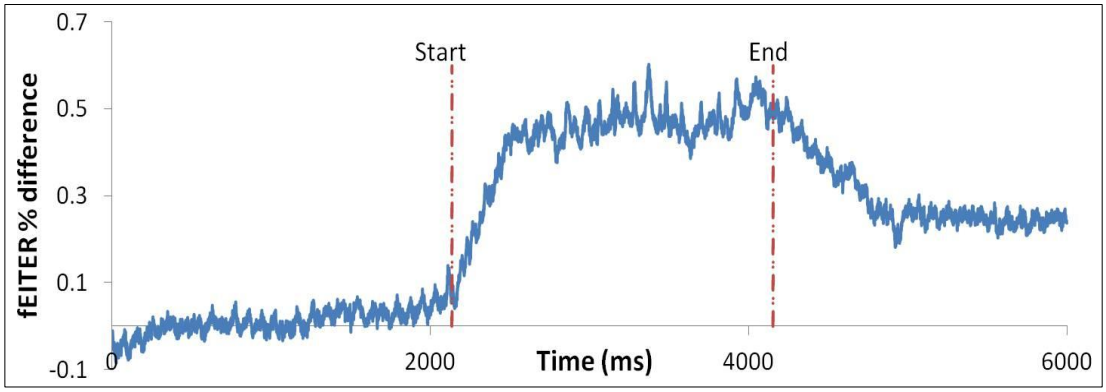

Figure 1. Average percentage differences for fEITER data recorded from 7 volunteers at injection pair FP1_O2 and measurement pair AF7_F7. Vertical lines indicate the start and end of visual stimulation.

References

1. Pastor MA, Artieda J, Arbizu J, Valencia M, Masdeu JC. *Human Cerebral Activation during Steady-State Visual-Evoked Responses.* 2003; **23:** 11621-11627
2. Sturzenegger M, Newell DW, Aaslid R. *Visually Evoked Blood Flow Response Assessed by Simultaneous Two-Channel Transcranial Doppler Using Flow Velocity Averaging.* 1996; **27:** 2256-2261
3. Tidswell T, Gibson A, Bayford RH, Holder D. *Three- Dimensional Electrical Impedance Tomography of Human Brian Activity.* 2001; **13:** 283-294